Study to quantify the combined interaction of tyre and surface water on asphalt surface performance

A thesis submitted for the degree of Doctor of Philosophy
By

Fauzia Saeed

Department of Civil and Environment Engineering
Brunel University London

July 2018

I. Abstract

Pavement surface failure is a dynamic and complicated process. Irrespective of the pavement type, the water on the pavement surface, the water build-up in the internal voids or the water pressure through cracks due to traffic action plays a significant role in the functional and structural failure of the pavement. Although extensive studies on water related material degradation have been conducted in the last fifty years, research on measuring water pressure due to dynamic action of load and its impact on pavement performance is very limited and disjointed.

The goal of this research was to investigate the formation of pavement surface damage in the laboratory environment, due to water pressure. A novel test method was developed to simulate dynamic loading-tyre-water-pavement interaction for the pore water pressure measurement. A custom build loading plate with different tyre characteristics was applied dynamically on submerged pavement surface with narrow pore. The compressed water under the tread pad generates a water pressure pulse in the pavement, and permits surface water to penetrate the pores in the asphalt slabs and creates a pores water pressure. The water pressure under the asphalt slabs was measured using a pressure sensor. It was found that dynamic water pressure increases significantly when high frequency loading combined with square type of tread, and water trapped inside the groove of the tread pad which generates pumping action. The water pressure also increases with thread thickness. Load magnitude and depth of surface water was found to have marginal impact on the water pressure in the pavement.

The combination of load magnitude, frequency, tyre parameters that created the highest pore water pressure, was used continuously to create surface damage in order to quantify asphalt surface performance. The influence of asphalt surface type, aggregate size, weather conditions and loading frequency were investigated. The results showed that depending on the type of asphalt surfaces, the presence of water accelerates surface cracking, rutting and other distresses such as ravelling. The cracking propensity was severe in highly open graded mixtures than the gap graded ones. Compared to dry condition testing, the appearance of surface crack was approximately seven times faster in highly open graded mixtures tested in the wet condition. The open graded mixtures demonstrated good rutting resistance compared to gap graded mixtures. In

the presence of water, the mixture gradations showed more influence on the load bearing capacity than the size of aggregates. Finally, for same mixture type, it appeared that aggregate size has more influence on the wet condition performance than air void contents in the mixture. The proposed test method showed good potential to be implemented as a screening test for different types of mixes.

Finally, two prediction models were developed. The first model was based on Fuzzy Inference System (FIS), a widely employed soft computing technique and the second method was a deterministic technique employing multiple regression analysis. The FIS method provided a set of "*if-then*" rules. After developing the model, a cross validation technique was employed to evaluate the model accuracy across the dataset. Furthermore, sensitivity analysis to assess the influence of each parameter in asphalt performance was conducted. The FIS model showed promising results to be implemented as a routine prediction model to differentiate the performance of different asphalt surfaces subjected to dynamic loading while submerged in water. The regression model on the other hand showed variability in the prediction and is being suggested to be used as an indicative predictive tool only. Further research is proposed to improve regression model.

II. Acknowledgements

Above all, I owe it all to Almighty God for granting me the health and strength to undertake this research task and enabling me to its completion.

Firstly, I would like to express my sincere gratitude to my principle supervisor, Dr Mujib Rahman for his excellent, valuable guidance, scholarly inputs and consistent encouragement I received throughout the research work. I would like also to present my sincere thanks to Prof Denis Chamberlain my industrial supervisor, for his valuable assistance and constructive suggestions throughout this research. I could not ask for better supervisors for my PhD research.

Great thanks go to Mr. Simon Le Geyt from Civil Engineering Research Center for his support and valuable comments during the lab work and thank you to Dr Ali Ahmadnia from Mechanical department for his support.

I want to dedicate my thesis to my beloved father Brigadier-general Mohammed Hamad Saeed who passed away in 2011, my mother Mrs. Kamala El-Fergany for thier wise counsel,endless love, encouragement and support.

I would like to thank my Husband Mr. Ezaldeen, who has always participated with and stood by me all the times. Also, my kind thanks also go to my lovely kids, Mohammed, Hasan, Batal and Abdulrahman.

I would like also to acknowledge the Ministry of Higher Education of Libya for providing me with the financial support and scholarship facilities to complete my PhD study in the UK.

III. Declaration

The research reported in this thesis was conducted at university of Brunel, Department of Civil and Environment Engineering, between August 2014 and July 2018.

I declare that the work is my own and has not been submitted for a degree at another university.

Fauzia Mohammed Hamad Saeed

London

2018

IV. Publication

The work detailed in this thesis has resulted in number of refereed publications, as follows:

Journal articles:

1. **F. Saeed**, M Rahman and D. Chamberlain. (2018). Impact of tire and traffic parameters on water pressure in pavement. *ASCE American Society of Civil Engineers, Journal of Transportation Engineering, Part B: Pavements*. [Chapter 4]. http://dx.doi.org/10.1061/JPEODX.0000065
2. **F. Saeed**, M Rahman and D. Chamberlain. (2018). *IJPEAT International Journal of Pavement Engineering and Asphalt Technology*. A novel laboratory test method to measure dynamic water pressure underneath a cracked concrete pavement, 19(2). [Chapter 4].
3. **F. Saeed**, M. Rahman D. Chamberlain and P. Collins. (2018) Asphalt Surface Damage Due to Combined Action of Water and Dynamic Loading. *Journal of Construction and building materials*. (Accepted, subject to minor correction). [Chapter 5].

Journal articles under preparation:

4. **F. Saeed**, M. Rahman and D. Chamberlain. (2019). A Fuzzy Inference System for Predicting Pavement Surface Damage. Submitted to Computer-Aided Civil and Infrastructure Engineering Journal.
5. **F. Saeed**, M. Rahman and D. Chamberlain. (2018). The State art review of pore water pressure in asphalt surfaces. [Chapter 2].

Publications in international conferences

6. **F. Saeed**, S. Qamariatul, M. Rahman and A Woodside (2015) 'The State of Pothole Management in UK Local Authority', 6th International Conference on Bituminous Mixtures and Pavements, June 10-12, Thessaloniki.
7. **F. Saeed**, M. Rahman, M. Mahmood and P. Collins (2019) Deterioration prediction model of asphalt surface damage due to combined action of water and dynamic loading, 98th TRB Annual Meeting, January 13-17, Washington, D.C. [Chapter 5 +Chapter 6]

8. **F. Saeed**, Rahman, M., Denis, C (2018) 'A novel laboratory test method to measure dynamic water pressure underneath a cracked concrete pavement', 17 th Annual International Conference on Asphalt, Pavement Engineering and Infrastructure. 21-22 February. Liverpool

Poster presentations at conferences:

9. F. Saeed. (2015). Moisture damage of Pavement Surface, Research Student Conference Poster. Brunel University. London, UK. 17-18 March.

V. Table of Content

VI. List of Figures

VII. List of Tables

VIII. List of Symbols

SQ	squared box tread
SL	square box with a channel tread
NT	non-treaded
1.5SQ4	1.5 means tread depth; SQ means a square box and four indicated to the water depth
8SL2	Eight means tread depth SL a square box with a channel and two indicated to the water depth
8SL4	Eight means tread depth; SL a square box with a channel and four indicated to the water depth
3SL2	Three means tread depth; SL a square box with a channel and two indicated to the water depth
3SL4	Three means tread depth; SL a square box with a channel and four indicated to the water depth
1.5SL2	1.5 means tread depth; SL a square box with a channel and two indicated to the water depth
1.5SL4	1.5 means tread depth; SL a square box with a channel and four indicated to the water depth
NT2	Non-treaded tyres and two indicated to the water depth
NT4	Non-treaded tyres and four indicated to the water depth
8SQ4-10	10 at the end indicate to load is 10 KN
8SQ4-5	5 at the end indicate to load is 5 KN
3SQ2-10	10 at the end indicate to load is 10 KN
3SQ2-5	5 at the end indicate to load is 5 KN
1.5SQ2-10	10 at the end indicate to load is 10 KN
1.5SQ2-5	5 at the end indicate to load is 5 KN
8SL2-10	10 at the end indicate to load is 10 KN
8SL2-10	5 at the end indicate to load is 5 KN
3SL2-10	10 at the end indicate to load is 10 KN
3SL2-5	5 at the end indicate to load is 5 KN
1.5SL2-10	10 at the end indicate to load is 10 KN

1.5SL2-5	5 at the end indicate to load is 5 KN
NT2-10	10 at the end indicate to load is 10 KN
NT2-5	5 at the end indicate to load is 5 KN
HRA	Hot Rolled Asphalt
SMA	Stone Mastic Asphalt
PA	Porous
HRA10-D	Hot rolled asphalt, 10 mm nominal aggregate size, D is Dry condition.
HRA10-w	Hot rolled asphalt, 10 mm nominal aggregate size, W is Wet condition
HRA14-D	Hot rolled asphalt, 14 mm nominal aggregate size, D is Dry condition.
HRA14-W	Hot rolled asphalt, 14 mm nominal aggregate size, W is Wet condition.
SMA6-D	Stone Mastic asphalt, 6 mm nominal aggregate size, D is Dry condition
SMA6-W	Open Stone Mastic asphalt, 6 mm nominal aggregate size, W is Dry condition
SMA10-D	Open Stone Mastic asphalt, 10 mm nominal aggregate size, D is Dry condition
SMA10-W	Open Stone Mastic asphalt, 10 mm nominal aggregate size, W is Dry condition
SMA14-D	Open Stone Mastic asphalt, 14 mm nominal aggregate size, D is Dry condition
SMA14-W	Open Stone Mastic asphalt, 14 mm nominal aggregate size, W is Dry condition
PA14-D	Porous asphalt, 14 mm nominal aggregate size, D is Dry condition
PA14-W	Porous asphalt, 14 mm nominal aggregate size, W is Dry condition
MIG	Metal Inert Gas
DAQ	data acquisition
RRV	Relative Ramp Waveform

CW	Cyclic waveform
ARW	Absolute Ramp Waveform
Ω	Ohm refers to the SI unit of electrical resistance
°C	Celsius
V	Voltage, electric potential difference
FIS	Fuzzy Inference Systems
μA(x)	Membership Function of Set A
Ci	Cluster Centre
U	Membership Matrix
mi	Number of Membership Functions for Input i
Yi	Dependent Variable
Xi	Independent Variable
SPSS	Statistical Package for the Social Sciences
R^2	Coefficient of Determination

Chapter 1 Introduction

1.1 Problem Statement

Flexible pavements are designed to withstand against mechanical and functional degradation due to traffic loading and environmental conditions (Cook and Dynkins, 1991; Dehnad et al., 2013; Shiwakoti, 2007; Little and Jones, 2003; Airey and Choia, 2002; Flynn, 1991; Lottman, 1982; Moulton, 1980). Premature failure leads to reduce service life, compromises the safe operation of traffic, and increases maintenance and rehabilitation cost. There are significant public concerns due to the rapid increase in the number of damages, namely potholes, in the asphalt surfaces (Saeed et al., 2015). These localized failed areas reduce the ride quality and potentially create a dangerous driving condition. A survey by Asphalt Industry Alliances in 2018 revealed that nearly one-third of the local authorities in the United Kingdom felt that the roads had to be shut down due to safety hazards (AIA, 2018).

Although it is well known that water ingress in pavement causes significant deterioration, the mechanism is not yet fully understood, especially its impact on the surface damage (AIA, 2018). When water enters the road surface, it creates significant hydrostatic pressure due to the action of moving vehicles. The magnitude of the pressure varies depending on the surface type, tyre tread depth and any presence of existing distress on the surface (Kringos, 2007). The high-water pressure under the tyre creates tensile stress at the mixture matrix, which in turn to damage under the repeated action of moving traffic. The water that enters the pavement coupled with the change in temperature results in freezing and thawing, making the asphalt mixture matrix more brittle, and that in turn cause rapid failure of the surface resulting in potholes (Willway,2008). Eventually, water may reach the subgrade layer which can then weaken the foundation, and can eventually result in a collapse of the road pavement.

There are two sources of water/moisture in asphalt pavement. internal and external. Inadequate drying of aggregate used in the mixes can be one familiar internal sources of moisture (Copeland, Youtcheff and Shenoy, 2007). An external source of water can come from three different ways; water enter the pavement from surfaces because of poor drainage, poor construction (compaction) or mixture design having high air voids content and so more permeability. Water can also seep into in pavements from the sides because of poorly constructed shoulders, poor side drainage and water beneath

the subgrade because of the high water table and poor drainage characteristics of a base and sub-base material (Ahmad, 2011).

Studies on water related damage are primarily investigate a material degradation of laboratory manufactured specimens by assessing the reduction of mechanical properties after several moisture conditionings cycles and determining the loss of adhesion and/or cohesion of the mixture matrix. Nevertheless, the interactions of tyre-water-pavement happen simultaneously, and it is vital to consider their combined influence on the overall performance of the asphalt pavement.

This research is to appraise the performance of various asphalt surfaces subjected to concurrent flooding and cyclic loading. This study displays a new laboratory test set-up to represent the combined action of water and traffic loading.

In the available literature on water pressure in a pavement, essentially studies are determined to be computational like (Kutay and Aydilek, 2007; Li and Deng, 2008; Cui et al., 2009; Li and Sheng, 2012; Guo, Sun and Dai, 2017) and/or analytical for examble (Li and Deng, 2008; Xiaoyong, 2008) and Experimental studies such as (Jiang, Zhang and Li, 2013; Gao, Guo and Liu, 2015), are limited. This is due to the complexity of measuring water pressure under traffic load in the laboratory environment as well as in in-situ. This research, consequently, focused on understand of the surface damage due to water pressure, a developing a laboratory test to measure water pressure under a repeated vertical load on pavement surface subjected to flooding. The impact of load magnitude, load frequency, tyre tread shape, and patterns, and depth of water on the surface were all studied.

1.2 Aims and Objectives

The primary aim of this research project is to quantify the impact of water pressure in asphalt surface damage due to combined interaction of traffic, and surface water. In order to achieve the aim, the following objectives were set to accomplish.

1. Develop a novel test method to measure water pressure inside the pavement.
2. Investigate the impact of traffic parameters, tyre parameters, and depth of surface water on water pressure inside the pavement.

3. Investigate the impact of combined interaction of tyre-water-pavement on formation of surface damage, due to water pressure.
4. Develop models to predict asphalt surfaces deterioration due to the combined interaction of traffic-water-pavement.

1.3 Work Package

To fulfil the objectives of the research, the project has been divided into four work packages.

Work package 1: A comprehensive literature review to cover different types of asphalt distresses, and in depth review of water related damages. The water related damages cover both material degradation due to continuous exposure to water and water pressure related damage when pavement is flooded with water and is subjected to traffic loading. The literature review also covered various models to select the most suitable one to predict deterioration of asphalt surfaces due to combined action of tyre -water-pavement.

Work package 2: In order to achieve objectives one and two, in this work package, a novel test method was designed to simulate combined interaction of tyre-water-pavement and to measure water pressure under the pavement. The testing was conducted to investigate the impact of load rate and magnitude, tyre characteristics, and depth of surface water on water pressure inside pavement. This work package was helping to determine the most severe combination, which were implemented in work package 3.

Work package 3: This work package is to fulfil objective three of this research. After determining the most severe combination of load, tyre characteristics and depth of surface water in work package 2, the case was applied load on different types of asphalt surfaces and was continued until asphalt surfaces showed significant damages. Comparison was made to evaluate the mixture performance in dry and wet condition testing. The influence of mixture gradation, and aggregate size were also evaluated.

Work package 4: The results generated from work package 2 and work package 3 will be utilised to develop models to predict asphalt surface deterioration when surface experience repeated load while submerged in water.

1.4 Structure of Thesis

The chapters of this research are constructed from systematic experimental and modelling works. The thesis structures and their relation to each objective and research methodology are given in Figure 1.1. A short description of each chapter is also presented in the following sections.

Chapter 2: Literature Review

Chapter 2 provides literature related to asphalt surface damage especially the impact of water pressure. The content of the review mainly focused on the fundamental of flexible pavement including asphalt surface damage due to water, studies related to pore water pressure, asphalt surface damage due to the interaction of traffic loading, tyre, water and pavement surface itself. Furthermore, a comprehensive review on various deterioration prediction models to select an appropriate technique for developing a prediction model from the experimental data in Chapter 5 for different types of asphalt surfaces.

Chapter 3: Methodology, Preliminary Investigations and Test Specifications

Chapter 3 provides a general description of the equipment, materials and approaches used for the experimental work. Manufactured moulds and details of testing equipment used in the laboratory are presented. A general preparation process of slabs is described. Testing techniques also for both pore pressure measurement and experiments to determine asphalt surface damage is also provided in full details.

Chapter 4: Impact of Tyre and Traffic Parameters on Water Pressure in Pavement

Chapter 4 presents the investigation related to pore water pressure measurement under various test conditions. The impact of load and tyre parameters are investigated in detail. Furthermore, analysis and interpretation of the test data and a comparison with previous related studies are presented.

Chapter 5: Asphalt Surface Damage Due to Combined Action of water and Dynamic Loading

Chapter 5 presents the results from the investigations to evaluate the combined influence of repeated loading with specific tyre characteristic and water on three widely used asphalt surfaces. The results are compared with relavent design standards to evaluate their comparative performance.

Chapter 6: Development of deterioration prediction model

Chapter 6 provides an extensive study for developing a multi-input model to predict deterioration of asphalt surfaces. The results from chapters 4 and 5 are used as input parameters for model development and validation.

Chapter 7: Summary, Conclusions and Recommendations

Chapter 7 outlines the conclusion of this research and the recommendations for future works.

1.6 Novel Research Contributions

This research contributes to develop better understand of pore water pressure in pavement where novel laboratory tests were exploited leading to the specific contributions as follows:

1) Develop a test method to simulate tyre-water-pavement surface interaction (refers to Chapter 3).
2) Measure water pressure in pavement under dynamic loading when the surface was flooded with water (refers to Chapter 4).
3) The influence of combined water and dynamic loading on surface damage was successfully simulated in the laboratory environment. The outcome of the test method has demonstrated a promising future for further development (refers to Chapters 5).
4) Develop a multi input models to predict deterioration of asphalt surfaces when subject to combined action of repeated traffic loads with specific tyre characteristics applied asphalt surfaces submerged with shallow water (refers to Chapters 5 and 6).

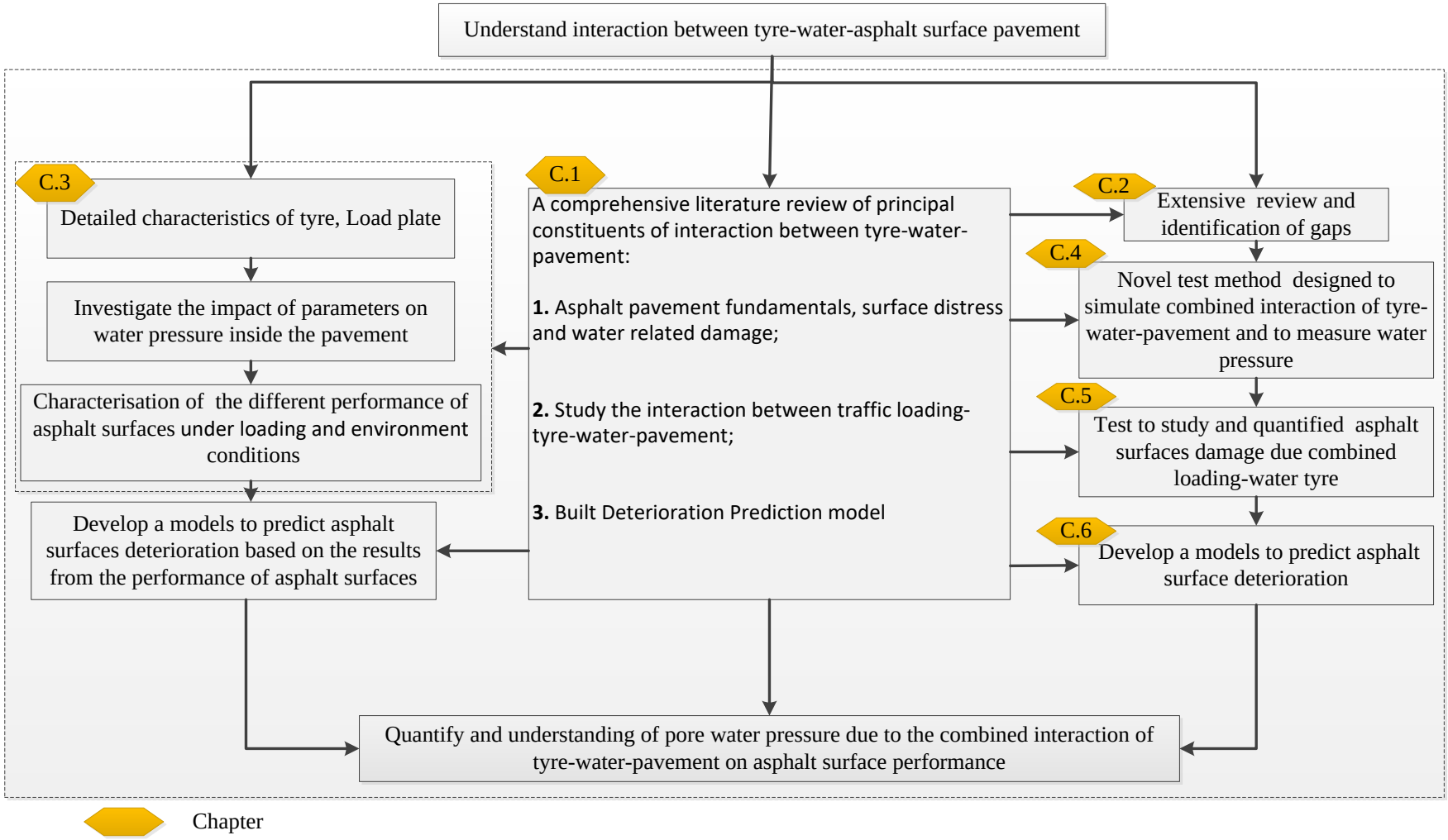

Figure 1.1 Thesis structure in relation to research objectives, methodology, and thesis chapters.

Chapter 2 Literature Review

2.1 Introduction

As discussed in Chapter one, the primary purpose of this research project is to study the impact of water pressure on the asphalt surface performance. This chapter will present the fundamental information on asphalt pavement and then will review literature related to asphalt surface damage, especially the influence of water pressure created by dynamic loading. This chapter has been divided into three main parts. The first part begins with a brief introduction on asphalt pavement including an evaluation of asphalt distress, especially distresses related to water. The second part presents a comprehensive review of relevant literature on moisture-related damage, studies related to pore water pressure, and asphalt surface damage due to the interaction of traffic loading, tyre, water and pavement surface itself. The third part will present a review of different deterioration prediction models to choose a suitable method for the utilisation of experimental data from this research to predict the performance against water pressure for different types of asphalt surfaces.

Part 1: Asphalt pavement fundamentals, surface distress and water related damage

2.1.1 Pavement Types

A road pavement is a structure consisting of multiple layers of prepared materials over a natural and/or stabilised soil sub-grade. The primary structural function of pavement is to provide enough support to withstand the imposed loads upon it and distribute them over a relatively wide area of soil (Nikolaides, 2014; Tom, 2008). Pavements are categorised into three groups based on the structural performance and layered structure. These are;

- Concrete pavement known as rigid pavement, where unreinforced or reinforced concrete slabs are laid on pavement foundation.
- Asphalt pavement known as flexible pavements where layers of bituminous material are laid on pavement foundation.
- Composite pavements are made with both concrete and asphalt layers.

As the scope of the project is limited to asphalt pavement and therefore, the following sections will explain asphalt pavement and related distresses.

2.1.2 Flexible Pavement

Asphalt pavement consists of aggregates which are bound together by a binder (bitumen). Asphalt pavement is a viscoelastic material. The visco-elasticity is commonly employed to describe that bitumen materials have viscous and elastic behaviour together; viscous behaviour at high temperature and/or slow loading, and elastic behaviour at a low-temperature and/or fast loading. Because of the viscoelastic response of flexible pavement, they have a higher susceptibility to permanent deformation, known as rutting, when exposed to prolonged loading time such as stationary or slow-moving traffic and/or at high temperature (Rahimzadeh, 2002; Airey *et al.*, 2016; Eustacchio and Fritz, 2014). Besides, asphalt pavement suffers from thermal and fatigue cracking due to repeated application of environmental and traffic loading at low and intermediate temperature respectively (Ozer *et al.*, 2018; Glaoui *et al.*, 2012; Osman, 2005).

A typical Asphalt pavement consists of surfacing (surface course and binder course), base and subbase built over a compacted subgrade. A brief overview of each layer is given in the following section, and a schematic diagram of a typical flexible pavement is given in Figure 2.1.

- **Surface Course**

A surface course should be capable of withstanding high tyre pressure, and mainly provides safety and comfort during driving, provides skid resistance in both dry and in wet condition and allow a path for surface water to drain quickly. As the surface course is directly exposed to sunlight and rain, the damage related to the environment is more significant in this layer. Depending on the traffic loading, type of the road and noise regulations, the thickness of this layer varies from as thin as 20 mm to maximum 50 mm (DMRB,2006).

- **Binder Course**

The binder course is to provide a uniform cushion for a surface course and allow imposed traffic to distribute in the base. The typical thickness of binder course is 50 mm to 100 mm, depending on the traffic and environmental conditions (DMRB, 2006).

- **Base**

The base is the main structural layer capable of taking traffic loading. This layer is mainly a dense layer with thickness varies from 100 mm to 200 mm (DMRB, 2006).

- **Sub-base**

Sub-base gives additional load distribution and provides to the sub-surface drainage. It may be formed of crushed stone and other untreated or stabilised materials (DMRB, 2006).

- **Sub-grade**

The subgrade is the in-situ materials upon which the pavement structure is placed. The subgrade must be able to support loads transmitted from the pavement structure.

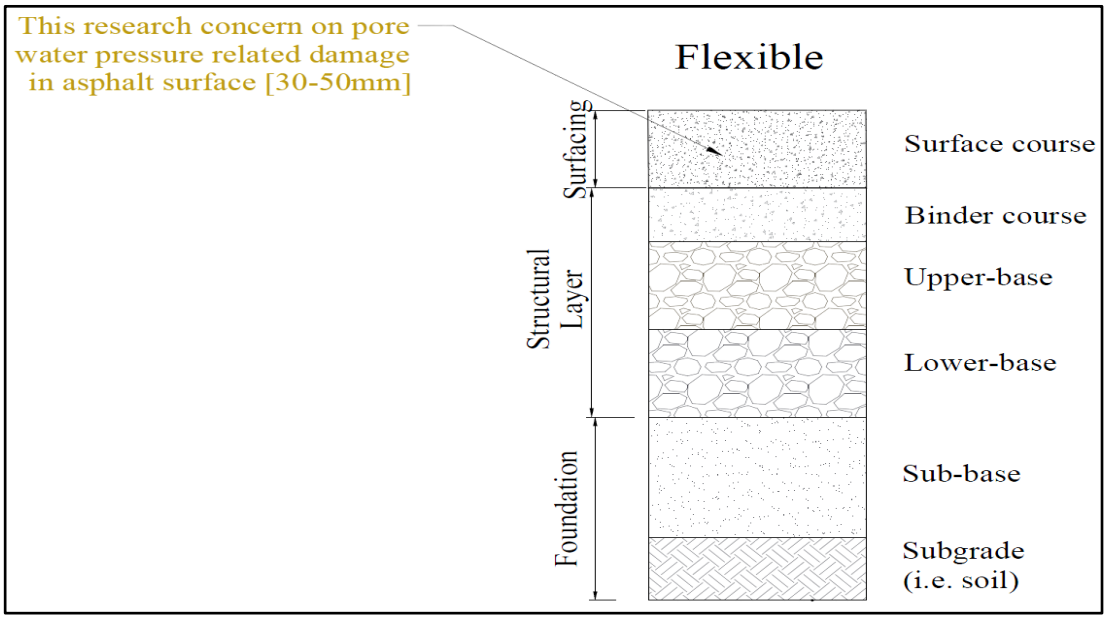

Figure 2.1 Typical pavement type using in highways (adopted from Tom, 2008)

2.1.3 Asphalt Mixture Type

Depending on the manufacturing process, asphalt mixtures are classified into two types, Hot Mix Asphalt (HMA) and cold mix asphalt (CMA). In HMA, materials are usually heated at approximately 150 to 160 C° and poured over the surface. On the other hand, the cold mix asphalt does not require any heating. Both HMA and cold mix asphalt can be designed for different gradation suitable for specific traffic and environmental conditions. There are three main types of gradations to design different types of asphalt mixtures. These are 1) gap graded asphalt 2) dense graded asphalt and 3) open graded asphalt. Figure 2.2 shows the typical gradations and the four types of asphalt surfaces such as Hot Rolled Asphalt, Porous Asphalt, Stone Matich Asphalt and Asphalt Concrete by utilising these three gradations.

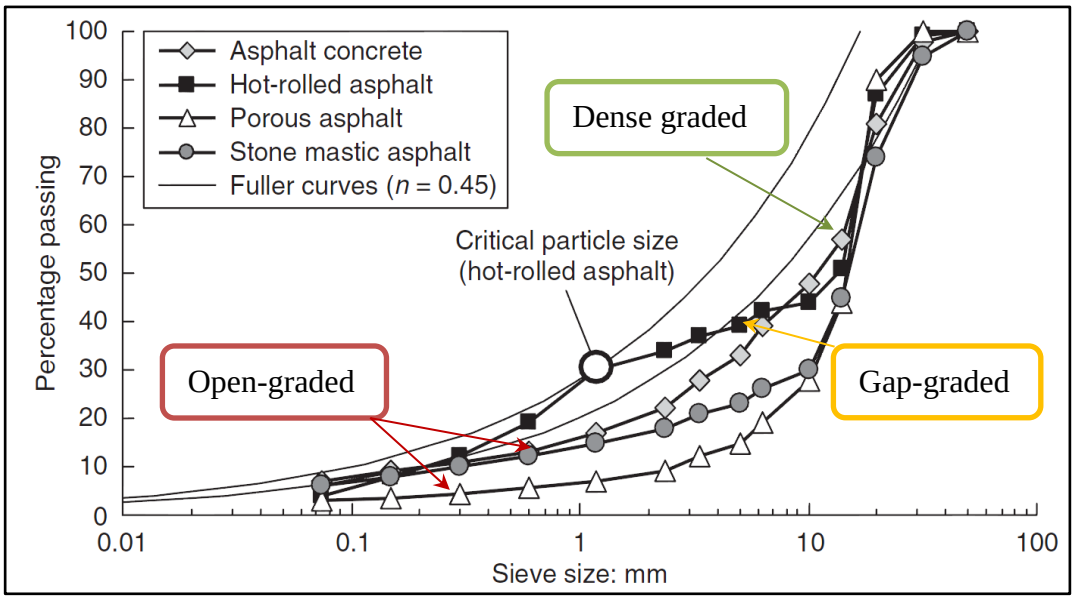

Figure 2.2 Aggregate gradations in asphalt mixtures (adopted from Thom, 2008)

- **Gap-graded Mixture**

In the gap-graded mixture, the particle size distribution is not continuous (Figure 2.3), and sizes of coarse aggregates are usually uniform. Thus, the high void content filled with sand, filler and bitumen. Depending on the required binder content, the gap-

graded mixture classified into mastic asphalt and hot rolled asphalt (HRA). The structural strength of gap-graded mixtures comes from bitumen and filler.

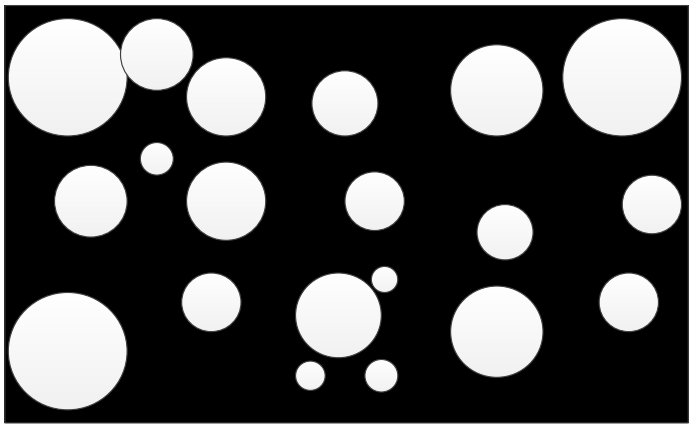

Figure 2.3 Conventional structure of HRA

- **Open graded Mixture**

An open-graded HMA mixture is designed to be water permeable. This study considered two ranges of used of open graded mixture open stone mastic asphalt and porous asphalt. Stone mastic asphalt (SMA) is an open-graded bituminous mixture with high contents of stone, filler and bitumen. The essential elements of mixture design include the formation of an interlocking stone skeleton that delivers high resistance to deformation. There are many additives to improve the characteristics of SMA. Typical applications in Europe have included heavily trafficked roads, airport taxiways and runways, bridge deck surfacing, container storage areas and bus stops. Figure 2.4 shows the conventional structure of stone mastic asphalt. SMA can be laid as thin as 20 mm, but 40 mm is generally the preferred thickness to serve more from the influence of the stone structure on performance. Typically, the property of SMA is the 11-micron film; the texture depth is mm based on a nominal size of aggregate and voids content ranges from 8-12% (BS EN 13108-5, 2016).

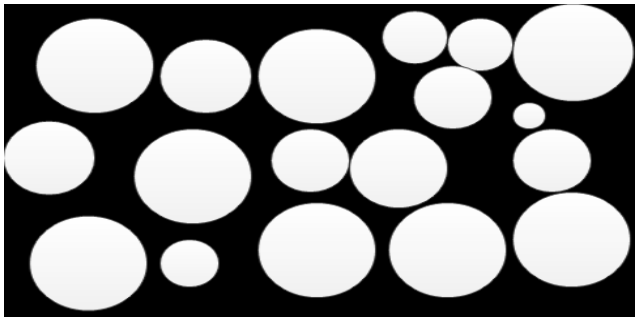

Figure 2.4 Conventional structure of OPEN SMA

Porous asphalt is also classified as open grades mixture. Due to the open-graded nature of the aggregates, they have higher voids content than traditional asphalt mixtures, which are approximately 15% to 25 % (Ongel, Harvey and Kohler, 2007). It contains relatively high and interconnected air voids after compaction which is permeable to water (Hamzah,2012). Sloping sites do create significant design issues; therefore, porous asphalt should not exceed 6% slopes (Palmer, 2013). Roadways do not require to be crowned, mainly if there is a longitudinal slope or free draining soils. Minimum air voids is normally 16% and maximum is 20% (Hamzah,2012). In the UK specifications, it is recommended that the binder should be either 100 or 200 penetration grades (Nielsen, 2006). It is interesting to perceive that as of 2006, in England, porous asphalt is not advised as a surface course material for new or old pavement. The principal cause was the premature failures noted in some schemes and its high cost (Nikolaides, 2014). Figure 2.5 shows the structure of porous asphalt.

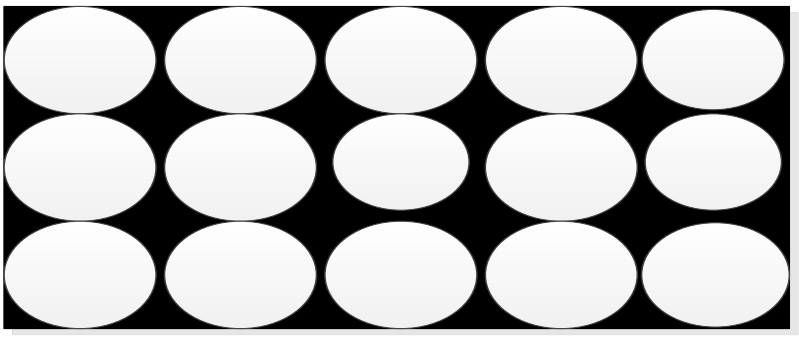

Figure 2.5 Conventional structure of Porous

- **Dense-graded Mixture**

A dense-graded mix is a well-graded distribution of aggregate particles from coarse to fine. Dense HMA mixture comprises aggregates and bitumen binder. Accurately designed and constructed mixtures are comparatively impermeable. Figure 2.6 shows the structure of dense-graded mixture.

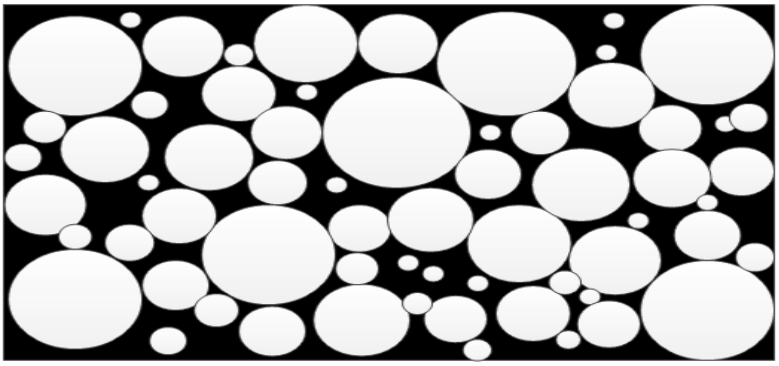

Figure 2.6 Conventional structure of dense graded mixture

Table 2.1 presents three the types of asphalt in term of mix type, aggregate gradation and each possible application in pavement structure based on The Manual of Contract Documents for Highway Works (DMRB, 2006) and specification to produce each category based on BE EN. In this research, the first three types are used as they are the most commonly used surfacing type material.

Table 2.1 Required layers for types of pavement bsed on DRMB and BS EN

Mixture Type	Specification of product	Use		
		Surface	Binder curse	base
Stone Mastic Asphalt	13108-5, 2016	✓	✓	
Hot Rolled Asphalt	13108-4, 2016	✓	✓	✓
Porous	13108-7, 2016	✓		
AC (Asphalt Concrete) thin layers.	13108-2, 2016	✓		

Table 2.2 provides the information regarding gradation type, nominal aggregate mixture, void contents, traffic loading, application and texture depth, aggregate size, and the benefit and limitations of each pavement type. This table based on review of information from BS EN 13108-5, 2016; BS EN 13108-4, 2016;. BS EN 13108-7, 2016; BS EN 13108-2, 2016 and Nikolaides, 2014.

Table 2.2 Pavement types' characteristic

Mixture Type	*Gradation*		*voids %*	*Traffic*	*Uses*	*Texture depth*	*Comments*
Stone mastic asphalt (SMA)	Open-graded	6, 10 and 14	8-12	Heavily trafficked roads were good deformation resistance is required;	Surface course, also a variation in mix design has seen it more frequently used on driveways, yards and house fronts.	1.2 - 1.4	Advantages: - can be produced and compacted with the same plant - surfacing may reduce reflective cracking from underlying cracked pavements due to its flexible mastic - durability (longer in-service life) Disadvantages: the increased material cost associated with high bitumen and filler content - increased mixing time and time is taken to add extra filler may result in reduced productivity - potential delays in openings (the road) as SMA should be cooled to 40°C to limit early flushing of the binder to the asphalt surface.
Hot Rolled Asphalt (HRA)	Gap-graded	10, 14 ,6	4-6	Motorways, National Routes and other heavily trafficked roads	Surface course (30/14F, 30/10F)*, base. Use of ramp and regulating with aggregate size 2, 10, 14 concerning layer thickness. Used in base	1.5	Advantages: -Waterproof – protects underlying layers - Flexible under foundation movement - Lasts a long time under low stress - Resistant to erosion. Disadvantages: -deforms under load and temperature - Needs extra width to lay - Requires the skill to lay - Noisy
Porous (PA)	Open-graded	14 and 20	16-20**	Motorway in the Netherlands	Surface course	1.5	Advantages: The use of PA prevented ponding water on road surfacing during heavy precipitation, so eliminating splash and spray and hydroplaning potential -noise reduction appears more appropriate in whole life value. Disadvantages: The major problem associated with PA is its short service life due to ravelling and cost more to repair. -loss permeability due to bitumen flow.

Asphalt Concrete for Very Thin Layers (AC)	Open-graded	11.2	3-5	Heavy traffic load and aircraft load, United States	Surface course	1.2-1.4	Advantages: They seem to be cost effective, fast to build and may have good surface properties. -Reduced traffic noise levels. -Increased traffic safety. Disadvantages:

*****Used in this research

** In practice PA cannot stand if void percentage exceeds 20%, although in recommending it gives a higher percentage of void contents.

2.1.4 Pavement Distress

Road structures are classified into three main types as previously mentioned, and each has several specific failure mechanisms. According to Kennedy, Roberts and Rauhut, (1979) the primary failures are:

- Fatigue cracking for all types of pavements,
- Permanent deformation (longitudinal rutting) for flexible and composite,
- Low-temperature cracking for flexible pavements,
- Reflection cracking for composite pavements and
- Faulting, spalling, low-temperature and shrinkage cracking, blow-ups, punch outs and steel rupture for rigid pavements, depending on their structural category

2.1.5 Description of Different Distresses

Based on the specific pavement failure in section 2.1.4, pavement deteriorates with time as result of one or more causes such as traffic loading, material ageing, environmental effects, construction inadequacy, design insufficiency, etc. To evaluate pavement surface condition at a particular time, pavement condition surveys are regularly conducted. Condition surveys generally provide different distress data such as deterioration types, severity, extent and location. Figure 2.7 shows all distress types in the pavement. Flexible pavement, distresses can be classified into five groups (Fwa, 2006):

- Surface deformation.
- Surface defects.
- Pothole and patches
- Cracks
- Miscellaneous distresses.

Figure 2.7 Destress types in pavement

- **Surface Defects**

Surface deteriorations are associated with the pavement surface and most of the time does not indicate structural distress in the asphalt pavement layers. They have a substantial influence on skid resistance and serviceability. The most common types of a surface defect in the flexible pavement are ravelling, polished aggregate and bleeding (Nikolaides, 2014; Fwa, 2006; Miller and Bellinger, 2003; Shahin and Walther, 1990).

- **Patching and Pothole**

A patch is a portion of the original pavement that has been cut off and replaced with new material to repair an insufficiency of serviceability or structural capacity in the pavement. A pothole is a shallow or deep hole in the pavement surface formed from a loss of surface or base course material (Nikolaides, 2014; Fwa, 2006; Miller and Bellinger, 2003; Shahin and Walther, 1990).

- **Cracking**

Cracks are fractures on the pavement surface in several modes; the range is from single cracks to interconnected patterns. Crack formation is of two types in asphalt layers, namely, top–down and bottom–up cracking. Top-down cracks (TDC) are longitudinal and transverse cracks initiating start at pavement surfaces and propagate downwards and outwards (Baladi et al., 2003). Savasdisant et al. (2002) reported that top-down cracking is a result of high tensile stresses because of traffic loading, temperature gradients, binder ageing and construction quality (material compaction and paving). Summary of pavement deficiencies is given in Table 2.3

i. Alligator Crack

An alligator crack is also termed as a crocodile /or fatigue crack. In addition, it is a single crack or/ a series of interconnected cracks (Fwa, 2006). It frequently initiates in the wheel path as longitudinal cracking and ends up as alligator cracking after severe distress.

ii. Block Cracking

Block cracking is where interconnected cracks split the pavement surface into roughly rectangular blocks (Nikolaides, 2014; Fwa, 2006; Miller and Bellinger, 2003; Shahin and Walther, 1990).

iii. Longitudinal and Transverse Cracks

They are one or more cracks parallel to the asphalt pavement's centreline, while transverse cracks are mostly vertical to the pavement's centreline (Nikolaides, 2014; Fwa, 2006; Miller and Bellinger, 2003; Shahin and Walther, 1990).

iv. Edge Cracking

Edge cracks are crescent-shaped cracks or continuous cracks that form just on unpaved shoulders (Nikolaides, 2015; Miller and Bellinger, 2003; Shahin and Walther, 1990).

v. Joint Reflection Cracking

Joint reflection cracks are distressed in asphalt concrete overlay surfaces which occur over joints in concrete slabs (Nikolaides, 2014; Miller and Bellinger, 2003; Shahin and Walther, 1990).

- **Surface Deformation**

This will be explained it in section 2.1.6.2 as part of mechanical properties of the asphalt surface.

Table 2.3 presents different type of distresses and possible cause behind them. The unit used to quantify each category are based on distress identification manual for the long-term pavement performance program (Miller and Bellinger, 2003). In addition, Table 2.4 explains in detail the severity level of each distress has summary from (Nikolaides, 2014; Fwa, 2006; Miller and Bellinger, 2003; Shahin and Walther, 1990).). The visual observation has been believed to be very important in level severity evaluation.

Table 2.3 Summaries of pavement surface defects (Nikolaides, 2014; Fwa, 2006; Miller and Bellinger, 2003).

Distress group	Distress type	Possible causes	Measure unit
Cracking	Alligator Cracking	Poor drainage, poor mix design, subgrade failure	m^2
	Block Cracking	Daily temperature cycling, asphalt pavement shrinkage	m^2
	Longitudinal	Natural causes or traffic loading	Not Measured
	Transverse	Surface shrinkage induced by low temperatures, hardening of the asphalt	m
	Edge Cracking	Frost-weakened base/or subgrade near the pavement edge, Traffic loading	m
	Joint Reflection Cracking	Thermal- or moisture- caused movement of the concrete slab beneath the asphalt pavement surface	n/a
Potholes	Potholes	Loss of material of surface/or base course	Number
Surface deformation	Rutting	High moisture content, poor compaction, inadequate surface thickness	mm
	Shoving	Braking or accelerating vehicles	Number, m^2
Surface defects	Bleeding	Excess bituminous material	m^2
	Ravelling and Pitting	Oxidized asphalt binder, ageing, poor compaction, letting the mix get cold when paving, overheating the mix during manufacture, dirty aggregate.	m^2
	Polished aggregate	Aggregate is susceptible to abrasion, subject to excessive studded tyre wear.	m^2
Miscellaneous Distress	Lane to shoulder drop-off	Erosion and settlement in the shoulder	Not measured
	Bleeding (or Flushing) and pumping	The high percentage of fine in the mix is very low void, an excess bituminous material in asphalt surface.	Number, m^2

Table 2.4 Destress severity levels in pavement (Nikolaides, 2014; Fwa, 2006; Miller and Bellinger, 2003; Shahin and Walther, 1990).

Distress group	Distress type	Severity level		
		Low	Moderate	High
Cracking	Alligator Cracking	A few joined cracks; cracks are not spalled or sealed.	Interconnected cracks; a complete pattern; cracks may be slightly spalled; cracks may be sealed.	Severely spalled interconnected cracks, a complete pattern; pieces may move when subjected to traffic; cracks may be sealed.
	Block Cracking	Mean cracks is ≤ 6 mm	Mean cracks is > 6 mm and ≤ 19 mm;	Mean cracks is > 19 mm.
	Longitudinal			
	Joint Reflection Cracking			
	Transverse			
	Edge Cracking	Cracks, no breakup or loss of material	Cracks and breakup and loss of material ≤10 % of the length of the affected portion.	Cracks with considerable breakup and loss of material ≥10% of the length of the affected section
Potholes	Potholes	< 25 mm deep.	25 mm to 50 mm deep.	> 50 mm deep.

2.1.6 Mechanical Properties of Asphalt Mixture

Two material characteristics are crucial in the analysis of procedures for the design of pavements. The first characteristic is the load deformation or stress-strain characteristic, which is employed during the computation of stress and strain in pavement structures. This characteristic includes the elastic stiffens and Poisson`s ratio of the materials. The second characteristic is material performance influencing mode of failure. The two main structural distress modes for the pavement layers are the fatigue cracking in bound layers and permanent deformation in bound and unbound layers.

2.1.6.1 Stiffness

The performance of bitumen layers can be assessed by using the stiffness of an asphalt mixture as an indicator. The elastic stiffness of the asphalt mixture indicates its capability to protect underlying layers and its capability of distributing wheel loading and influencing traffic-induced stress and strains. The stiffness of bituminous material can be used in the calculation of required layer thickness in pavement design. The stiffness parameter is generally evaluated as the ratio between the maximum stress and maximum strain.

2.1.6.2 Permanent Deformation

Permanent deformation, whether consolidated (primary) or instability (secondary) is characterised by the longitudinal surface depression within the wheel path and may have associated transverse displacement, decreasing serviceability and safety of a flexible pavement. Rutting can be the result of the permanent reduction in volume (consolidation/traffic densification), permanent movement of the material at constant volume (plastic deformation/shear) or a combination of both (Roque et al., 2004). Bituminous mixture is a time, temperature and stress-dependent material, which, when exposed to repeated loading exhibits elastic/ plastic/visco-elastic/plastic responses. It is measured in square feet or square metres of the affected area (Nikolaides, 2014; Fwa, 2006; Miller and Bellinger, 2003; Shahin and Walther, 1990).

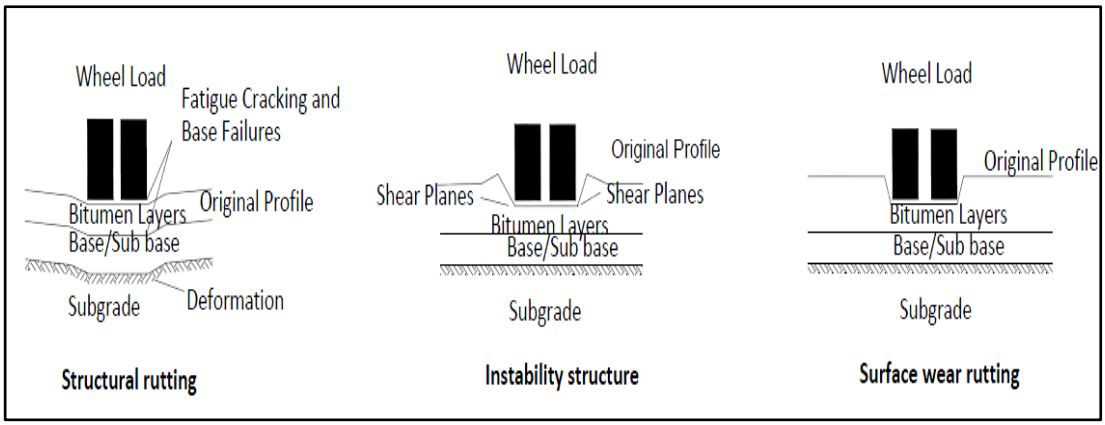

Figure 2.8 Type of rutting in asphalt pavement (Nguyen and Le, 2016)

Figure 2.8 shows three main type of rutting in asphalt surface (Nikolaides, 2014; Nguyen and Le, 2016) as below:

Structural Rutting: The structural rutting affects all pavement layers and foundation. This type of distress is related to inadequate pavement design and construction, weak subgrades, poor drainage combined with heavy traffic loading.

Instability Structure: The instability structural rutting modes only in asphalt layers and is connected to the mechanical properties of asphalt mixture, air voids content and mixture resistance to rutting. Weak asphalt layers (weak aggregate structure, excessive bituminous, moisture damage) are potential causes due to its low shearing capacity

Surface Wear Rutting: The surface course rutting modes confined within the asphalt top layer, which is caused by progressive loss of coated aggregate particles from the pavement surface due to combined impact of environment and traffic loading (see Figure 2.8).

2.1.6.3 Cracking

Cracking is one of the most critical concerns that can influence pavement condition and performance through its operation life. This problem is usually considered as essential for old pavements that as a result of renewed by laying new asphalt overlay, but undesirable cracking can likewise happen in relatively new pavements that include stiff, rigid base courses, such as aggregates, or soils bound with hydraulic binders. It

should be indicated that the issue of cracking susceptibility of asphalt mixtures also affects the fundamental pavement characteristics, such as fatigue life and ageing-related performance. Even new pavements, which can be structurally and long-lasting, if built with asphalt mixtures that are stiff and susceptible to cracking lead to premature deterioration, usually earlier than predicted.

2.1.7 Moisture Damage in Asphalt Pavement

The primary cause of repeated pavement maintenance operations is moisture damage. High-performance asphalt is an essential investment for any country. Moisture damage can destroy cohesive bonds inside an asphalt binder and/or adhesive bonds between aggregates and binders. The primary objective of designing asphalt mixtures is the elimination of the origin or source of moisture damage (Kakar, Hamzah and Valentin, 2015), which has been considered a primary cause of deterioration in asphalt pavements since the 1900s (Cui, 2010). Vehicle movement produces stress that decreases the inner strength of hot mix asphalt and may result in initial rutting, fatigue cracking, ravelling and pothole in this layer (Kok and Yilmaz, 2009).

If distress occurs one or two years after a road is opened to traffic movement (Kandhal, 1994) and is mainly attributed to moisture damage (Cui et al., 2009). Moisture damage can be defined as the loss of strength and durability of an asphalt mixture owing to the effects of moisture (Little and Jones, 2003). Such damage in asphalt pavements is a complicated subject that has been the focus of several studies for six decades (Solaimanian et al., 2003; Miller and Bellinger, 2003).

2.1.7.1 Impact of the Moisture in Asphalt Pavement

Water plays a crucial role in the severity and expansion of distress on pavements, but it does typically does not initiate cracking, permanent deformation and ravelling (Kakar, Hamzah and Valentin, 2015). Moisture-related damage does not occur without the presence of water and traffic. Figure 2.9 shows the potential route of moisture in asphalt pavement. Moisture in an asphalt pavement comes from internal and external sources. Inadequate drying of aggregates used in asphalt mixes can be a conventional internal source of moisture (Santucci, 2002). Technologies used for warm mixes

produce moisture in the form of steam generated when water contacts hot bitumen (Read and Whiteoak, 2003). Meanwhile, moisture is also caused from three different sources. Moisture entering the pavement from the surface result poor drainage, poor construction (compaction) or mixture design having high air void content and increased permeability. Moisture entering from the sides is a result of poorly constructed shoulders and poor side drainage. Moisture coming from beneath the subgrade is a result of the high-water table and poor drainage characteristics of base and sub-base materials as mentioned in chapter one.

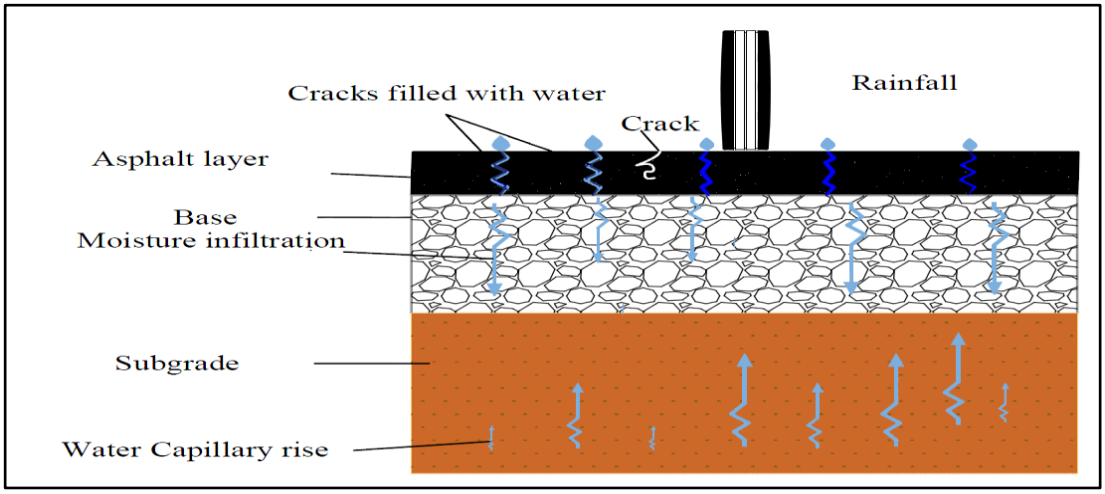

Figure 2.9 Recourse of moisture in asphalt pavement (adopted from Zornberg et al., 2017)

2.1.7.2 Mechanisms of Moisture Damage

Several contributing mechanisms are associated with moisture damage, namely, pore pressure, hydraulic scour, spontaneous emulsification, sequences of the environment upon the asphalt-aggregate system and detachment (Yilmaz and Sargin, 2012). A brief overview of various moisture damage mechanism is given below;

- Detachment is the microscopic separation of bitumen (bitumen-filler mastic) films from the aggregate surface owing to the presence of thin films of water or moisture without an apparent break in the bitumen films. The thin films of water or moisture probably result from either aggregate that is not completely

dry or interstitial pore water or moisture, which vaporises and condenses on the aggregate surface (Johnson and Freeman, 2002).

- Displacement occurs when the bitumen films are removed from the aggregate surface with water or moisture. Compared with the detachment, displacement occurs because of the intrusion of water or moisture in the aggregate surface through breaks of the bitumen films.
- Spontaneous Emulsification is inverted emulsion of water or moisture in the bitumen phase. As reported by (Fromm, 1974), an inverted emulsion of water or moisture in bitumen phase causes bituminous particles to separate from one another (cohesive failure) and ultimately leads to adhesive failure.
- Hydraulic Scouring is caused by capillary tension and compression around moving traffic on a wet pavement surface. Dust mixed with water or moisture during traffic enhances the abrasion of bitumen films from the aggregates.
- Water Pressure, this research based on the concept of pore water pressure in asphalt surface.

2.1.7.3 Influence of Air Voids on Moisture Damage of Asphalt Pavement

Moisture transport is influenced significantly by the air void structure in asphalt concrete (Caro et al., 2008); the air void in asphalt mixtures categories into three types effective, semi effective and improbable as shown in Figure 2.10 (Chen et al., 2004). Stripping and loss of cohesion result from water penetrating through the cracks of asphalt concrete (Chen, Lin and Young, 2004). The influence of cracks in asphalt allied with moisture damage is significant; the air void content increases owing to cracks, so permeability in an asphalt mixture is increased because water infiltrates through voids and cracks; these interactions may lead to weak and saturated asphalt (Chen, Lin and Young, 2004).

Several studies showed that asphalt pavements commonly have an anisotropic and a heterogeneous internal pore structure, which directly affects the degree of permeability in various directions (Kutay and Aydilek, 2007; Hunter and Airey, 2005; Masad et al., 2004; Masad et al., 1999). The effects of another condition, that is, increased flow-induced pore pressure at the pore–solid interfaces, on moisture damage

affecting the textures of asphalt pore structures remain are not advanced. Critical pore pressures values can be significant and must be investigated for the precise evaluation of directional flows in asphalt surfaces (Kutay and Aydilek, 2009).

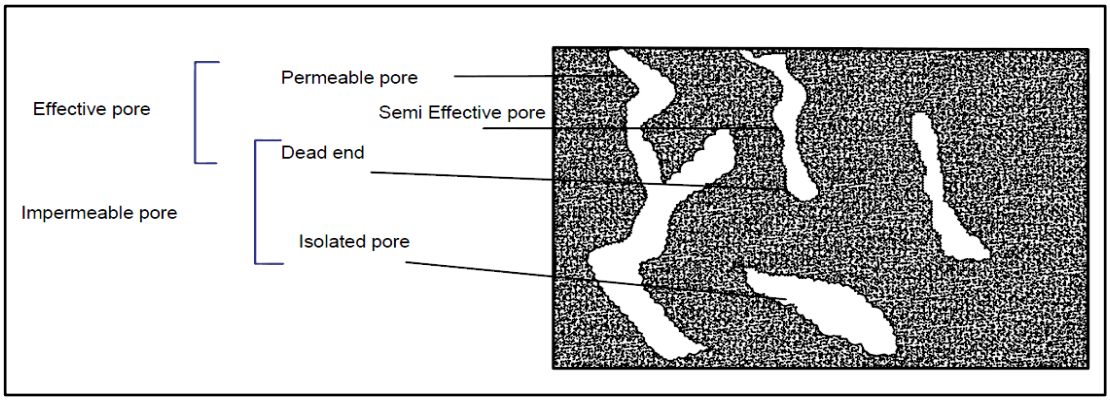

Figure 2.10 Three different types of void (Chen et al., 2004)

2.1.7.3.1 Permeability

Permeability is correlated to the air void, the interconnection of air voids and pore structure. The external pressure also influences the permeability. Chen et al. (2004) found that the relationship between permeability and air void is exponential. As bitumen content was increased, the effective air void content was reduced, so reducing permeability. They also categorised the air voids regarding the permeability (k) as shown in Table 2.5.

Table 2.5 Classification of Voids in Terms of Permeability (Chen et al, 2004)

K (cm/s)	Preamble condition	Void	Mixture type
$\leq 10^{-4}$	Impervious	Impermeable	Dense
10^{-4}- 10^{-2}	Poor drainage	Semi effective	Stone mastic asphalt
$\geq 10^{-2}$	Good drainage	Effective	Porous

Table 2.5 is related to Figure 2.9 and summarises the relationship between air voids and permeability. It is impossible to study the permeability without counting the air voids range and its complication. Castelblanco (2004) found that the moisture damage would be increased if the percentage of air voids is between 7 and 13%.

Each mixture type has a unique voids-permeability relationship. The relationship between the air voids and permeability may be referred to density as well. Low density in asphalt mixture is caused by bad compactions and can lead to oxidation, water damage and crack (Hainin et al., 2013). The gradation is also another factor that determines the permeability of asphalt mixtures as mentioned previously. According to previous studies, the permeability is higher with coarsely graded mixes together with larger aggregate size and the large aggregates with lack of fine aggregates to fill the voids leads to high permeability (Hainin et al., 2013). The study by Mallick et al. (2003) demonstrated that mixes with different gradations and nominal maximum aggregate size have the significant increase in permeability to varying voids in total mix content. The relationship between the water infiltration rate and water pressure exhibits a roughly linear curve (Gao, Guo and Liu, 2015). The permeability of asphalt mixture which is typically considered as impermeable possibly significantly increased and up to 1241.2 ml/min if the vehicle transport with high speed. Excessive water will penetrate deep into the pavement and be deposited on the base, which could directly cause the moisture deterioration in asphalt pavement (Gao, Guo and Liu, 2015).

2.1.8 Examination of Moisture Sensitivity

The durability of an asphalt pavement degrades over time owing to age and moisture exposure. Many laboratory tests have been conducted for the quantification of moisture sensitivity in asphalt mixtures. These tests are mainly aimed at preventing the premature failure of road pavements based on bitumen aggregate adhesion characteristics.

Testing techniques for the assessment of moisture sensitivity are conducted either on loose coated aggregates or compacted aggregates. Tests on compacted asphalt mixtures such as Immersion mechanical tests, Marshall stability test (AASHTO T245), Lottman test, Texas freeze–thaw pedestal test, Immersion compression test (AASHTO T165, ASTM D1075), Duriez test (NFP 98-251-1), Tunnicliff and Root procedure, Modified Lottman procedure (AASHTO T283), LINK bitutest water sensitivity protocol, Immersion wheel tracking tests and Hamburg wheel tracking. While the Tests on Loose Coated Aggregate such as Static immersion tests (AASHTO Tl82, ASTM Dl664), Rolling bottle method, Dynamic immersion test, Chemical

immersion test (by use of sodium carbonate), Ultrasonic method, Boiling water stripping test, Ancona stripping test, Net adsorption test (SHRP, MOOl) and Modified net adsorption test (Ahmad, 2011)..

Different conditioning procedures are employed for the simulation of field exposure conditions, and conditioned specimens are inspected visually or mechanically for moisture sensitivity assessment (Ahmad, 2011).

It has been apparent that water has a significant impact on asphalt surface performance. The next part will explain in more details the interaction between the traffic- tyre-water –asphalt surface.

Part 2: Interaction between Traffic Loading-Tyre-Water-Pavement

2.2 Introduction

In asphalt pavement, the water pressure is dependent on tyre characteristics (tyre pressure, tread shape, depth, and patterns), traffic characteristics (magnitude, speed) as well as mixture configurations such as size and gradation of aggregate, voids content and level of compaction (Vaiana et al, 2012). For example, in dense and close graded surface course (voids less 4%), the water infiltration is relatively low and slow, whereas water drains freely in high void content mixtures such as in porous asphalt. Uniformly graded mix with intermediate void content, 6%-12%, may experience water infiltration and water storage within the mixture (Sonebi,2016). Besides, water may also pass through cracks or blocked interconnected voids caused by debris and creates the capillary force at the interface when subjected traffic, which may eventually be damaging to interlinked bonds by adhesion failure (Apul et al., 2002). In concrete pavement, water infiltration through crack/joints can lead to water pressure generated at the bottom of the slab when traffic passes through the water-filled crack/joint. This can potentially lead to under slab voiding and poor load transfer efficiency of the joints/crack (Rahman et al., 2011). This part provides a brief review of the tyre properties, a review of relevant literature on how water infiltrates in the pavement and finally review on the tyre - water -pavement interaction.

2.2.1 Tyre

A tyre is composed of rubber and steel reinforcement serves three essential functions (Gillespie, 1992).

- Supports the vertical load wheel cushioning against road shock, and this characteristic is a crucial advantage of the pneumatic tyre.
- Develops longitudinal forces of acceleration and braking capability of vehicles to start, stop and turn corners as consequences from friction between the road and the tyres.
- Enables the directional change of the vehicle and develops lateral forces for braking.

The primary function of a tyre is to provide an interface between a vehicle and road. The contact area of rubber for all four tyres for a typical mid-size vehicle is less than that of a 215.9mm x 279.4mm sheet of paper (Gent and Walter, 2006).

A tyre is a simple visco-elastic toroid with modern refinement and optimised properties. Regarding the mechanical structure, the elastic torus of a tyre is composed of a flexible carcase of high-tensile strength cords fastened to steel cable beads that firmly anchor the assembly to the rim. The internal (inflation) pressure stresses the structure in such a way that any external force is causing deformation in the carcase results in a tyre reaction force. The behavioural characteristics of the tyre depend not only on the operating conditions but also on the type of construction (Gillespie, 1992).

2.2.2 Tyre Construction

Tyre is carefully constructed using a series of various processes and up to 200 raw materials (kwikfit, 2018). When design tyre there is seven key components as shown in Figure 2.11 and Table 2.6 give a brief description of a function in each element of the tyre (Goodyear, 2015).

- Ply*:* The ply is the layer of fabric that constitutes the skeleton of a tyre and is classically made of interwoven fibre cords coated with rubber.
- Belt Steel: belts reinforce the strength and contribute the rigidity of tyres.

- Shoulder: The tyre has a small bevelled edge where the tread meets the sidewall.
- Sipe and Groove: The tread blocks are divided by the deep grooves that allow the tyre to disperse water, snow and mud.
- Beads: The beads, created from high-strength braided steel coated in rubber, produce an airtight seal between the tyre and the rim
- Sidewall: The sidewall is the area of extra-thick rubber that runs from the bead to the tread and gives the tyre lateral stability.
- Rib: The middle of the tyre is the weak part. Therefore, some brands have a rib that runs down the centre, serving as reinforcements.

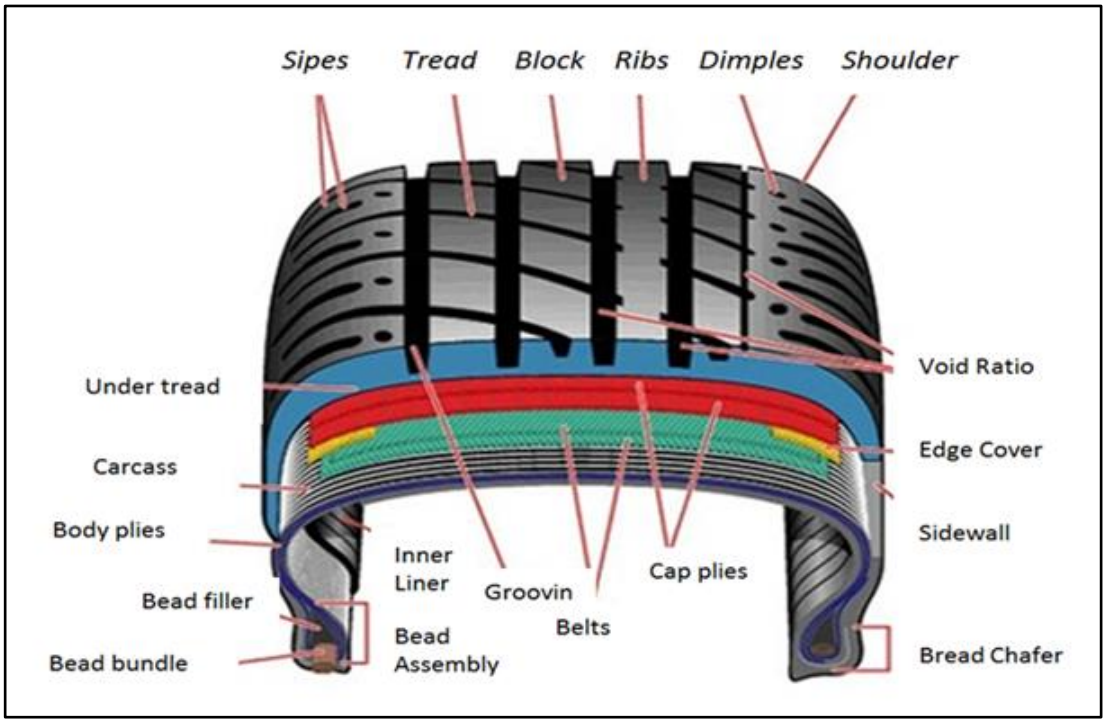

Figure 2.11 Tyre structure (Goodyear, 2015)

Table 2.6 Tyre function and description (Goodyear, 2015)

Tyre component	*Description*	*Function*
Ply	A Layer of fabric that constitutes the skeleton of a tyre and is classically made of interwoven fibre cords coated with rubber	Providing strength
Belt	Made of woven sheets of rubber-coated steel wires.	Steel belts reinforce the strength and contribute the rigidity of tyres.
Shoulder	Occasionally, Kevlar cord is also added for durability, additional strength and puncture resistance	Play significant parts in how the tyre supports taking corners.
Sipes and groove	A small bevelled edge where the tread meets the sidewall.	Sipes build resistance to aquaplaning. Groove to improve the tyre's braking effectiveness and steer ability and prove decisive in the rolling noise level.
Beads	Inner circle of the tyre and connects the tyre to the rim	Demanded to have a balancing effect on vehicle tyres
Sidewall	Sipes is the narrow voids and passageways on the tyre lugs.	Contains all manufacturer information about the tyre.
Rib	Groove are similar to sipes but often much longer and deeper	Serving as reinforcements

2.2.3 Tread Pattern

About 16,000 different tread patterns used in a tyre in 2004, and keep on increasing with time (Hanson, 2004). The tyre tread pattern is aimed as a compromise between grip, handling, ride, noise safety and tyre durability criteria.

The number of ribs and groove spacing influence the way water is eliminated to avoid hydroplaning. Shoulder slot size and orientation can affect traction, handling and water exit paths. The number of pitches and pitch sequence, as well as the placement of tie-bars and sipes, can affect traction, noise, wear and the tendency to wear non-uniformly. Moreover, tread designs must be acceptable aesthetically and must match the perception of the customer about product performance.

Tyres are designed with various kinds of tread, and every pattern indicates different road conditions and driving styles. Tyre treads have four different types (Pep boys, 2016).

- **Asymmetrical Tyre Treads**

This type of pattern used in sports cars because it is capable of maximising grip in wet and dry roads. The exterior of the tyre has large tread blocks, which enables the maximisation of torn capability on dry road surfaces, whereas the interior and middle sections of tyres are useful in wet road surfaces.

- **Symmetrical Tyre Treads**

This type has the same pattern, continuous grooves and/or independent lugs, across the whole tyre. This tyre can rotate in several ways to prolong the service life and increase versatility.

- **Directional (Unidirectional)**

This type is designed to roll in only one direction. It incorporates lateral grooves on both sides of the centreline that point in the same direction and results in V-shaped tread blocks.

The grooves enhance hydroplaning resistance at high speeds by pumping water more efficiently through the tread pattern. Except they are dismounted and remounted on their wheels to accommodate use on the other side of the vehicle, directional tyres are to be used on only one side of the vehicle and are designed to be rotated from the front to the rear axle. If different tyre sizes are used on the front versus rear axle, the tyres become location-specific and prohibit rotation unless remounted (Tirerack, 2016).

- **Directional/Asymmetrical**

Asymmetric and directional tread patterns have V-shaped tread grooves that are offset compared with the centreline of the tyre. Tyre pattern is discharged away from the water from the tyre. Asymmetric and directional tread patterns must be treated as directional tyres for tyre rotation. However, if different tyre sizes are used on the front versus rear axle, they become location-specific and prohibit any tyre rotation possibilities (Tirerack, 2016). Figure 2.12 shows the image of the three tread patterns.

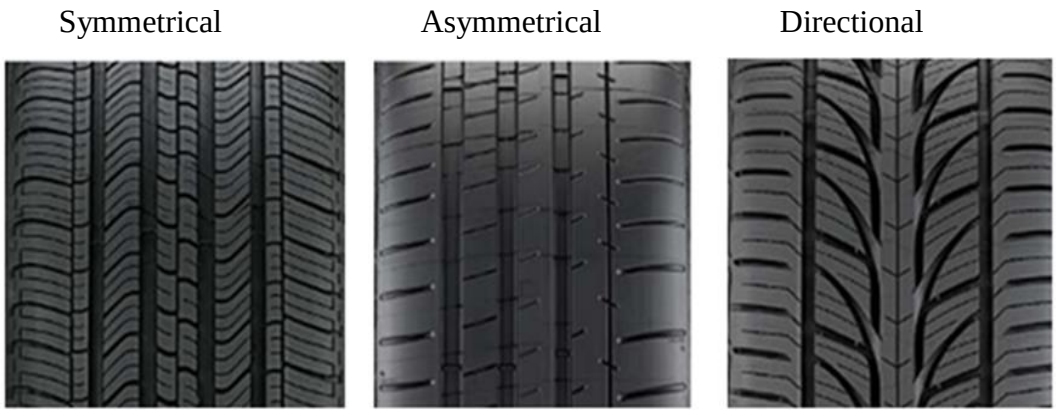

Figure 2.12 Types of tread pattern

2.2.4 Legislation on Tyre Treads Depth

Different legislation requirements have been specified for tyres from vehicle safety because tyres are essential elements of a vehicle. Japan Automobile Tyre Manufacturers Association found that each country has its legislation defining the standards, and the tyres are requested to meet the standards of the country where they are to be used (JATMA, 2011).

Jansen et al., (2014) studied the legislation and recommendation of tread depth are based on questionnaires in some countries such as Croatia, Denmark, Finland, Germany, Greece, Italy, Netherlands, Spain, Poland and Sweden. The results showed a variation of legislation of tread depth for both summer and winter tyres. Tread depth for passenger car tyres, however this study does not include the UK, Japan and USA.

2.2.5 Infiltration of Water into Pavement Structure

Water enters the pavement structure by infiltration via the pavement surface, shoulder, melting ice during freezing-thawing cycles, seasonal changing in the water table and capillary action (Ridgeway, 1982). In the past, it was the general thought that high water table and capillary water are principal reasons of excess water on the asphalt road. The investigations found that surface infiltrated water is the primary reasons for moisture increase in the subgrade (Ridgeway, 1982) Infiltration of water into the asphalt pavement can distress the durability of that asphalt pavement. This, in turn,

increases pore pressure, leading to excessive deflection, cracking, and decrease in load carrying capacity of the asphalt pavement (Lindly and Elsayed, 1995).

The infiltration rate through a pavement for the design is assumed 2.8 $.10^{-3}$ l/s per meter run of crack (Ridgeway, 1976). In the UK, maintenance intervention level of 10 % area cracked was considered by (Baldwin et al., 1997) to equal to a crack length of 0.2 m/m^2. In sequence, this interpreted to an infiltration rate of 2 l/m^2 per hour (Reid et al., 2006).

2.2.6 Concept of Tyre-Water-Pavement Interaction

When water enters the asphalt surface, it creates hydrostatics pressure due to the action of moving vehicles. The magnitude of pressure varies, depending on the surface type, tyre tread depth and presences of existing distresses on the surface (Dawson, 2008). The conceptual illustration of tyre-water-pavement interaction is shown in Figure 2.13.

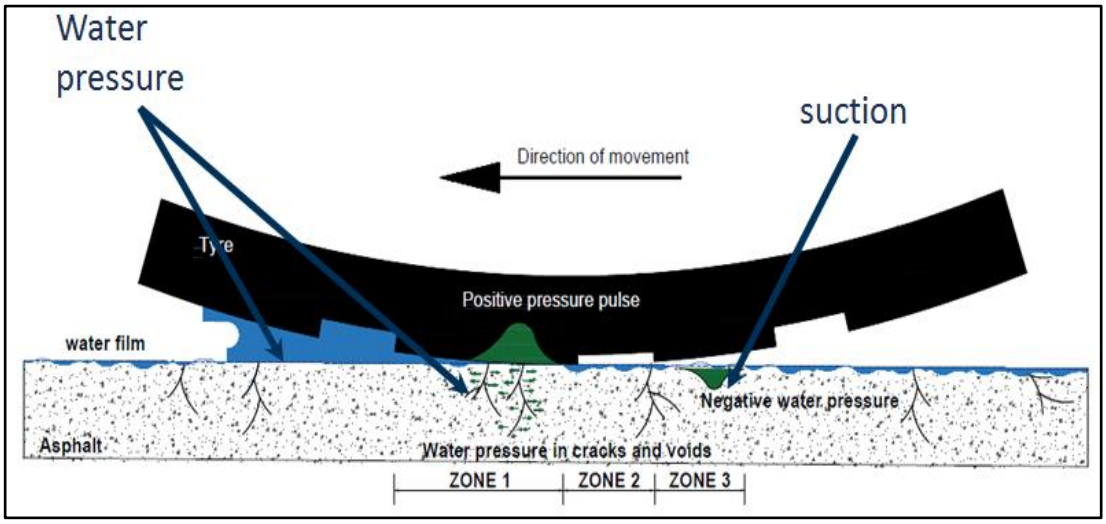

Figure 2.13 Conceptual illustration of tyre-water-pavement interaction (adopted from Heisler, 2002)

The interaction of tyre pavement can be divided into 3 zones when rolling on a wet surface (Cerezo et al. 2014). Zone 1 is the significant part to drain the stagnant water film covering the road surface, and this part depends on the water depth, the speed,

tyre tread depth and the road surface macrotexture. With increasing speed and water depth, it will be more difficult to drain the water from the road surface, thus creating a possible scenario for water infiltration and moisture damage. However, with the help of tread depths, this can be minimized (Dixon,1996). After pass through the zone 1, the remaining water on the surface goes to zone 2, or middle zone and this zone is responsible for the final removal of water, this assisted by sipes and grooves along the contact patch. The squeezing of water on zone 2 will dissipate the remained fluid to all directions; especially to beneath the tread blocks and ribs, and this pressure may cause further infiltration in the pavement. The water film in zone 3 has almost completely been squeezed out, so in this region, the contact between the tyre and pavement start, to happen (Dixon,1996).

The prone zones to develop water infiltration and overpressure on micro voids (Figure 2.13) are one and two because in these areas the amount of water still high and not totally dissipated. Thus, in roads with cracks, the possibility to create moisture damage problems is higher than new roads because of distresses already present on the surface. The water is a relatively difficult fluid to drainage when compared with air for example Dixon (1996). The density of water is approximately 999.2 kg/m³ and viscosity is $1.14x10^{-3}$ Ns/m². Therefore, the water after being squeezed out from the longitudinal channels will be directed sideways to help drainage. Dixon (1996) demonstrates a "drainage" number to explain the problem with water drainage through the tread channels. It is a non-dimensional measure and correlates the cross-sectional area of the channel in front view, divided by the cross-sectional area of the approaching water. According to this, if the number is greater than 1.0, the channels will be sufficient to drain the water; however, if the number is less than 1.0, the tyre will need the help of lateral drainage to provide a good flow of water. The time of the contact of the tyre is extremely important as well, for example, if the car is at in high speed it will be more difficult to drain the water compared with slow speed. According to Dixon (1996) the time that the rubber contacts with the footprint are normally 6 ms at a speed of 30 m/s and the water will be drained in only 2 or 3 ms.

2.2.7 Influence Dynamic Loading on Amplitude of the Pore Water Pressure in Asphalt Surface

Traffic loading is the main input in the road design procedure (other inputs are subgrade strength and temperature). Typically, converting every real traffic load (wheel loads of different magnitudes and repetitions) into an equivalent number of a standard axle loading – ESAL (equivalent 80 kN single axle load) is convenient (Highway Research Board, 1962). Several loading waveforms are employed to simulate traffic loading in the laboratory. Sinusoidal, the most common, approximates the traffic load in the field more realistically. Loading frequency and duration influence the fatigue life; increasing the frequency or decreasing the duration of load pulse increases the stiffness; thus, the fatigue life increases (Read, 1996). The presence of water in bound materials brings danger of accelerated ageing to the bitumen–aggregate bond. Besides, the application of high pressure on the tyre will induce pore water pressure and rapid local flows of water between voids, particularly at the base of a poorly compacted layer, and this effect can wash binder clean off the aggregate (Thom, 2008).

Pore pressure increase as a result of entrapped water can lead to pavement distress. Stresses imparted to the trapped water from repeated traffic load will aggravate the deteriorate since the continued build up in pore pressure rapture the asphalt film from the aggregate surface /or can create the progression of micro-cracks in the asphalt mastic (Little and Jones, 2003).

This project uses cyclic load to provide a more realistic representation of the measured pore pressure in the pavement. The capability of hot mix asphalt to prevent water from entering the pavement structure is one of the critical factors controlling pavement performance (Masad et al., 2004).

Measurement of dynamic water pressure in asphalt surface is a key to improve the resistant of asphalt mixture to water damage (Jiang, Zhang and Li, 2013). Gao et al., (2015) investigated the pore hydraulic pressure in asphalt pavement and its influences on permeability and observed that the pore hydraulic pressure increased with increasing traffic speed. Because of repeated tyre loading in the road surface, the

external pressures on a saturated pavement pore structure are often dynamic (Kutay and Aydilek, 2007).

2.2.7.1 Traffic Speed and Water Pressure

Moisture damage is a complicated process that is determined by material factors, their combinations, construction and external influences such as environment and loading (Gao, Gue and Lui, 2015; Cui, 2010). Pore water is an essential factor for the reason of moisture damage (Cui, 2010; Li and Sheng, 2012). Repetitive of traffic loading generates a high-velocity flow of pore water. Pump suction phenomenon produced by the high flowing velocity of pore water causes moisture damages directly (Lei et al., 2017). Continuation effect of moisture caused weakening of material and traffic load caused mechanical damage that will induce progressive dislodgement of the aggregates. In many cases, this distressing mode become a dominant pattern of failure and a cause for reducing road safety. Consequently, these are great significance to study moisture damage of asphalt pavement (Guo et al., 2017). The same study found that there is a positive correlation between the pressure and the vehicle speed. Repetitive traffic loading might lead to emulsification, shift and peeling of the asphalt film. Besides, the bigger size of the exit slit is the high velocity of the fluid.

Perhaps increase speed leads to reduce the contact area and a load of tyre concentrated on a small area so lead to apply more force in water in a road surface, so influence to force the water to infiltrate into cracks and this lead to more damage as explained before.

2.2.8 Influence of Void in Pore Water Pressure

The effects of pore water pressure occur when air voids in asphalt pavements decrease because of loading, and water in these voids is compressed by water pressure against bitumen films. When pore water pressure increases to a high level, bitumen films on aggregates rupture, enabling water to access the surfaces of the aggregates.

The voids are interconnected and permit water transport throughout the pavement. When an asphalt pavement becomes increasingly dense, the resulting interconnected voids close and trap water. Excessive densification leads to pore collapse and increases

water pressure. Several reasons attributed to the increase in pore pressure include traffic loadings, thermal expansion and freezing expansion (Lottman, 1982). When the asphalt film ruptures, the displacement mechanism then removes the asphalt film (Karlson, 2005).

The pore water pressure can influence the pavement structure even while the asphalt pavement is not thoroughly saturated. The unsaturated voids can generate a capillary tension within the pavement, causing the pore pressure to become negative. On the other hand, once a load is applied to the pavement, the total stress and the pore pressures increase according to the load intensity. In sequence, the effective stresses within the asphalt pavement reduce and cause cyclic of compression and tension within the voids (Karlson, 2005).

The pore pressure mechanism, as the asphalt at the bottom of a pavement layer, is in tension because of the traffic load and is often subjected to prolonged exposure to moisture from water trapped in the granular subbase above the subgrade. The distribution of air voids in compacted field mixtures shows that the top and the bottom of the layer have higher air voids and higher permeability, whereas the middle of the layer has lower air voids and less permeability (Masad et al., 2005). The high permeability parts of the compacted layer are more probable to contain moisture, resulting in pore pressures caused by vehicle loadings. For pavements with a source of moisture beneath the pavement, stripping from the bottom-most permeable part of the asphalt layer is expected (Karlson, 2005).

2.2.9 Previous Studies of Measurement of Pore Water Pressure in Asphalt Surface

Research on pore water pressure in the road surface is limited and disjointed. Some studies calculated and analysed pore water in asphalt pavement by creating numerical simulation models (Kutay and Aydilek, 2007; Li and Deng, 2008; Cui et al., 2009; Li and Sheng, 2012; Guo, Sun and Dai, 2017). Other researchers measured and investigated pore water pressure using experimental work (Jiang, Zhang and Li, 2013; Gao, Guo and Liu, 2015), the rest studied thus using mathematical methods (Li and Deng, 2008; Xiaoyong, 2008).

2.2.9.1 Numerical Simulation Model

Li and Sheng (2012) applied a 2D finite element method built on porous elastic theory to replicate the pore water pressure produced in the base layer of rigid pavement under the vehicle load. They found that the maximum pore pressure is created in the middle depth of the base layer (Li and Sheng, 2012). They assume all the gradients produced by fluid pressure or external force is in the vertical direction, the specific weight of pore fluid is assumed to be 276.8 × 103 N/m^3. For computing results and analysis, the distributed load is around ¼ car`s weight (2500 N), the Young`s modulus of concrete cement materials is 31000 Mpa, and Poisson`s ratio is 0.15, permeability coefficient is 1× $10^{-5}$ cm/s, these are parameters of materials of cement concrete surface while the parameters of base materials are Young's modulus of 2500 Mpa, Poisson`s ratio of 0.25, the permeability of 1× 10^{-3} cm/s. The pore water pressure of this position is investigated to evaluate the base layer performance under different vehicle speeds, the difference between pore water pressure when vehicles speed 10 m/s and 60 m/s is 1.91 kPa. The numerical simulation results indicated that the dissipation time decreases with increasing vehicle speed, 1.04 s at 60 m/s and 1.37 s at 10 m/s. The results also displayed that the high vehicle speed has a high impact on base erosion (Li and Sheng, 2012). Li and Sheng (2012) applied the finite element method built on the porous elastic theory to replicate the pore water pressure produced in the base layer of rigid pavement under the vehicle load. Figure 2:14 and Figure 2.15 shows the computation model of pore water pressure under different vehicle speed and loading area respectively. While Figure 2.16 and Figure 2.17 show the results of pore water pressure under different vehicle speed and dissipations time respectively.

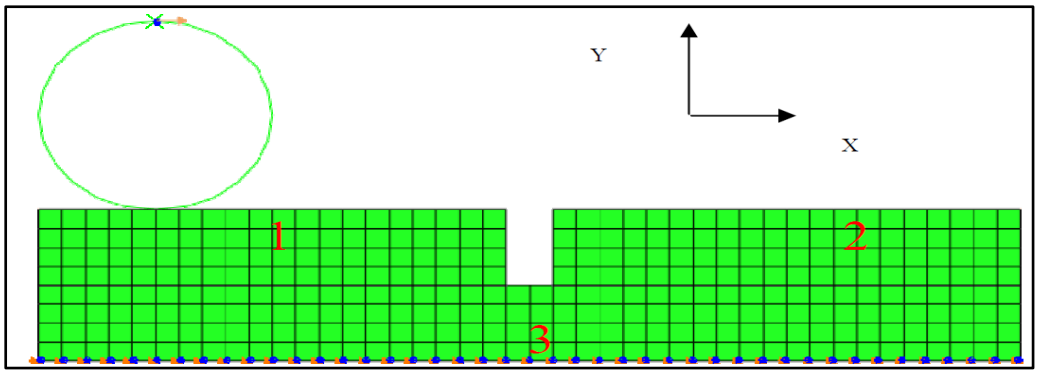

Figure 2.14 Computation model of pore water pressure under different vehicle speed (Li and Sheng, 2012).

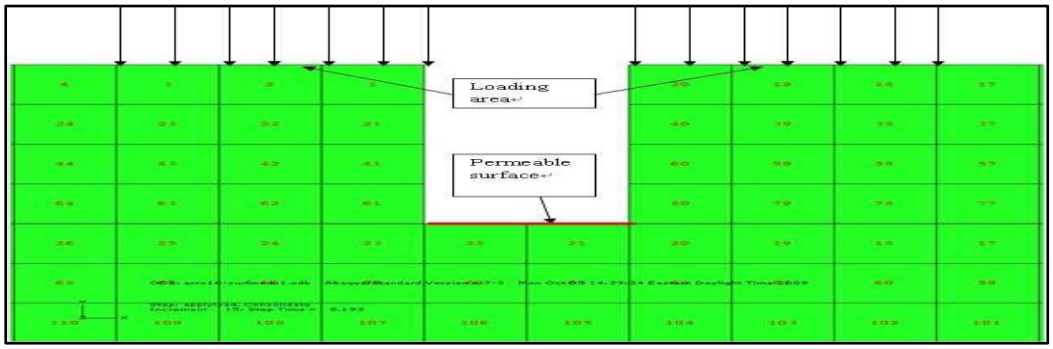

Figure 2.15 Loading area and permeable surface of the base (Li and Sheng, 2012)

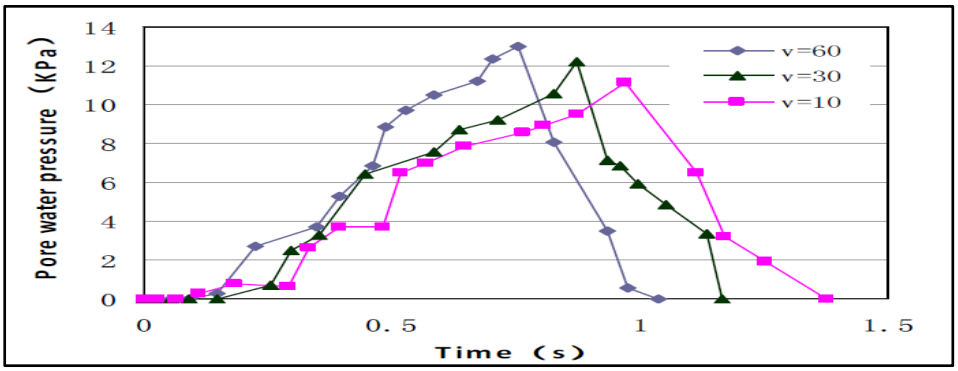

Figure 2.16 Pore water pressure under different vehicle speed at 10 cm depth (Li and Sheng, 2012)

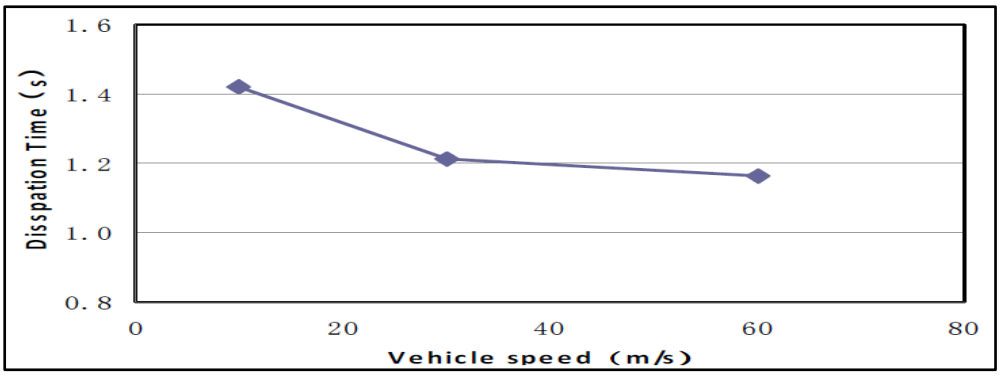

Figure 2.17 Dissipations time of pore water pressure under different vehicle speed (Li and Sheng, 2012)

Other techniques such as the Finite Difference Method (FDM) and the Biot Dynamic Consolidation theory were applied to investigate the dynamic response of the saturated asphalt pavement, and the results demonstrated that the positive pore water pressure under wheel is associated with pumping action. However, the negative pressure refers to the suction in pavement surface where water is sucked cyclically under traffic loading. This suction increases with vehicle speed lead to increasing dynamic pore water pressure (Cui et al., 2009). A three-dimensional fluid flow model was built on Lattice Boltzmann to study the unsteady dynamic fluid flow in asphalt pavements (Kutay and Aydilek, 2007). This study investigated samples with different hydraulic conductivity resulting from aggregate angularities, orientations and fine distribution. Considering, these samples have the same nominal size of aggregate and same compaction energy. It is found that dynamic fluid pressure influences the moisture transport inside the asphalt concrete.

Kutay and Aydilek (2007) performed a three-dimensional fluid flow model built on Lattice Boltzmann to study the unsteady dynamic fluid flow in asphalt pavements. Using X-ray computed tomography imaging technique to create a three-dimensional pore structure of asphalt samples to input it into the numerical model to calculate the dynamic hydraulic conductivities on some asphalt pavement the pulsatile pressure was applied. This study observed that samples with simulation having different compaction level and nominal maximum aggregate size (NMAS) have variant hydraulic conductivities resulting in variant aggregate orientations, angularities and distribution of fine. From this, different internal pore structure occurred. This study

concluded that dynamic fluid pressure influences the moisture transport inside asphalt concrete. Also there was a micromechanical model established by Guo, Sun and Dai, (2017) used the fluid dynamics theory, they calculated the pressure when the asphalt was saturated and was exposed to repeated traffic, and found that the maximum pressure inside pore was occurred at the junction between exit slits the pore wall, they also found that there is positive correlation between pressure and traffic speed because of repeated traffic loading where it may cause emulsification, shift and peeling of asphalt membrane. The model used for calculation of thesis pressure shown in Figure 2.18.

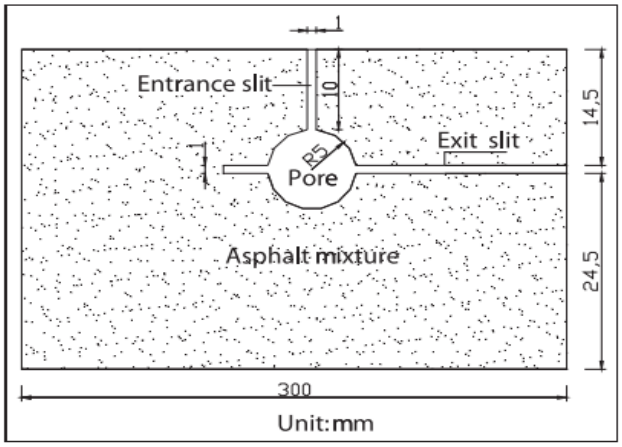

Figure 2.18 Calculating model (Guo, Sun and Dai, 2017)

Zhou et al., (2007) computed the peak value of pore water pressure in flooded asphalt pavement using Finite Element Method (FEM) built on Biot consolidation theory and viscoelastic incremental constitutive equations and found out that when the permeability coefficient of asphalt mixture is 1× 10-4 cm/s and the load duration is 0.005 s, the pore water pressure is 0.566 MPa.

2.2.9.2 Experimental Studies

There are a limited number of studies found in the literature that have experimentally tried to measure and evaluate the impact of water pressure in the overall pavement structure.

The in-situ study (Gao, Guo and Liu, 2015) designed a fibre optic hydraulic pressure sensor (FOHPS) to measure the in-situ pore water pressure Figure 2.19. Three sensors were installed at different depth under traffic load, as illustrated in Figure 2.20. The drill cavities B, and C were filled with water by a fine steel pipe and sealed. Drill hole A, through a roadway flusher, to sprinkle water, to make sure that the pavement was in the condition of water flowing and as on a raining day. During measuring of the pore water pressure, a vehicle was driven to the passage above the holes A, B and C at the speeds of 20 Km/h, 40 Km/h, 60 Km/h, 80 Km/h and 100 Km/h. For a reason the vehicle possibly cannot pass appropriately above the sensors, so the test was repeated a number of times as showed in Figure 2.21.

The tests results showed that the pore water pressure increase with the increasing vehicle speed. However, the lifetime of pore water pressure is directly related to the load duration. And the load duration is inversely proportional to the vehicle speed. So, the lifetime of pore water pressure decreases with the increasing speed (Gao, Guo and Liu, 2015), Which is consistent with the findings the theoretical investigation presented by Li et al., (2007) on the pore water pressures as well indicated a build-up in pore water pressure on pavement surface with increasing vehicle.

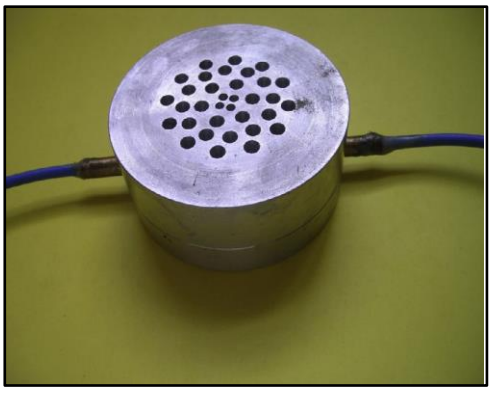

Figure 2.19 Fibre optic hydraulic pressure sensors (Gao, Guo and Liu, 2015)

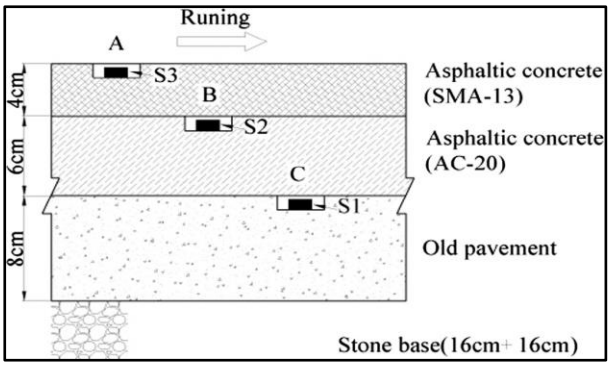

Figure 2.20 Asphalt pavement cross section showing sensors (Gao, Guo and Liu, 2015)

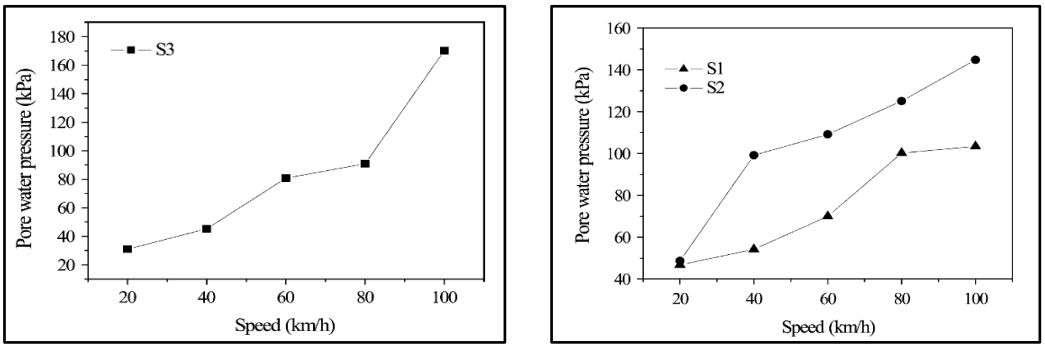

Figure 2.21 Relationship between vehicle speeds and pore water pressure at Pavement surface and in pavement respectively (Gao, Guo and Liu, 2015).

Dong et al., (2007) calculated the pore water pressure in the asphalt pavement surface, whose value is 0.44 MPa. Also, Gao et al., (2009) measured the dynamic water pressure in the asphalt pavement surface. The results showed that when car speed is 80 km/h, the water pressure is about 0.2 MPa. Despite several decades of comprehensive studies, moisture damage in asphalt pavement stills an issue of discussion among researchers (Kakar et al., 2015).

2.2.9.3 Mathematical Method

Li and Deng (2008) developed a theoretical model whereby the asphalt pavement was regarded as an axially symmetrical body of multi-layered saturation elastic half-space (Cui et al., 2009) the pore water pressure in asphalt pavement under mobile load was

calculated. The results demonstrated that the pore water pressure in the internal asphalt pavement has a close relation to the permeation coefficient of the surface, surface thickness, wheel speed and material parameters. The pore pressure at the interface between surface layers and the base layer of the asphalt pavement is maximised when the pore of pavement is entirely saturated, under the loading action. Under the repeated act of loading, the pavement fatigue cracking may happen, a process which accelerates the development of the cracking of asphalt pavement.

On effective stress and dynamic pressure against time, Li and Deng, (2008) constructed a theoretical model in which the asphalt pavement was regarded as an axially symmetrical body of multi-layered saturation elastic half space, and pore water pressure in asphalt pavement under mobile load was calculated; The results show that the pore water pressure in the internal asphalt pavement has close relation to permeation coefficient of surface, surface thickness, wheel speed and material parameter. Pore fluid stress at the interface between the surface layer and base layer of the asphalt pavement is maximum when the pore of pavement is entirely saturated, under loading act. Under the iterative action of load, the pavement fatigue cracking may occur, which accelerates the developing of cracking of asphalt pavement.

Table 2.7 summarise water pressure related research in terms of study type, the assumption used to obtain the results and the outcome of each study.

Table 2.7 Summery of pore water pressure studies

Authors	Study type	Aims	Assumption	Output
(Jiang, Zhang and Li, 2013)	Experimental work	Study the relation among the wheel load, pore pressure, and water erosion on pavement water damage.	The water pressure is equal to the air pressure	-Asphalt mixture with 8% void contents showed minimum resistance to water damage. - powder escaped, shear failure happened
(Gao, Guo and Liu, 2015)	Experimental work in situ	Measure pore water pressure in asphalt pavement and its effects on permeability.	Uniform pressure	- Pore water pressure increase with the increasing car's speed. -Water infiltration rate increases on an approximate linear curve as the hydraulic pressure increased from 40 kPa to 350 kPa.
(Lei et al., 2017)	Experimental work in situ	Investigate influence of vehicle speeds on the hydrodynamic pressure of pavement surface.	five fiber Bragg grating (FBG) sensors was designed and utilized to measure the surface hydraulic characteristics	-The hydrodynamic pressure of the pavement surface increased with the increase in vehicle speed -The directional anisotropy of the hydraulic pressure was found to be dependent on vehicle speed.
(Zhou et al., 2007)	Numerical model. Based on Biot' s theory and viscoelastic incremental constitutive equations	Analysis the dynamical pore water pressure in saturated asphalt concrete pavement.	-impervious in bottom surface but non-watertight in the top surface except the pan area. -the pavement, is water-proof on the lateral surface	-Numerate dynamic response of stress and pore water pressure in asphalt pavement. -Correlative curve equation of influences on the maximal pore water pressure by permeability coefficient and loading speed is obtained. - Fluctuations and distribution of pore water pressure are obtained.
(Cui *et al.*, 2009)	Numerical model. Based on fast Lagrangian finite difference method and Biot dynamic consolidation theory.	Investigate the accelerating role of dynamic pressure in moisture damage of asphalt pavement.	-Asphalt mixtures as porous medium. -Course is assumed to be not penetrable. -Wheel loads were simplified as uniform pressure on two circles.	-The dynamic pore pressure increases with vehicle velocity. -Effective stress and deflection of pavement all decrease due to the dynamic pore pressure. -The maximum dynamic pore pressure occurs at the bottom of the surface course.

			-The interface between surface course and base course is impervious.	
(Kutay and Aydilek, 2009)	Numerical model used field cores and laboratory- prepared specimens using the lattice boltzmann (lb).	Study the development of flow-induced pore pressure and viscous shear stress distributions at the pore–solid interfaces, on moisture damage in an asphalt pore structure.	The 3D internal structures of the specimens were obtained using the non-destructive X-ray CT imaging technique.	-The pore water pressure gradient is highly nonlinear within the pore structure of asphalt specimens, as opposed to a linear gradient normally observed in homogeneous pore structures such as granular soils. -The viscous shear stresses were observed to be the largest at the constrictions located at the mid-depth of the specimens.
(Cui, 2010)	Numerical model. Based on the Biot consolidation theory, 3D Fast Lagrangian Analysis of Continua	Investigate the dynamics mechanism of the inhibitory effect of permeable base on moisture damage	-Large stone porous asphalt mixture and permeable base -Wheel load simplified as uniform pressure circle.	-Dynamic flow velocity of fluid is very small and the dynamic flow in asphalt pavement is laminar flow. -Water pumping out of and sucking into the pavement under the moving loads was proved
(Li and Sheng, 2012)	Numerical model. The poro-elasticity theory using ABQUS.	Compute the pore water pressure development in the base layer underneath joints.	-Distributed loading is applied on the partial surface near the joint gap. -Gravity is neglected. - All the gradients caused by external force or fluid pressure will be in the vertical direction due to boundary condition.	-Pore water pressure reaches the peak value in a shorter time for higher speed vehicle.
(Guo, Sun and Dai, 2017)	Numerical model ,based on fluid dynamic theory	The aim to build model could be used to calculate several kinds of data when the asphalt pavement under the influence of traffic loading is in water-saturated condition.	a micromechanical model, -saturated pavement -repeated traffic loading	- Positive correlation between traffic and pressure. -Existing micro crack in asphalt films lead to accelerate the cumulative damage and lead to peel of the asphalt film.
(Xiaoyong, 2008)	Mathematical method. Using thermal Boit consolidation theory and seepage flow equation.	To calculate the pore water pressure in asphalt pavement is based on some mathematic methods such as Hankel and Laplace integral transformations.	-Penetrate is constant. -Asphalt concrete entirely saturated and homogenous. -Both pore water pressure and concrete cannot be compressed.	-Pore water pressure inner surface has close relation to: . Permeation coefficient of surface. . Thickness of surface, materials parameter and wheel speed. -Pore fluid is stress at interface between surface layer and base layer of flexible pavement is max when the pore of pavement is full of water under the action of load.

				-Under the iterative action of load, pavement fatigue cracking may occur, which accelerate the appearing of breakage of pavement

Part 3: Deterioration Prediction Model of Asphalt Surfaces Performance

2.3 Introduction

Performance is a general term defining how pavement condition changes or how pavement structures serve their intended purposes with accumulating use (George, Rajagopal and Lim, 1989). A need has been considered the several implementing organisations to develop an intelligent pavement performance model that can prioritise pavement maintenance and repair pavement surfaces, as this includes cost economics. The flexible pavement deterioration models involve the complex interaction between traffic loading and the environment and the structure and pavement surfaces. The pavement deterioration models forecast the deterioration of the pavement over time and under changing environmental conditions, which, usually, is shown in different types of distresses. Each mode of distress develops and progresses at various rates in several environment scenarios. Performance models correlating the pavement material characteristics to different environmental factors are analysed and developed by researchers.

2.3.1 Pavement Deterioration Prediction Models

There are two basic types of performance models: deterministic and probabilistic. Deterministic deterioration model kinds are those which predict a single value of the response variable like a performance indicator, distress quantity, pavement life, etc., for a particularised number of independent variables such as time, age, traffic loading, usage rate, environmental effect, level of preservation activity, etc (Mahmood, 2015). For deterministic models, the usual common analysis approach is statistical regression (Haas et al., 1994; Lytton, 1987).

The all most of deterministic deterioration models were built based on linear or nonlinear statistical analysis techniques (Mahmood, 2015). Kerali et al. (1996)developed a nonlinear regression model to predict rut depth by analysing traffic loading, base materials and thickness. It was determined that the combined

consequences of the base layer materials and base layer thickness impact rutting. Ningyuan et al. (2001) showed a dynamic prediction model considering particular treatment consequences to predict a condition index for each treatment (Ningyuan et al., 2001). Prozzi and Madanat (2004) developed a nonlinear deterioration model to predict pavement serviceability by employing the laboratory and field data of the American Association of State Highways Officials (AASHO) Road Test.

The deterministic models of pavement deterioration were developed to predict particular distress progression without studying other distress kinds. Besides, the majority of these models may not reflect the contribution of the most critical variables to pavement deterioration (Mahmood, 2015).

The probabilistic deterioration model is different from deterministic models in that it predicts a distribution of such events (Mahmood, 2015). To deal with the inadequate availability of archival data, the most of probabilistic deterioration models were developed utilising the Markov chain procedure for forecast defect value or an overall performance index (Lytton, 1987). Alsherri and George (1988) founded a simulation model for determining the reliability-performance of pavements and the expected pavement life. Henning established continuous probabilistic models to predict the crack initiation and accelerated rutting for New Zealand's pavement network. A Logit model form, which is especially useful in predicting the possibility of a defect event happening, was applied (Henning, 2008).

Almost of probabilistic models were based on the deterioration rate remaining constant throughout the examination period (Mahmood, 2015).

In addition, in order to address uncertainty and nonlinearity, soft computing techniques are increasingly gaining popularity in pavement engineering (Mahmood, 2015). The advancement of computational power in data processing, good learning and adaptive capacities, adequate data storage and management, have helped soft computing techniques to be employed in pavement engineering (Mahmood, 2015).

Due to the nature of this research, soft-computing technique was adopted. In order to determine most appropriate technique, a comprehensive review has been done on different soft-computing techniques and is presented in the following sections.

For any prediction model, there are three key parameters to consider- input, thresholds/rules, and output. A short description of generating rules is given in Section 6.2.4.

2.3.2 Soft Computing

For solving complex problems, significant achievements for pavement classification in algorithmic development have been made through modelling techniques based on biological mechanisms and natural intelligence. These algorithms of soft computing comprise artificial neural networks and fuzzy logic (Engelbrecht, 2007). All these artificial intelligence techniques help to consider the partial truth.

2.3.2.1 Genetic Algorithm (GA)

A genetic algorithm (GA) is an 'intelligent' probabilistic search algorithm which simulates the process of evolution by using a population of solutions and applying genetic operators in each reproduction. Each solution in the population is evaluated according to some fitness measure. Highly fit solutions in the population are given opportunities to reproduce. New 'offspring' solutions are generated, and unfit solutions in the population are replaced. This evaluation–selection–reproduction cycle is repeated until a satisfactory solution is found (Chu and Beasley, 1997).

GA is based on converting each feasible solution to a chromosome; by applying selection, crossover and mutation, it can locate the optimum global option with more probability (Vadood, Semnani and Morshed, 2011). GA evolves a population of individuals to better ones (Gopalakrishnan et al., 2010). GA is employed to efficiently solve highly nonlinear and mixed integer optimisation problems (Uysal and Bulkan, 2008). Because of the relationship between variable used to build prediction model in this project is mixed linear and nonlinear; therefore, the best method to use is fuzzy logic.

2.3.2.2 Artificial Neural Networks (ANN)

"A neural network can be defined as a model of reasoning based on the human brain" (Negnevitsky, 2002). Neural networks are computational models that model the

relationship between some input variables and output variables. The artificial neural network is similar to the human brain includes many simple, highly interconnected processors that are named neurons (Agatonovic-Kustrin and Beresford, 2000) . Neurons are linked together by a large number of weighted links, with each neuron getting input from several resources (Naveep ,2017). The weights, known as synaptic weights, additional increase the correspondence between the real and artificial neurons (Wells, 2003). The input components get their inputs from external sources while other components get their inputs from the specific output which each component generates (Sussil and Abbott, 2009).

A neural network is an interconnected network of neurons where one neuron's output acts as a stimulus to another one. Through the connection, it can obtain more than a single input, but it is not allowable to provide more than a single output (Agatonovic-Kustrin and Beresford, 2000). The benefit of artificial neural networks is the capability to compute nonlinear functions and detect all possible interactions between predictor variables by learning from knowledge. Pavement condition assessment is subjected assessed by road experts and engineers. The artificial neural network method has adopted a computational model to simulate the human decision-making process.

2.3.2.3 Fuzzy Logic

Human expert controllers usually perform superbly well under conditions of uncertainty and imprecision employing inherently approximate reasoning (Berenji et al., 1989). They choose control actions built on a quick evaluation of the process which they are controlling. Learning to manage a physical system has been regarded as one kind of intelligence (Connell,1986). Control theorists have successfully dealt with a large class of control problems by mathematically modeling the process and solving these analytical models to generate control actions(Berenji et al., 1989). However, the analytical models tend to become complicated, especially in large, intricate systems. The non-linear behaviour of several practical methods makes this analytical method indeed more complex (Berenji et al., 1989). A challenge facing many applications of Al in control is how to manage imprecision in the knowledge expressed by expert controllers (Berenji et al., 1989). Fuzzy set theory - suggested by Zadeh gives the

facility to express the imprecise knowledge by employing linguistic variables (Zadeh, 1988).

The crisp set theory is governed by the logic that employs one of only two values: true (1) or false (0) (Mahmood, 2015). It cannot represent vague concepts and fails to provide the answers to the paradoxes. An element in fuzzy set theory has a certain degree of membership. It resembles human decision making, so is neither true nor false. It may be partly true or partly false to any degree. The degree is generally chosen as a real number in the interval [0, 1] (Zadeh, 1969). As a replacement for using crisp sets of classic rules which derive from the human expertise decision, the fuzzy set uses the rule of *if-then* to represent expert human thinking. Sometimes, this technique is not feasible when facing a complicated task or when humans are not present. An active substitute is to generate the fuzzy interface system model automatically from data by employing learning methods (Riza et al., 2015). The significant advantage of fuzzy logic is that it offers a practical approach for automating complicated data analysis, data fusion and inference processes that are commonly performed by human experts with years of official training and extensive knowledge (Munakata and Jani, 1994).

Several methods have been used for learning methods, such as gradient descent learning method, neural- fuzzy approach, heuristic methods, the clustering method, GAs and space partition-based procedure (Wang and Mendel, 1992) which is used in this study. Moreover, a fuzzy rule-based system was developed for the representation of expert knowledge through fuzzy *if-then* rules. The advantages of this approach include the mechanism of reasoning in human thinking, the capability of gaining linguistic information from human experts and combining it with numerical data and ability to estimate complicated nonlinear functions with simpler models (Dehzangi et al., 2007). The fuzzy system generates several sets of random crisp data for the independent and the dependent variables. The least squares non-linear regression is applied to these data to determine the coefficients of the prediction model. Two separate models are available, one for each distress (cracking and rutting) using Wang and Mendel's approach (WM).

2.3.3 Adopted Method

The pavement performance is computed based on pavement deterioration data, such as the kind of distress and severity level, which are collected by distress measurements (See Chapter Five Section 5.4), Simple and effective models are developed that is capable of coping with uncertain data gathering from an experimental study. This research proposes a fuzzy rule-based system or fuzzy inference system (FIS) for deterioration prediction model pavement, considering three type of asphalt pavement surface, three aggregate sizes, weather conditions (wet, dry), number of cycles, void content, load and two frequencies as input variables. A FIS is one of the most popular methods used in classification problems (Mahmood, 2015). The FIS is a method which interprets the values in the input vector and, based on predefined rules, assigns quantities to the output vector. The benefit of this procedure is that knowledge can be expressed in the form of *If-Then* rules.

Firstly, pavement distress data are extracted and manipulated to build a fuzzy rule-based system for pavement deterioration prediction models with a severity level for each output.

A new deterioration prediction models developed, the parameters of three type of asphalt pavement surface, three aggregate sizes, weather conditions (wet, dry), number of cycles, void content, load and two frequencies are used as FIS inputs. The severity level is determined by using the distress based Distress Identification Manual for the Long-Term Pavement Performance Program (2003) for cracking, for rutting based on studied by (Vaitkus Cygas, and Kleiziene, 2014; Nguyen and Le, 2016). Cracking is the output of the FIS and rutting is the output of second model of the FIS.

There is the challenge of the generation of the fuzzy rules and membership functions in FIS with a high-dimensional problem. To defeat this problem, the membership functions of inputs are created based on the k-means clustering technique using the Fuzzy Inference System Professional (FISPro) software (Mahmood, 2015). "FISPro offers the possibility to generate fuzzy inference systems and to use them for reasoning purposes, especially for simulating a physical or biological system" (Guillaume, Charnomordic and Lablee, 2002). It can design a fuzzy inference system from the expert knowledge or the numerical data. For each parameter type, three triangular

membership functions representing the range of variability (low, medium, and high) are generated. The seven triangular membership functions of output are generated manually. Moreover, to address the challenge of fuzzy rules generation. The Wang & Mendel technique is adopted to create fuzzy rules mechanically from numerical data. FISPro software selected to reduce time and effort; it is used for the generation of membership functions and fuzzy rules from the numerical data.

2.3.3.1 Wang and Mendel Method

This method is used to generate fuzzy logic from numerical data and was presented by (Wang and Mendel, 1992) using five steps, as follows:

1) Equally split the input and output spaces of the specified numerical data into fuzzy regions as the database. Fuzzy regions refer to intervals for the linguistic conditions. Thus, the length of the fuzzy regions is correlated to the number of linguistic conditions.
2) Generate fuzzy *if-then* rules covering the training data using the database from steps first; compute degrees of the membership function (MF) for all values in the training data. For each instance and each variable, a linguistic value is determined as the linguistic term whose membership function is maximal in this case. Then, repeat the process for all instances in the training data to construct fuzzy rules covering the training data.
3) Assign a degree for each rule. Degrees of each rule is assigned by accumulating the degrees of membership functions in the antecedent and consequent parts. In this case, the product aggregation operators can be used.
4) Obtain a final rule base after removing redundant rules. Considering the degrees of rules, a redundant rule with a lower degree can be deleted (Riza et al., 2015).
5) Defuzzification technique obtains mapping based on fuzzy rules (Wang and Mendel, 1992).

The application of Fuzzy based soft computing can be an attractive choice for practicing engineers because the real-life engineering decisions are made in an ambiguous environment that needs a very high level of reliable human knowledge (Mahmood, 2015).

2.4 Summary

This chapter reviewed information on asphalt pavement based on that three types of pavement surface were selected based on aggregate gradation and void contents, and those types are open graded included Open stone mastic asphalt and porous asphalt. Then reviewed literature related to asphalt surface damage particularly the influence of water pressure and selected to types of distress (surface cracking and rutting) to investigate the influence of loading water and pavement type in asphalt surface damage. Also presented a comprehensive review of relevant literature on moisture-related damage, research related to pore water pressure. Moreover, was an apparent gap in measure pore water pressure in the pavement surface. The third part presented a study of different deterioration prediction models to establish a rationale to select the technique for the application of experimental data from this research to predict the performance versus water pressure for several kinds of asphalt surfaces.

Chapter 3 Methodology, Preliminary Investigations and Test Specifications

3.1 Introduction

A comprehensive review on asphalt pavement distresses and the influence of water on asphalt pavement performance is presented in the Chapter 2. Previous studies related to experimental, numerical and analytical studies on pore water pressure measurement in asphalt pavement are reviewed in detail. It was evident that research in pore water pressure and its impact on asphalt surface damage is limited and disjointed. In addition, past studies did not cover the impact of combined interactions of repeated traffic load-tyre-water-pavement surface (as explained in conceptual illustration in section 2.2.12 in Chapter 2) on long-term performance. It was also evident that there is no test that can simulate the combined interaction of traffic load- tyre-water-pavement surface. A new experiment is necessary due to the absence of standard laboratory test method. This chapter presents the design and create of new test method, together with the methodology used to design and execute the experimental programme. This chapter has been divided into three main parts.

Part 1: Preliminary study: An investigation has been conducted to understand how water flows under a moving wheel and utilising this concept to design a laboratory test for measuring water pressure under a slab when the slab was flooded with water while subjected to dynamic loading.

Part 2: Adopted test set-up: Based on the results from Part 1, the test was modified and semi-automated to perform the test and for data collection

Part 3: This section will present the specifications of materials, mixture design, and test parameters used in the research.

Part 1 Preliminary Study

A simple test was designed to idealise the concept of tyre-water-pavement interaction in section 2.2.12 in Chapter 2. The purpose of the test was to measure water pressure consistently under a pavement. In addition to the water pressure, the preliminary study was also used to design a loading plate capable of adapting different tread pattern and shape and was used to determine the pore water pressure range and subsequent selection of pore water measuring sensor for automatic collection of the test data. A schematic diagram and an image of the preliminary test set-up are given in (Figure 3.1

a) a brief description of each component including test procedure is given in the following sections. The test set-up that includes eight channel manometer, concrete base with 16 no 2mm full depth holes, a loading plate with rubber pad and loading frame. Figure 3.1 b shows the actual test set-up.

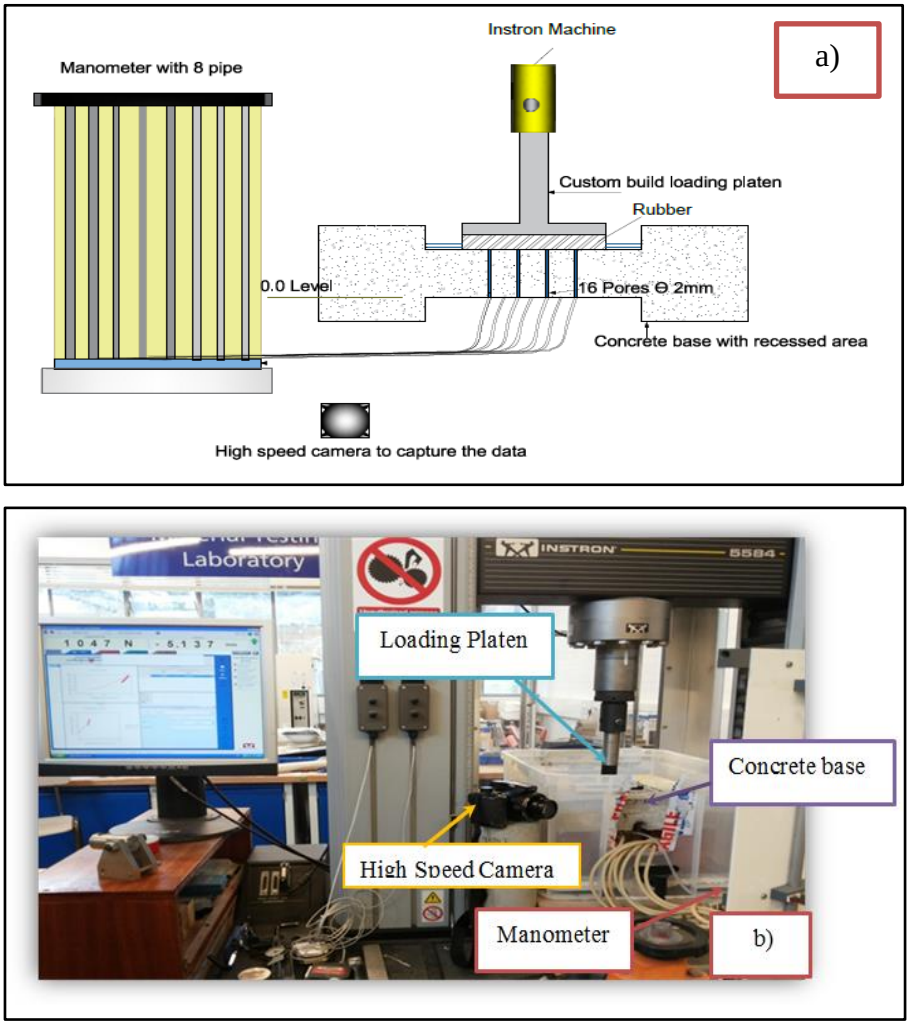

Figure 3.1 a) Schematic diagram of initial test-set-up, b) Image of initial test-set-up

The manumater is used to measure pore water pressure, the following section will explain the concept of static pressure, dynamic pressure and method measuring it when use instrument such as sensor. Static pressure, or hydraulic pressure, is the pressure of a fluid at rest considering the fluid is not moving; static pressure is the outcome of the fluid's weight. There are two different methods to determine static pressure the first and most common calculate is to take the force exerted by fluid and diveded by the area over weighted. The second conventional method for measuring static pressure is

to calculate the head. Measure the pressure head is how much the fluid can go up when the force confining the fluid is removed.

The pressure equation is the relation of force and area (P_{static} =Force/Area), but the force can be characterised by mass (m) × gravitational acceleration (g). So, the question can be demonstrated as

$$P = m \times g/area$$

If water is used as a meduim then

$$m = \text{density of water } (\rho) \times \text{volume of water (v)}$$

$$\Delta P = \rho \times v \times g / area$$

$$\Delta P = \rho \times area \times h \times g / area$$

$$\Delta P = \rho . g . h$$

Dynamic pressure is a pressure exerted perpendicular to the direction of the flow and is represented by the symbol q. The equation for dynamic pressure is as follows:

$$q = \frac{1}{2} \rho V^2$$

Where V is speed of fluid m/s.

$$\text{Total Pressure (P) = Static Pressure+ Dynamic Pressure}$$

$$P = \rho . g . h + \frac{1}{2} \rho V^2$$

3.1.1 Concrete Base

As shown in Figure 3.2, the test set-up consisted of a concrete base (300 mm × 300 mm × 100 mm) C40 concrete slabs with (150 mm × 150 mm × 20 mm) recessed area with 16 no, 2 mm full depth pores connected with a flexible tube under the slab. The rationale to choose rigid concrete base was to avoid the effect of visco-elasticity under loading and to minimise the effect of texture depth on the water pressure. It was intended that if this trial gives meaningful and repeatable measurement of pore water pressure, the concept could be implemented to other loading and frequencies as well as on asphalt surface with different voids, aggregate size and macro textures.

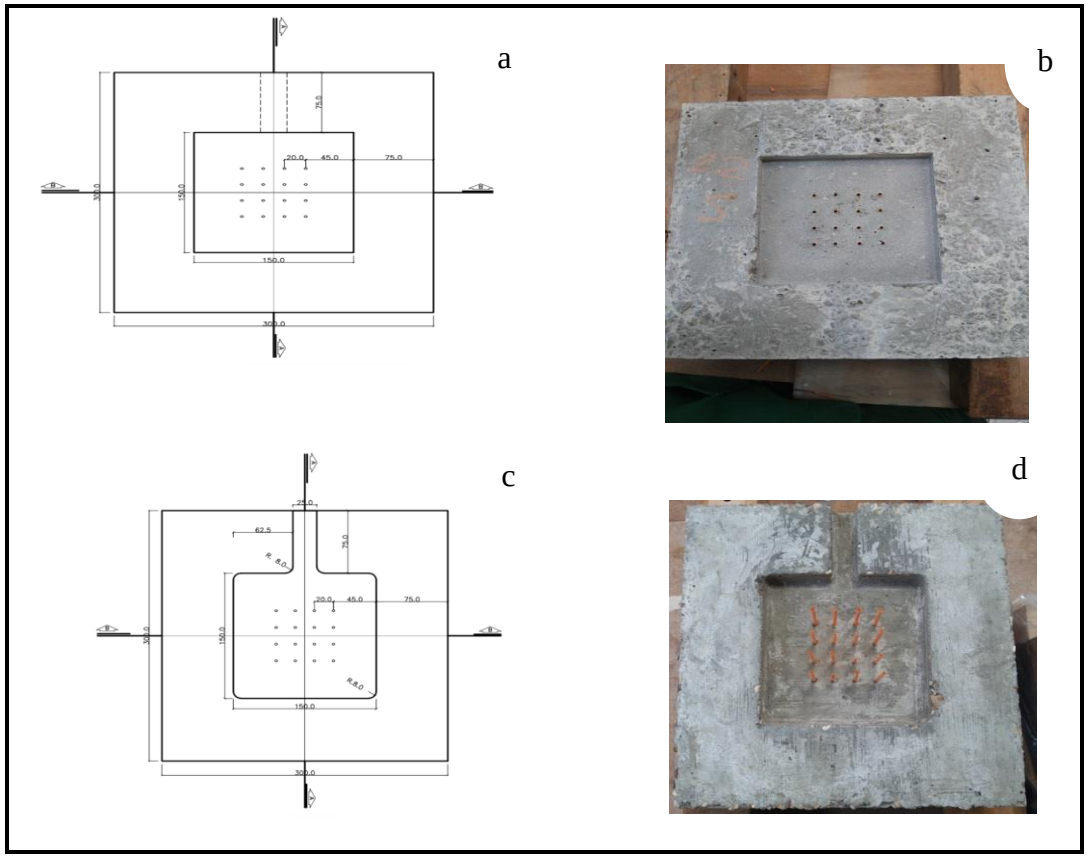

Figure 3.2 (a) Top plane viewing of concrete slab, (b) Top of manufactured slab (c) Down plane viewing of concrete slab, (d) Down of manufactured slab

The other end of the tube was connected to an eight-channel manometer to measure water pressure under dynamic loading. Whilst there were 16 pores in the concrete slab, eight of them were connected by tubes at one time and other eight were closed. The position of the tube was changed to evaluate pressure profile at different locations in the contact patch. In addition, as the loads are dynamic, the maximum pressure was difficult to read accurately on the manometer. To overcome this difficulty, a high speed camera was used to record the movement of water when loads are applied.

3.1.2 Loading Plate

Typical contact patch of a tyre varies between 150 mm to 300 mm. However, the effective treaded area could be between 100 mm to 250 mm. This is because the wall of the tyre is un-treaded, therefore it was considered to have 100 mm contact patch be sufficient to simulate the effective treaded area (description is given in Chapter 2,

section 2.2.4). In addition, for simplicity in manufacturing, the loading head was designed as a square rather than circular. A picture of the loading head is given in Figure 3.3. Similar concept was applied in earlier research by Rahman and Thom (2012).

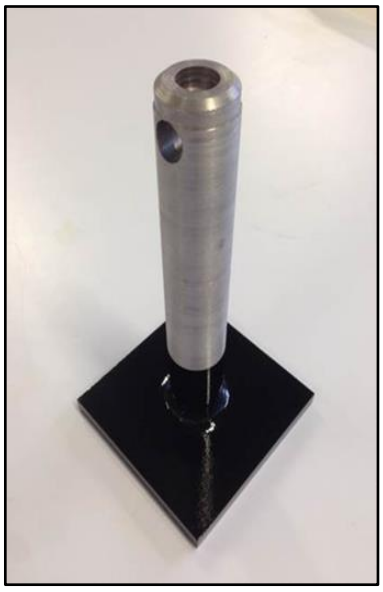

a) 100mm X100mm loading head b) Picture of the exposed (head) part

Figure 3.3 loading device

The device was made using bright mild steel bar welded to a square mild steel base plate, painted by enamel gloss paint to help with corrosion protection. The exposed face of the square part of the platen was kept rough so that tread part can be glued. The handle part was made with 25 mm diameter stainless steel rod to attach with loading frame.

3.1.3 Idealised Tyre Characteristics

As mentioned in Section 2.2.3 in Chapter 2, the shape, pattern and depth of tyre tread is vastly different for different types of tyres and their manufacturers. It was therefore, necessary to simplify the tread pattern and shape so that the effect of key features can be simulated in the laboratory. It was evident from the literature review that the main purposes of the tyre tread, are to allow traction between tyre and road surface and to

allow water under the wheel drain adequately to reduce chances of aquaplaning (Gillespie, 1992). In general, irrespective of tread pattern and shape, the treaded area in tyre has predominantly two types, a grove and a grove with channel to drain water. Therefore, the idealised sections were deigned to simulate grove and grove with channel. In addition, depending upon the manufacturer and age, tyres have different hardness, reinforced with tread and cord. Different hardness will response differently under loading, which will create inconsistency in water pressure measurement. To avoid this variability, a silicon rubber with uniform hardness was used to manufacture idealised tread pattern. A picture of the tread shape and pattern is given in Figure 3.4.

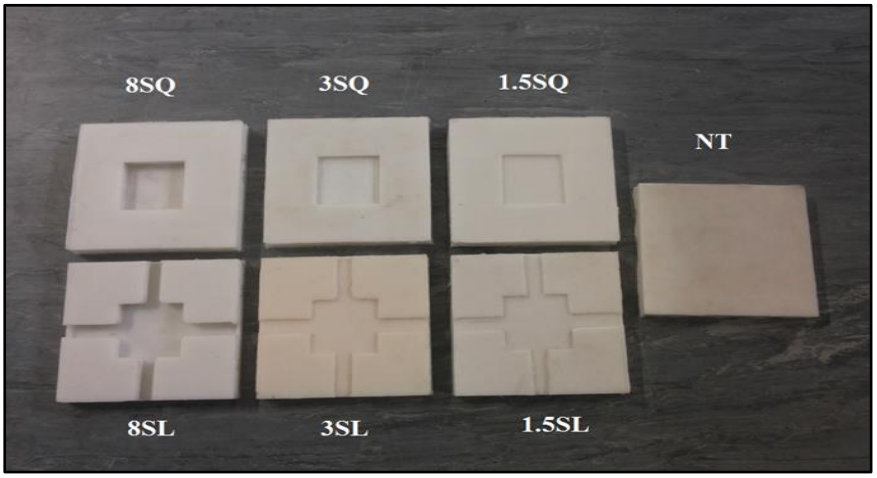

Figure 3.4 Idealised tread shape and pattern

The characteristics of the rubber pad used in this research are as follows:

- Overall thickness: 12 mm.
- Tread shape: a squared box (SQ) to represent Sipes, groove and dimple of the tyre and a square box with a channel (SL) to represent block and ribs of the tyre and non-treaded tyres (NT).
- Tread depth: 8 mm tread depth to represent new tyre, 3 mm to represent part worn tyre and 1.5 mm to represent worn tyre.

The notation, 8SL, is referred to 8mm tread depth in square box with channel tread pattern. Similar notations were used for the other tread depths and patterns.

3.1.4 Testing

The recessed part of the slab surface was flooded with 2 mm and 4 mm water prior to the application of load. A 5 kN repeated compression load at 1 Hz frequency was applied and water pressure was measured manually from the manometer. As mentioned earlier, higher frequency loading at this stage was avoided as it was not possible to measure water pressure manually due to the fast movement of water level in the manometer bar. The close-up image of the application of load is given in Figure 3.5.

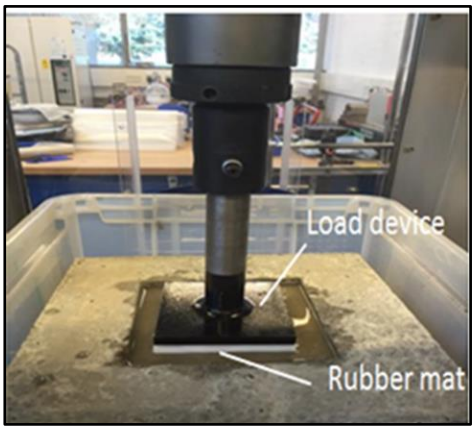

Figure 3.5 Attached load device with rubber

3.1.5 Test Outcome

Figure 3.6 shows the location of each pore number and cross symbol to represent closed pores. This arrangement was chosen to collect representative pore pressure at all locations. The centre pores (pores no 2, 5, 6 & 7) are directly under the load, while pores no 1, 3, 4, 8 are located at the edge of the loading plate.

Each test was repeated for four times and the average water pressure readout from the manometer is given in Figure 3.7 and Figure 3.8 for 4mm and 2mm surface water respectively. The results are shown for different tread characteristics at different pore locations.

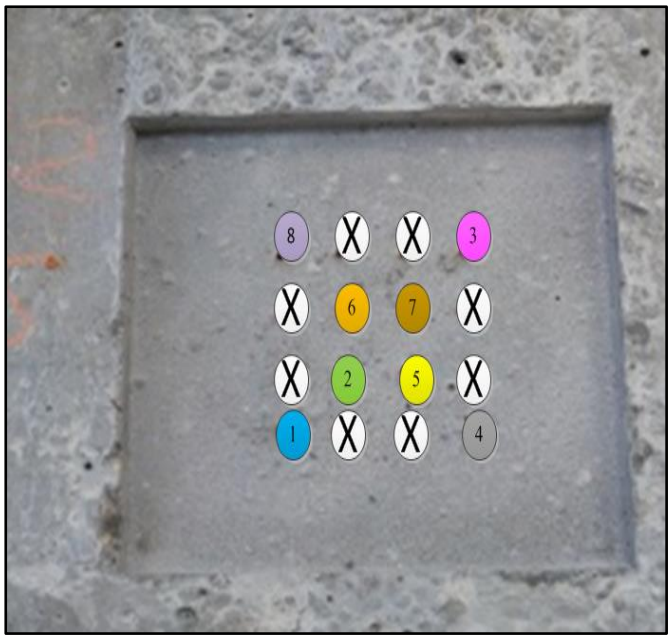

Figure 3.6 Pore locations

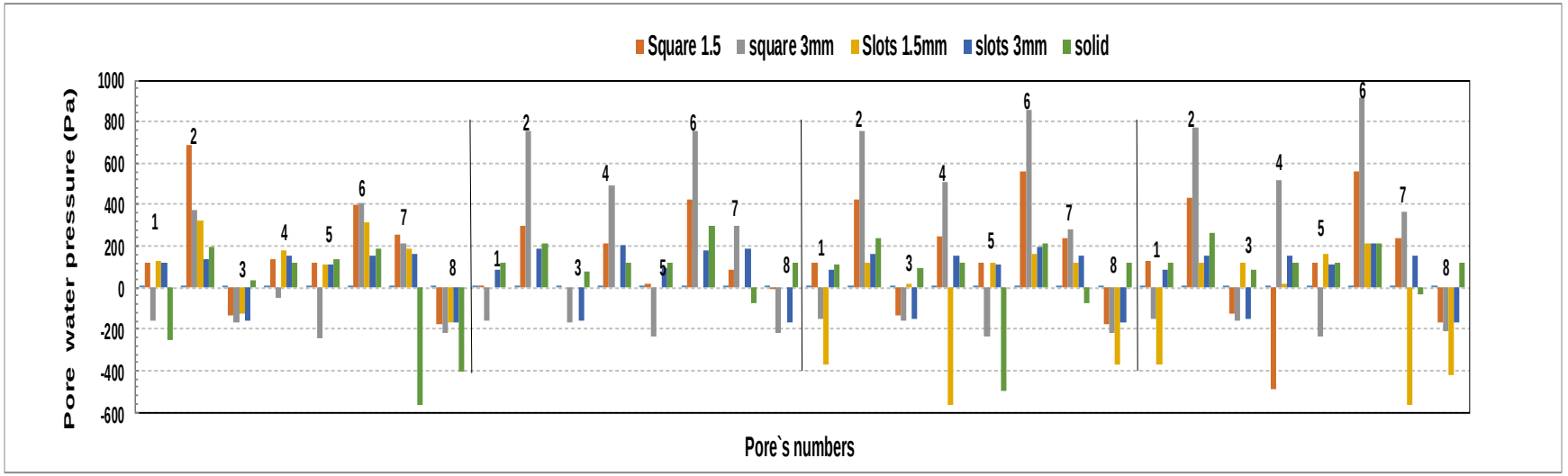

Figure 3.7 Pore water pressure magnitude when the slab was flooded with 4 mm water

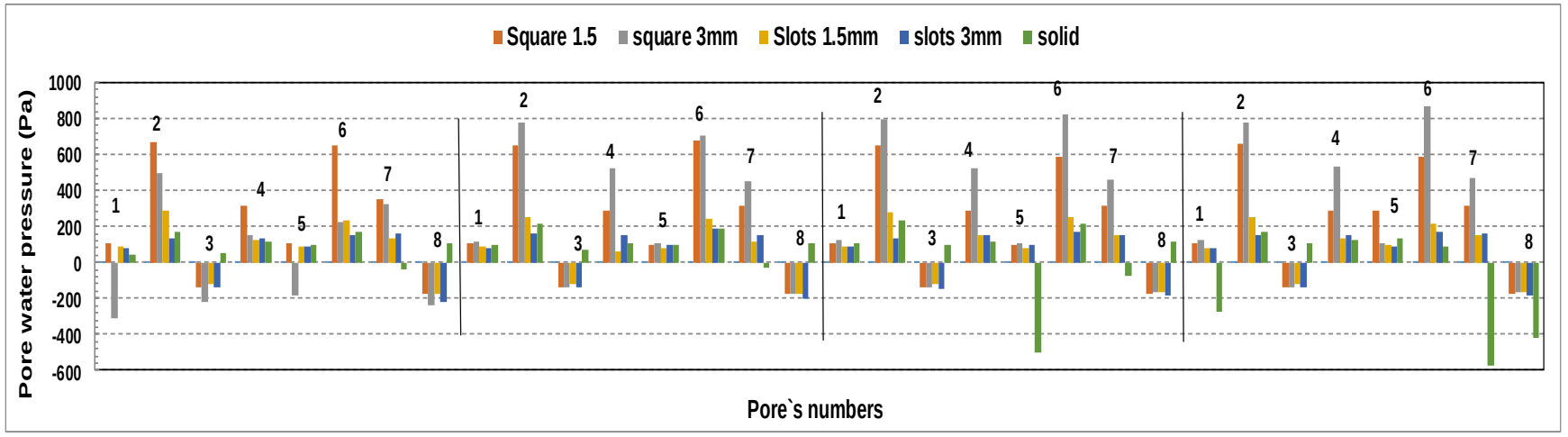

Figure 3.8 Pore water pressure magnitude when the slab was flooded with 2 mm water

As shown in the above Figures, depending on the location of measurement, the pressure distribution is non-uniform under the loaded patch. The pressure distribution also varies due to the change in tread pattern and depth of the tread. It is interesting to note that depending on the location of the measurement, suction on pore 3 and 8, the pressure can be negative, indicating suction due to repeated compression load.

Preliminary study showed, irrespective of tread shape and pattern, the maximum water pressure could be approximately 913 Pa, which occurred in one of the middle location directly under the loading plate (pores no 2, 6, 7, and 5). The magnitude of the pressure was significantly less at the edges (pores no pores no 1, 3, 4, 8). This value was used to select water pressure measuring sensor and locations to attach the sponsor for adopted testing presented in the following sections.

Part 2 Adopted Test Set-Up

As analysed in section 3.1.5, the maximum pressure was found at the centre of contact patch. Therefore, it was decided to take measurement at the centre of the contact patch rather than sixteen different locations. The final set-up consisted of developing a complete sequence of testing programme to semi-automatically collect data at different loads and frequencies. The flow chart of test sequences is given in Figure 3.9, with a brief description of each test component is given in the following sub-sections.

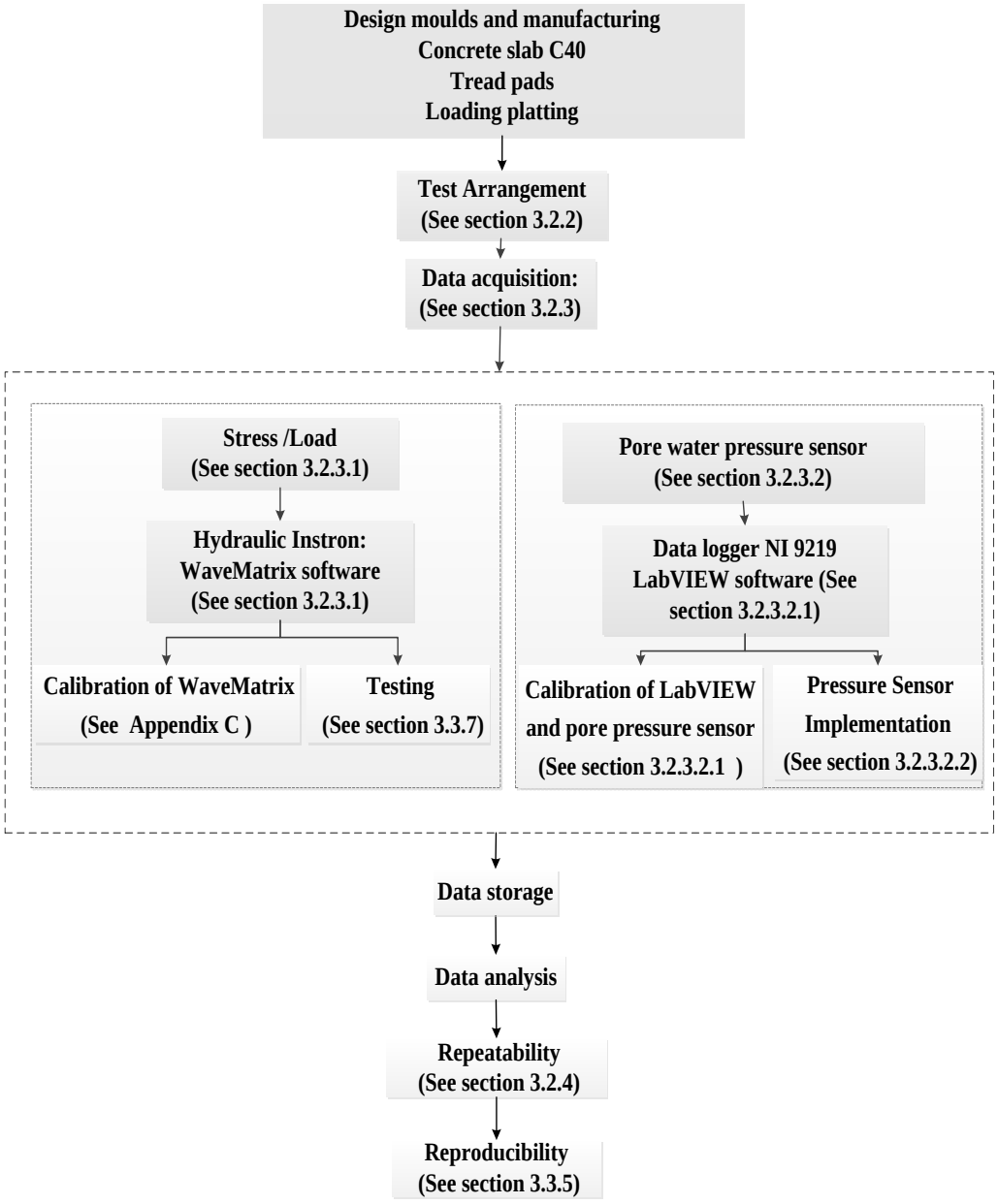

Figure 3.9 Flow chart of adopted test set-up

3.2.1 Idealised Pavement

The actual asphalt pavement construction and response of different layers under loading is rather complex due to different types of materials used in the construction. The idealised structure, as explained below, was therefore adopted to avoid some of the complexities.

Scenario 1: This state is similar to preliminary testing, but to measure water pressure at different load magnitudes and frequencies. As reported in section 3.1.3, this was done to avoid the influence of bituminous layer on water pressure measurement. Figure 3.10 represents an idealised concrete pavement, for which, instead of subbase granular material, a 40 mm rubber pad was placed on plywood to represent the pavement foundation.

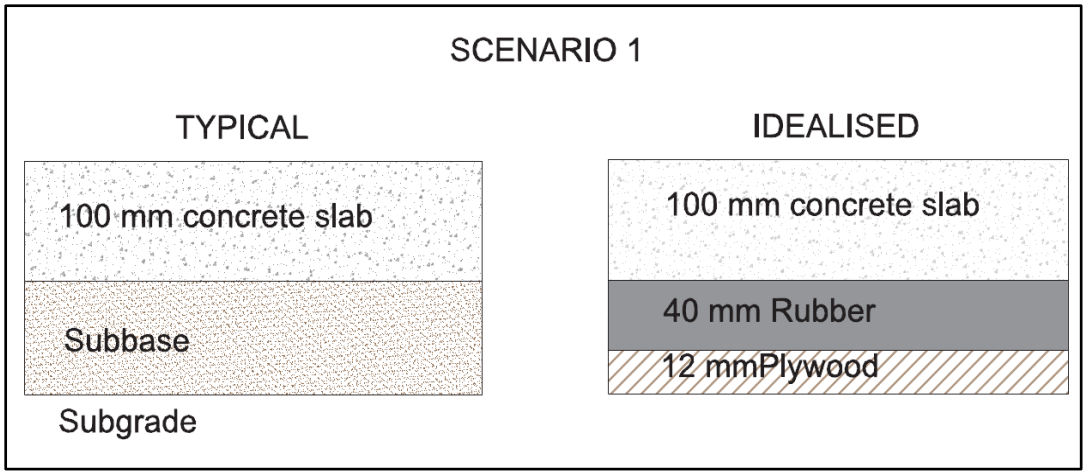

Figure 3.10 Scenario 1

Scenario 2: In scenario 2, a 20mm asphalt surface was laid on top of the concrete slab to evaluate the impact of asphalt surface on pore water pressure. Figure 3.11 shows a schematic diagram of an idealised pavement with asphalt surface for scenario 2 testing. The concrete slab helped to avoid the viscoelastic response from lower asphalt layers (binder and base). In addition, the concrete slab eliminated the possibility of water infiltration to lower layers.

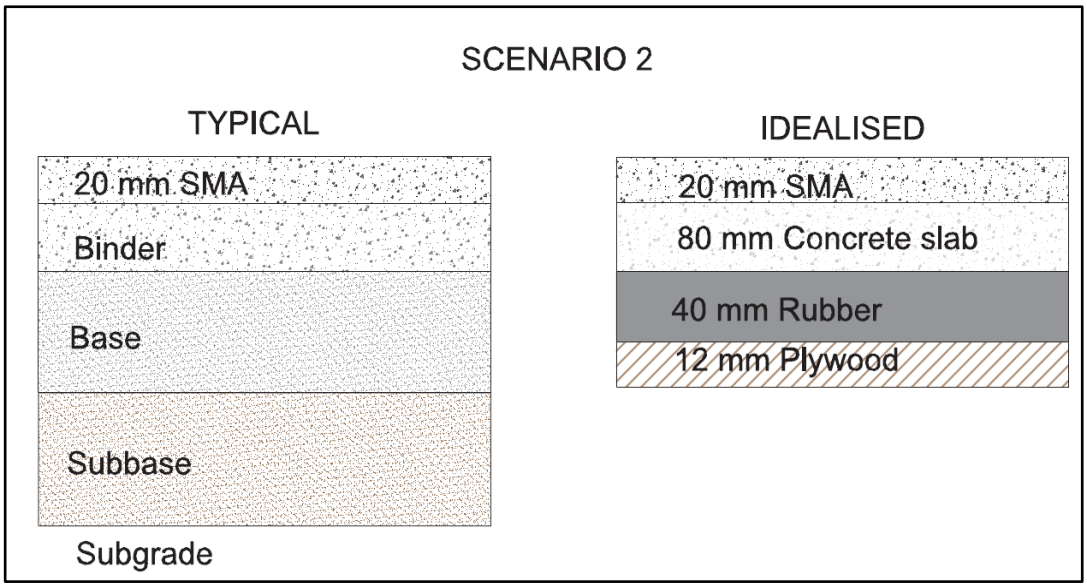

Figure 3.11 Scenario 2

3.2.2 Test Arrangement

The schematic diagram of scenario No 1 and Scenario No 2 is given in Figures 3.12 and 3:13 respectively and a picture of complete test arrangements is shown in Figure 3.14.

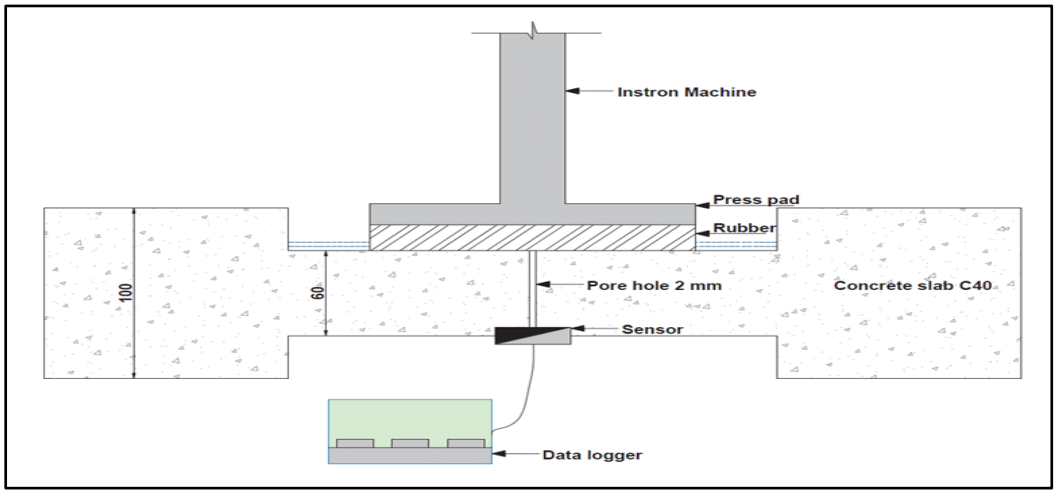

Figure 3.12 Scenario No. 1

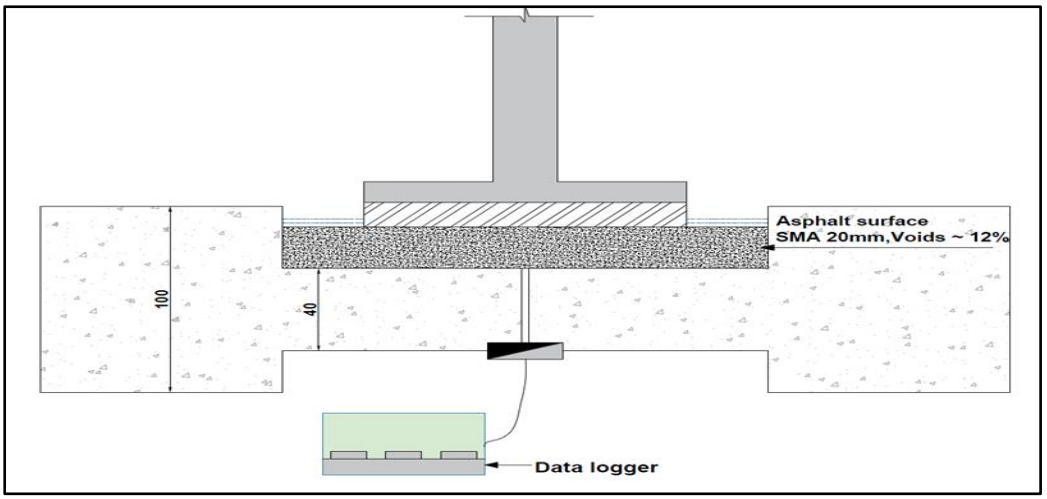

Figure 3.13 Scenario No. 2

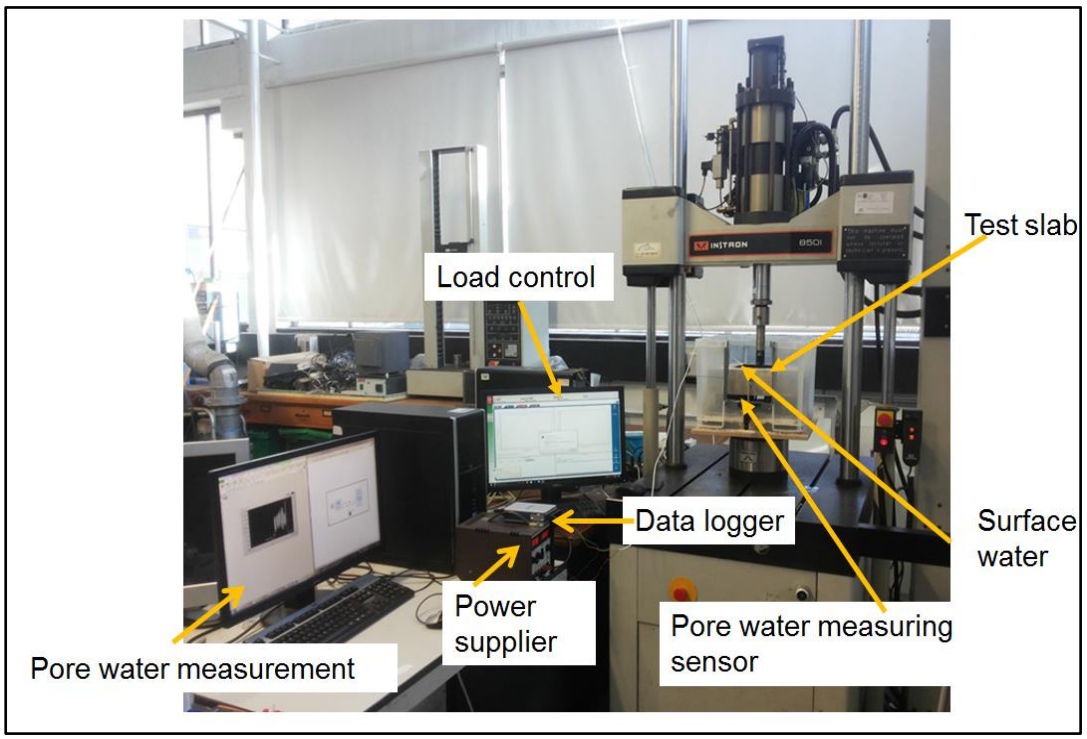

Figure 3.14 Test setup

As shown in Figure 3.14, the idealised pavement section was placed inside a watertight plastic crate, similar to set-up in preliminary testing. The recessed part of the slab was flooded with water and the loading head was placed on top of it. The handle of the loading plate was then attached with an INSTRON 8501 load cell. The INSTRON 8501 is a servo-hydraulic testing rig, with fully-integrated dynamic and fatigue testing

systems capable of applying loads at 0.1Hz to 50Hz in the 1kN to 100 kN load range. Testing was operated in a controlled load/stress mode.

3.2.3 Data Acquisition

Two separate data acquisition (DAQ) systems was used- the first one was to operate INSTRON 8501 servo-hydraulic testing rig for load/stress control and the second one was to measure pore water pressure during dynamic loading. A brief description of the data acquisition of each system is given below.

3.2.3.1 DAQ for Load/Stress Control

The INSTRON 8501 is equipped with WaveMatrix software to operate the equipment and loading in different waveforms such as a simple static ramp, to cyclic waveforms through to complex multi-step. The software has advance graphical user interface (GUI) integrated in tabular screens (Instron, 2015). The test sequence was divided in three steps, each one to perform a specific action as presented below. A detail description of test setup is described in appendix A. (Instron, 2015).

Step 1: Relative Ramp Waveform (RRV) is a relative ramp moves to a value relative to its starting value, at a specified duration. The RRV was necessary to lower down the ramp at a specific rate so that it does not damage the specimen.

Step 2: Cyclic waveform (CW) a cyclic waveform is defined by its amplitude and frequency parameters. The CW was used to control the specified load and frequencies and number of cycles.

Step 3: Absolute Ramp Waveform (ARW). An absolute ramp moves to an absolute end point over a specified period of time. This was necessary to end the test safely and to collect and store test data.

3.2.3.2 DAQ for Pore Pressure Sensor

The NI 9219 DAQ system was used to measure signals from pressure sensor by making quarter-bridge measurements (120 Ω), with built-in voltage and current excitation. The gain error was (±0.1, ±0.5) at temperature (25 °C ±5 °C) (Omega, 2015) in the data acquisition (DAC). LabVIEW software with charting window was used to show data in a graphical format for absolute time, pre-set the saving and recording of measurement data.

3.2.3.2.1 Signal Proccing to Capture Pressure Data

The DAQ assistant in the LabVIEW coded front panel was used to measure pressure and the magnitude of pressure. In the front panel, the block diagram contains the code, as shown in Figure 3.15, which were then connected the data assistant with sensor and feed the data to write in measurement file. Figure 3.16 gives visual representation of the DAQ assistant, sensor and the voltmeter used to check the connection of sensor, data logger and power supply at the beginning of each test.

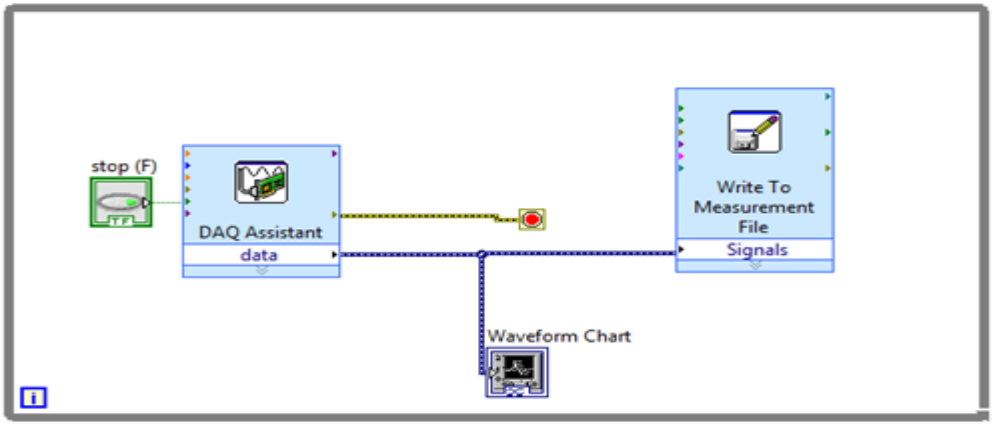

Figure 3.15 The Block Diagram

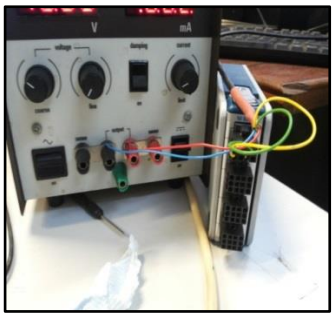

Data logger and power supplier

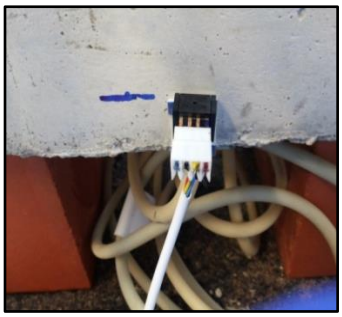

Sensor

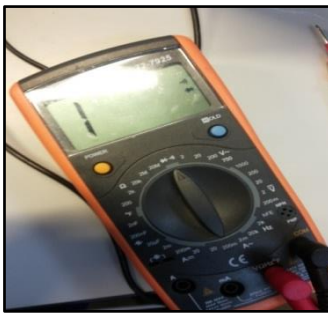

Voltmeter

Figure 3.16 The DAQ assistant, Sensor and Voltmeter

3.2.3.2.2 Pressure Sensor Implementation

The pressure sensor, model PX26-001GV, from Omega was used to measure water pressure (Omega, 2015). This sensor has a silicon diaphragm and unique conductive seal to increase reliability. The measurement range of the sensor is converted 0-1 psi to (0-6900 Pa) and it requires a 10V DC supply. It does not require external calibration. The PX26-001GV has guaranteed long-term stability, low hysteresis effects, and high output repeatability. Similar attributes were mentioned in the earlier research as a requirement for water pressure measurement (Browne, 2005). The PX26-001GV pressure sensor has an output voltage of 0-16.7 mV/V over its full range the accuracy 1% Fs (full scale), with response time 1 msec. It is worth to mention that the PX26-001GV is a gauge referenced pressure transducer, so at atmospheric pressure it will read zero.

3.2.4 Repeatability of the Test

For each test configuration, three tests were performed to evaluate the repeatability of the test. The number of tests done was [(2(water depth) × 2(Loading rate) x 4 (Frequencies)x 7(tread shape and depth) =112 cases] and each case repeats three times which equal to 336 tests for scenario 1 and 336 for scenario 2. The results showed agreement within 5%, which is indicative of good repeatability of the adopted method. Results are discussed in Chapter 4.

3.2.5 Reproducibility of the Test

After completing the first series of test, the same test configuration was repeated with different sensor to measure water pressure. The degree of agreement was found within 5% range. This indicates good reproducibility of the test method. Details descriptions are given in Chapter 4.

Part 3 Material Selection and Mixture Design

The material used to make concrete base and asphalt surfaces including their mixture design are presented in the following section.

3.3.1 Concrete Base Slab

Nominal maximum size 10mm limestone aggregate was used to produce C40 concrete base slab. The size of the slab was 300 mm × 300 mm × 100 mm with void 200 mm × 200 mm × 50 mm. Figure 3.17 shows the schematic of the manufactured concrete base. The aggregate gradation and w/c ratio were according to BS EN 1766. As mentioned in section 3.2.1, the purpose of the concrete base was to provide boundary and robust platform for asphalt surface, to provide a means of adding water, and to minimize water penetration to the lower layer. This arrangement was found useful to minimize the influence of lower asphalt layer on the performance of asphalt surface. The slotted concrete slabs were used to provide confinement and an impermeable base so that all water is stored within the asphalt surface, i.e. no water percolate in the lower layer. This is to simulate the worst-case scenario on the flooded surface.

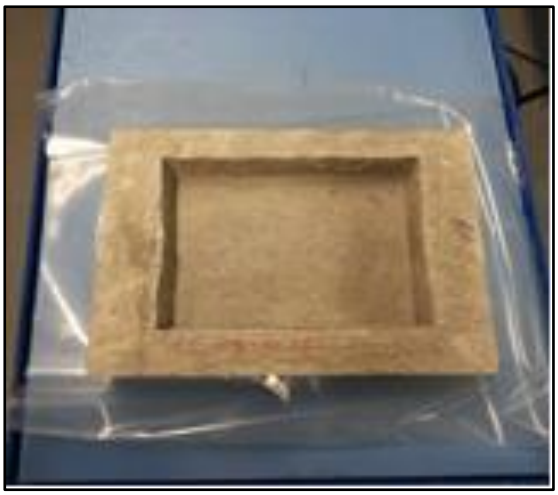

Figure 3.17 Manufactured concrete base

3.3.2 Asphalt Surface

The coarse, fine and filler aggregate fractions used to manufacture asphalt surface course mixtures were supplied by CONEXPO, (NI) LTD (CONEXPO, 2016). The specifications of the material conform to BS EN 13043:2002. A softer grade bitumen 150/100 pen was used for all mixtures. The bitumen was supplied by Total Bitumen UK (Total, 2016).

The specific gravity for the coarse and fine aggregates, filler and bitumen fractions of the mixtures were made available by the producers. The grading and specifications of the aggregate, filler and bitumen are listed in Table 3.1.

Table 3.1 Aggregate and bitumen specification

Component	Type	Size specifications			Specific gravity
		14mm	10mm	6mm	
Coarse aggregate	Granite	6.3/14	4/10	2/6mm	2.70
Fine aggregate Filler	Granite	0/4mm			2.70
Bitumen	Total	100/150 Pen			1.01

3.3.3 Mixture Design

Three various range of void contents used surface course mixtures were chosen. They were stone mastic asphalt (Open SMA), hot-rolled asphalt (HRA) and porous asphalt (PA). Mixtures were designed using relevant BS EN standards. The gradation of each mix, together with its reference to standard is given in Table 3.2. The 6 mm HRA and 10 mm Porous asphalts were not tested, as they are not widely used surfacing type. The gradation curves are given in Figures 3:18 to Figure 3.23.

Table 3.2 Mixture design gradation

Sieve size	HRA BS EN 13108-4:2016		Open SMA BS EN 13108-5:2016			PA BS EN 131087:2006
	Nominal maximum aggregate size (mm)					
	14mm	10mm	14mm	10mm	6 mm	14 mm
22.4	-	-	-	-	-	100
20	100	-	100	-	-	-
16	-	-	-	-	-	94
14	96.5	100	96.5	100	-	-
11.2	-	-	-	-	-	75
10	75	98	47.5	93	100	-
6.3	-	42	29	28	96.5	-
5.6	-	-	-	-	-	20
4.76	-	-	-	-	33.5	-
2	66	40	23	16	27	15
0.5	35	19	-	-	-	8
0.25	27.5	9	-	-	-	-
0.063	9	6	9	8	11	4.5
Bitumen Grade	150/100	150/100	150/100	150/100	150/100	150/100
%Bitumen content by mass	8.2	8	5.8	6.2	6.6	4.5

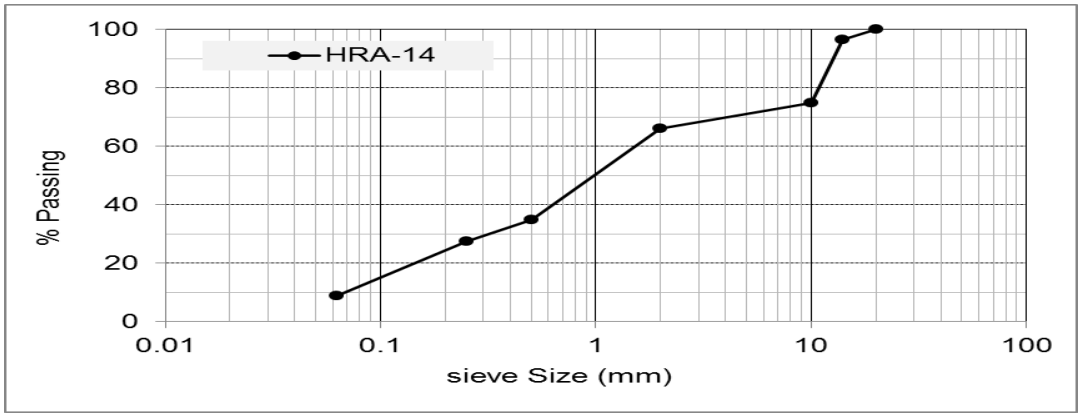

Figure 3.18 Gradation curve for 14 mm HRA

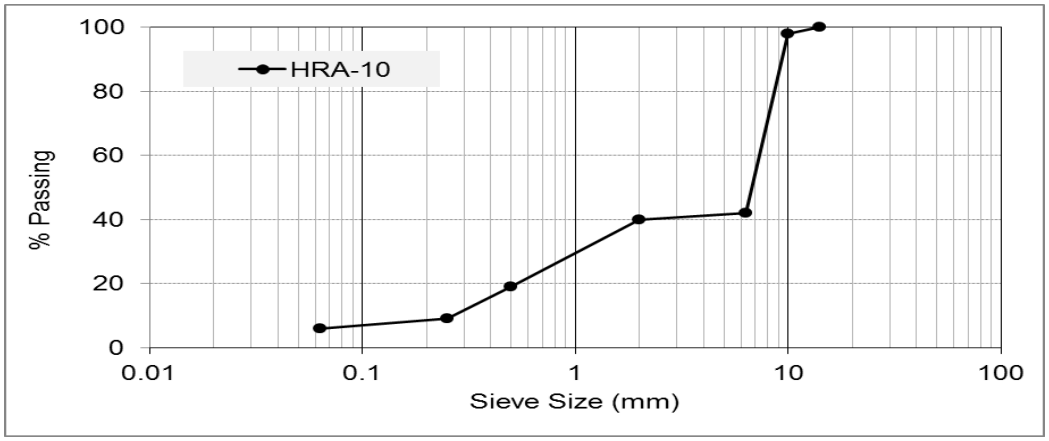

Figure 3.19 Gradation curve for 10 mm HRA

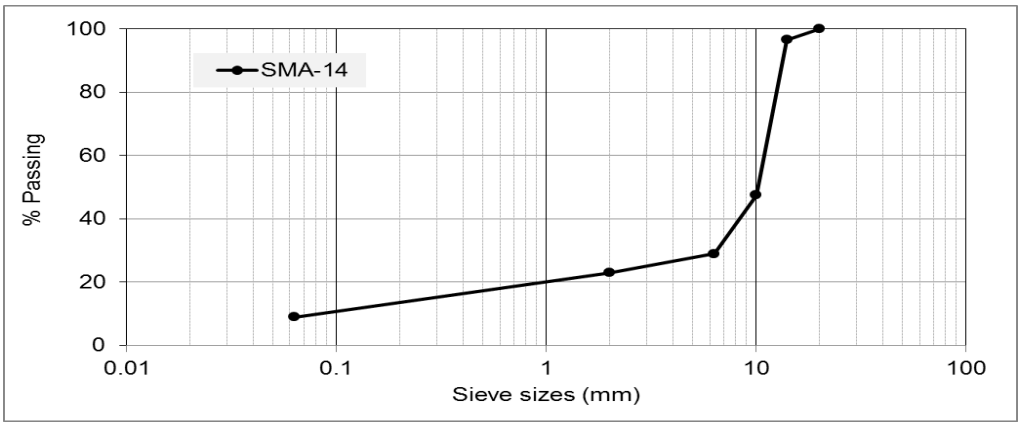

Figure 3.20 Gradation curve for 14 mm Open SMA

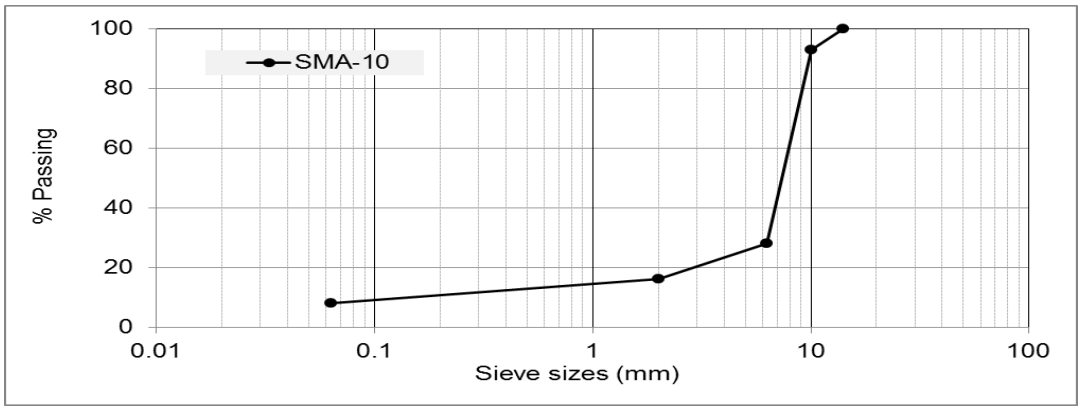

Figure 3.21 Gradation curve for 10 mm Open SMA

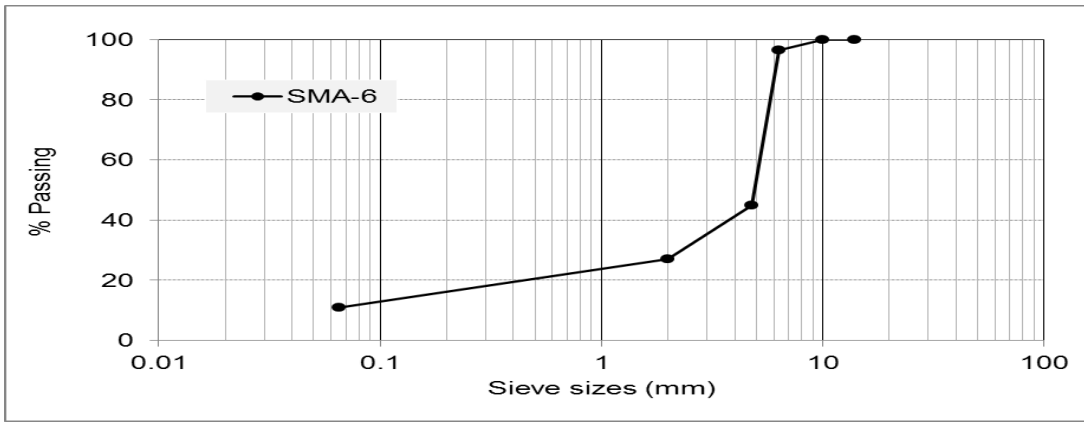

Figure 3.22 Gradation curve for 6 mm Open SMA

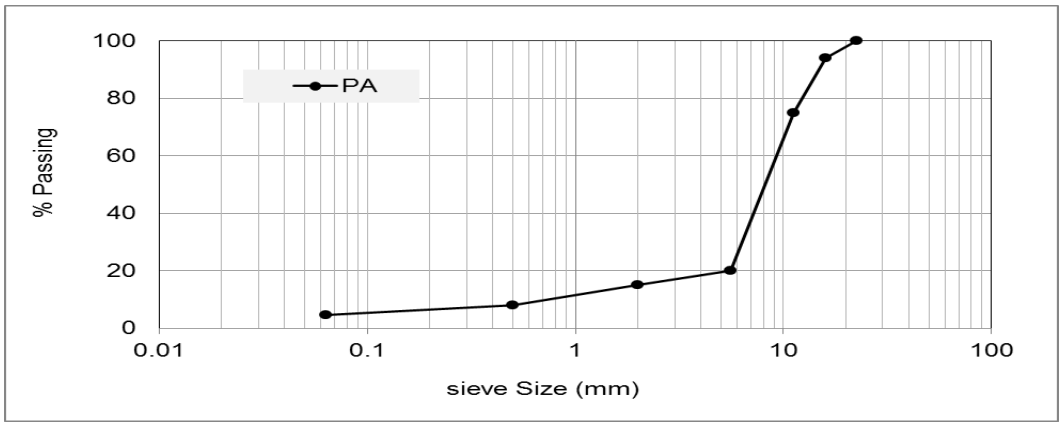

Figure 3.23 Gradation curve for 14 mm PA

The volumetric propoertions of all mixtures with 14mm maximum aggregate size are given in Figure 3.24.

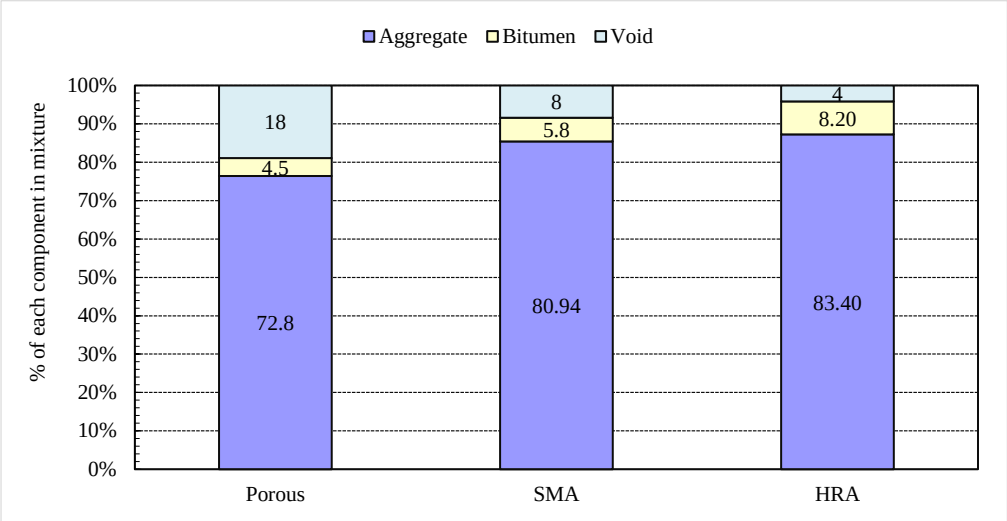

Figure 3.24 Percentages of each component by mass for 14 mm (PA, Open SMA and HRA)

Proportions of other mixtures and detail calculations are given in Appendix D.

Additional slabs were made by replacing the filler with substituting mineral fillers for 10mm Open SMA, 14mm Open SMA, 10mm HRA and 14mm HRA mixtures.

3.3.4 Mixing

The mixing process of aggregate, filler and bitumen is given in Figure 3.25. The material was thoroughly mixed prior to the addition of pre-heated bitumen. The mixing continued at 145^0C until all material thoroughly mixed together. The aggregates, bitumen and filler were mixed according to BS EN 12697-35: 2004 (British Standards Institution, 2004).

Figure 3.25 Mixing of asphalt material

3.3.5 Asphalt Compaction

The loose mixture was then poured into a preheated custom build split 200 mm × 200 mm × 50 mm square steel mould (shown in Figure 3.26) at 140 C° and then compacted using a handheld vibrating compactor to the desired slab thickness to achieve the required air void content. It was easier to place the mixture into the square mould with removable base, and after compaction, it was easier to remove the specimen without disturbing the mixture matrix.

Figure 3.26 Removable base mould for aspahlt surface

A picture of the compaction device, compacted specimens and the specimen inside the slotted section in the concrete slab is shown in Figure 3.27.

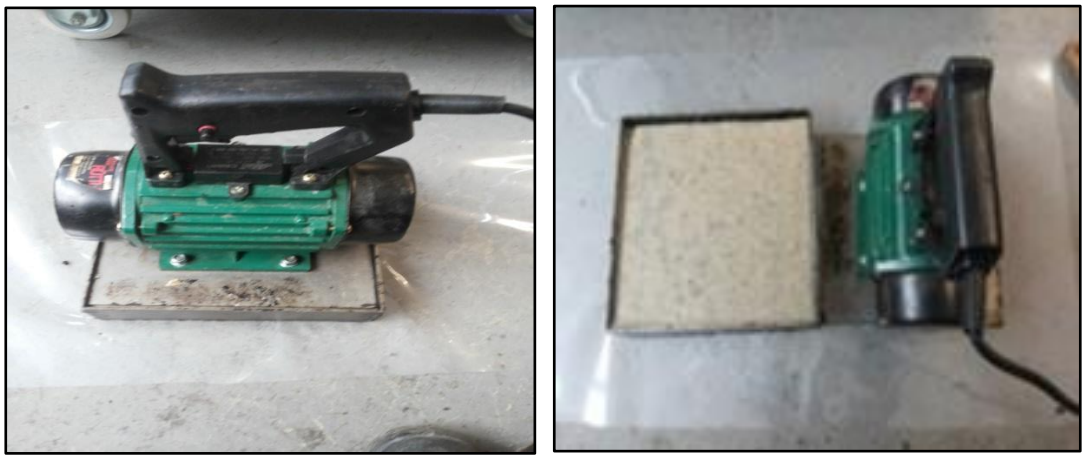

Figure 3.27 Slabs and hand held vibrating plate

It should be noted that the direct force applied to the slab, and the vibration frequency were chosen before compaction and therefore, can be assumed as constant throughout the compaction process. Previous research has demonstrated that the procedure could be used to simulate field compaction (Georgiou and Loizos, 2014). The compacted samples for OPEN SMA mixtures are shown in Figure 3.28.

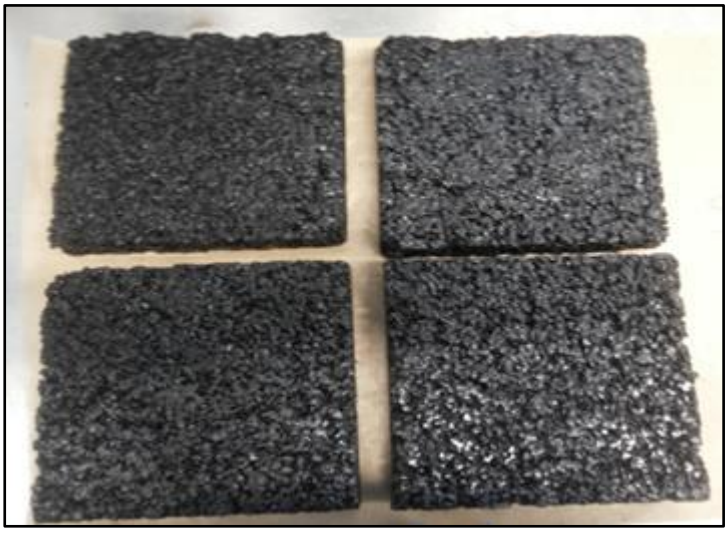

Figure 3.28 6 mm Open SMA slabs

3.3.6 Mixture Volumetric

The dimensions of each specimen were measured and then tested for bulk density as detailed in BS EN 12697-6: 2003 (British Standards Institution, 2003). The actual percentage of air voids of each test specimen were calculated according to BS EN 12697-8: 2003 (British Standards Institution, 2003). The target void content was 8-13% for the Open SMA (Stone Mastic Asphalt); it was 4-6% for the HRA (Hot Rolled Asphalt) and >16% for the PA (Porous Asphalt). The sample properties are given in Table 3.3.

Table 3.3 Specimens properties

Mixture Type	Aggregate properties			No of sample	Specimen Size (mm^3)	Void contents (%)		
	Nominal maximum size (mm)	Type	Filler			Max	Min	Std
HRA	10	Granite	Granite	6	200×200×50	7.81	5.97	0.736
	14	Granite	Granite	6	200×200×50	8.00	5.20	1.017
Open SMA	6	Granite	Granite	6	200×200×50	12.78	8.97	1.421
	10	Granite	Granite	6	200×200×50	13.63	10.36	1.371
	14	Granite	Granite	6	200×200×50	12.50	10.33	1.024
PA	14	Granite	Granite	6	200×200×50	20.89	18.00	1.315

3.3.7 Testing Programme

Six identical specimens were produced for each mixture combination to evaluate test repeatability and the sufficient number of specimens for statistical analysis. The specimens were kept inside the mould for 24 hours at room temperature and then extracted and placed inside a similar size prefabricated slot in a 305 mm ×305 mm × 100 mm size C40 concrete slab. Adopted test setup is given in Figure 3.29 and Figure 3.30 shows asphalt specimens in concrete slab ready for testing.

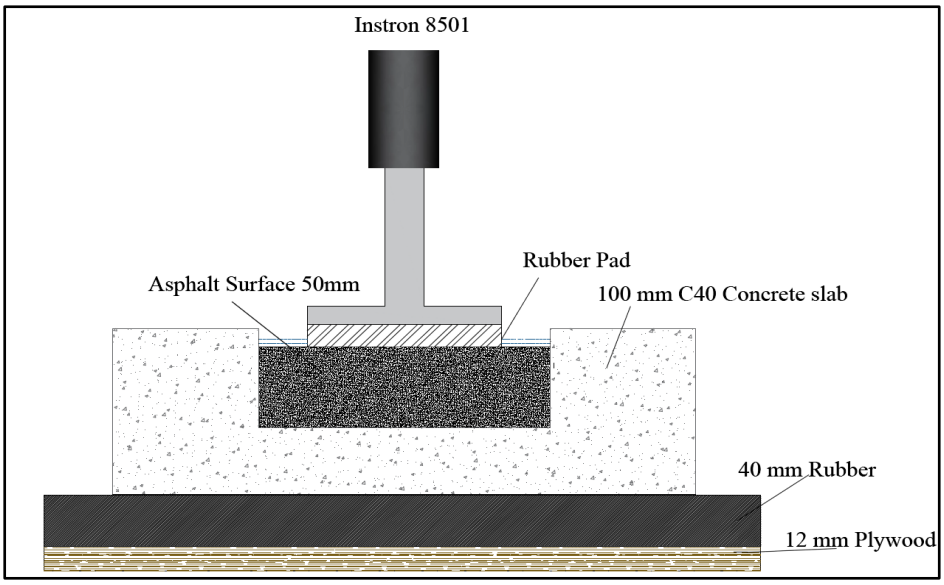

Figure 3.29 Lab site and asphalt specimens in concrete slab ready for testing

Figure 3.30 Specimens in concrete slab ready for testing

The testing programme was divided into the following two parts,

- The first part (presented in Chapter 4) was to measure water pressure under dynamic loads with different tyre characteristics and depth of surface water on concrete base alone and concrete base overlaid with stone mastic asphalt surface. This chapter will also present results from repeatability and reproducibility tests.

- The second part (presented in Chapter 5) was to select most severe case for water pressure from part 1 and continue the test until the surface damage becomes eminent. This series of test was done on all three types of surfaces.

The details test specifications are given in the relevant chapters.

3.4 Summary

In this chapter, the detail explanation of initial test, design of adopted test, material specification and testing programmes are presented. The preliminary study showed that highest water pressure occurs at the centre of the loading plate. Based on the preliminary test results, the adopted test method was designed to automatically control loadings at different frequencies and collect water pressure data under the slab with shallow flooding. The purpose of the adopted test was not only to measure water pressure, but also to investigate asphalt surface performance when subjected to combined interaction of loading-tyre-water-pavement.

The preliminary investigation determined that highest water pressure happens at the middle of the loading plate with the maximum pore water pressure at low frequency loading (1Hz) was about 913Pa. Based on the preliminary outcomes, a 913Pa pore water pressure sensor was employed in the adopted test and was optimized to use a single sensor directly under the loading plate.

The next chapter will present detail experimental programme and results on water pressure measurement in both idealised pavement scenarios.

Chapter 4 Impact of Tyre and Traffic Parameters on Water Pressure in Pavement

4.1 Introduction

The adverse impact of water on pavement durability is a well-known concern in the pavement engineering community. As mentioned in the literature review (Chapter 2), studies on water related distresses are predominantly manifested towards material degradation due to loss of adhesion and/or cohesion of the mixture matrix for asphalt pavement or failure of joints and foundation in concrete pavement. In addition, many modern types of asphalt road surfaces, such as stone mastic asphalt (OPEN SMA), porous asphalt (PA), experience premature failure in the form of ravelling and cracking, leading to pothole and/or other structural failure.

Review of available literature showed that the water pressure is reliant on tyre characteristics (tyre pressure, tread shape, depth, and patterns), traffic characteristics (magnitude, speed) and mixture configurations such as size and gradation of aggregate, void contents and level of compaction. For instance, in dense and close graded surface course (voids content < 4%), the water infiltration is comparatively low and slow, whereas water drains freely in high void content mixtures such as in porous asphalt. Uniformly graded mixture with intermediate void contents, 6%-12%, may experience water infiltration and water storage inside the mixture. Besides, water may also pass through cracks or blocked interconnected voids caused by debris and creates a capillary force at the layer interface when subjected to traffic loading, which may eventually be damaging to interlinked bonds. In concrete pavement, water infiltration within crack/joints may cause water pressure produced at the bottom of the slab when traffic crosses over the water-filled crack/joint. This infiltration can create voiding under a slab, which eventually can cause asymmetric loading and poor load transfer across joints/crack.

It is generally believed that the water on the surface or water build up inside the pavement exacerbates this pressure, which may result in pavement surface layer spalling or loosening, cracking, rutting and leading to localised and eventually structural damage (Kim et al., 2008; Willway et al., 2008; Karlson, 2005; Lindly and Elsayed, 1995; Dong et al., 2007). Some of the distresses directly related to water and others are accelerated by the action of water. So, the presence of water, either directly or indirectly, influences the performing of asphalt pavement.

In the available literature on water pressure in pavement (presented in chapter 2), most studies were found to be computational and/or analytical. Experimental studies are extremely limited as simulating tyre pavement interaction and related water pressure accurately in real pavement and even in the laboratory environment are extremely difficult. This is due to the complexity of tyre interaction with the pavement structure, variability of materials and influence of other factors such as layer deboning, vehicle speed, tread shape and pattern, for example.

In this chapter, the concept illustrated in section 3.2.1 in chapter 3 was used to study the influence of tread depth, tread pattern, loading range and frequency range and water depth on the magnitude of water pressure under dynamic loading. The procedure for test set-up, test specifications, results from repeatability and reproducibility of the test, and finally, analysis and interpretation of test data are presented in this chapter. All tests were done on both idealised pavement structures presented in section 3.2.1 and results were also compared with previous similar studies found the literature.

4.2 Test Set-Up

Two C40 concrete slabs (300 mm x 300 mm x 100 mm) were manufactured (details are in chapter three section 3.1.1). Preliminary study was carried out to measure pore water pressure in eight pore holes under the loading patch, by using a manometer. The test results, presented in Chapter 3, showed that the maximum pressure is generated at the middle pore hole. Therefore, it was decided to use single pore measurement. As this study is mainly to evaluate the impact of tyre characterises, loading frequencies and depth of surface water on water pressure, the distribution under the contact patch was not included.

The test was conducted in two scenarios as explained below (detailed descriptions and schematic layout are presented in section 3.2.1)

- In scenario 1, the recess area in concrete surface was filled with water to simulate water pressure under the slab when water is forced through a narrow crack (2 mm) during traffic loading. This scenario is also used to test experimental setup for its consistency and repeatability of the test. Schematic diagram is given in Figure 3.12 in Chapter 3.

- The purpose of scenario 2 was to evaluate the impact of a 20 mm semi permeable asphalt surface laid on the 100 mm concrete slab with 2 mm wide full depth crack. The average texture of the asphalt surface was measured as 1.27 mm. The asphalt surface was saturated to minimise the impact of surface texture and maximise the effect of internal voids. The concrete slab was used in the idealised pavement structure to simulate the lower layers of asphalt (binder and base). The impermeable concrete slab eliminates the complication of water saturation in lower asphalt layers, which could potentially influence the water pressure. A schematic diagram of the idealised pavement in scenario 2 is given Figure 3.13 in Chapter 3.

4.3 Test Specifications

The test performed in this project is a non-destructive in nature for measuring pore water pressure under asphalt concrete. The test was suitable for this project, as it can apply a repeated sinusoidal vertical load. This would be a reasonable reproduction of the on-field conditions of a load generated by the traffic load. The test was a controlled stress type test in which the magnitude of the applied stress pulse is maintained constant for the required number of cycles. Therefore, the principle of this testing was that a specimen is exposed to repeated sinusoidal compressive load, developing a relatively uniform tensile stress both perpendicular and parallel to the direction of the applied load. Test setup given in Figure 3.14 in Chapter 3.

As mentioned in section 3.3.3 (in Chapter 3), the testing was conducted using an INSTRON 8501 servo-hydraulic testing rig, capable of applying loads at 0.1Hz to 50Hz in the 1kN to 100 kN load range. The test consisted of running the equipment at a required load for a given frequency and water depth, recording the resulting amplitude of water pressure under the slab. By repeating the test on each tread enables the influence of tread shapes to be evaluated. There were some variations in the water pressure measurement. This was due to the difficulty of maintaining constant level of surface water during load applications.

Each test case was repeated for three times to check the repeatability and reproducibility. The test specifications are given in Table 4.1 and the flow chart of test sequence are given in Figure 3.9 in Chapter 3.

As shown in Table 4.1, the depth of surface water was kept to 2mm and 4mm, to avoid complete submerging of the loading plate. Four tread depths and three tread shapes were used according to idealised cases presented in Chapter 3 section 3.1.3. The magnitude of applied dynamic compression loads were selected to as 5kN and 10kN to simulate light and heavy vehicle loading and they were applied in four different frequencies. The wave form of the load was chosen as sinusoidal to simulate actual traffic movement and allow time for water to fill the loaded area between loading cycles. It should be noted that the maximum frequency used in this research was 15 Hz due to safety reasons and also difficulty of maintaining water depth at very high frequency testing. To convert frequencies (Hz) to speed (Km/h), equation developed by Brown (1974) was used (see section 4.4.9).

Table 4.1 Pore water pressure test specifications

Variable	Specifications
Surface water depth (mm)	2, 4
Tyre Tread Type	Square, Slot, No tread
Tread Depth	0, 1.5, 3 and 8 mm
Load (KN)	5, 10
Loading Frequency (Hz)	1, 5, 10 and 15
Loading speed (Km/h)	0.69, 3.84, 8.02 and 12.48
Type of Load	Dynamic compression
Load Duration (sec)	6.7-10

In total 112 cases had been tested. The test was named as 8SQ4, which refers to 8mm tread depth, square tread pattern and 4mm water depth and so on (detail explanation is given in Chapter 3 section 3.1.3). For each frequency, the test was run to capture ten continues pulses and was repeated for three times. The average, maximum and minimum values were used for analysis.

4.4 Results and Analysis

4.4.1 Signal Output

Figures 4.1 and 4.2 show the load/stress signal at 1Hz - 5kN and 1Hz-10kN respectively, and corresponding pore water pressure when pavement was submerged with 2mm surface water is presented in Figures 4.3 and 4.4.

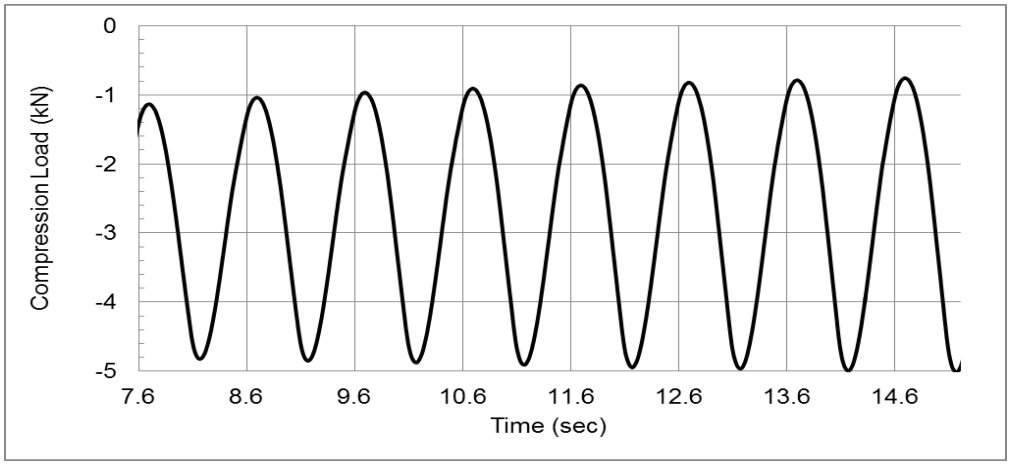

Figure 4.1 Load/Stress signal of 5kN at 1Hz

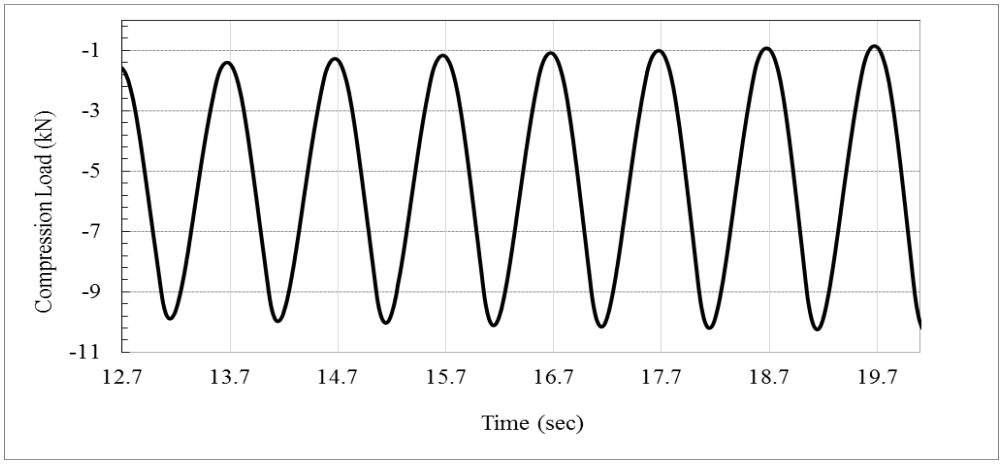

Figure 4.2 Load/Stress signal of 10 kN at 1Hz

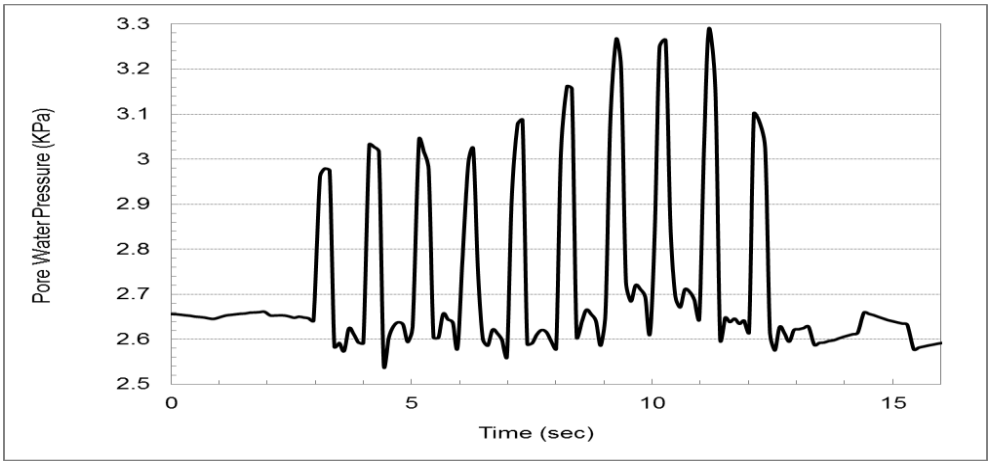

Figure 4.3 Signal of pore water pressure of 10 kN at 1Hz

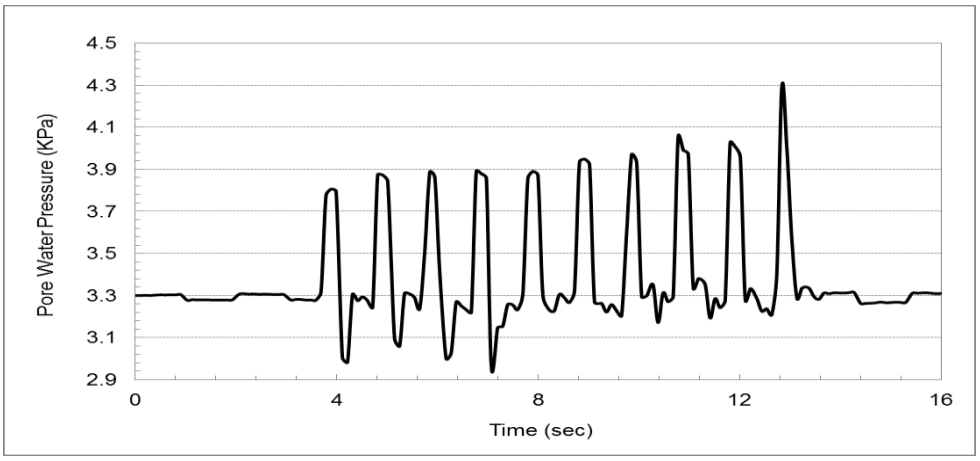

Figure 4.4 Signal of pore water pressure of 10 kN at 1Hz

It is evident in Figures 4.3 and 4.4 that the dynamic pressure was formed while the film of water on slab surface was pressurised by repeated vertical load. Positive pressure was generated in the pore at the bottom of the slab. It is important to note that the accuracy of load pulses was very good with no visible sign of signal distortion. However, despite cyclic nature, the corresponding pore water pressure signal was variable. This variability was higher in high frequencies as shown in Figure 4.5 for 10Hz frequency water pressure pulse.

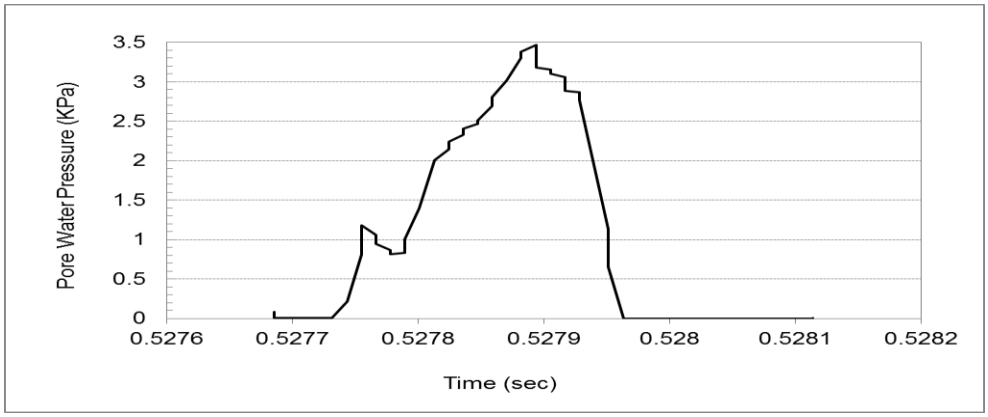

Figure 4.5 Signal of pore water pressure of 5 kN at 10 Hz

At low frequency loading, sufficient time between load intervals allows water to move under the loading plate and fill the pore. However, there was not enough time to fill the pore between load pulses when applied at high frequencies. To reduce this issue, constant water feeding was maintained. It should be noted that, despite this variability, the maximum water pressure at a particular frequency was similar in the repeat test.

4.4.2 Repeatability

For each test configuration, three tests were performed to evaluate the repeatability of the test method. The signal outputs for three tests at 1Hz 10kN load is presented in Figure 4.6. It can be seen that the load pulses are very similar in all cases. Testing at other load and frequencies showed similar level of accuracy.

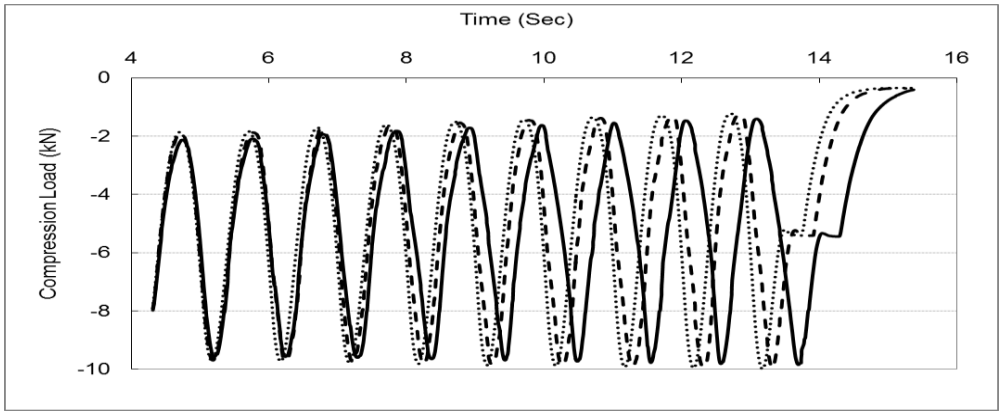

Figure 4.6 Signal output from three repeat tests at 10kN and 1Hz

The pore water pressure signal output for 1 Hz, 10 Hz and 15Hz at 5kN load configuration for three repeat tests are given in Figure 4.7 to Figure 4.9.

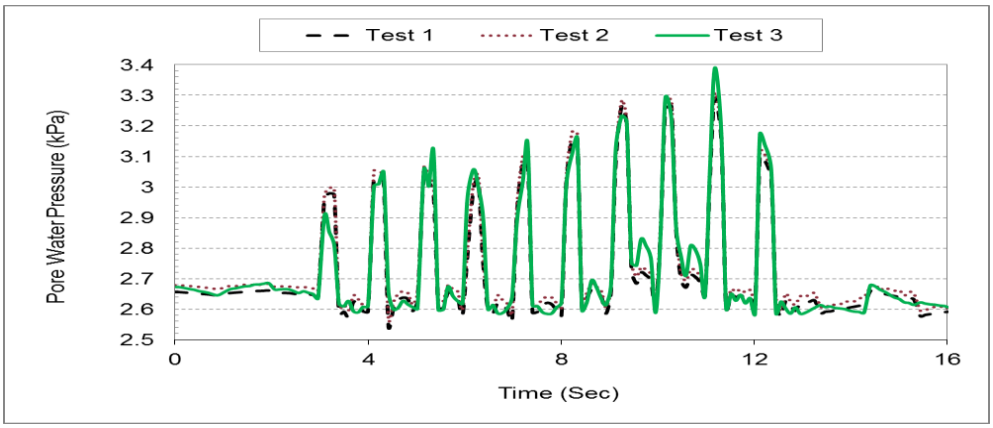

Figure 4.7 A repeated typical signals output at 1Hz and 5kN test configuration

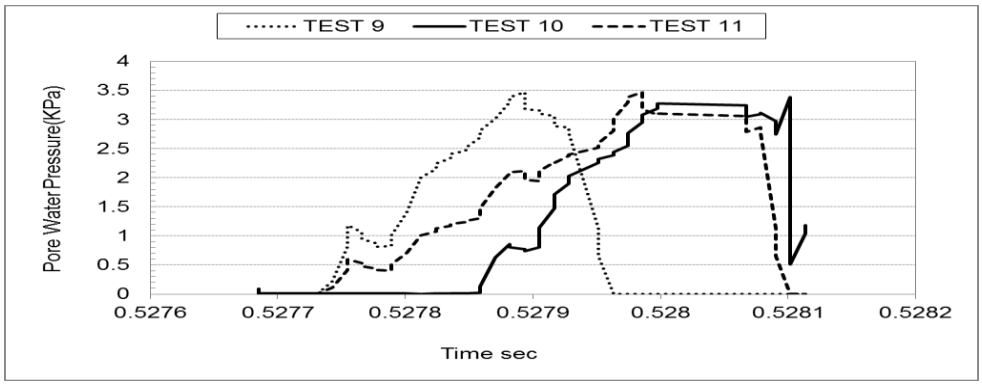

Figure 4.8 Signals output for three test at 10 Hz and 5kN load configuration

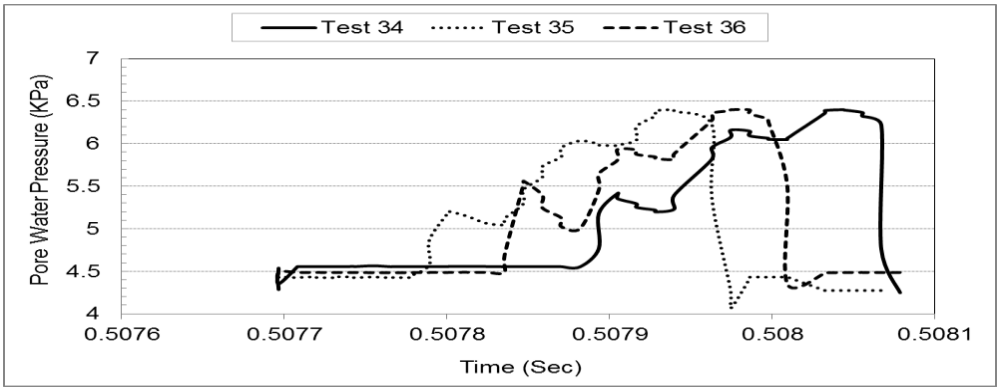

Figure 4.9 Signals output for three test at 15 Hz and 5kN load configuration

As mentioned in the previous section, unlike load pulse, the signal outputs for pore water pressure were not smooth. The variability increased with increasing frequency with highest being in 15Hz frequency. However, despite the variability of signal output, the maximum magnitude for each test was close. For example, the maximum water pressure at 10Hz-5kN load was close to 3.5kPa, whereas at 15Hz-5 kN case the magnitude was close to 6.5 kPa in all three tests. Similar results were obtained for other test cases. For brevity, the maximum and minimum and STDV were presented in appendix B.

4.4.3 Reproducibility

After completing the first series of test, the same test configuration was repeated with different sensor to measure water pressure. The degree of agreement was found within 5% range. This indicates good reproducibility of the test method.

4.4.4 Results of Pore Water Pressure in Both Scenarios

The data are analysed to evaluate the influence of load magnitude and frequency, tread patterns and depth on the pore water pressure through a 2mm pore extended through the depth of the slab. The average of maximum pore water pressure from three tests for all test cases is presented in Tables 4.2 and 4.3. The test results are also shown in graphical forms in Figures 4.12, to 4.15; for scenario 1 and in Figures 4.16, to 4.19 for scenario 2.

Table 4.2 Observed pore water pressure under the concrete slab

Test No	ID	FREQ.	Max				Min				STDV			
			Water Depth 4mm		Water Depth 2mm		Water Depth 4mm		Water Depth 2mm		Water Depth 4mm		Water Depth 2mm	
			5KN	10KN	5KN	10KN	5KN	10KN	5KN	10KN	5KN	10KN	5KN	10KN
1-4	1.5 SQ	1HZ	2.712	3.710	2.702	3.633	2.645	3.559	2.180	3.459	0.034	0.082	0.287	0.092
5-8	1.5 SQ	5HZ	3.858	4.577	2.793	3.822	3.747	4.321	2.730	3.718	0.059	0.128	0.033	0.053
9-12	1.5 SQ	10HZ	3.732	4.907	3.242	4.851	3.600	4.775	3.149	4.756	0.076	0.066	0.050	0.048
13-16	1.5 SQ	15HZ	4.894	5.213	4.893	5.133	4.870	5.042	4.301	4.985	0.014	0.093	0.319	0.079
17-20	3 SQ	1HZ	3.080	4.662	2.991	3.150	3.029	4.528	2.946	3.015	0.027	0.072	0.025	0.078
21-24	3SQ	5HZ	4.266	5.390	3.900	5.240	4.172	5.215	3.796	5.161	0.048	0.088	0.059	0.040
25-28	3 SQ	10HZ	4.713	5.431	3.943	5.390	4.637	5.395	3.866	5.309	0.040	0.020	0.042	0.046
29-32	3SQ	15HZ	5.371	5.921	4.613	4.877	5.330	5.702	4.576	4.765	0.022	0.115	0.021	0.060
33-36	8SQ	1HZ	4.638	5.843	2.851	3.895	4.163	5.685	2.796	3.783	0.258	0.089	0.031	0.056
37-40	8SQ	5HZ	4.725	5.556	4.633	5.433	4.652	5.454	4.558	5.240	0.037	0.055	0.038	0.096
41-44	8SQ	10HZ	5.861	6.214	5.431	5.959	5.793	5.968	5.329	5.865	0.037	0.133	0.056	0.048
45-48	8SQ	15HZ	6.383	6.893	6.234	6.653	6.199	6.665	6.125	6.585	0.097	0.088	0.055	0.036
49-52	1.5SL	1HZ	2.790	3.690	2.728	3.603	2.729	3.559	2.642	3.519	0.031	0.069	0.046	0.043
53-56	1.5SL	5HZ	2.779	3.844	2.225	3.714	2.755	3.733	2.185	3.676	0.012	0.056	0.022	0.020
57-60	1.5SL	10HZ	2.715	4.882	3.252	4.861	2.599	4.763	3.151	4.741	0.063	0.065	0.058	0.065
61-64	1.5SL	15HZ	3.149	5.209	4.403	5.091	3.048	5.073	4.321	4.985	0.051	0.074	0.047	0.053
65-68	3SL	1HZ	2.104	4.649	1.863	2.128	2.043	4.528	1.753	2.066	0.032	0.061	0.059	0.031
69-72	3SL	5HZ	2.362	3.402	1.932	3.325	2.294	3.373	1.903	3.290	0.035	0.014	0.015	0.019
73-76	3SL	10HZ	2.504	5.249	1.993	4.798	2.422	4.954	1.940	4.679	0.041	0.150	0.027	0.069
77-80	3SL	15HZ	3.501	5.425	2.276	5.413	3.329	5.303	2.228	5.269	0.090	0.065	0.025	0.079
81-84	8SL	1HZ	2.820	3.604	2.245	3.524	2.758	3.591	2.200	3.493	0.032	0.007	0.023	0.017
85-88	8SL	5HZ	3.023	4.363	2.515	4.281	2.939	4.338	2.441	4.232	0.045	0.014	0.037	0.026
89-92	8SL	10HZ	3.399	5.106	3.365	5.044	3.390	4.834	3.311	4.802	0.005	0.137	0.027	0.138
93-96	8SL	15HZ	4.232	5.467	3.711	5.225	4.214	5.319	3.614	5.131	0.009	0.082	0.049	0.051
97-100	NT	1HZ	1.315	1.333	0.692	1.302	1.272	1.303	0.672	1.275	0.022	0.015	0.012	0.014
101-104	NT	5HZ	1.346	1.377	0.894	1.335	1.308	1.361	0.866	1.323	0.020	0.008	0.016	0.006
105-108	NT	10HZ	1.544	1.629	1.008	1.507	1.496	1.582	0.974	1.473	0.025	0.024	0.020	0.017
109-112	NT	15HZ	1.618	1.690	1.102	1.588	1.581	1.651	1.024	1.534	0.019	0.021	0.041	0.027

Table 4.3 Observed pore water pressure under concrete slab using asphalt overlay

Test No	ID	FREQ.	Max				Min				STDV			
			Water Depth 4mm		Water Depth 2mm		Water Depth 4mm		Water Depth 2mm		Water Depth 4mm		Water Depth 2mm	
			5KN	10KN	5KN	10KN	5KN	10KN	5KN	10KN	5KN	10KN	5KN	10KN
1-4	1.5 SQ	1HZ	2.378	2.631	2.102	2.311	2.254	2.581	2.244	2.081	0.063	0.026	0.035	0.011
5-8	1.5 SQ	5HZ	2.512	3.244	2.372	3.107	2.462	3.218	2.353	3.082	0.027	0.014	0.009	0.012
9-12	1.5 SQ	10HZ	3.105	3.311	3.075	3.095	3.014	3.242	3.011	3.091	0.049	0.036	0.032	0.002
13-16	1.5 SQ	15HZ	3.293	4.131	3.194	3.689	3.249	4.103	3.163	3.660	0.024	0.014	0.016	0.015
17-20	3 SQ	1HZ	2.512	2.773	2.443	2.626	2.462	2.753	2.419	2.551	0.027	0.011	0.014	0.039
21-24	3SQ	5HZ	3.360	3.584	3.044	3.339	3.313	3.528	3.028	3.243	0.024	0.030	0.009	0.051
25-28	3 SQ	10HZ	3.634	3.995	3.172	3.388	3.530	3.982	3.155	3.342	0.054	0.007	0.009	0.023
29-32	3SQ	15HZ	3.690	4.984	3.534	3.698	3.559	4.949	3.530	3.682	0.069	0.019	0.002	0.009
33-36	8SQ	1HZ	3.863	3.383	3.383	2.586	3.787	3.263	3.363	2.521	0.041	0.064	0.010	0.032
37-40	8SQ	5HZ	4.103	3.540	3.462	4.564	3.984	3.510	3.411	4.529	0.060	0.015	0.027	0.020
41-44	8SQ	10HZ	4.290	5.596	4.292	4.984	4.202	5.559	4.259	4.934	0.047	0.019	0.017	0.026
45-48	8SQ	15HZ	5.192	5.765	5.250	5.262	5.042	5.763	5.090	5.231	0.075	0.001	0.084	0.016
49-52	1.5SL	1HZ	1.948	2.153	2.298	2.108	1.915	2.138	2.253	2.066	0.016	0.007	0.023	0.022
53-56	1.5SL	5HZ	1.853	2.358	2.365	3.094	1.799	2.315	2.358	3.065	0.027	0.021	0.004	0.015
57-60	1.5SL	10HZ	2.304	3.392	3.034	3.096	2.175	3.372	3.010	3.088	0.065	0.010	0.013	0.004
61-64	1.5SL	15HZ	2.460	3.461	3.191	3.692	2.443	3.411	3.172	3.662	0.009	0.027	0.011	0.016
65-68	3SL	1HZ	2.165	2.372	2.112	2.096	2.158	2.333	2.072	2.066	0.004	0.020	0.020	0.015
69-72	3SL	5HZ	2.410	3.289	2.328	2.307	2.363	3.252	2.306	2.284	0.025	0.019	0.011	0.012
73-76	3SL	10HZ	2.881	3.388	2.654	2.391	2.818	3.344	2.600	2.343	0.032	0.022	0.029	0.026
77-80	3SL	15HZ	2.962	3.452	2.902	3.082	2.877	3.421	2.877	3.006	0.043	0.016	0.013	0.042
81-84	8SL	1HZ	2.511	2.444	2.453	2.665	2.452	2.439	2.432	2.635	0.030	0.002	0.011	0.015
85-88	8SL	5HZ	3.292	3.634	3.114	2.637	3.223	3.631	3.112	2.561	0.036	0.002	0.001	0.039
89-92	8SL	10HZ	4.069	4.247	3.998	3.054	3.994	4.241	3.986	3.015	0.041	0.003	0.006	0.020
93-96	8SL	15HZ	4.242	4.554	4.189	3.699	4.162	4.521	4.072	3.662	0.044	0.018	0.059	0.018
97-100	NT	1HZ	0.995	1.120	0.861	0.945	0.969	1.101	0.840	0.923	0.013	0.009	0.012	0.011
101-104	NT	5HZ	1.198	1.130	1.128	1.050	1.167	1.097	1.088	1.025	0.016	0.016	0.020	0.013
105-108	NT	10HZ	1.212	1.300	0.682	1.130	1.210	1.291	0.662	1.097	0.001	0.005	0.010	0.017
109-112	NT	15HZ	1.761	1.985	1.948	1.799	1.720	1.928	1.925	1.760	0.021	0.029	0.011	0.020

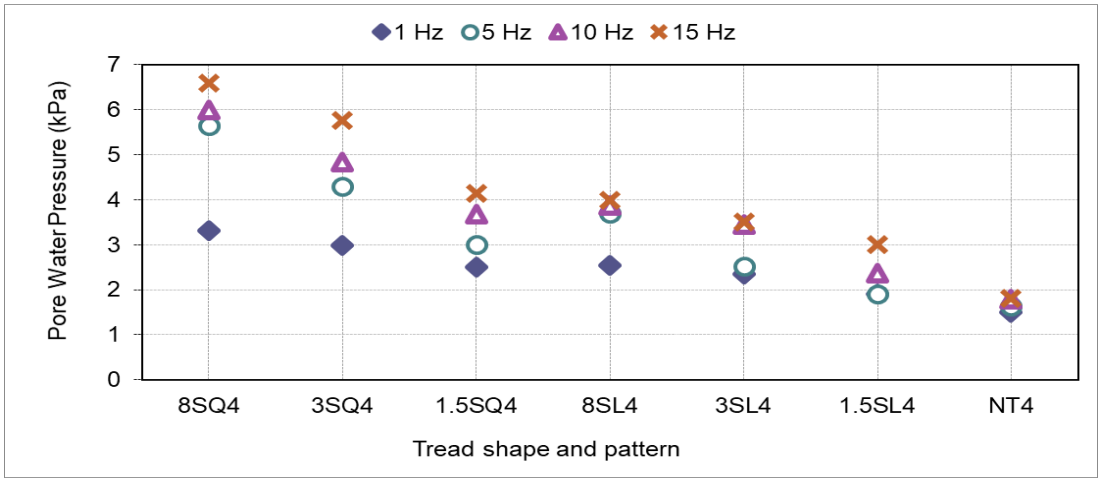

Figure 4.10 4mm surface water, load 5kN, no asphalt surface

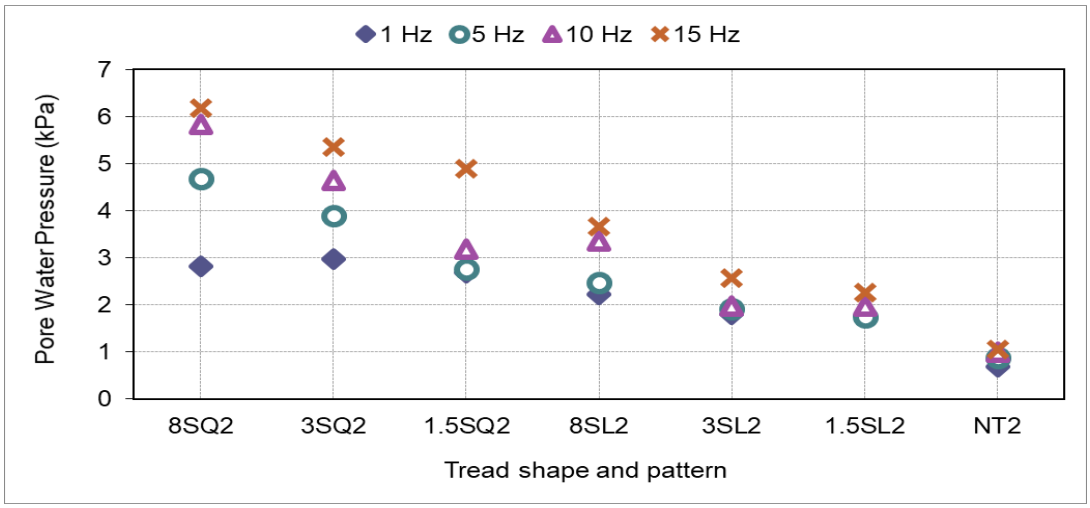

Figure 4.11 2mm surface water, 5 kN load, no asphalt surface

Figure 4.12 4mm surface water, 10kN load, no asphalt surface

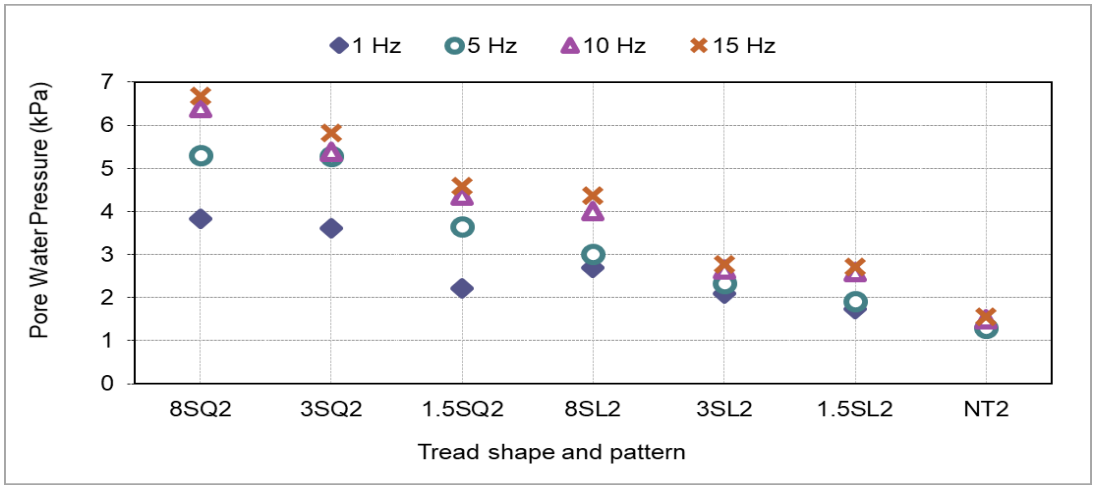

Figure 4.13 2mm surface water, 10 kN load, no asphalt surface

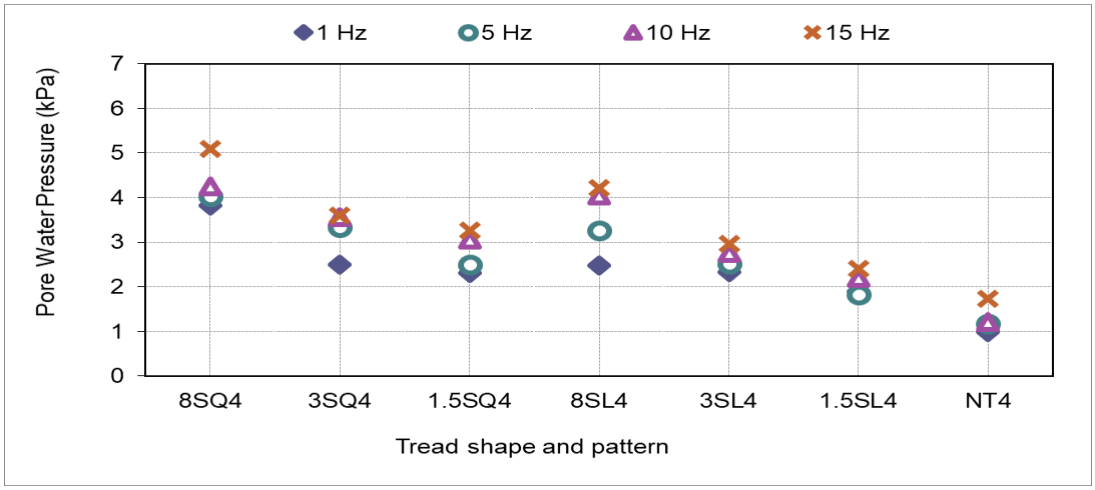

Figure 4.14 4mm surface water, 5kN load, with 20mm asphalt surface

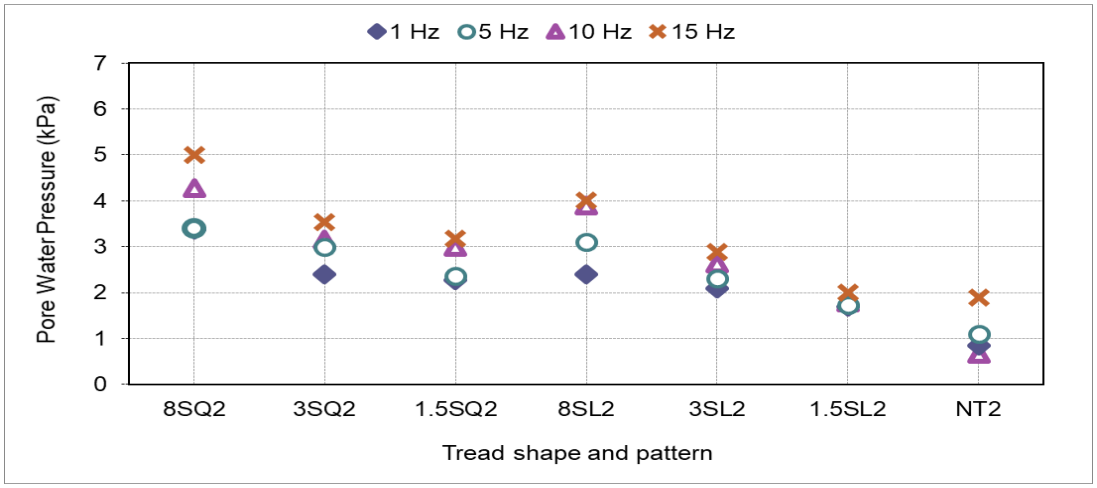

Figure 4.15 2mm surface water, 5kN load, with 20mm asphalt surface

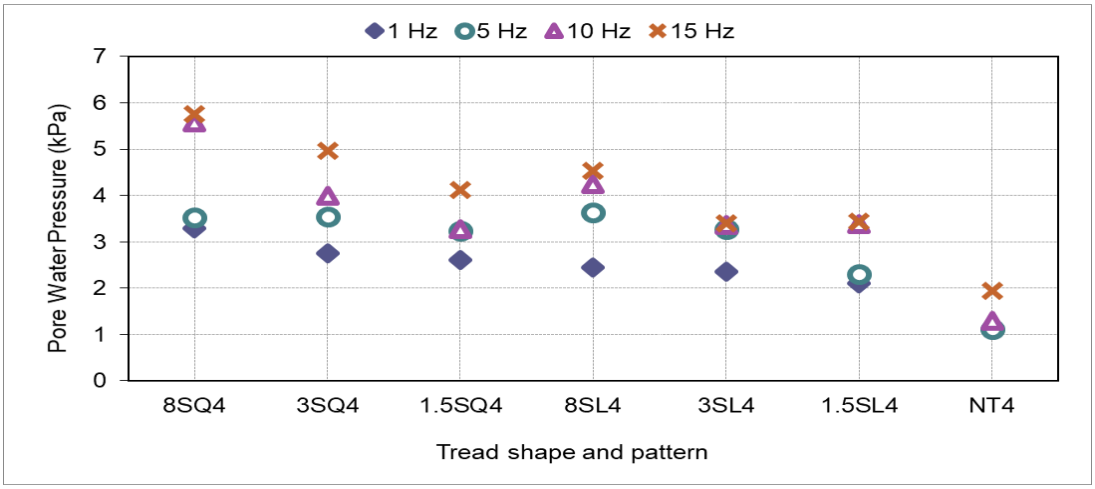

Figure 4.16 4mm surface water, 10kN load, with 20mm asphalt surface

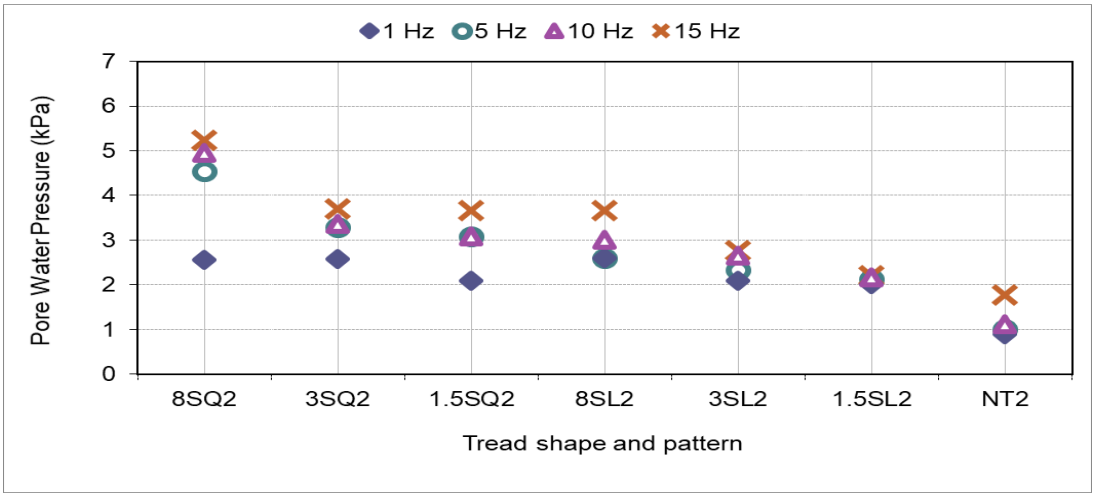

Figure 4.17 2mm surface water, 10kN load, with 20mm asphalt surface

4.4.5 Influence of Tread Shape and Pattern

It can be seen in Figures 4.10 to 4.17 that, at a specific frequency, irrespective of applied load, the maximum water pressure was occurred with the 8mm square tread (8SQ4) whilst the pressure decreases with decreasing tread depth, reaching minimum at the no tread situation. The maximum water pressure at 8SQ4 was 6.89 kPa, 3SQ4 was 5.921 kPa, and 1.5SQ4 was 5.213 kPa. And no tread cases it was 1.69 kPa. It is interesting to note that whilst water pressure was increasing with loading frequencies

in all treaded cases, in no tread cases only marginal changes happened despite increasing either load frequency or load magnitude.

4.4.6 Influence of Loading

From Figures 4.10 to 4.16, irrespective of surface water depth and load magnitude, the water pressure increases with increasing frequency. The pressure was 5.921 kPa, 5.371 kPa of 3SQ under loading 10kN and 5kN respectively. For 8SQ4 was 6.383 kPa and 6.893 kPa in under 5kN and 10KN. Pressure under 8SL4 was 5.467 kPa and 4.232 kPa under loading 10kN and 5kN. The water pressure decreases as tread depth decreases. As expected, for a specific frequency, water pressure was higher in a square tread than slot cut tread shape as more water was possible to drain out during the load pulse. It is worth to note that irrespective of loading frequency, change in water pressure on flat loading plate negligible; i.e no treads depth.

4.4.7 Influence of Depth of Surface Water

As shown in Figures 4.6 to 4.9 and percentage difference of water pressure between 2mm and 4mm surface water is given in Figure 4.17. The results are plotted for both 5kN and 10kN load cases. It can be seen that pressure difference, with the exception of six cases, majority of the pressure differences were less than 15%. This indicates that the depth of surface only has marginal impact on the water pressure. The slight increase in water pressure was observed at high frequency, whereas the changes are negligible at low frequencies.

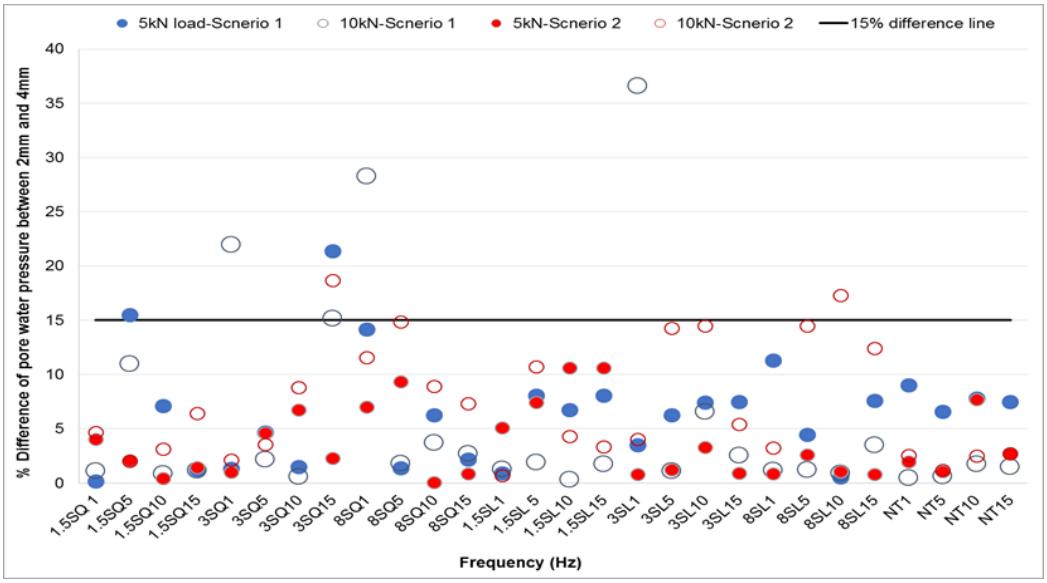

Figure 4.18 Percentage changes in pore water pressure between 2mm and 4mm surface water

4.4.8 Influence of Load Magnitude

As with surface water, the magnitude of load appears to have only marginal influence on the pore water pressure at in all tread shape, tread patterns and loading frequency, majority of the results are showing only marginal increase in water pressure (3%-25%) between 5kN and 10 kN load as shown in Figure 4.18.

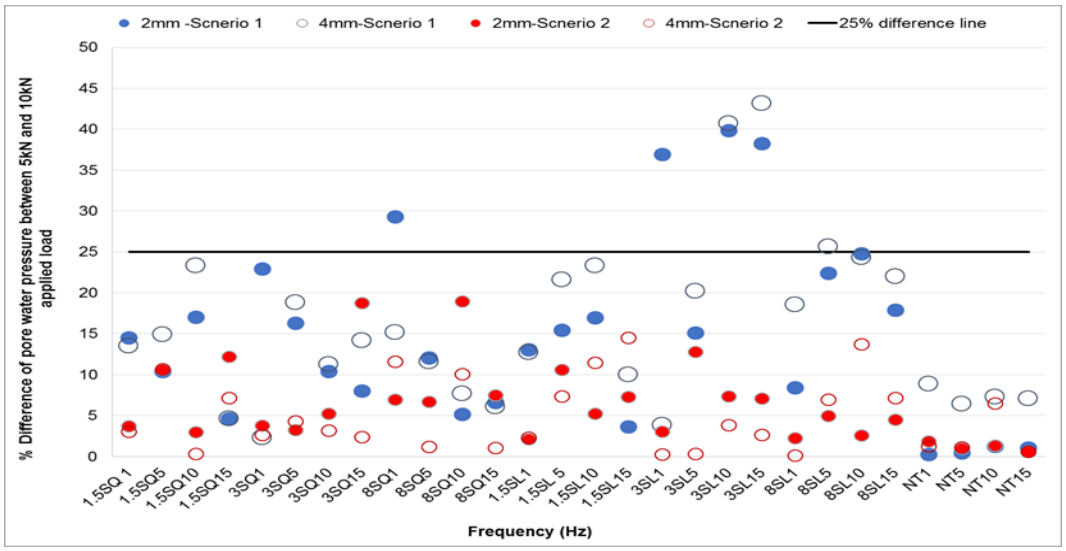

Figure 4.19 Percentage changes in pore water pressure between 2mm and 4mm surface water

4.4.9 Influence of Tyre and Load Parameters

From Figures 4.13 to 4.17, it can be seen that the worst-case scenario for maximum pore water pressure in both scenario 1 and scenario 2 are to be at high loading frequency, when water is trapped in a deep square groove (8mm in this) of the tyre. At the worst-case scenario (8mm square tread 8SQ4, 15 Hz frequency), the maximum pore water pressure in this test was approximately 7kPa at the bottom of the slab, which equates to approximately 1.4%-0.7% of the actual contact stress is 0.5 Mpa ($5/0.01^2$) and is 1Mpa ($10/0.01^2$) respectively. It should be noted that the tread depth in a new truck tyre could be as deep as 15mm, which may increase pore water pressure significantly.

To extrapolate the pore water pressure to high speed traffic, the following equation developed by Brown (1974) was utilised.

$$\log (t) = 0.5d - 0.2 - 0.94\log(v)$$

Where, t = loading time (sec); d = pavement depth (m), 0.1m slab thickness; and v = vehicle speed (km/h). f (Hz)=1/t (NCHRP, 2004).

Brown's equation relates to loading time to vehicle speed and pavement depth profile. The loading time was considered as the average of the pulse times of the stresses in three directions as obtained from the elastic layered theory (Brown 1974). The extrapolated graph relating to water pressure and vehicle speed is shown in Figure 4.20. From (a) to (g) the figures represent scenario 1 and from figures (h) to (n) represent scenario 2. Each graph was extrapolated the four main cases of pore water pressure produced using tread pad.

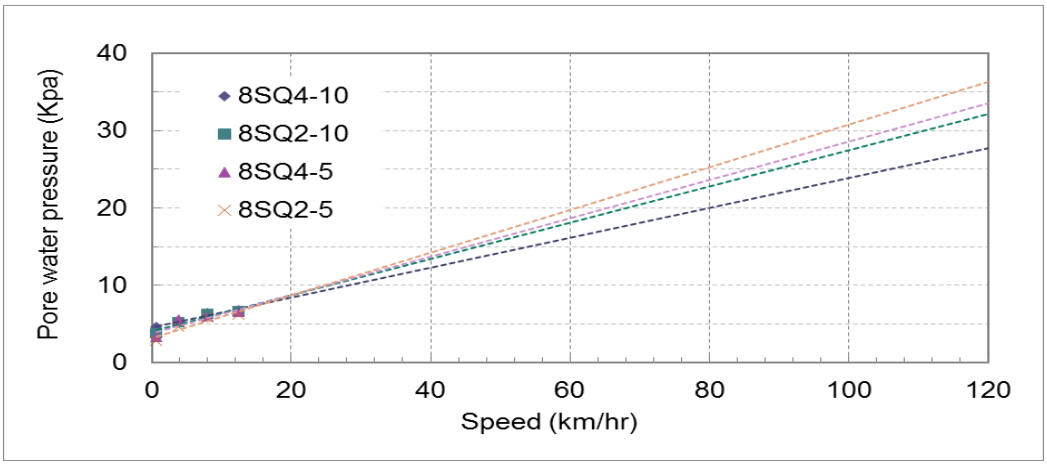

a) Extrapolated relation between water pressure, vehicle speed and 8SQ

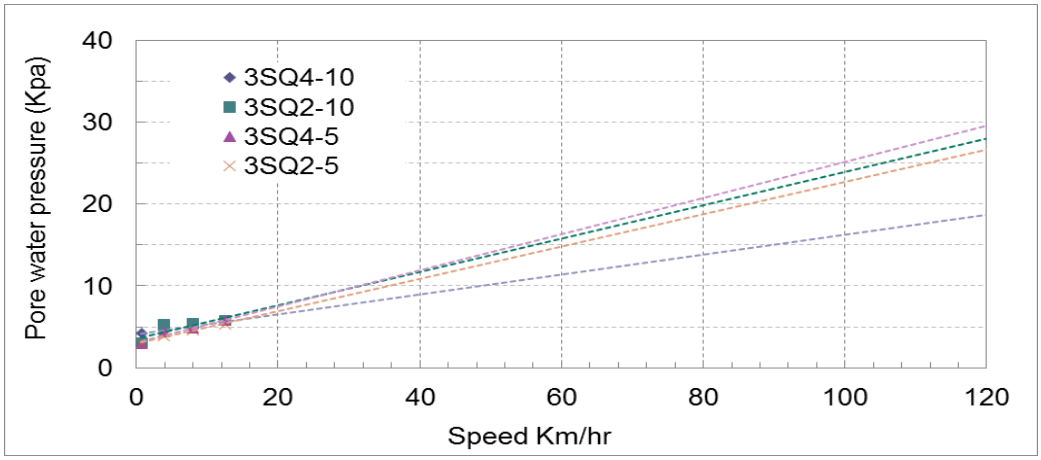

b) Extrapolated relation between water pressure, vehicle speed and 3SQ

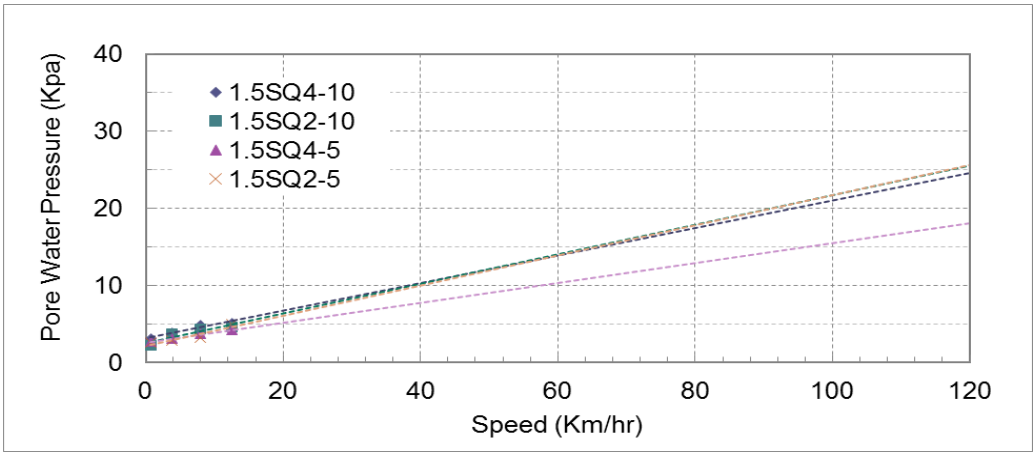

c) Extrapolated relation between water pressure, vehicle speed and 1.5SQ

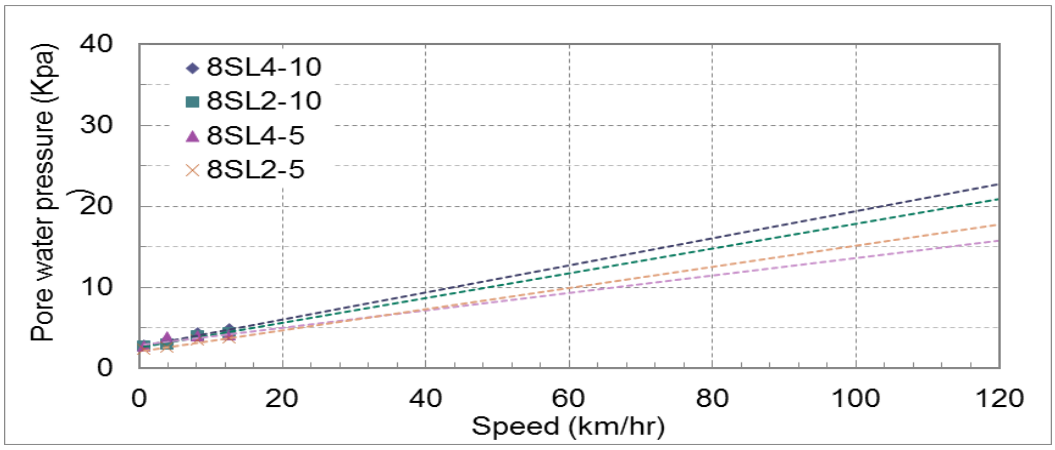

d) Extrapolated relation between water pressure, vehicle speed and 8SL

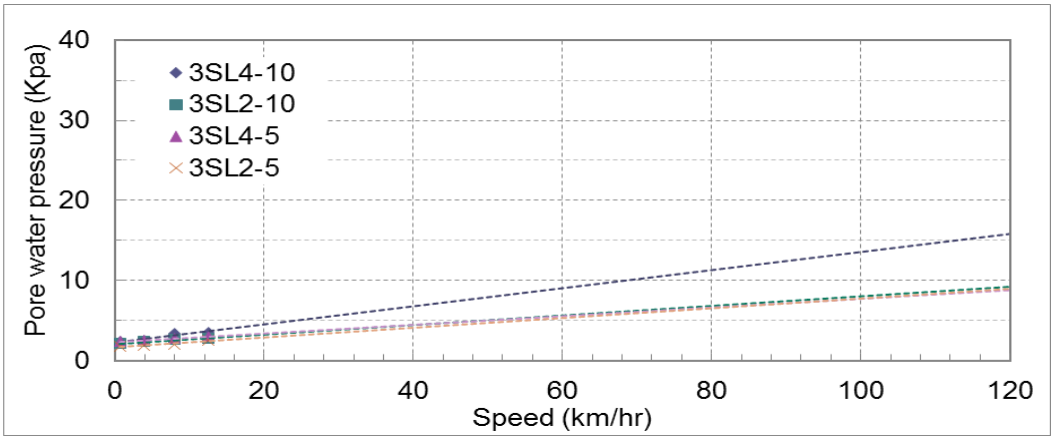

e) Extrapolated relation between water pressure, vehicle speed and 3SL

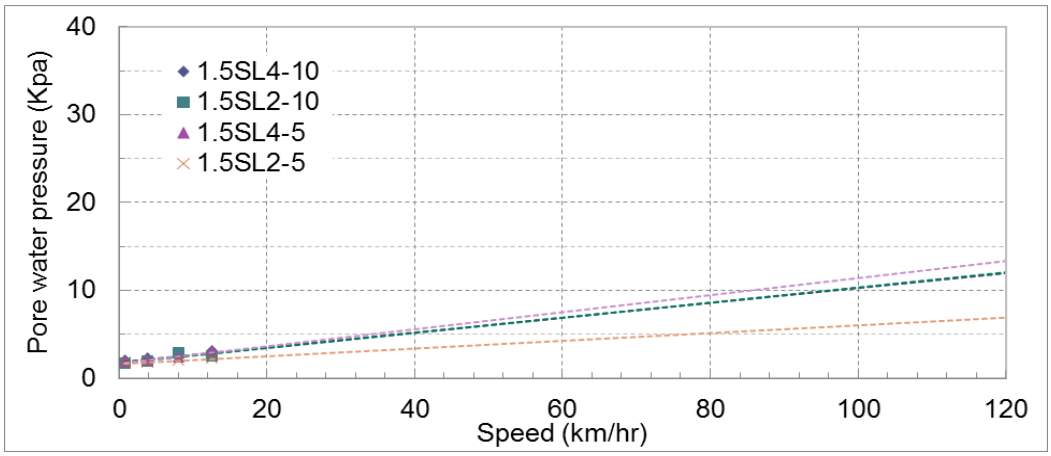

f) Extrapolated relation between water pressure, vehicle speed and 1.5 SL

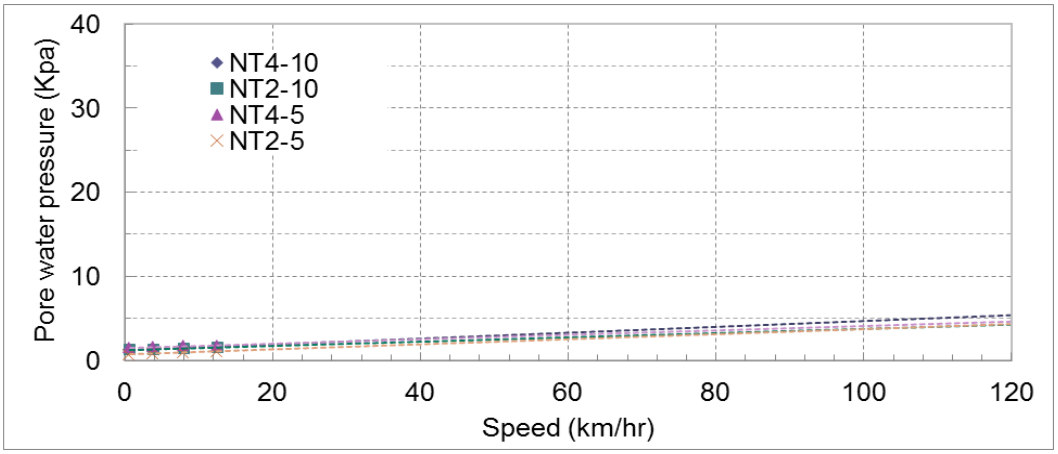

g) Extrapolated relation between water pressure, vehicle speed and NT

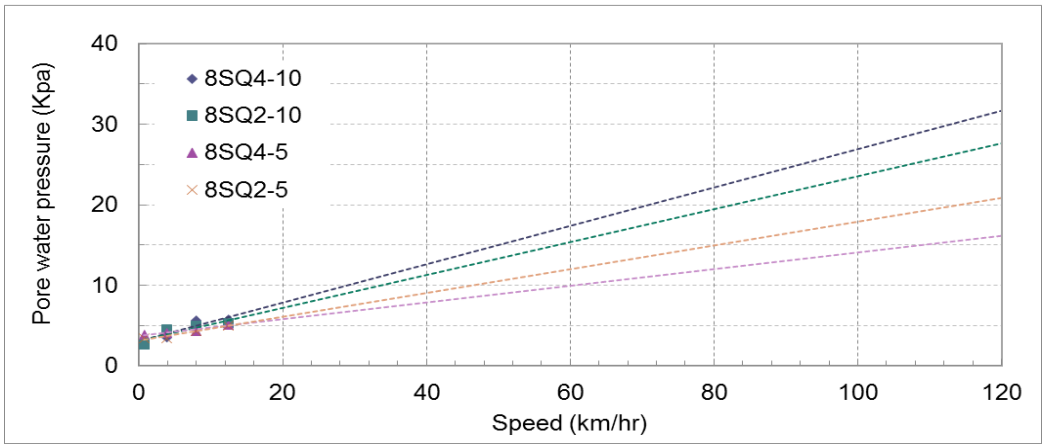

h) Extrapolated relation between water pressure, vehicle speed and 8SQ

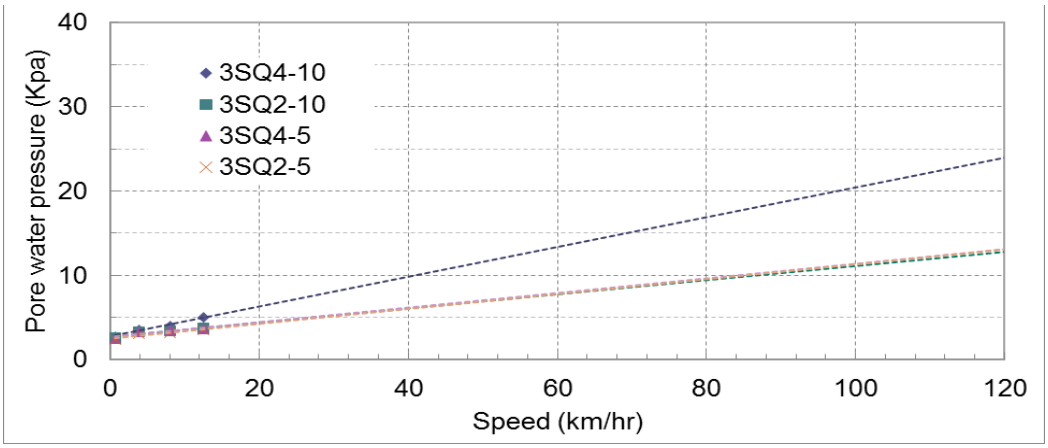

i) Extrapolated relation between water pressure, vehicle speed and 3SQ

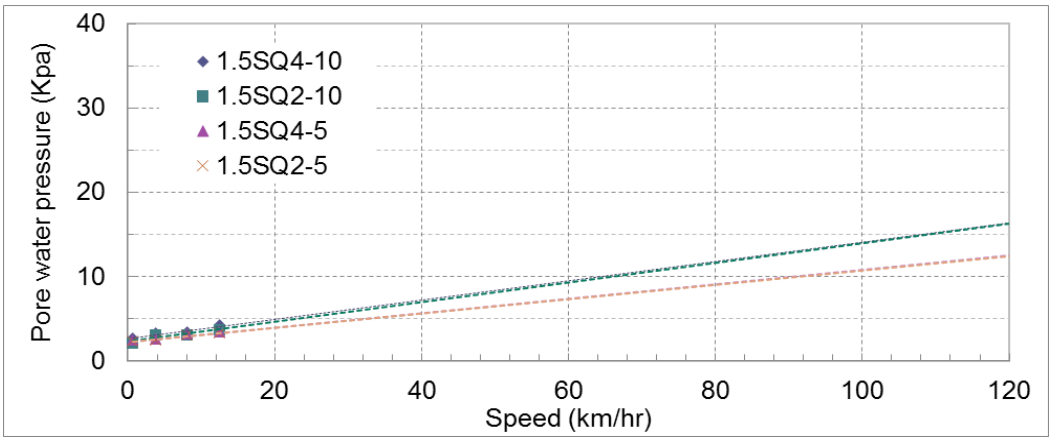

j) Extrapolated relation between water pressure, vehicle speed and 1.5SQ

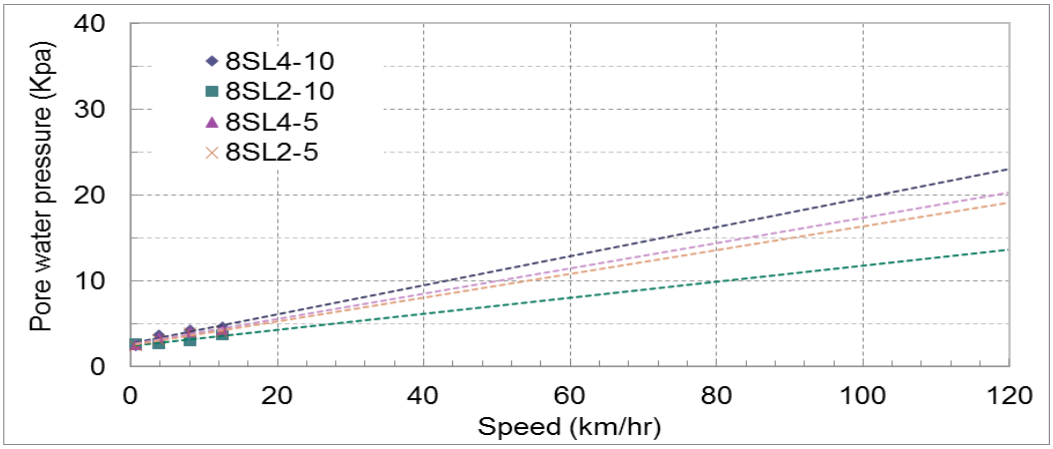

k) Extrapolated relation between water pressure, vehicle speed and 8SL

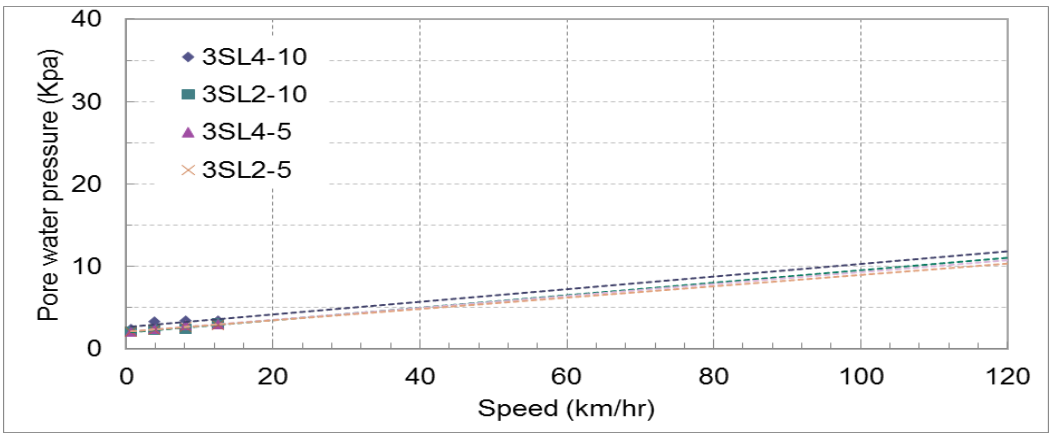

l) Extrapolated relation between water pressure, vehicle speed and 3SL

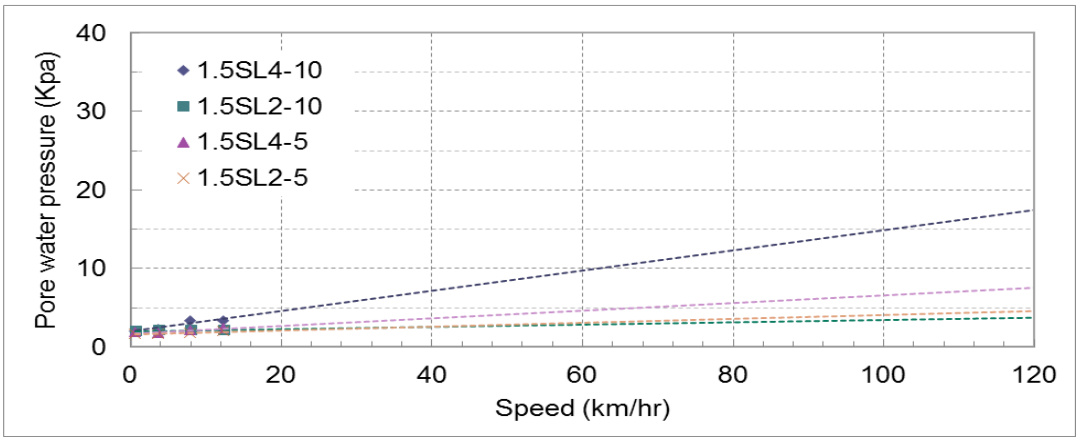

m) Extrapolated relation between water pressure, vehicle speed and 1.5 SL

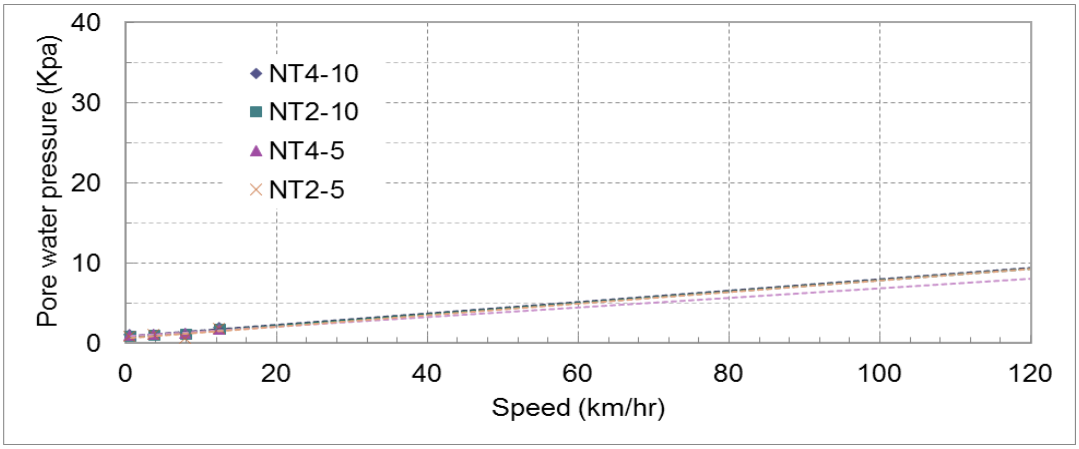

n) Extrapolated relation between water pressure, vehicle speed and NT

Figure 4.20 Extrapolated relation between water pressure and vehicle speed and each specific tread shape

Table 4.4 and Table 4.5 represent equation and R^2 of each case in the Figure 4.20

Table 4.4 Equations and R^2 for scenario 1

ID	Water depth mm	Loading (KN)	Equation	R^2
8SQ	4	10	y = 0.1925x + 4.6055	0.9638
	2	10	y = 0.2341x + 4.0527	0.9003
	4	5	y = 0.247x + 3.8443	0.779
	2	5	y = 0.2762x + 3.1466	0.8708
3SQ	4	10	y = 0.1213x + 4.0962	0.935
	2	10	y = 0.203x + 3.6196	0.6998
	4	5	y = 0.2208x + 3.0908	0.95

ID	Water depth mm	Loading (KN)	Equation	R^2
	2	5	y = 0.1971x + 2.9814	0.9815
1.5SQ	4	10	y = 0.0583x + 3.0139	0.9473
	2	10	y = 0.0626x + 2.4392	0.8562
	4	5	y = 0.0418x + 2.5352	0.9916
	2	5	y = 0.1961x + 2.104	0.8752
8SL	4	10	y = 0.054x + 2.6866	0.9884
	2	10	y = 0.0493x + 2.5298	0.9621
	4	5	y = 0.0352x + 2.8179	0.7114
	2	5	y = 0.0423x + 2.0756	0.9554
3SL	4	10	y = 0.1134x + 2.2228	0.8682
	2	10	y = 0.0592x + 2.0922	0.9506
	4	5	y = 0.0537x + 2.3115	0.9977
	2	5	y = 0.061x + 1.6782	0.8245
1.5SL	4	10	y = 0.0841x + 1.901	0.9327
	2	10	y = 0.0859x + 1.746	0.6463
	4	5	y = 0.0972x + 1.6867	0.9218
	2	5	y = 0.0441x + 1.6592	0.9045
NT	4	10	y = 0.0098x + 0.7025	0.9272
	2	10	y = 0.0082x + 1.2441	0.9228
	4	5	y = 0.0084x + 1.5115	0.9026
	2	5	y = 0.0098x + 0.7025	0.9272

The equations of extrapolated of scenario 2 are showed in Table 4.8

Table 4.5 Equations and R^2 for scenario 2

ID	Water depth mm	Loading (KN)	Equation	R^2
8SQ	4	10	y = 0.2387x + 3.0441	0.8743
	2	10	y = 0.2053x + 3.0407	0.7464
	4	5	y = 0.1037x + 3.6536	0.9038
	2	5	y = 0.1482x + 3.0829	0.9442
3SQ	4	10	y = 0.1773x + 2.7058	0.9793
	2	10	y = 0.0837x + 2.7035	0.8445
	4	5	y = 0.0862x + 2.7084	0.7222
	2	5	y = 0.088x + 2.4722	0.916
1.5SQ	4	10	y = 0.1146x + 2.5906	0.9084
	2	10	y = 0.1169x + 2.2509	0.8338
	4	5	y = 0.0855x + 2.2452	0.9598
	2	5	y = 0.0856x + 2.1671	0.9279
8SL	4	10	y = 0.1698x + 2.6498	0.8766
	2	10	y = 0.0939x + 2.3775	0.8985
	4	5	y = 0.1478x + 2.5727	0.9078
	2	5	y = 0.1386x + 2.4825	0.8949
3SL	4	10	y = 0.0767x + 2.6177	0.6303

ID	Water depth mm	Loading (KN)	Equation	R^2
	2	10	y = 0.0752x + 1.9721	0.8804
	4	5	y = 0.072x + 2.1123	0.9113
	2	5	y = 0.0686x + 2.0507	0.9968
1.5SL	4	10	y = 0.1285x + 2.0008	0.8747
	2	10	y = 0.0147x + 2.033	0.8458
	4	5	y = 0.0487x + 1.7751	0.8618
	2	5	y = 0.0248x + 1.6497	0.883
NT	4	10	y = 0.0712x + 0.9172	0.8252
	2	10	y = 0.0712x + 0.7518	0.8414
	4	5	y = 0.0591x + 0.9076	0.8687
	2	5	y = 0.0713x + 0.6838	0.4528

At 100 km/hr (~60 mph), the water pressure can be around 31 kPa, which is approximately 6.2% of the applied pressure. Although this is unlikely to create any immediate damage to the road, repeated action of the load will eventually lead to bond deterioration in the mixture matrix and at interface between two layers. Another point to note is that if the pore opening reduced from 2mm to 1mm, the pressure will increase significantly due to capillary action of the water.

4.4.10 Reduction of Water Pressure Due to Asphalt Surface

A comparison between two scenarios at 5kN applied load on 4mm surface water is shown in Figure 4.21 and Figure 4.22. Depending on the loading frequency and tread shape and pattern, reduction of approximately 5% to 38% maximum water pressure was measured when concrete slab was overlaid with a semi permeable 20mm SMA asphalt. This reduction could be due to texture in the surface and water storage in side mixture matrix. The tread shape & thickness and frequencies are the main contributory factors for changes in water pressure. The load magnitude, as with scenario 1, has only marginal effect. It is interesting to note that, in the case of no tread case (NT4), the pressure at 15Hz was slightly higher in scenario 2 (Figures 4.16 to Figure 4.19) than scenario 1 (Figures 4.12 to Figure 4.15). It can be due to water build up in the interconnected voids forcing water through the cracks.

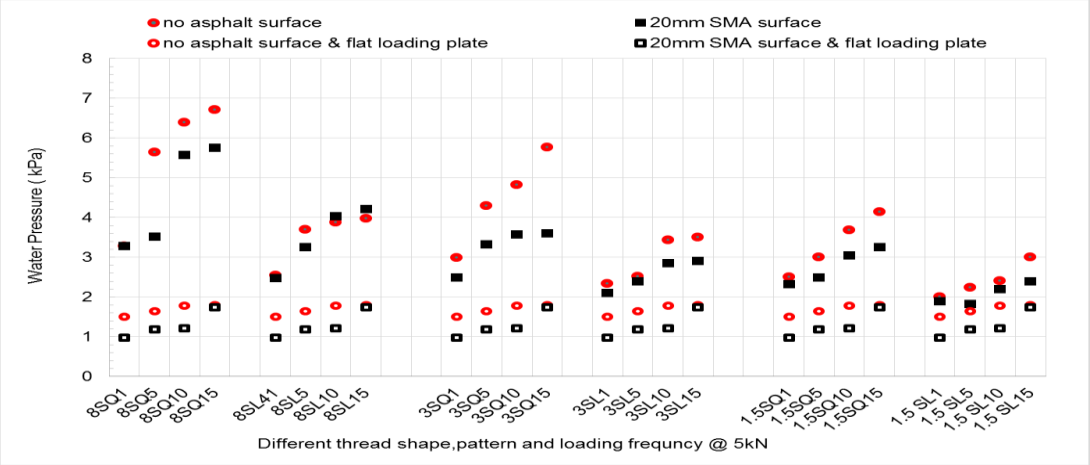

Figure 4.21 Comparison of water pressure at different frequencies on pavement with and without asphalt surface@ 5kN.

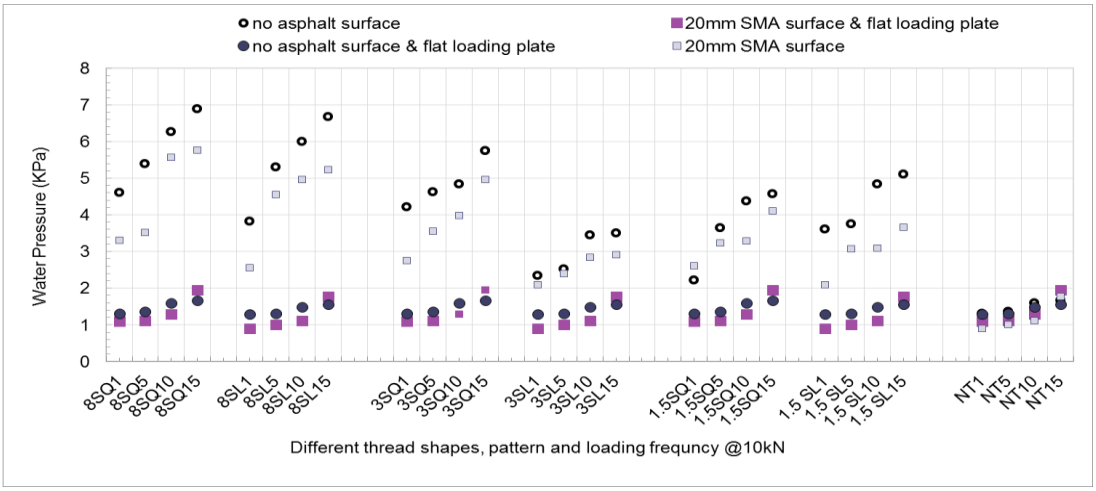

Figure 4.22 Comparison of water pressure at different frequencies on pavement with and without asphalt surface @10kN.

4.4.11 Comparison with Previous Studies

The experimental study by Gao et al (2015) (details given in section 2.2.9.1 in Chapter 2) on an in service pavement was used to compare the results obtained from this study. The water pressure at different speeds from Geo et al (2015) study has been plotted in Figure 4.23. The used custom build sensor and placed the first sensor (S3) at surface 0mm, second sensor (S2) at 40mm and third sensor (S1) at 100mm. The pavement

type was stone mastic asphalt. It can be seen, at 12.48 km/h (15Hz), the water pressure is approximately 16 kPa.

This value is higher than measured maximum dynamic pore water pressure in this research 6.89 KPa at 15 Hz (12.48 km/h). However, there wasn't any indication of including atmospheric pressure in their measurement and whether custom build sensor was capable of neutralised atmosphere pressure. As explained in Chapter 3, the sensor used in this study uses atmospheric pressure 101 KPa as a reference. Therefore, the combined pressure (atmospheric and dynamic) was 107.89 KPa.

When considered companied pressure at the similar depth and speed, this pressure was higher than previous studies by Gao, et al (2015), this was due to the forced infiltration of the water through void structure in the slab was measured. This difference was also attributed due to the difference measurement conditions such as different tyre treads and different asphalt type.

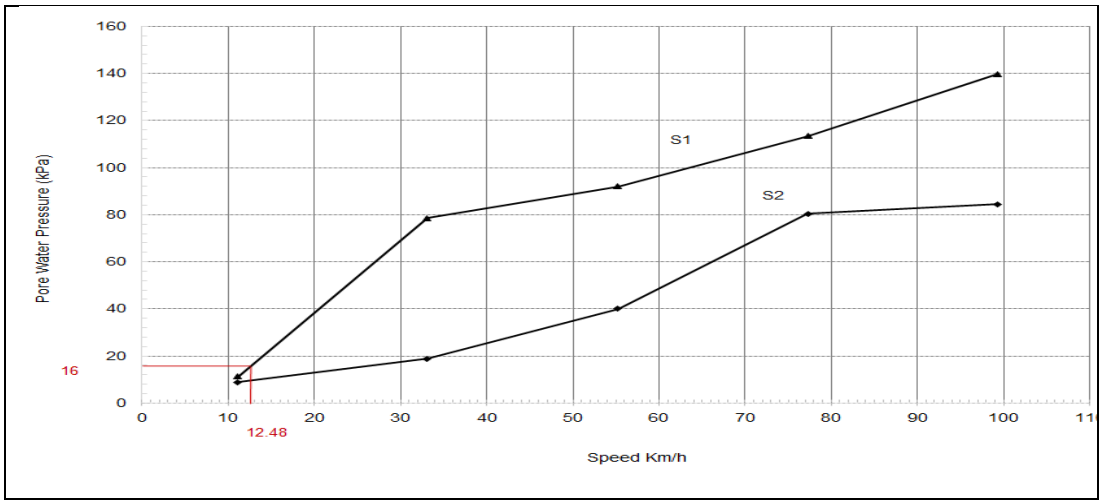

Figure 4.23 Comparison of water pressure finding with (Gao at el., 2015).

In addition, recent simulation study by Guo, Sun and Dai, (2017), (details are given in section 2.2.9.1 in Chapter 2) established that there was a positive correlation between the pressure and the vehicle speed; they reported that the repeated traffic loading caused emulsification. They found that at slits which already has micro cracks the cumulative damage will be accelerated due to repeated traffic and the asphalt film may be peeled easily (Guo, Sun and Dai, 2017).

4.5 Summary

The outcomes from this chapter are increasing load frequency increases pore water pressure in the pavement. But, water pressure increases significantly when high frequency loading combined with square kinds of tread with deep tread depth when water trapped inside the groove. Square tread with channel permits water to drain, which decreases pore water pressure. Irrespective of tread pattern, 8mm tread thickness gave the highest value of water pressure. However, the pressure reduces significantly in 1.5mm tread thickness. It is likely that increasing tread depth will increase the water pressure in the pavement.

Load magnitude has a marginal influence on the pore water pressure. The water pressure diffidence between 5kN and the 10kN load was found an only range from 3% to 25% in all tread patterns, thicknesses and loading frequencies. Furthermore, the depth of surface water seems to have a minimum impact on water pressure. It is possible that pore water pressure will build up if pores are filled with water, and there is a minimum value of water on the surface. The asphalt surface can decrease water pressure underneath the pavement range from 5% to 38% based on the vehicle speed, tread patterns and thickness. This significant variation also indicates that, for given surface type, the tyre characteristics and vehicles speed will determine the pore water pressure. While the magnitude of water pressure is only approximately 8% of the contact pressure, smaller but continuous voids can significantly increase this pressure, which finally can lead to degradation of foundation material and progressive deterioration to asphalt surface resulting fretting, ravelling or stripping.

Chapter 5 Asphalt Surface Damage Due to Combined Action of water and Dynamic Loading

5.1 Introduction

Several studies have been conducted on water-related deterioration, focusing towards material degradation of lab manufactured specimens by assessing the reduction of mechanical properties after number of moisture conditionings cycles and determining the loss of adhesion and cohesion of the mixture matrix (Cook and Dynkins, 1991).On the other hand, the interaction of tyre-water-pavement occurs simultaneously, and it is important to study their combined influence on the overall performance of the asphalt surface. Furthermore, previous studies into pavement performance prediction has paid little serious attention to surface-originating damage, despite a recent TRL (Transport Research Laboratory) study highlighting that surface cracking and ravelling were the dominant failure modes on major roads in the UK (Nicholls et al., 2010). It is believed that much of these surface related failures are directly related to tyre-water-pavement interaction. A significant knowledge gap, therefore, exists which this chapter aims to address by comparing performance of different asphalt surfaces subjected to concurrent flooding and repeated loading.

In Chapter 4, details studies are conducted to evaluate the influence of tyre, traffic and surface water on pore water pressure under a pavement. The experiments were done for limited number of cycles with different combinations of tyre, traffic and surface variables. In this chapter, the combination that creates maximum pore water pressure was chosen to apply continuously until the surface shows significant failure.

Three asphalt surfaces were studied; a gap graded hot rolled asphalt (HRA) mixture and two open-graded mixtures, stone mastic asphalt (Open SMA) and porous asphalt (PA). Those mixtures, Open SMA, HRA and PA were chosen because they are replicate the three high void content, medium void content and low void content also used as surface layers usually. Moreover, 50 mm thickness layer was used in all cases. The aggregate gradations for Open SMA, HRA and PA are given in Figure 3.18 to Figure 3.23 in Chapter 3 and mixture design and specimen manufacturing processes are also given in sections 3.3.3 to 3.3.7 in Chapter 3.

All mixtures were tested in dry and in wet conditions in a controlled laboratory environment by applying vertical dynamic load while the asphalt surface was submerged with up to 2mm water. The impact of voids contents and size of aggregates

were also studied. This chapter presents the test set up, the test specifications, results concerning surface cracking, permanent deformation and other visual distress such as material loose due to dynamic loading at different frequencies.

5.2 Test Set-Up

In chapter 3, a schematic diagram of the test set up is given in Figure 3.29. An additional feature, such as a microscope, was added to measure distress during the testing. A picture of the modified test set-up is given in Figure 5.1.

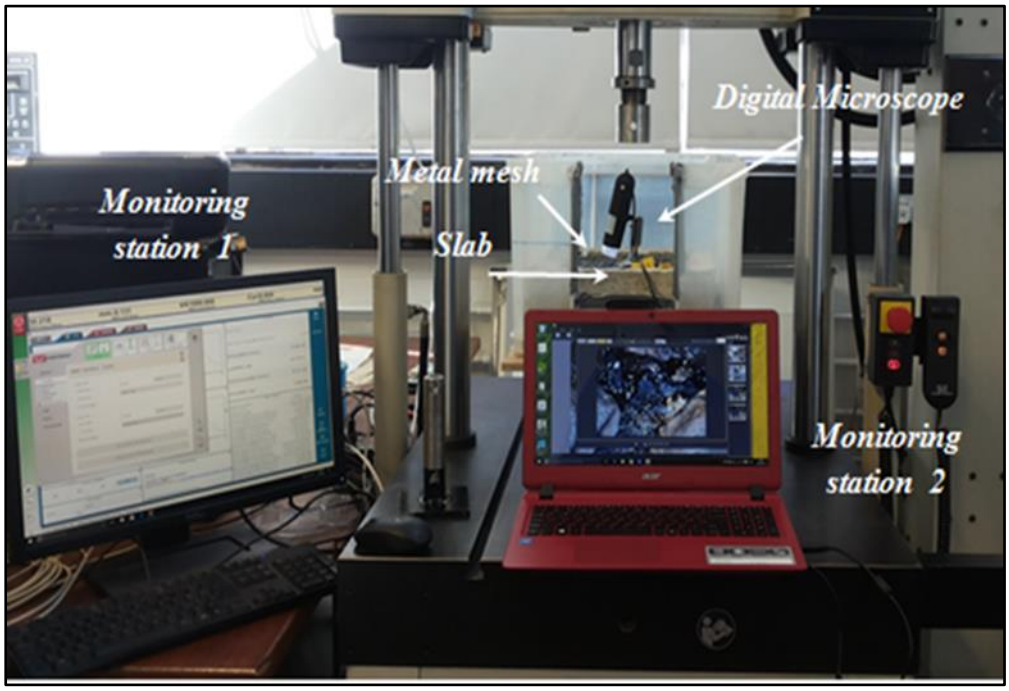

Figure 5.1 Test arrangement with attached microscope to measure cracks and disintegration on the surface.

A 5kN sinusoidal compression load at a frequency of 5Hz was applied. First, the loading plate was lowered on the surface with pre-load 4.5kN to ensure load plate is firmly placed on the surface, and then 0.5kN load was applied continuously until the test is completed, i.e. the magnitude of maximum and minimum load was 4.5kN and 0.5kN respectively. The selection of load and tyre characteristics were based on the outcome of Chapter 4 as the results showed that the significant pore water pressure

was generated in 8SQ tread when subjected to high frequency (details are in chapter 4).

5.3 Test Specifications

As mentioned earlier, the test specifications were designed to investigate the impact of load magnitude, load frequency, tyre properties, surface water and asphalt surface type.

For each mixture type, three specimens were tested in dry condition and three in wet condition. The surface was submerged with 1-2mm water and this depth was kept constant during the duration of test by constant feeding of water. Specimens tested in wet condition went through overnight conditioning in water at room temperature to ensure saturation prior to testing.

The samples were exposed to a total 20,000 to 40,000 load cycles depending on the level of damage observed on the surfaces. All 6mm and 10mm HRA and OPEN SMA mixtures were tested for 20,000 cycles while testing for all 14mm HRA, OPEN SMA and PA mixtures were ceased after 40,000 cycles due to excessive amount of failure. Table 5.1 presents testing specification.

Table 5.1 Test specifications for repeated loading on different asphalt surfaces

Asphalt type and tests conditions	Load (kN)	No of Sample	Frequency (Hz)	Water depth	No of pulses	Tread depth & Pattern (mm)
HRA10-D	5	3	5,10	1-2	20,000	8SQ
HRA10-W	5	3	5,10	1-2	20,000	8SQ
HRA14-D	5	3	5,10	1-2	40,000	8SQ
HRA14-W	5	3	5,10	1-2	40,000	8SQ
Open SMA6-D	5	3	5,10	1-2	20,000	8SQ
Open SMA6-W	5	3	5,10	1-2	20,000	8SQ
Open SMA10-D	5	3	5,10	1-2	20,000	8SQ
Open SMA10-W	5	3	5,10	1-2	20,000	8SQ
Open SMA14-D	5	3	5,10	1-2	40,000	8SQ
Open SMA14-W	5	3	5,10	1-2	40,000	8SQ
PA14-D	5	3	5,10	1-2	40,000	8SQ
PA14-W	5	3	5,10	1-2	40,000	8SQ

In addition to the slabs presented in Table 5.1, a limited number of slabs manufactured in the lab by replacing the filler by mineral filler in mix design of 10 mm Open SMA, 10mm HRA, 14mm Open SMA, and 14 mm HRA to study the influence of filler on performance of asphalt mixture mentioned in the sections 5.5.1.

5.4 Distress Measurements

After each 1000 load cycles, the resulting vertical deformation of the asphalt slab and the length of the cracks appearing on the surface were measured. The procedure to measure distresses is given in the following sections.

5.4.1 Visual Observation

The visual observation due to accumulative cycles on individual crack length, rutting and other distresses were recorded in a standard survey sheet and photographic records by camera and microscope. A mesh plate and ruler were used to measure pattern and length of cracks (mm), and depth of rutting (mm). Other distresses such as corner cracking, loss of particles after every 1000 cycles were also recorded. The close image of crack and surface disintegration measurement set-up is shown in Figure 5.2 and selected pictures of distresses are given in Figure 5.3.

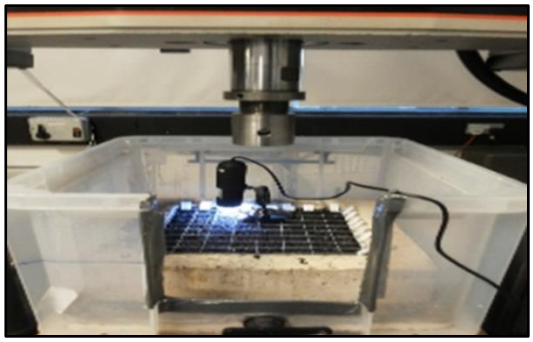

Figure 5.2 Microscopic measurement of cracks and surface disintegration

a) Missing aggregate on OPEN SMA surfaces

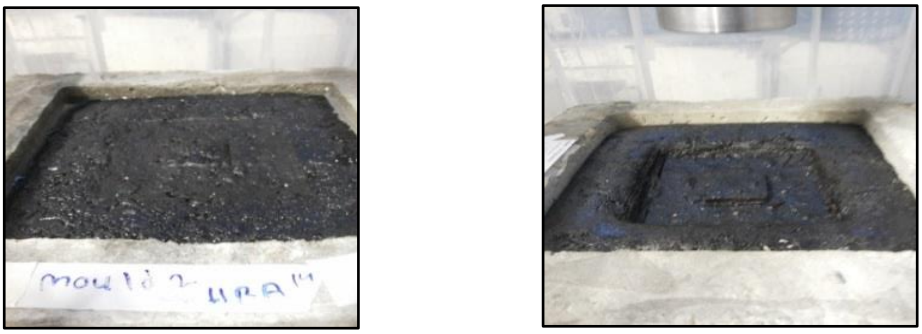

b) Rutting in HRA surfaces

Figure 5.3 Distresses on asphalt surfaces

5.4.2 Crack Measurement

After each 1000 cycles, the load device was lifted so that the slab surface can be seen. Then, the sample was evaluated, and the presence of surface cracks was measured. Once a crack initiated, a picture was taken using the microscope with 400X magnifications to measure the length of crack using the build in image processing software in the microscope. The length of the crack was recorded, marked and accumulated to get a total length of the crack for subsequent 1000 cycles. Similar procedure was followed in wet condition testing; accept after lifting the load device, the asphalt surface was dried by a blotting paper prior taking any measurement. Slab with marked cracked is showed in Figure 5.4.

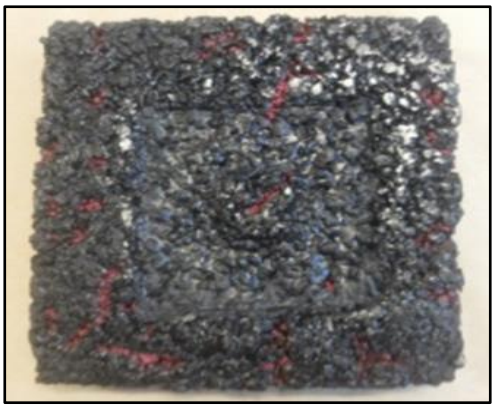

Figure 5.4 Slab marked in 10mm OPEN SMA

5.4.3 Rutting Measurement

The rutting of the asphalt slab surface was measured after each 1000 load cycles by placing the straight plate in a plane perpendicular to the load direction and the bottom surface of the plate was parallel to longitudinal slope of the asphalt slab surface. The measurement set-up is shown in Figure 5.5. Five measurements were taken for each case to ensure the accuracy.

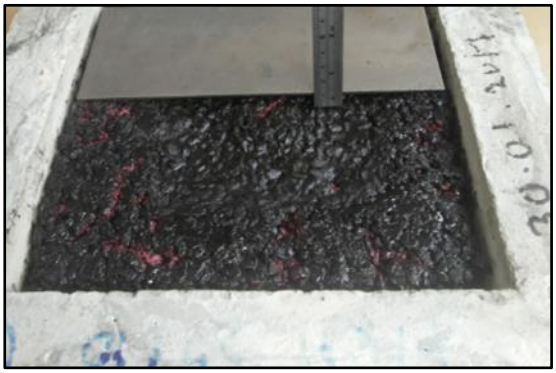

Figure 5.5 Deformation measurement

5.4.4 Ravelling Measurement

The ravelling was measured by visual and microscopic observation and by manually counting the number of missing aggregates within the loaded area.

5.5 Results and Analysis

The results are analysed in terms of cracking and rutting severity of different types of surfaces tested in dry and wet conditions. The influence of mixture characteristics, and load frequencies are also investigated.

5.5.1 Cracking on different asphalt surfaces

5.5.1.1 Influence of Water on Surface Cracking

The average cumulative length of cracking for each mixture tested in dry and in wet condition is shown in Figures 5.6 and Figure 5.7a to 5.7f show the cumulative crack result of individual specimen for all mixtures tested in dry and in wet conditions. The results are consistent for each mixture, and cracks patterns are similar in three individual dry tests and in three individual wet tests.

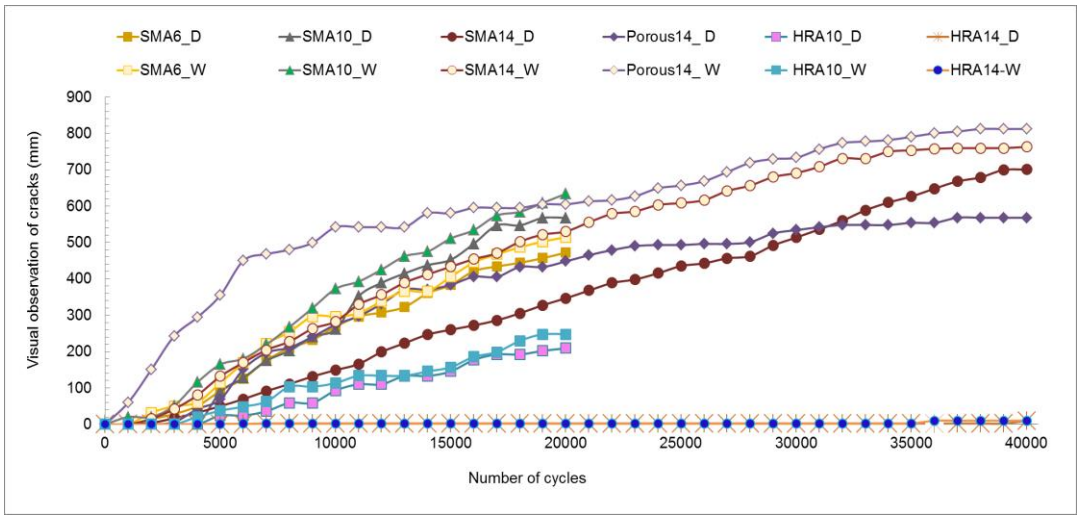

Figure 5.6 Average cumulative cracking for all mixtures tested in dry and wet treated condition at 5Hz

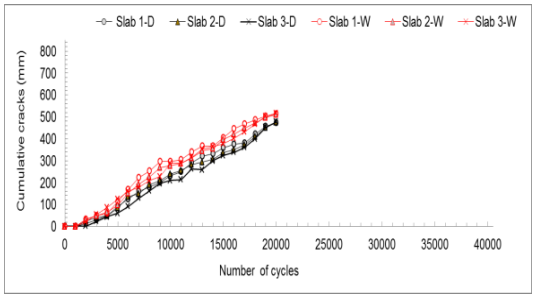

a) Measured crack in six 6mm Open SMA slabs in wet and dry conditions

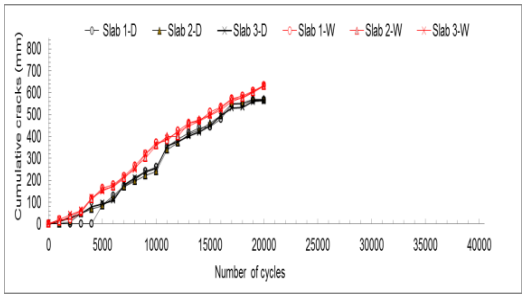

b) Measured crack in six 10mm Open SMA slabs in wet and dry conditions

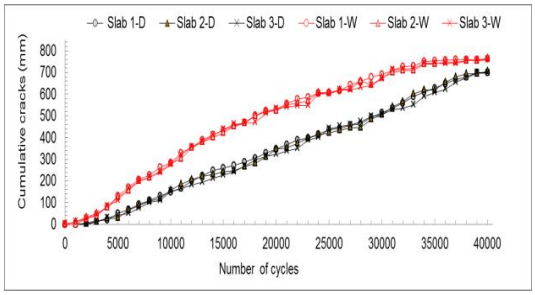

c) Measured crack in six 14mm OPEN SMA slabs in wet and dry conditions

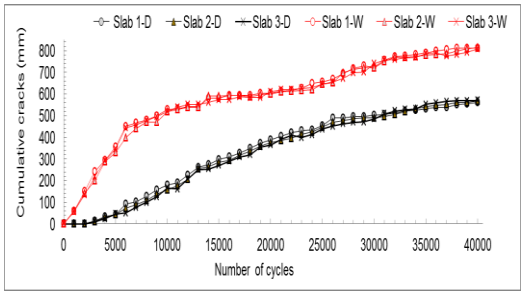

d) Measured cracks in six 14mm PA slabs in wet and dry conditions

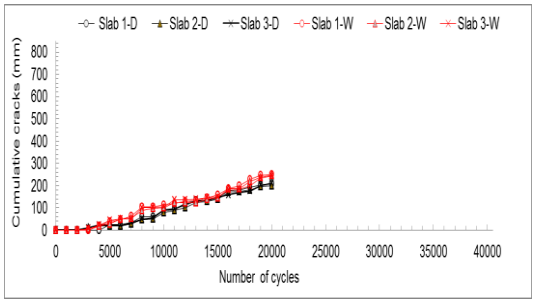

e) Measured crack in six 10mm HRA slabs in wet and dry conditions

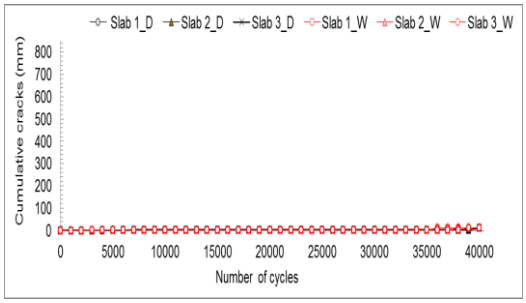

f) Measured crack in six 14mm HRA slabs in wet and dry conditions

Figure 5.7 Cumulative cracking for individual slab for each mixture

It is evident from the test results that, in most cases, the presence of water accelerates surface cracking. The affect is more severe in 14 mm porous asphalt (Figure 5.7d), then respectively to 14, 10 and 6 Open SMA and least in 10 mm and 14 mm HRA. The cracking was almost negligible in 14 mm HRA (Figure 5.7f).

Crack severity

In terms of dry versus wet crack severity, the relative effect is shown in Figure 5.8 where the ratio between wet and dry cracking at each load pulse is presented.

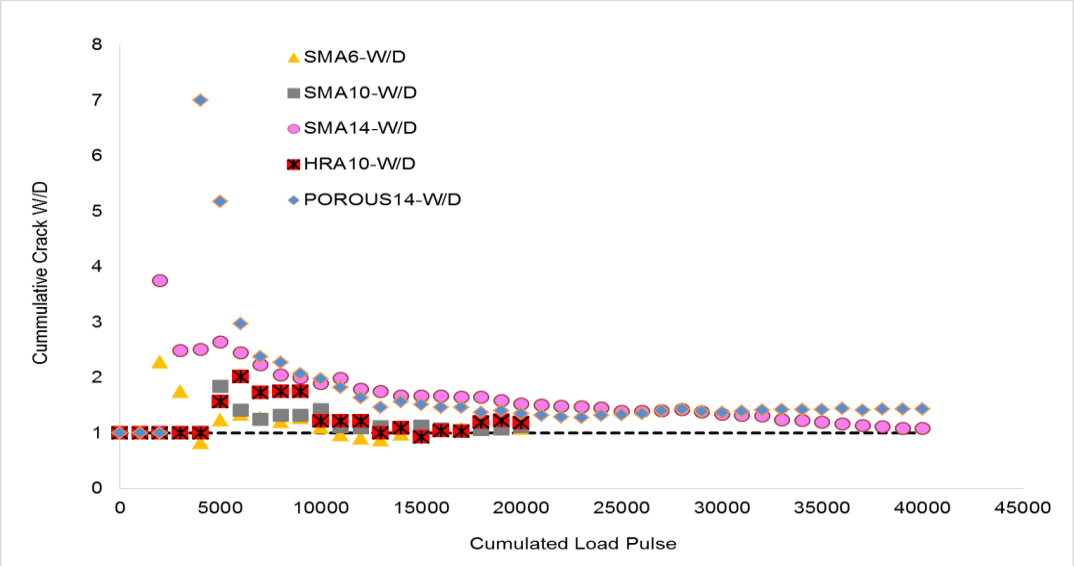

Figure 5.8 Comparison between wet and dry cracking

It can be seen that the crack appearance on the wet porous surface was more than seven-times the dry state at the same load cycle. On the other hand, it is approximately twice in OPEN SMA mixtures. Both mixtures showed maximum cracking in dry and in wet conditions. In Table 5.2, the number of load cycles for 1st cracks and propagation of cracks and their severity level based on LTPP (2003) classification for alligator cracking is given.

Table 5.2 Impact of combined action of surface water and loading on surface cracking based on distress identification manual from the LTPP study (Miller and Bellinger, 2003).

Mixture ID	Number of load pulse and corresponding cumulative length of crack			
	1st	70 mm to 100 mm with a few connecting cracks	100 mm to 150 mm with interconnected cracks	> 150 mm interconnected cracking forming a complete pattern and pieces move with loading
HRA10-D	4042	9320	10236	14664
HRA10-W	3050	7180	7820	15096
HRA14-D	6000	40,000*	-	-
HRA14-W	5000	40,000*	-	-
Open SMA6-D	1070	4350	5120	6420
Open SMA6-W	1030	4313	4780	5640
Open SMA10-D	4012	4785	5192	6448
Open SMA10-W	50	3290	3712	4576
Open SMA14-D	1250	6037	7360	10001
Open SMA14-W	1065	3732	4344	5420
PA14-D	2160	5025	5400	5960
PA14-W	17	1110	1432	2000

*The cracks length in a 14 mm HRA mixture was 10 mm for both cases with number of load pulse 40,000.

Appearance of first crack

LTPP crack severity classification is based on measurement of crack in 300 mm on longest and recorded in square meter. This was scaled down to 70 mm to 100 mm with a few connecting cracks in tested 200 mm^2 for low severity (L), 100 mm to 150 mm with interconnected cracks for moderate severity (M), greater than 150 mm interconnected cracking forming a complete pattern and pieces move with loading for high severity (H) (Miller and Bellinger, 2003).

It can be seen in Table 5.2 that crack appears within the first 17 load cycles in wet condition testing of 14mm PA. While in dry condition, it took 2160 load pulses for first crack to appear for same mixtures. Similarly, crack appears within first 50 cycles in 10mm OPEN SMA wet testing, compared to 4012 load cycles in dry condition. The

first cracks for mixtures in wet and dry conditions for 6mm OPEN SMA dry 1070 load pulses and wet 1030 cycles, 10mm HRA dry 4042 load cycles and wet 3050 load pulses, 14mm HRA dry 6000 load cycles and wet 5000 cycles. This implies that moisture makes a physical change to the material properties. Especially in the open graded mixtures, this exhibits itself in the early development of damage patterns which, without the moisture, may have not occurred or may have occurred in a much later stage of the pavements. The observed and measurement of first crack appearance indicated that if the road surface is designed for 10 years, the cracks may appear on the surface within the first few years.

Crack expansion

As 5 Hz load frequency, crack expansions in wet and dry conditions were divided into three stages, for low severity from 70mm to 100mm for 14mm OPEN SMA, the load cycle was 6037, where's in wet condition it was 3732. For 14 mm PA, it was 5025 load cycles for dry and only 1110 load cycles for wet condition. For 10 mm OPEN SMA it was 4785 for dry condition and in wet condition it was 3290.

In medium severity, crack length from 100mm to 150mm, for 14mm OPEN SMA dry it was 7360 and for wet it was 4344 load pulses. Similarly, for PA dry, load pulses were 5400 but it reduced drastically to only 1432 in wet condition. For 10mm OPEN SMA, a dry testing load pulse was 5192 which reduced to 3712 in wet condition. For 10mm HRA dry it was 10236, whereas in wet it was 7820.

In high severity, crack length > 150mm, for 14mm OPEN SMA dry test, load pulses were 10,001 but in wet, it was halved to 5420. For 14mm PA, load pulses were 5960 in dry but reduced to more than 50% to 2000 load pulses in wet testing. Similarly, for 10 mm OPEN SMA dry testing, load pulses were 6448, which reduced approximately 30% to 4576 load cycles in wet testing.

It is clear from the above analysis that, wet condition not only reduces resistance to crack but also, depending on the mixture type, the rate of deterioration accelerates.

Similar observations were noted for 10Hz testing. A comparative analysis of observed distresses between 5Hz to 10Hz testing is given in later part of this chapter.

5.5.1.2 Influence of Mixture Parameters on Surface Cracking

Aggregate size has influence on accelerated damage in wet condition as shown in Figure 5.7a and Figure 5.7c for 6mm Open SMA, 10mm Open SMA and 14mm Open SMA mixtures respectively. It is evident that cracking accelerates faster in 14mm Open SMA, compared to 10mm Open SMA and 6mm open SMA. This is due to the notable interactions, both chemically and physically, between bitumen and the aggregate fractions of an asphalt mixture. It has been proposed that the bond between coarse aggregate and asphalt mastic may be governing part in moisture damage (Apeagyei, Grenfell and Airey, 2015). In 14mm Open SMA after 14,000 pulses, 400 mm cumulative cracks were measured while in dry condition same cumulative cracks happened after 21000 pulses. Compared to 14mm Open SMA, the influence of water appears to be less severe in both 6mm and 10mm Open SMA. In PA, as shown in Figure 5.7d, the response was similar to 14mm Open SMA with. Similar cumulated of cracks were generated in wet condition after 14800 pulses while in dry condition that happened after 40,000 pulses.

The aggregate gradation also has an impact on surface cracking. For example, comparing 10 mm OPEN SMA with 10mm HRA, the influence of water was higher in 10mm OPEN SMA compared to 10mm HRA. 10mm HRA showed the best performance among all asphalt mixtures. This might be due to medium size of aggregate and a high percentage of fine aggregate and high (8%) bitumen content in the mixture.

With respect to the impact bitumen of content, as presented in Table 3.2 in Chapter 3, 14mm OPEN SMA with bitumen content 5.8% and PA with 4.5% bitumen content have lower film thickness compared to 14 mm HRA which has 8.5% bitumen content. It is likely that lower bitumen content and thin binder film, allied with aggregate dominant mixture gradations of OPEN SMA and PA, accelerate damage in wet condition.

5.5.1.3 Influence of Load Frequency on Surface Cracking

Figure 5.9 shows the cumulated cracks when slabs were exposed to 5kN loading applied at 10 Hz.

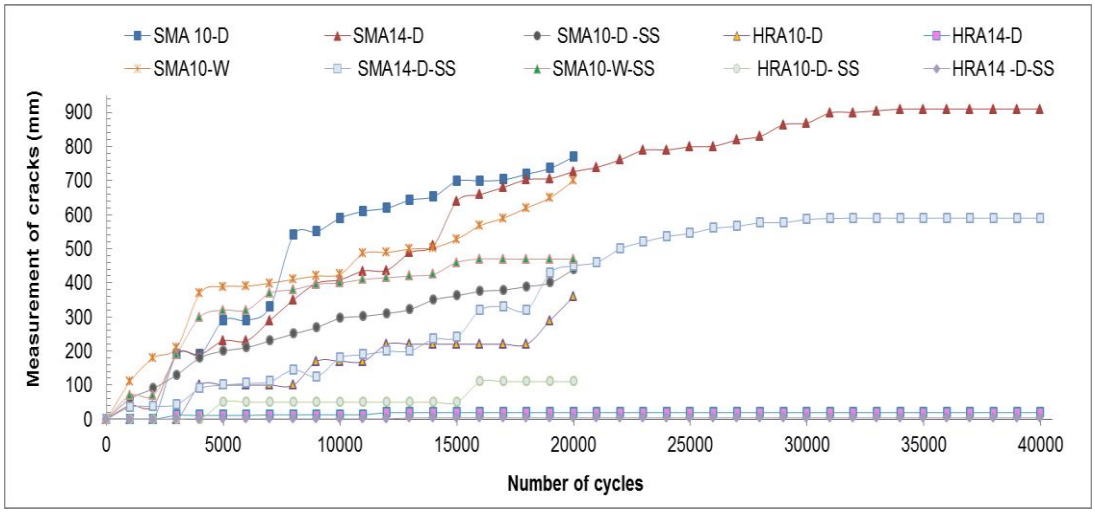

Figure 5.9 Average cumulative cracking mixtures tested in dry and wet condition at 10 Hz

Comparing with 5Hz results, presented in Figure 5.6, it is evident that increasing load frequency leads to accelerating damage. For example, in 10mm OPEN SMA dry test, after 5000 load pulses the crack was 290mm at 10Hz, whereas it was 89mm at 5Hz. Similarly, in wet conditions, crack length was 389mm at 10Hz and 164.5mm at 5Hz. For 14mm OPEN SMA dry test at 10Hz, crack length was 230mm, and at 5Hz it was 50mm. Finally, for 14mm HRA showed maximum cracking increase at high frequency loading, cracking was 0.2mm at 5Hz was 0.2mm but increased to 11 mm at 10Hz.

Comparing the influence of filler after 20,000 load pulses at 10Hz and 5kN the use of steel slag filer improved the resistant of cracking 24% in 10mm OPEN SMA and 22% in 10mm HRA. For 10 mm OPEN SMA dry test with granite filler the cracks was 770mm while with steel slag filer the cracks were 470mm. The cracks in 10mm OPEN SMA wet condition were 700mm while 10mm OPEN SMA-SS was 470mm. Moreover, in 10mm HRA dry condition was 360mm, and 10mm HRA-SS, it was 110mm.

The relative impact of load frequency was studied and the ratio of cracking at 5Hz and 10Hz at particular load pulse is presented in Figure 5.10.

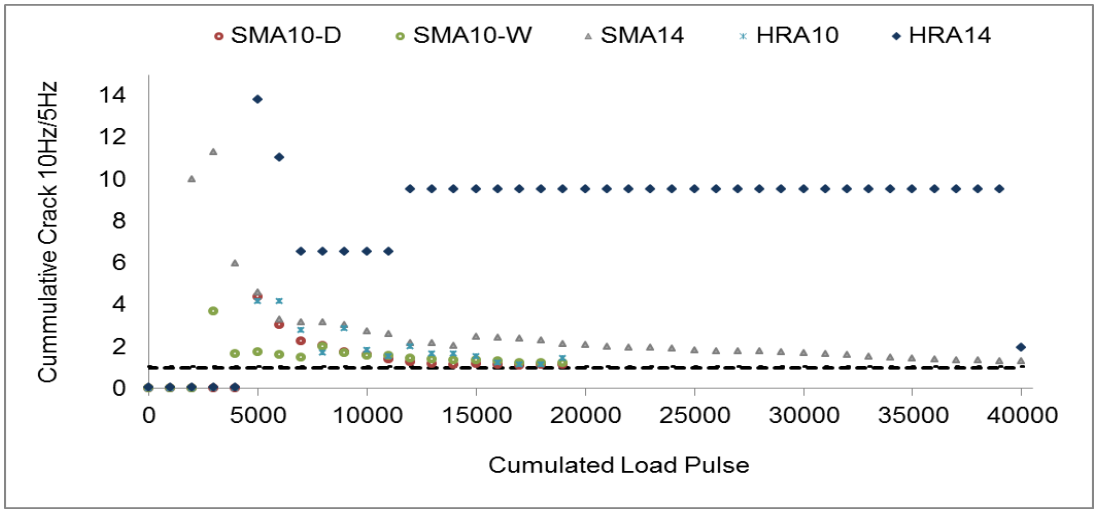

Figure 5.10 Comparison between 10Hz and 5Hz cracking

10mm Open SMA showed 3.25 times increase in cracking between 5Hz to 10Hz, 14mm Open SMA showed the 11.28 times from 5Hz to 10Hz and for 10mm HRA it was 4.16 times. Although, the cracking in 14mm HRA was very low but comparing between low and high frequencies, cracking increase nearly 55 times.

5.5.2 Rutting on Different Surfaces

Rutting is one of the principal factors that affect pavement performance and has resulted in various premature pavement failures. Factors considered in this study included types of asphalt mixtures, loading frequency, weather conditions, and aggregate size.

The average maximum rutting in both dry and wet condition testing for all mixtures are shown in Figure 5.11. The cumulative rutting for each mixture tested in dry and in wet condition was also studied. Figures 5.12a to 5.12f show the cumulative rutting result of individual specimen for all mixtures tested in dry and in wet conditions.

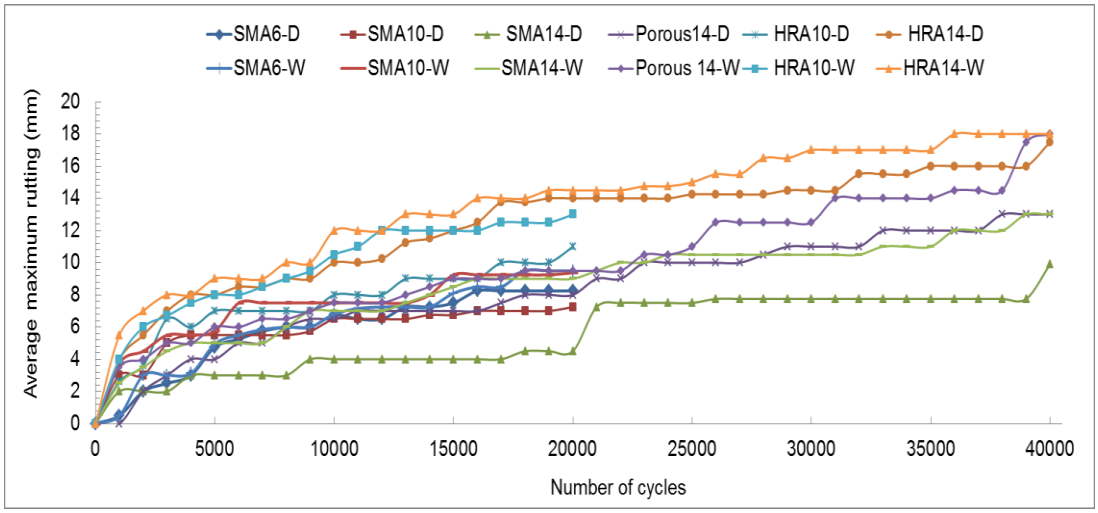

Figure 5.11 Average maximum rutting for all mixtures at 5Hz

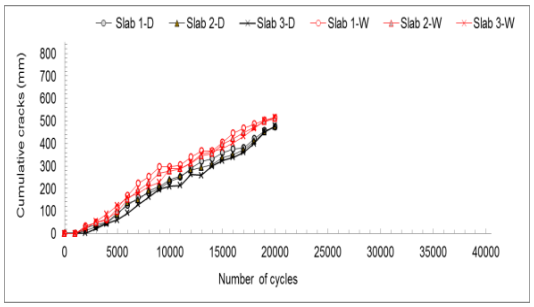

a) Measured rutting in six 6mm Open SMA slabs in wet and dry conditions

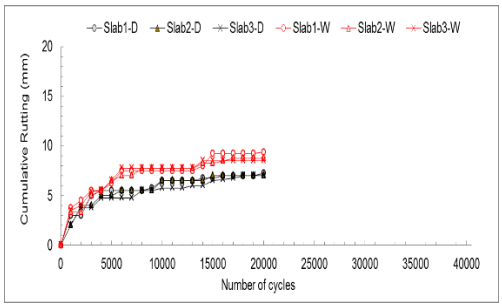

b) Measured rutting in six 10mm Open SMA slabs in wet and dry conditions

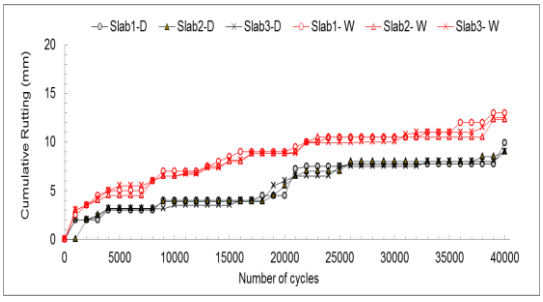

c) Measured rutting in six 14mm Open SMA slabs in wet and dry conditions

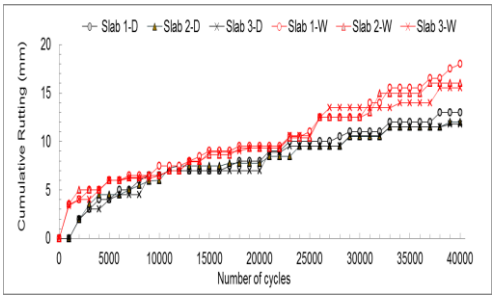

d) Measured rutting in six 14mm PA slabs in wet and dry conditions

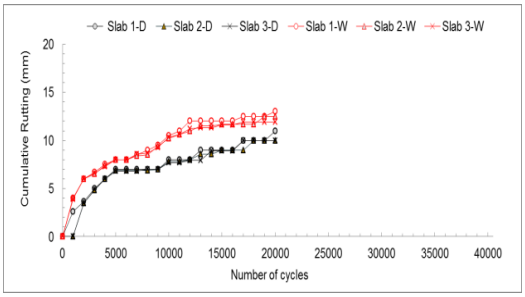

e) Measured rutting in six 10mm HRA slabs in wet and dry conditions

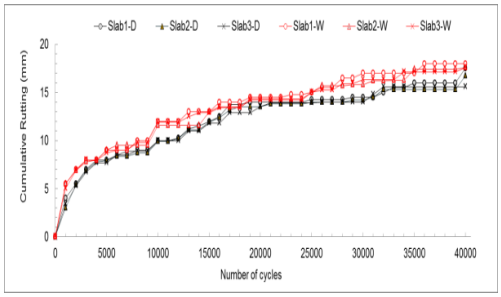

f) Measured rutting in six 14mm HRA slabs in wet and dry conditions

Figure 5.12 Cumulative rutting for individual slab for each mixture

It can be seen that the results are consistent for each mixture, and rutting patterns are similar in three individual dry tests and in three individual wet tests.

5.5.2.1 Influence of Water on Rutting

The result of rutting presented in Figure 5.11, irrespective of mixture types, the resistance to permanent deformation of the asphalt mixtures decreases with the presence of water.

Table 5.3 shows the level severity of each type of asphalt mixture based on studied by (Vaitkus Cygas, and Kleiziene, 2014; Nguyen and Le, 2016). After 20,000 load cycles, the rutting in 10mm HRA and 14 mm HRA reached high severity levels. For the same load cycles, presence of water accelerates rutting in 14mm Open SMA from low severity 4.5mm in dry testing to medium severity 9 mm in wet testing, an increase in 50%. For the rest of asphalt mixture, presence of water accelerated the rutting too. For example, for 10mm Open SMA, 7.5mm rutting was measured in dry testing, which increased to approximately 20% to 9.4mm in wet testing. In 14 mm PA, the dry testing rutting was 8.2mm, but it increased to 9.5mm in wet testing, an approximately 16% increase.

After 40,000 cycles, rutting in 14mm HRA dry testing was 14.5mm, but in wet testing it was 18mm, approximately 25% increase. In 14mm Open SMA, 9.9mm rutting in dry testing, which went up to 13mm in wet testing, an increase of approximately 32%.

Similarly, in 14mm PA, 8mm rutting in dry test, increased to 13mm in the presence of water, 55% increased.

Table 5.3 Maximum rutting

Mixture ID	@ 20,000 load cycles		@40,000 load cycles	
	Measured rutting (mm)	Low Severity <6 mm, Medium Severity <11 mm, High severity <20 mm	Measured rutting (mm)	Low Severity <6 mm, Medium Severity <11 mm, High severity <20 mm
HRA10-D	11.4	H	-	-
HRA10-W	13.2	H	-	-
HRA14-D	14.3	H	14.5	H
HRA14-W	17.5	H	18	H
Open SMA6-D	8.3	M	-	-
Open SMA6-W	9.5	M	-	-
Open SMA10-D	7.5	M	-	-
Open SMA10-W	9.4	M	-	-
Open SMA14-D	4.5	L	9.9	M
Open SMA14-W	9.0	M	13	H
PA14-D	8.2	M	13	H
PA14-W	9.5	M	18	H

5.5.2.2 Influence of Mixture Parameters on Rutting

Both 10 mm and 14 mm HRA mixtures showed significant rutting after 20,000 load cycles compared to any OPEN SMA or Porous asphalts. The 14 mm HRA surface appears to perform the worst. The mechanical properties of the HRA come from the cohesion of the binder within the fine aggregates, so HRA can be less resistant to internal movement but it can be better in fatigue crack resistant.

The best performance was observed in 10 mm OPEN SMA. The mixture gradation appeared to have more influence on load bearing capacity than the size of aggregates.

Interesting to note that air voids do not seem to influence wet condition performance in OPEN SMA mixtures. For example, despite similar void contents in Open SMA 14 and Open SMA 10, Open SMA 10 was not very sensitive to wet conditions as it was in a 14 mm Open SMA. It has appeared that aggregate nominal size may have an impact on wet condition performance.

At the end of 40,000 pulses, the porous asphalt showed significant rutting. It is likely that the permeability of porous asphalt is also subjected to different properties of

clogging material (i.e. types, concentration, and particle size distribution) as well as the loading state (cycle of clogging). Since the clogging limits the ability of porous asphalt layer to transmit water internally, it will create internal pressure resulting breaking and deforming of the bond (Hassan et al., 2015). Despite its benefits, the presence of water, the performance and service life of porous asphalt pavement is limited due to poor durability and loss of permeability because of clogging.

Influence of steel slag filer at 10Hz in mixture showed improvement in resistance to rutting, for example, the range was 39.3% in 10mm HRA dry tests to 30.4% in 10mm OPEN SMA dry conditions.

5.5.2.3 Influence of Load Frequency on Rutting

Figure 5.13 presents the cumulated rutting when slabs were exposed to 5kN loading applied at 10 Hz.

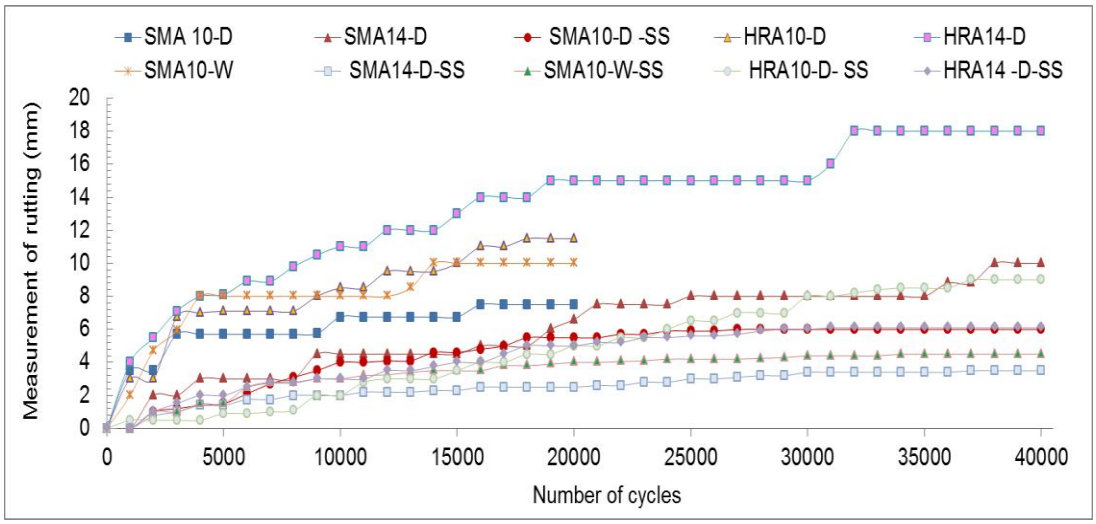

Figure 5.13 Measuring of rutting at 10Hz

Comparing with 5Hz results, shown in Figure 5.11, it can be seen that increasing load frequency caused accelerating rutting. For instance, in 14mm OPEN SMA dry test, after 20,000 load pulses, the rutting was 6.5mm at 10Hz corresponding to medium severity level, while it was 4.5mm at 5Hz which is in the low severity level.

Furthermore, in 10 mm OPEN SMA wet test, after 4000 load pulses, rutting was 8mm at 10Hz (medium severity level) and 5.5mm at 5Hz which falls into low severity level.

The relative influence of load frequency was investigated, and the ratio of rutting at 5Hz and 10Hz at a specific load pulse is shown in Figure 5.14.

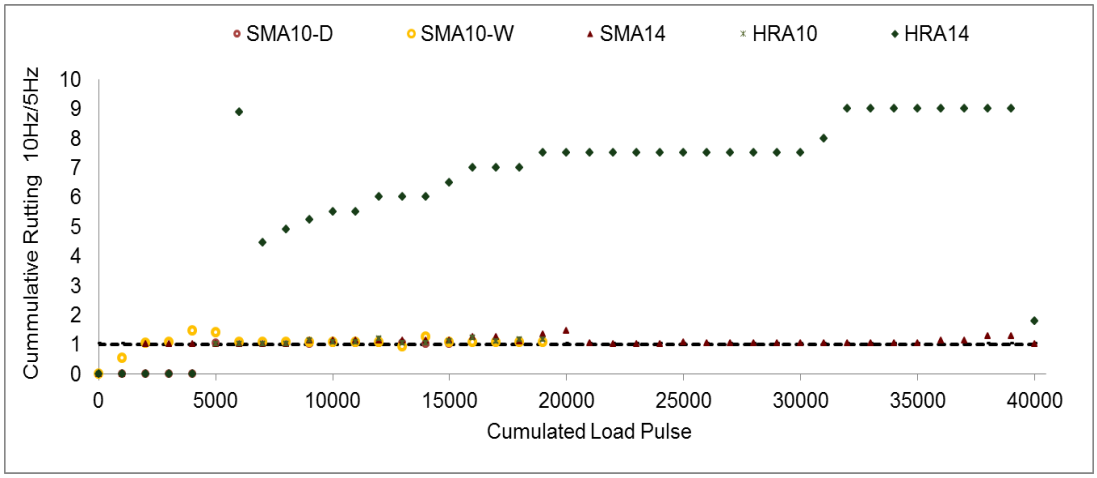

Figure 5.14 Comparison between 10Hz and 5Hz rutting

14mm HRA showed low resistant to rutting and, comparing between low and high frequencies, rutting increase approximately ten times.

Increasing load frequency, rutting was accelerated in the rest of the mixtures, and the range was from 1.27 times in 10mm OPEN SMA dry test to 1.47 times in 14mm OPEN SMA dry conditions.

5.6 Discussions

5.6.1 Overall Asphalt Surface Damage

Concerning dry versus wet damage severity after every 1000 pulses for all asphalt mixtures, the relative effect on cracking and rutting is shown in Figure 5.15 and Figure 5.16 respectively. The differences in the percentage of each type of asphalt mixture in wet and in dry conditions was calculated using the following simple formula; the difference in percentage = ((distress in wet-distress in dry)/total distress) × 100

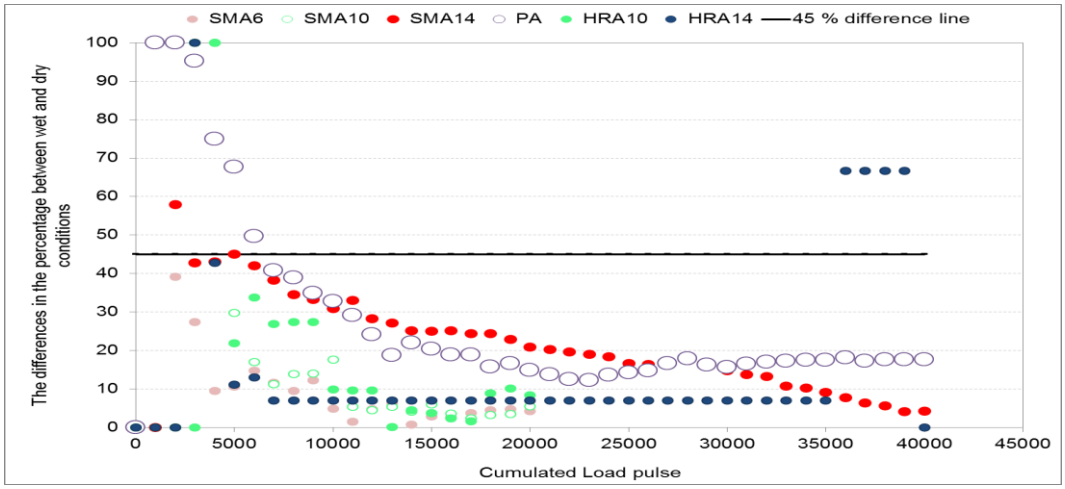

Figure 5.15 Difference in percentage at every 1000 cycles between wet and dry cracking

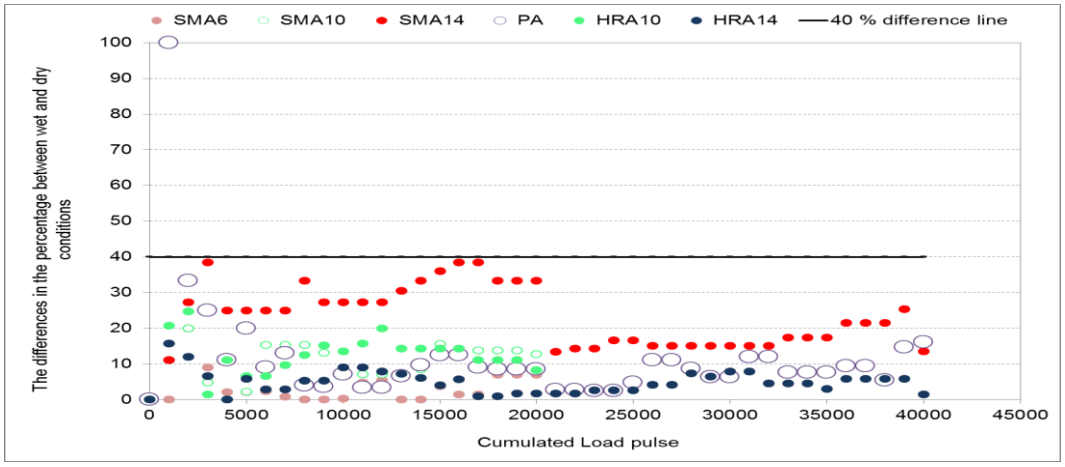

Figure 5.16 Difference in percentage between wet and dry rutting

The presence of water in the same asphalt mixture, compacted in the same manner, leads to increased cracking by up to 45% and rutting was up to 40%.

As discussed in section 5.5.1.2, it has appeared that the gradation has more influence on cracking than actual size of aggregate. For example, 6mm and 14 mm OPEN SMA appears to have inferiors cracking resistance than 10 mm Open SMA.

Water on the surface has minimum impact on the HRA surface cracking (Figure 5.6). This is primarily due to the gradation of the mixtures, as PA and Open SMA mixtures contain aggregate contact whereas HRA has more binder in the mix making it resilient

to crack. It is likely that water or moisture entrapped within the asphalt mixtures can lead to the pore pressure build-up due to the repeated traffic loads. The continuation of the process of the pore pressure ultimately leads to the degradation of the adhesive bond strength of the mastic (bitumen-filler) and that of the aggregates resulting in the growth of micro-cracks in the asphalt mixtures. As both Open SMA and Porous asphalt have more aggregate contact with relatively thin binder film thickness, these mixtures are more prone to cracking, than HRA mixtures with high binder content.

It is also interesting to note in Figure 5.6 that the air voids do not seem to have influence on wet condition. For example, despite similar void contents in OPEN SMA 14 (12.5% voids, shown in Chapter 3.3.6) and OPEN SMA 10 (13.63% voids), OPEN SMA 10 was not very sensitive to wet conditions as it was in OPEN SMA14. It is appeared that aggregate nominal size may have an impact on wet condition performance.

In addition to cracking, Figure 5.11 shows the influence of water on the rutting on different surfaces. It is clear that although rutting is a high-temperature phenomenon, the influence of water significantly deteriorated the resistance capacity of all tested mixtures even at 20^0C.

In addition to rutting and cracking, some ravelling was also observed in all OPEN SMA and Porous asphalt mixtures after the wet test, but it was negligible in mixtures tested in dry condition. Very little material loss was found in both HRA mixtures. It is important to note that the damage pattern and relative quantity of damage were similar in all three-specimens tested for each mix in dry condition and three specimens tested in the wet situation.

Furthermore, it is evident that irrespective of mixture type, loading frequency accelerates surface damage in wet condition. The severity in many cases was almost double when loading frequency was doubled from 5Hz to 10Hz. The higher speed appears to create more pore water pressure in the mixture, as demonstrated in Chapter 4, resulting faster break down of the mixture integrity.

This indicates the method developed in this research has the potential to be used to evaluate the performance of different asphalt surfaces under combined loading and water saturation condition.

5.6.4 Assessment of Combined Damage

As cracking and rutting occur simultaneously and were measured in mm, both damaged were combined and presented in Figure 5.17 evaluate their overall effect on different asphalt surfaces.

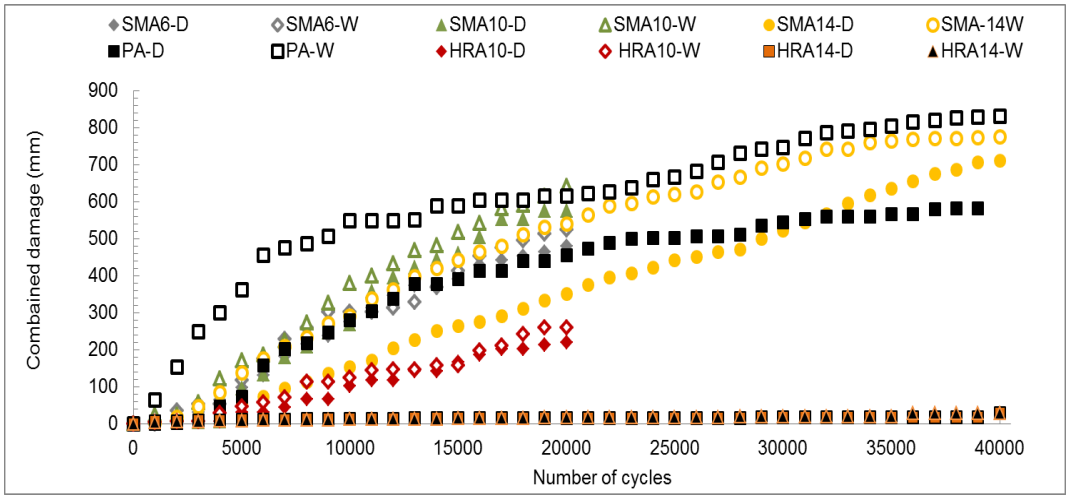

Figure 5.17 Overall performance of different asphalt slab surfaces

As amount of cracking (up to 800 mm) on the surfaces were far higher than the maximum rutting (up to 20 mm), the impact of cracking on the overall performance was significantly higher. This can be clearly seen that despite significant rutting in 14mm HRA, the very minimum cracking, has put this mixture in best performance. Other mixtures, with significant amount of cracking showed overall inferior performance despite good rutting resistance. Whilst both rutting and cracking on asphalt surfaces will have negative impact on pavement serviceability (ride quality) performance, significant surface cracking would allow water to ingress in lower structural layers, aiding to further structural deterioration.

5.6.5 Comparison with Previous Studies

Abo-Qudais and Shatnawi (2007) conducted comparative research on three different HMAs with a maximum nominal size of 12.5, 19 and 25 mm. This research was aimed to predict the number of cycles that produce a fracture of hot-mix asphalt (HMA) based on the number of cycles at which the slope of accumulated strain turned from

decreasing to increasing mode. Also, the impact of aggregate gradation and temperature on fatigue behaviours of HMA was evaluated.

They found that the larger gradation had the lower fatigue life, which means, the gradation has 12.5 mm maximum nominal size had the highest fatigue life followed by the gradation containing 19 and 25 mm maximum nominal sizes.

In this research found the 14 mm aggregate size have more sever to cracking in porous asphalt and Open SMA. The finding showed the same trend of the research done by Abo-qudais and Shatnawi (2007).

5.7 Summary

The main conclusion from this chapter is the influence of combined water and dynamic loading on surface damage was successfully simulated in the laboratory environment. The outcome of the test method has demonstrated promising future for further development as a screening test for different types of mixtures. Depending on the type of asphalt surfaces, the appearance of water accelerates surface damage concerning cracking, rutting and other distresses such as ravelling. The cracking trend was severe in extremely open graded porous asphalt PA, then semi impermeable Open SMA and gap graded hot rolled HRA asphalt mixtures. Compared to dry condition testing, the form of surface crack was approximately seven times faster in porous asphalt experimented in wet conditions. It is likely that the water pressure builds up inside the pore increases during cycling loading which then lead to extra stress and strains, resulting accelerated damage. It is interesting to note that while porous asphalt is designed to drain water within open voids, the constant presence of water on the surface as result of heavy rain combined with loading can significantly diminish their load bearing capacity. All tested Open SMA mixtures proved good wet condition rutting resistance compared to porous and hot rolled mixtures, although their cracking resistance was significantly decreased in the presence of water.

Both 10mm and 14mm HRA showed the best performance regarding resistance to cracking; the rutting was significantly higher compared to the other two mixtures. However, at the end of 40,000 pulses, the porous asphalt showed significant rutting.

The best performance was observed in 10mm SMA. In the presence of water, the mixture gradation seemed to have more impact on load bearing capacity than the size of aggregates.

In the next chapter, two deterioration prediction models based on Fuzzy Inference System (FIS) and Multiple Variables Regression Analysis have been developed using the input from this chapter. These inputs are aggregate size, weather conditions, asphalt surface types and frequencies and experientially measured distresses such as rutting and cracking.

Chapter 6 Development of Deterioration prediction model

6.1 Introduction

As presented in Chapter 5, rutting, and cracking are the two mains distresses that can happen in asphalt surfaces when pavement is flooded with water and experiences repeated traffic loading. Once the deterioration has been quantified, it is important to develop a model to predict the performance of different types of asphalt surfaces. A prediction model usually is done by learning from the past for which actual data is gathered and analysed to investigate the resulting pattern (Vaidehi *et al.*, 2008).There are a plethora of prediction models available in the literature, from simple deterministic linear regression model to a probabilistic Markov chain to artificial intelligence based (Abaza, 2016; Saleh, Awda and Ahmed, 2008; Al-Mansour, Sinha and Kuczek, 1994). All these methods have their merits and short-comings. A review of these methods has been presented in Chapter 2. After a careful literature review, in this study, a Fuzzy Inference system (FIS) has been used (Mahmood, Rahman and Mathavan, 2018). FIS modelling has excellent learning capabilities, requires less computational effort, suitable to deal with high dimensional problems and easier to implement (Sheta, 2006). A brief overview of the method has been given in chapter 2, section 2.3.3 and specific details on model development is described in the modelling section of this Chapter.

The primary objective of this chapter is to develop a multi input models to predict deterioration of asphalt surfaces due to the combined action of repeated traffic loading with specific tyre characteristics applied on submerged asphalt surfaces. The input parameters for this study were asphalt surface type, aggregate size, initial void contents, weather condition and loading frequency. Three asphalt surfaces, namely, hot rolled asphalt (HRA), stone mastic asphalt (OPEN SMA) and porous asphalt (PA) were chosen as these were evaluated in Chapter 5 as a most commonly used surfacing type. Each of these mixtures was produced with different sizes of aggregates to assess their impact on mixture performance. The testing was done at two frequencies and both in dry and in wet conditions. In the prediction models, both rutting and cracking were considered as the main predicted distress. After developing the model, validation exercise and sensitivity analyses were carried out to evaluate the model accuracy and the influence of each parameter in model output.

A single equation of prediction model generated using multiple variable regression analysis and finally with key conclusions.

6.2 Deterioration Prediction Model by FIS (Fuzzy Inference Systems)

The theoretical background of fuzzy logic and adopted method is given in sections 2.3.2 and 2.3.3 respectively.

Fuzzy interface system (FIS) is one of the most popular methods used in classification and prediction problems (Mahmood, 2015). It interprets the values in the input vector and, based on user-defined rules, assigns values to the output vector (Borkar and Atulkar, 2013). Dehzangi et al., (2007) found the benefits of this method that is represented by the knowledge in the form of *If-Then* rules, interpreting the mechanism of logic in human-understandable terms. It can take linguistic information from human experts and combine it with numerical data. In addition, it can approximate complex nonlinear functions with simpler models (Dehzangi *et al.*, 2007).

Fuzzy based model was developed in three main steps, generation of membership functions, data clustering and fuzzy rules. A short description of each of these steps is given below.

6.2.1 Membership Functions Generation

Within the fuzzy approach, the fuzzy set *A* of universe *X* is determined by the function $\mu_A(x)$, named the membership function of set *A* (Negnevitsky, 2002)

$$\mu_A: \times \rightarrow [0, 1]$$

Where $\mu_A(x) = 1$ if *x* is totally in *A*; $\mu_A(x) = 0$ if x is not in A; $0 < \mu_A(x) < 1$ if *x* is partly in *A*. in this research, the membership functions of inputs variables are generated by data clustering method.

6.2.2 Data Clustering

Numerical data clustering is the foundation of various modelling and classification algorithms to evaluate their performance (Jain, 2010). It separates the data set into many data subsets, such that the similarity within a subset is higher than between the subsets. A similarity among elements of input vectors is an essential feature to achieve data clustering (Naik, 2004). The most common clustering method, one has been used in this study, is k-means clustering. The fundamental thought of this clustering technique is to choose k initial cluster means, or centres randomly. After many repetitions, certain initial cluster means are updated in such a way that they represent the data clusters as much as possible (Christiansen, 2007). A limitation of the k-means clustering algorithm is that the number of clusters is fixed; after k is chosen, there will always be k cluster means or centres (Mahmood, 2015). The k-means algorithm can avoid this limitation by eliminating the excess clusters. A cluster centre may be removed if it does not have enough samples. It is likely to prevent this problem by picking a large enough k (Naik, 2004). The steps for k-mean clustering technique are as follows;

i. Initialise C_i by randomly choosing C points from among all the data points.
ii. Compute the membership matrix (U), where the element (u_{ij}) is 1 if the j^{th} data point x_j belongs to the group i and 0 oppositely.
iii. Compute the fitness function by using the following equation. Stop if the fitness function value is lower than a certain threshold value:

$$J = \sum_{i=1}^{c} = Ji = \sum_{i=1}^{c} (\sum k, x_k \in c_i \| x_k - c_i \|^2)$$

Update the cluster centre C_i and calculate the new matrix (U). The k-means clustering algorithm is iterative. Accordingly, it is hard to forecast its convergence to the best solution (Mahmood, 2015).

6.2.3 Fuzzy Rules

A rule containing several fuzzy If-Then rules (Jang, 1993), and they were,

1) A database which defines the membership functions in the fuzzy sets used in the fuzzy rules;

2) A decision-making unit which performs the inference operations on the rules;

3) Fuzzification interface which transforms the crisp inputs into degrees of a match with linguistic values;

4) Defuzzification interfaces which transform the fuzzy results of the inference into a crisp output.

The number of rules of a complete rule set is equal to

$$\Pi_i^n = 1^{m_i}$$

Where *m* is the number of membership functions for input *i*, and *n* is the number of inputs

The fuzzy rules are generated either from skilful experience or numerical data (Nelles, Fischer and Muller, 1996). In this study, the widely used Wang & Mendel technique was adopted to create fuzzy rules mechanically from numerical data (Wang and Mendel, 1992). This method needs predefined fuzzy membership functions for each input and output (Mahmood, 2015; Chen and Chen 2002). It begins by performing one rule for each data pair of the training set the ith pair rule is as follow:

$$\text{IF } x_1 \text{ IS } A_1^i \text{ AND } x_2 \text{ is } A_2^i \ldots \text{ AND } x_p \text{ THEN } y \text{ is } C^i$$

The fuzzy sets A_1^i are those for which the degree of match of X_j^i is maximum for each input variable j from pair i. The fuzzy set Ci is the one for which the degree of match of the observed output, y, is maximum (Guillaume, Charnomordic and Lablee, 2002).

6.2.4 Inputs and output Parameters

As mentioned earlier for development of prediction model, the key element to be considered is rules, input and output parameter. The rule generation are explained in

previous section and a brief overview on input and output parameters used in this research is given below.

The primary challenge for predicting deterioration of in-service pavement is the existence and use of the various factors influencing pavement performance that require being respected.

These factors are traffic loading, Weather condition, initial design, pavement age, construction, and maintenance effect (Fwa, 2006). In this project, the following parameters are considered as inputs for the deterioration prediction models.

6.2.4.1 Weather Condition

Climate is one of the key contributors to pavement structural distress, and the climatic effect is represented by precipitation quantity and freeze-thaw cycles. Structural damage reduces the load-carrying capacity of a pavement, which causes distress such as cracking, rutting and ravelling (Al-Mansour et al., 1994; Fwa, 2006). It is challenging to represent environmental effects mathematically in a prediction model. Therefore, environmental impacts were inserted by generating a prediction model. These are wet and dry conditions.

6.2.4.2 Traffic

Usually, the influences of traffic related deterioration consider are the traffic volume, vehicle type, load repetition and axle load type. The study conducted in Chapter 4 indicated that load frequency has more impact water pressure. Therefore, it was decided to use 5kN load magnitude with two frequencies 5Hz and 10Hz.

6.2.4.3 Pavement Type and Construction

The type and construction of a pavement section have a significant impact on its performance. Usually, pavement design consists of two main parts: the pavement type and asphalt layer thickness. In performance prediction analysis, all pavement sections should be the same pavement type; that is, flexible or rigid (Fwa, 2006). Since pavement structure and construction have a significant effect on deterioration, three

asphalt types are employed to reflect structural design variations in this research. In addition, three size of aggregate has been used for asphalt mixtures.

6.2.4.4 Output Parameters

There are many types of asphalt distress as explained in detail in sections 2.1.4 and 2.1.5 in this research, the section will consider two major types of damages rutting and cracking. A crack can permit water to enter the asphalt surface and lead to the development of a pothole or stripping and rutting will hold water in the rut and can create optional unsafe driving.

6.3 Development of Deterioration Prediction Model

Figure 6.1 shows the flowchart of two stages in the damage prediction model. Stage one was based on experimental work in Chapter 5, and stage two shows the development of deterioration prediction model using the information from stage 1. A short description of each of these steps in stage 2 is given below.

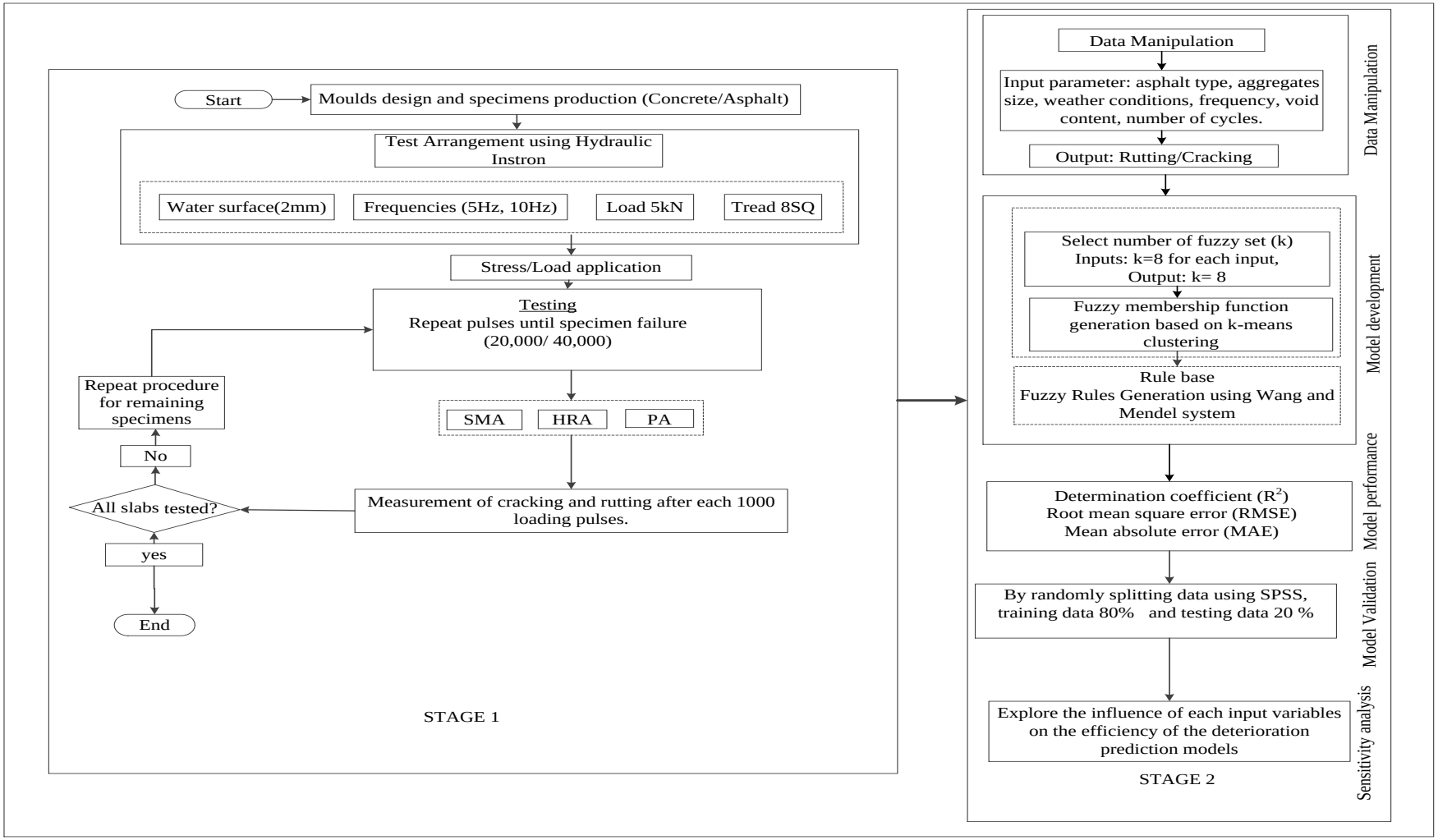

Figure 6.1 Flowchart of a pavement damage prediction model based on FIS.

6.3.1 Data Manipulation

For building a pavement deterioration model in FIS, the three asphalt types, three different aggregate size, two weather conditions, one load, three void contents and two frequencies were used as FIS inputs, and a measured cracking was defined as the FIS output. The same process was used to build the deterioration model for rutting. Cracking and rutting were used as an output parameter in the first model and the second model respectively. It was assumed that the void content remains constant even it changes due to progressive damage of the asphalt surfaces during testing.

The severity level of each distress type, as shown in Table 5.2 and Table 5.3 in Chapter 5, was determined by using the Distress Identification Manual for the Long-Term Pavement Performance Program (Miller and Bellinger, 2003). All input variables were converted to either linguistic or numerical number. For example, each mixture was given a numerical identification number, such as HRA=1, OPEN SMA=2, PA=3, and for aggregate sizes, 14 was for a large stone, 10 for medium size stone and 6 for small size stone. The dry condition was referred to as 0 while the wet condition was given number 1. A summary of threshold values and their corresponding linguistic abbreviation is given in the following Table 6.1.

Table 6.1 Linguistic/numerical identification of different mixture input and output parameters

Input	Name	Input variable conversion for FIS	
		Linguistic	Numerical
Mixture type	HRA	HRA	1
	Open SMA	Open SMA	2
	PA	PA	3
	Open SMA-SS*	HRA-SS	4
	HRA-SS*	Open SMA-SS	5
Aggregate size	14mm	Large	14
	10mm	Medium	10
	6mm	Small	6
Void content	Low	Low	<5
	Medium	Medium	>5 <12
	High	High	>12
Frequency	5 Hz	Low	5
	10 Hz	High	10
Weather	Dry	Dry	0
	Wet	Wet	1

*SS- same mixture with different mineral fillers. These additional mixtures were tested to include in the deterioration model.

6.3.2 Membership Function

The membership functions of input variables were generated by *k*-means clustering using Fuzzy Inference System Professional (FisPro.) software (Guillaume and Charnomordic, 2002). Rutting and cracking occur in asphalt surface simultaneously. Therefore, the membership functions for inputs variables of both rutting and cracking in the deterioration model were kept same. However, the output variables were different. For each parameter type, triangular membership functions representing the range of variability (low, medium, and high), as shown in Table 5.3 and 5.4 in Chapter 5, were generated. The seven triangular membership functions (MFs) of output were generated manually. The membership functions are shown in Figures 6.2 to 6.4.

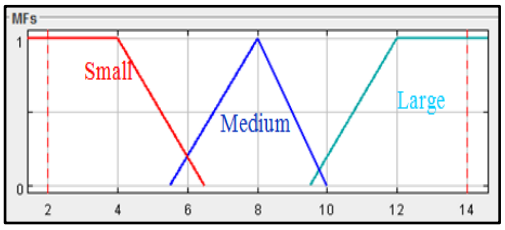

Aggregate sizes MFs

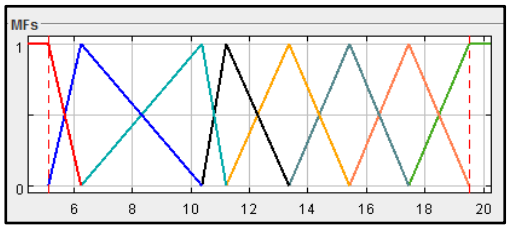

Void contents MFs

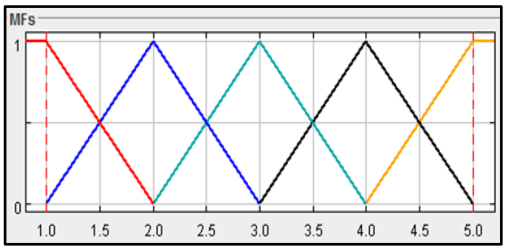

Asphalt type MFs

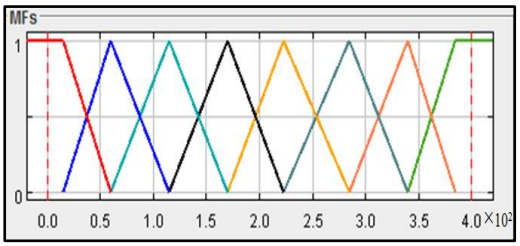

Cumulated load pulse MFs

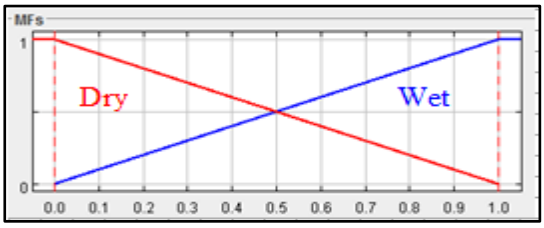

Weather Conditions MFs

Figure 6.2 Membership functions for models

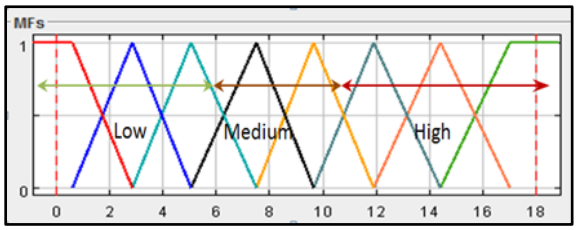

Figure 6.3 Rutting MFs

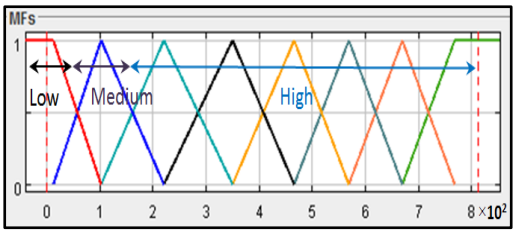

Figure 6.4 Cracking MFs

6.3.3 Fuzzy Rule

The FisPro software was used for automatic generation of fuzzy rules from the numerical data. The generation of fuzzy rules of the deterioration model reported in this study is challenging and complicated as it consists of six inputs and one output for each model. To overcome the problem of generation of the fuzzy rules and membership functions with a high-dimensional problem, the membership functions of inputs parameters were created based on the k-means clustering technique in (FisPro) software (Mahmood, 2015). FisPro offers the possibility to generate fuzzy inference systems and to use them for reasoning purposes, especially for simulating a physical or biological system (Chen and Chen, 2002). In total 140 rules were created for each model using the logic given in the fuzzy inference system. Fuzzy *If-Then* rules generated for cracking and for rutting are given in the following Table 6.2 and Table 6.3. An example of multi-input rules, as shown in Table 6.1 was " If aspahlt type is OPEN SMA, if aggrgate size is large, if whather is dry, if loading frequency is 5Hz, if void contents are medium, if no of load cycles are 0-6000" then output cracking severity level is "low". Similar logics were used for rutting output (shown in Table 6.3)

Table 6.2 Fuzzy If-Then rules generated for Cracking

Rules	Input Rule - If "Type Asphalt" is … and "Size Aggregate" is …						Output Rule- The Cracking Severity Level is …
	Asphalt Type	Aggregate Size	Weather	Frequency	Void Content	No of Cycles	
1.	Open SMA	Large	Dry	Low	Medium	0-6000	Low
2.	PA	Large	Dry	Low	High	0-6000	Low
3.	HRA	Medium	Dry	Low	Medium	0-6000	Low
4.	HRA	Large	Dry	Low	Medium	0-6000	Low
5.	Open SMA_SS	Medium	Dry	High	Medium	0-6000	Low
6.	OPEN SMA	Large	Dry	High	Medium	0-6000	Low
7.	HRA	Medium	Dry	High	Low	0-6000	Low
8.	HRA_SS	Medium	Dry	High	Low	0-6000	Low
9.	Open SMA	Large	Wet	Low	Medium	0-6000	Low
10.	PA	Large	Wet	Low	High	0-6000	Low
11.	HRA	Medium	Wet	Low	Medium	0-6000	Low
12.	HRA	Large	Wet	Low	Medium	0-6000	Low
13.	Open SMA_SS	Medium	Wet	High	Medium	0-6000	Low
14.	Open SMA	Small	Dry	Low	Medium	0-6000	Low
15.	Open SMA	Medium	Dry	Low	Medium	0-6000	Low
16.	Open SMA_SS	Large	Dry	High	Medium	0-6000	Low
17.	HRA	Large	Dry	High	Medium	0-6000	Low
18.	HRA_SS	Large	Dry	High	Medium	0-6000	Low
19.	Open SMA	Small	Wet	Low	Medium	0-6000	Low
20.	Open SMA	Medium	Wet	Low	Medium	0-6000	Low
21.	Open SMA	Medium	Wet	High	Medium	0-6000	Low
22.	Open SMA	Medium	Dry	High	Medium	0-6000	Low
23.	Open SMA	Large	Dry	Low	Medium	1500-11500	Low
24.	PA	Large	Dry	Low	High	1500-11500	Low
25.	HRA	Medium	Dry	Low	Medium	1500-11500	Low
26.	HRA	Large	Dry	Low	Medium	1500-11500	Low
27.	Open SMA_SS	Medium	Dry	High	Medium	1500-11500	Low
28.	Open SMA	Large	Dry	High	Medium	1500-11500	Low
29.	Open SMA_SS	Large	Dry	High	Medium	1500-11500	Low
30.	HRA	Medium	Dry	High	Low	1500-11500	Low
31.	HRA_SS	Medium	Dry	High	Low	1500-11500	Low
32.	HRA	Large	Dry	High	Medium	1500-11500	Low
33.	HRA_SS	Large	Dry	High	Medium	1500-11500	Low
34.	Open SMA	Large	Wet	Low	Medium	1500-11500	Low
35.	PA	Large	Wet	Low	High	1500-11500	High
36.	HRA	Medium	Wet	Low	Medium	1500-11500	Low

Rules	Input Rule - If "Type Asphalt" is … and "Size Aggregate" is …						Output Rule- The Cracking Severity Level is …
	Asphalt Type	Aggregate Size	Weather	Frequency	Void Content	No of Cycles	
37.	HRA	Large	Wet	Low	Medium	1500-11500	Low
38.	Open SMA	Medium	Wet	High	Medium	1500-11500	Low
39.	Open SMA_SS	Medium	Wet	High	Medium	1500-11500	Low
40.	Open SMA	Small	Dry	Low	Medium	1500-11500	Low
41.	Open SMA	Medium	Dry	Low	Medium	1500-11500	Low
42.	Open SMA	Small	Wet	Low	Medium	1500-11500	Low
43.	Open SMA	Medium	Wet	Low	Medium	1500-11500	Low
44.	Open SMA	Medium	Dry	High	Medium	1500-11500	Low
45.	Open SMA	Medium	Dry	Low	Medium	6000-17000	High
46.	Open SMA	Large	Dry	Low	Medium	6000-17000	Low
47.	PA	Large	Dry	Low	High	6000-17000	High
48.	HRA	Medium	Dry	Low	Medium	6000-17000	Low
49.	HRA	Large	Dry	Low	Medium	6000-17000	Med
50.	Open SMA_SS	Medium	Dry	High	Medium	6000-17000	Low
51.	Open SMA	Large	Dry	High	Medium	6000-17000	Low
52.	Open SMA_SS	Large	Dry	High	Medium	6000-17000	Low
53.	HRA	Medium	Dry	High	Low	6000-17000	Low
54.	HRA_SS	Medium	Dry	High	Low	6000-17000	Low
55.	HRA	Large	Dry	High	Medium	6000-17000	Low
56.	HRA_SS	Large	Dry	High	Medium	6000-17000	Low
57.	Open SMA	Small	Wet	Low	Medium	6000-17000	High
58.	Open SMA	Large	Wet	Low	High	6000-17000	High
59.	PA	Large	Wet	Low	High	6000-17000	High
60.	HRA	Medium	Wet	Low	Medium	6000-17000	Low
61.	HRA	Large	Wet	Low	Medium	6000-17000	Low
62.	Open SMA	Medium	Wet	High	High	6000-17000	Low
63.	Open SMA_SS	Medium	Wet	High	High	6000-17000	Low
64.	Open SMA	Medium	Dry	Low	High	6000-17000	Low
65.	Open SMA	Medium	Dry	High	High	6000-17000	Low
66.	Open SMA	Medium	Wet	Low	High	6000-17000	High
67.	Open SMA	Large	Dry	Low	High	11507-22352	Low
68.	PA	Large	Dry	Low	High	11507-22352	High
69.	HRA	Medium	Dry	Low	Medium	11507-22352	Low
70.	HRA	Large	Dry	Low	Medium	11507-22352	Low
71.	Open SMA_SS	Medium	Dry	High	Medium	11507-22352	Low
72.	Open SMA	Large	Dry	High	High	11507-22352	Low
73.	Open SMA_SS	Large	Dry	High	High	11507-22352	Low
74.	HRA	Medium	Dry	High	Low	11507-22352	Low
75.	HRA_SS	Medium	Dry	High	Low	11507-22352	Low

Rules	Input Rule - If "Type Asphalt" is … and "Size Aggregate" is …						Output Rule- The Cracking Severity Level is …
	Asphalt Type	Aggregate Size	Weather	Frequency	Void Content	No of Cycles	
76.	HRA	Large	Dry	High	Medium	11507-22352	Low
77.	HRA_SS	Large	Dry	High	Medium	11507-22352	Low
78.	Open SMA	Large	Wet	Low	High	11507-22352	High
79.	PA	Large	Wet	Low	High	11507-22352	High
80.	HRA-SS	Medium	Wet	Low	Medium	11507-22352	Low
81.	HRA-SS	Large	Wet	Low	Medium	11507-22352	Low
82.	Open SMA	Medium	Wet	High	High	11507-22352	High
83.	Open SMA_SS	Medium	Wet	High	High	11507-22352	High
84.	Open SMA	Small	Dry	Low	Medium	11507-22352	High
85.	Open SMA	Medium	Dry	Low	High	11507-22352	High
86.	Open SMA	Small	Wet	Low	Medium	11507-22352	High
87.	Open SMA	Medium	Wet	Low	High	11507-22352	High
88.	Open SMA	Medium	Dry	High	High	11507-22352	High
89.	Open SMA	Small	Dry	Low	Medium	17000-28500	High
90.	Open SMA	Medium	Dry	Low	High	17000-28500	High
91.	HRA	Medium	Dry	Low	Medium	17000-28500	High
92.	Open SMA	Small	Wet	Low	Medium	17000-28500	High
93.	Open SMA	Medium	Wet	Low	High	17000-28500	High
94.	HRA	Medium	Wet	Low	Medium	17000-28500	low
95.	Open SMA	Large	Dry	Low	High	17000-28500	High
96.	PA	Large	Dry	Low	High	17000-28500	High
97.	HRA	Large	Dry	Low	Medium	17000-28500	Low
98.	Open SMA_SS	Medium	Dry	High	Medium	17000-28500	High
99.	Open SMA	Large	Dry	High	High	17000-28500	High
100.	HRA	Medium	Dry	High	Low	17000-28500	Low
101.	HRA_SS	Medium	Dry	High	Low	17000-28500	Low
102.	Open SMA	Large	Wet	Low	High	17000-28500	High
103.	PA	Large	Wet	Low	High	17000-28500	High
104.	HRA	Large	Wet	Low	Medium	17000-28500	Low
105.	Open SMA_SS	Medium	Wet	High	High	17000-28500	High
106.	Open SMA_SS	Large	Dry	High	High	17000-28500	Low
107.	HRA	Large	Dry	High	Medium	17000-28500	Low
108.	HRA_SS	Large	Dry	High	Medium	17000-28500	Low
109.	Open SMA	Large	Wet	High	High	17000-28500	High
110.	Open SMA	Large	Dry	High	High	17000-28500	High
111.	PA	Large	Dry	Low	High	22352-34000	High
112.	HRA	Large	Dry	Low	Medium	22352-34000	Low
113.	Open SMA	Large	Dry	High	High	22352-34000	High
114.	HRA_SS	Large	Dry	High	Low	22352-34000	Low

Rules	Input Rule - If "Type Asphalt" is … and "Size Aggregate" is …						Output Rule- The Cracking Severity Level is …
	Asphalt Type	Aggregate Size	Weather	Frequency	Void Content	No of Cycles	
115.	PA	Large	Wet	Low	High	22352-34000	High
116.	Open SMA	Large	Dry	Low	High	22352-34000	High
117.	Open SMA_SS	Large	Dry	High	High	22352-34000	High
118.	HRA	Large	Dry	High	Medium	22352-34000	Low
119.	HRA_SS	Large	Dry	High	Medium	22352-34000	Low
120.	Open SMA	Large	Wet	Low	High	22352-34000	High
121.	Open SMA	Large	Dry	Low	High	28500-38500	High
122.	PA	Large	Dry	Low	High	28500-38500	High
123.	HRA	Large	Dry	Low	Low	28500-38500	Low
124.	Open SMA	Large	Dry	High	High	28500-38500	High
125.	Open SMA_SS	Large	Dry	High	High	28500-38500	High
126.	HRA	Large	Dry	High	Medium	28500-38500	Low
127.	HRA_SS	Large	Dry	High	Medium	28500-38500	Low
128.	Open SMA	Large	Wet	Low	High	28500-38500	High
129.	PA	Large	Wet	Low	High	28500-38500	High
130.	HRA	Large	Wet	Low	Medium	28500-38500	Low
131.	Open SMA	Large	Dry	Low	High	34000-40000	High
132.	PA	Large	Dry	Low	High	34000-40000	High
133.	HRA	Large	Dry	Low	Low	34000-40000	Low
134.	Open SMA	Large	Dry	High	Medium	34000-40000	High
135.	Open SMA_SS	Large	Dry	High	Medium	34000-40000	High
136.	HRA	Large	Dry	High	Medium	34000-40000	Low
137.	HRA_SS	Large	Dry	High	Medium	34000-40000	Low
138.	Open SMA	Large	Wet	Low	Medium	34000-40000	High
139.	PA	Large	Wet	Low	High	34000-40000	High
140.	HRA	Large	Wet	Low	Medium	34000-40000	Low

Table 6.3 Fuzzy If-Then rules generated for Rutting

Rules	Input Rule - If "Type Asphalt " is … and "Size Aggregate" is …						Output Rule- The Rutting Severity Level is …
	Asphalt Type	Aggregate Size	Weather	Frequency	Void Content	No of Cycles	
1.	Open SMA	Large	Dry	Low	High	0-6000	Low
2.	PA	Large	Dry	Low	High	0-6000	Low

Rules	Input Rule - If "Type Asphalt " is … and "Size Aggregate" is …						Output Rule- The Rutting Severity Level is …
	Asphalt Type	Aggregate Size	Weather	Frequency	Void Content	No of Cycles	
3.	HRA	Medium	Dry	Low	Medium	0-6000	Low
4.	HRA	Large	Dry	Low	Medium	0-6000	Low
5.	Open SMA_SS	Medium	Dry	High	Medium	0-6000	Low
6.	Open SMA	Large	Dry	High	High	0-6000	Low
7.	HRA	Medium	Dry	High	Low	0-6000	Low
8.	HRA_SS	Medium	Dry	High	Low	0-6000	Low
9.	Open SMA	Large	Wet	Low	High	0-6000	Low
10.	PA	Large	Wet	Low	High	0-6000	Low
11.	HRA	Medium	Wet	Low	Medium	0-6000	Low
12.	HRA	Large	Wet	Low	Medium	0-6000	Low
13.	Open SMA_SS	Medium	Wet	High	High	0-6000	Low
14.	Open SMA	Small	Dry	Low	Medium	0-6000	Low
15.	Open SMA	Medium	Dry	Low	Medium	0-6000	Low
16.	Open SMA_SS	Large	Dry	High	Medium	0-6000	Low
17.	HRA	Large	Dry	High	Low	0-6000	Low
18.	HRA_SS	Large	Dry	High	Low	0-6000	Low
19.	Open SMA	Small	Wet	Low	Medium	0-6000	Low
20.	Open SMA	Medium	Wet	Low	Medium	0-6000	Low
21.	Open SMA	Medium	Wet	High	Medium	0-6000	Low
22.	Open SMA	Medium	Dry	High	Medium	0-6000	Low
23.	Open SMA	Large	Dry	Low	Medium	1500-11500	Low
24.	PA	Large	Dry	Low	High	1500-11500	Low
25.	HRA	Medium	Dry	Low	Medium	1500-11500	Medium
26.	HRA	Large	Dry	Low	Medium	1500-11500	Low
27.	SMA_SS	Medium	Dry	High	Medium	1500-11500	Low
28.	Open SMA	Large	Dry	High	Medium	1500-11500	Low
29.	SMA_SS	Large	Dry	High	Medium	1500-11500	Low
30.	HRA	Medium	Dry	High	Low	1500-11500	Low
31.	HRA_SS	Medium	Dry	High	Low	1500-11500	Low
32.	HRA	Large	Dry	High	Medium	1500-11500	Low
33.	HRA_SS	Large	Dry	High	Medium	1500-11500	Low
34.	Open SMA	Large	Wet	Low	Medium	1500-11500	Low
35.	PA	Large	Wet	Low	High	1500-11500	Low
36.	HRA	Medium	Wet	Low	Medium	1500-11500	Medium
37.	HRA	Large	Wet	Low	Medium	1500-11500	Medium
38.	Open SMA	Medium	Wet	High	Medium	1500-11500	Low
39.	SMA_SS	Medium	Wet	High	Medium	1500-11500	Low
40.	Open SMA	Small	Dry	Low	Medium	1500-11500	Low
41.	Open SMA	Medium	Dry	Low	Medium	1500-11500	Low
42.	Open SMA	Small	Wet	Low	Medium	1500-11500	Low
43.	Open SMA	Medium	Wet	Low	Medium	1500-11500	Medium
44.	Open SMA	Medium	Dry	High	Medium	1500-11500	Low
45.	Open SMA	Medium	Dry	Low	Medium	6000-17000	Medium
46.	Open SMA	Large	Dry	Low	Medium	6000-17000	Low

Rules	Input Rule - If "Type Asphalt " is … and "Size Aggregate" is …						Output Rule- The Rutting Severity Level is …
	Asphalt Type	Aggregate Size	Weather	Frequency	Void Content	No of Cycles	
47.	PA	Large	Dry	Low	High	6000-17000	Medium
48.	HRA	Medium	Dry	Low	Medium	6000-17000	Medium
49.	HRA	Large	Dry	Low	Medium	6000-17000	Medium
50.	Open SMA_SS	Medium	Dry	High	Medium	6000-17000	Low
51.	Open SMA	Large	Dry	High	Medium	6000-17000	Low
52.	Open SMA_SS	Large	Dry	High	Medium	6000-17000	Low
53.	HRA	Medium	Dry	High	Low	6000-17000	Low
54.	HRA_SS	Medium	Dry	High	Low	6000-17000	Low
55.	HRA	Large	Dry	High	Medium	6000-17000	Low
56.	HRA_SS	Large	Dry	High	Medium	6000-17000	Low
57.	Open SMA	Small	Wet	Low	Medium	6000-17000	Medium
58.	Open SMA	Large	Wet	Low	Medium	6000-17000	Medium
59.	PA	Large	Wet	Low	High	6000-17000	Medium
60.	HRA	Medium	Wet	Low	Medium	6000-17000	Medium
61.	HRA	Large	Wet	Low	Medium	6000-17000	Medium
62.	Open SMA	Medium	Wet	High	Medium	6000-17000	Medium
63.	Open SMA_SS	Medium	Wet	High	Medium	6000-17000	Low
64.	Open SMA	Medium	Dry	5Hz	Medium	6000-17000	Medium
65.	Open SMA	Medium	Dry	High	Medium	6000-17000	Low
66.	Open SMA	Medium	Wet	Low	Medium	6000-17000	Medium
67.	Open SMA	Large	Dry	Low	Medium	11507-22352	Low
68.	PA	Large	Dry	Low	High	11507-22352	Medium
69.	HRA	Medium	Dry	Low	Medium	11507-22352	Medium
70.	HRA	Large	Dry	Low	Medium	11507-22352	High
71.	Open SMA_SS	Medium	Dry	High	Medium	11507-22352	Low
72.	Open SMA	Large	Dry	High	Medium	11507-22352	Low
73.	Open SMA_SS	Large	Dry	High	Medium	11507-22352	Low
74.	HRA	Medium	Dry	High	Low	11507-22352	Low
75.	HRA_SS	Medium	Dry	High	Low	11507-22352	Low
76.	HRA	Large	Dry	High	Medium	11507-22352	Low
77.	HRA_SS	Large	Dry	High	Medium	11507-22352	Low
78.	Open SMA	Large	Wet	Low	Medium	11507-22352	Medium
79.	PA	Large	Wet	Low	High	11507-22352	Medium
80.	HRA	Medium	Wet	Low	Medium	11507-22352	Medium
81.	HRA	Large	Wet	Low	Medium	11507-22352	High
82.	Open SMA	Medium	Wet	High	Medium	11507-22352	Medium
83.	Open SMA_SS	Medium	Wet	High	Medium	11507-22352	Low
84.	Open SMA	Small	Dry	Low	Medium	11507-22352	Medium
85.	Open SMA	Medium	Dry	Low	Medium	11507-22352	Medium
86.	Open SMA	Small	Wet	Low	Medium	11507-22352	Medium
87.	Open SMA	Medium	Wet	Low	Medium	11507-22352	Medium
88.	Open SMA	Medium	Dry	High	Medium	11507-22352	Medium
89.	Open SMA	Small	Dry	Low	Medium	17000-28500	Medium
90.	Open SMA	Medium	Dry	Low	Medium	17000-28500	Medium

Rules	Input Rule - If "Type Asphalt " is … and "Size Aggregate" is …						Output Rule- The Rutting Severity Level is …
	Asphalt Type	Aggregate Size	Weather	Frequency	Void Content	No of Cycles	
91.	HRA	Medium	Dry	Low	Medium	17000-28500	Medium
92.	Open SMA	Small	Wet	Low	Medium	17000-28500	Medium
93.	Open SMA	Medium	Wet	Low	Medium	17000-28500	Medium
94.	HRA	Medium	Wet	Low	Low	17000-28500	Medium
95.	Open SMA	Large	Dry	Low	Medium	17000-28500	Medium
96.	PA	Large	Dry	Low	High	17000-28500	Medium
97.	HRA	Large	Dry	Low	Medium	17000-28500	High
98.	Open SMA_SS	Medium	Dry	High	Medium	17000-28500	Low
99.	Open SMA	Large	Dry	High	Medium	17000-28500	Low
100.	HRA	Medium	Dry	High	Low	17000-28500	Medium
101.	HRA_SS	Medium	Dry	High	Low	17000-28500	Low
102.	Open SMA	Large	Wet	Low	Medium	17000-28500	Medium
103.	PA	Large	Wet	Low	High	17000-28500	Medium
104.	HRA	Large	Wet	Low	Medium	17000-28500	High
105.	Open SMA_SS	Medium	Wet	High	Medium	17000-28500	Low
106.	Open SMA_SS	Large	Dry	High	Medium	17000-28500	Low
107.	HRA	Large	Dry	High	Medium	17000-28500	Medium
108.	HRA_SS	Large	Dry	High	Medium	17000-28500	Low
109.	Open SMA	Large	Wet	High	Medium	17000-28500	Medium
110.	Open SMA	Large	Dry	High	Medium	17000-28500	Low
111.	PA	Large	Dry	Low	High	22352-34000	Medium
112.	HRA	Large	Dry	Low	Medium	22352-34000	High
113.	Open SMA	Large	Dry	High	High	22352-34000	Low
114.	HRA_SS	Large	Dry	High	Low	22352-34000	Medium
115.	PA	Large	Wet	Low	High	22352-34000	Medium
116.	Open SMA	Large	Dry	Low	Medium	22352-34000	Medium
117.	Open SMA_SS	Large	Dry	High	Medium	22352-34000	Low
118.	HRA	Large	Dry	High	Medium	22352-34000	Medium
119.	HRA_SS	Large	Dry	High	Medium	22352-34000	Low
120.	Open SMA	Large	Wet	Low	Medium	22352-34000	Medium
121.	Open SMA	Large	Dry	Low	Medium	28500-38500	Medium
122.	PA	Large	Dry	Low	High	28500-38500	Medium
123.	HRA	Large	Dry	Low	Medium	28500-38500	High
124.	Open SMA	Large	Dry	High	Medium	28500-38500	Low
125.	Open SMA_SS	Large	Dry	High	Medium	28500-38500	Low
126.	HRA	Large	Dry	High	Medium	28500-38500	Medium
127.	HRA_SS	Large	Dry	High	Medium	28500-38500	Low
128.	Open SMA	Large	Wet	Low	Medium	28500-38500	Med
129.	PA	Large	Wet	Low	High	28500-38500	High
130.	HRA	Large	Wet	Low	Medium	28500-38500	High
131.	Open SMA	Large	Dry	Low	Medium	34000-40000	Medium
132.	PA	Large	Dry	Low	High	34000-40000	Medium
133.	HRA	Large	Dry	Low	Low	34000-40000	High
134.	Open SMA	Large	Dry	High	Medium	34000-40000	Low
135.	Open SMA_SS	Large	Dry	High	Medium	34000-40000	Low

Rules	Input Rule - If "Type Asphalt " is … and "Size Aggregate" is …						Output Rule- The Rutting Severity Level is …
	Asphalt Type	Aggregate Size	Weather	Frequency	Void Content	No of Cycles	
136.	HRA	Large	Dry	High	Medium	34000-40000	Med
137.	HRA_SS	Large	Dry	High	Medium	34000-40000	Low
138.	Open SMA	Large	Wet	Low	Medium	34000-40000	Medium
139.	PA	Large	Wet	Low	High	34000-40000	High
140.	HRA	Large	Wet	Low	Low	34000-40000	High

6.3 Results and Discussion

As mentioned earlier, two deterioration models were developed, one for cracking, and another one for rutting. For each model, six input variables such as asphalt type, aggregate sizes, weather conditions, frequencies, void contents and cycles numbers were used to generate output for rutting and cracking. The results are given below.

6.3.1 Pavement Deteriorations (Rutting and Cracking)

The prediction models for mixtures and for individual mixtures are presented below.

6.3.1.1 Prediction Model All mixtures

Figure 6.5 and Figure 6.6 show model correlation for rutting and cracking respectively. It can be seen that a correlation of approximately 94.1% was achieved between measured and predicted rutting and 96.6% correlation between measured and predicted cracking. This indicates a very good accuracy of both models.

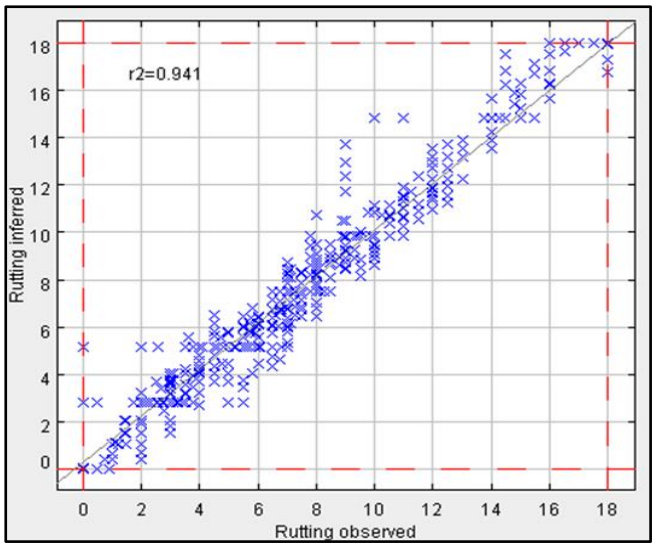

Figure 6.5 Relationship between measured and predicted rutting

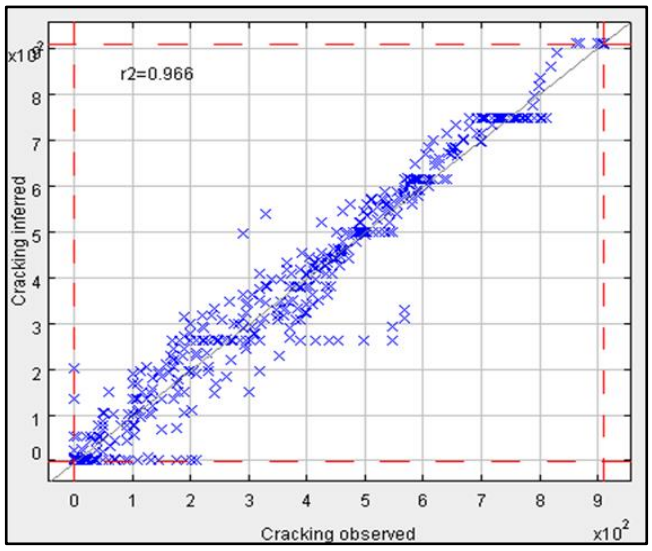

Figure 6.6 Relationship between measured and predicted cracking

Table 6.4 shows the coefficient of determination (RMSE) and (MAE). Mean Absolute Error (MAE) measures the average magnitude of the errors in a set of predictions. Furthermore, Root mean squared error (RMSE) measures square root of the average of squared differences between prediction and actual observation. Both MAE and RMSE express average model prediction error in units of the variable of interest. Since the errors are squared before they are averaged, the RMSE gives a relatively high weight to significant errors. This means the RMSE should be added beneficial when significant errors are particularly undesirable.

Table 6.4 Model performances of asphalt deteriorations

Deteriorations Types	R^2 (%)	RMSE	MAE
Rutting	94.1	1.112	0.732
Cracking	96.6	50.553	30.687

Both RMSE and MAE are very small for rutting, but high in the cracking. This is because the measurement of rutting was only up to 20mm and it was concentrated in confined areas under the loading plate. On the other hand, cracking was distributed across the slab and measured up to 900mm after the test. Despite this, these levels of correlations in both cases indicate good model accuracy.

6.3.1.2 Cracking Prediction model of each mixture

A pavement section's design and construction have the significant impact on its performance. Usually, pavement design consists of two principal parts, pavement kind and asphalt layer thickness. In performance prediction analysis, all pavement segments should be the same pavement kind, either flexible or rigid pavement. Thus, the performance of each type of asphalt mixture has studied, and the results are shown in Figure 6.7 to 6.9.

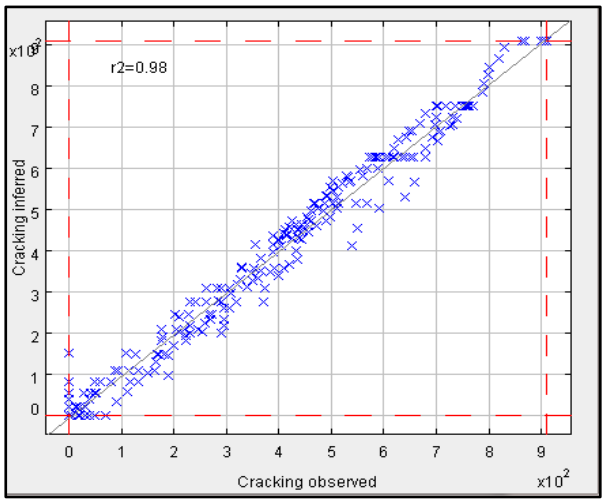

Figure 6.7 Relationship between measured and predicted cracking in Open SMA

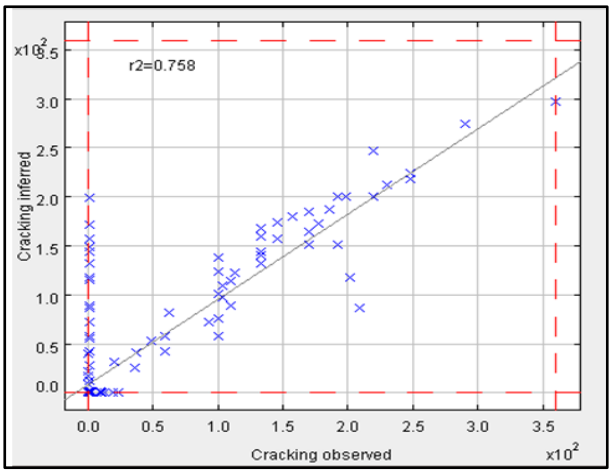

Figure 6.8 Relationship between measured and predicted cracking in HRA

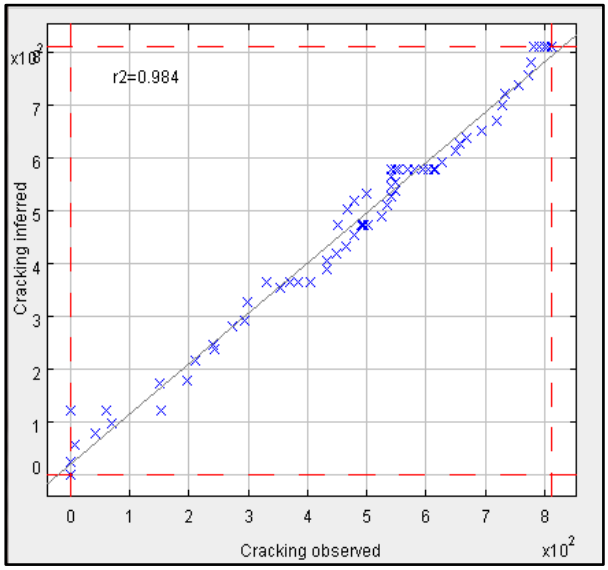

Figure 6.9 Relationship between measured and predicted cracking in PA

Table 6.5 Cracking Model performances of asphalt types

Asphalt Types	R^2 (%)	RMSE	MAE
Open SMA	89	37.315	28.571
HRA	75.8	37.761	19.013
PA	89.4	28.799	22.678

From Table 6.5 it can be seen that a correlation for open graded mixtures (PA, SMA) approximately 89.4% and 89% was achieved between measured and predicted

cracking while gap graded (HRA) showed 75.8 %. The performance of HRA was lower due to a 14mm HRA has negligible cracking and this influence the correlation value.

6.3.1.2 Rutting Prediction model of each mixture

Figures 6.10 to 6.12 show rutting model correlation of SMA, HRA, PA respectively. It can be seen that a correlation presented in Table 6.6 approximately 91.5%, 91.3% and 95.8 was achieved between measured and predicted rutting. This indicates a very good accuracy of three models

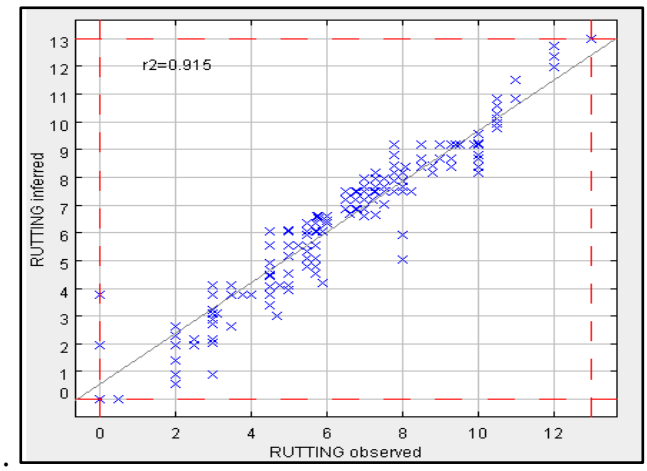

Figure 6.10 Relationship between measured and predicted rutting in Open SMA

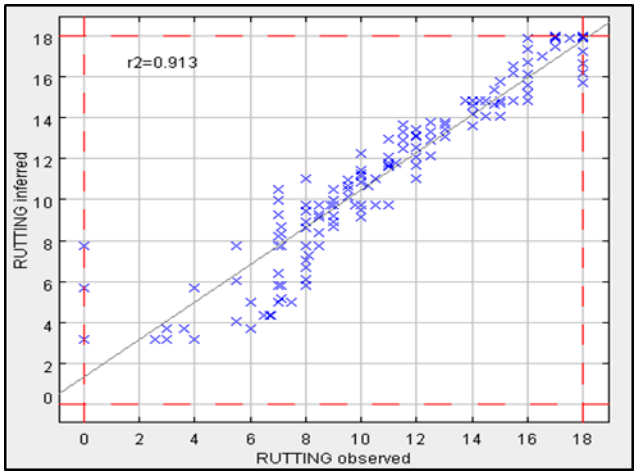

Figure 6.11 Relationship between measured and predicted rutting in HRA

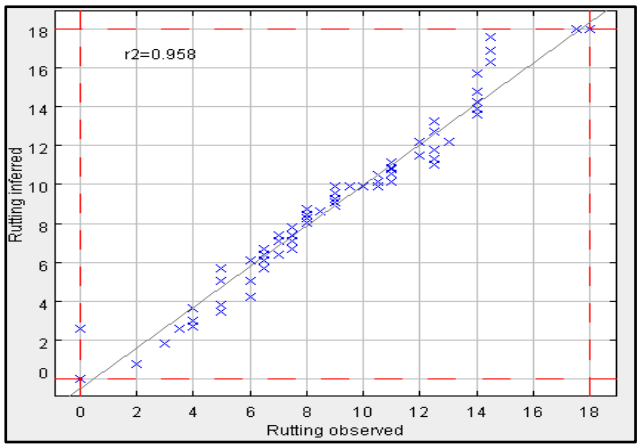

Figure 6.12 Relationship between measured and predicted rutting in PA

Table 6.6 Rutting Model performances of asphalt types

Asphalt Types	R^2 (%)	RMSE	MAE
Open SMA	91.5	0.795	0.552
HRA	91.3	1.362	0.962
PA	95.8	0.843	0.591

6.3.2 Cross Validation Method

The cross-validation method was conducted to assess how well models can predict cracking/rutting across the dataset. The entire data set used to develop the prediction model were randomly split into training data (around 80%) and testing data (around 20%). The training data were used to generate the prediction models while the testing data were used to validate the models. The data for both models were split by using SSPS software (Landau, 2004). SPSS can automatize this selection process without requiring multiple steps. The process to split training data and testing data has been repeated to run models five times for both cracking and rutting to ensure all data were included. The models are presented in Figure 6.7 and Figure 6.8.

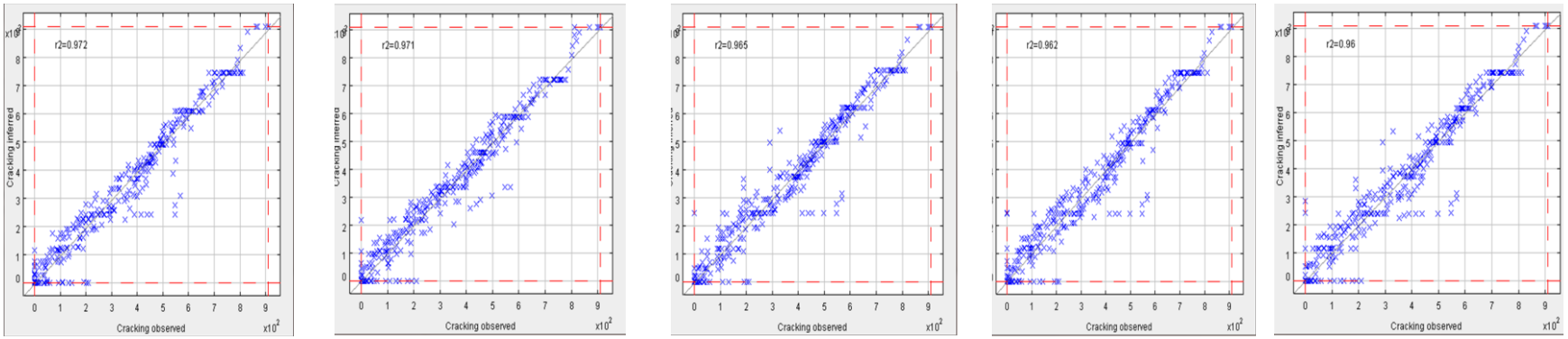

1 2 3 4 5

Cracking Model performance (training data 80% of all data)

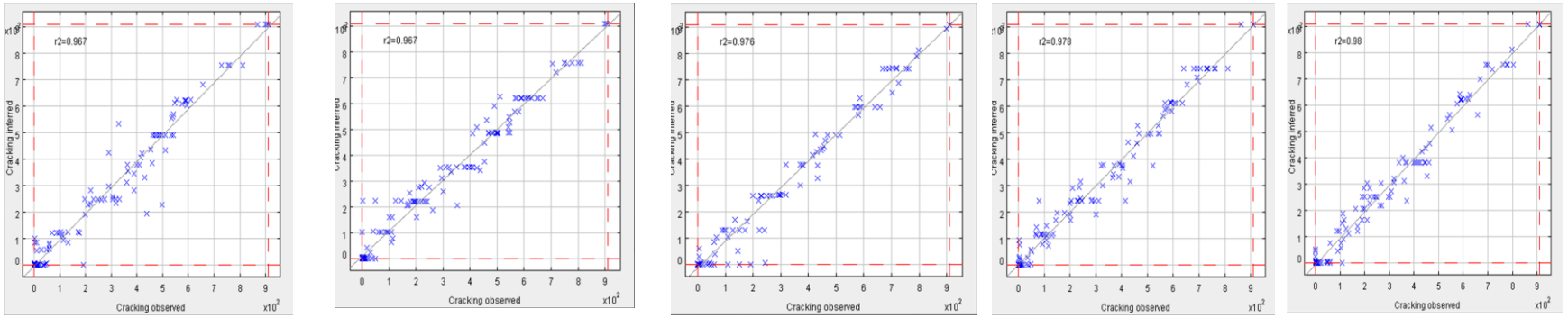

1 2 3 4 5

Cracking Model performance (testing data 20% of all data)

Figure 6.13 Cross validation of cracking models' performance

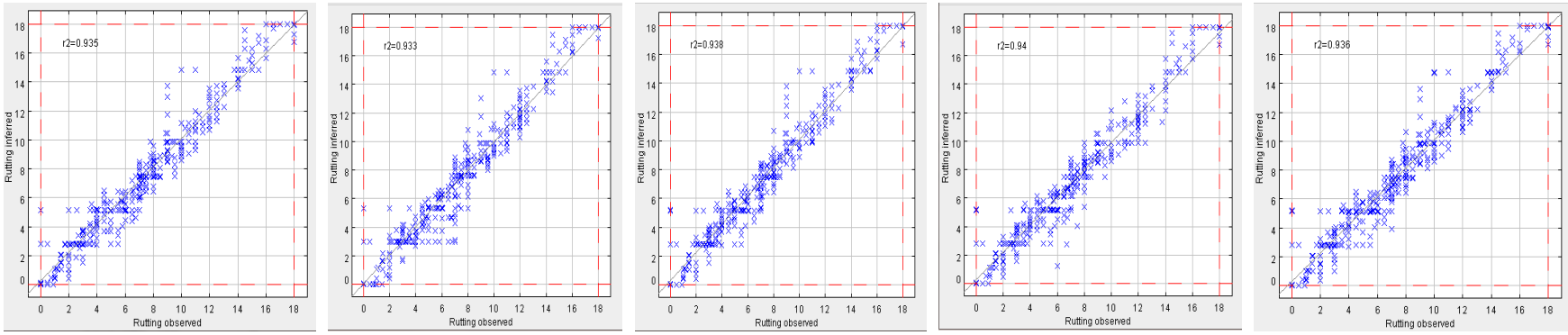

1 2 3 4 5

Rutting Model performance (training data 80% of all data)

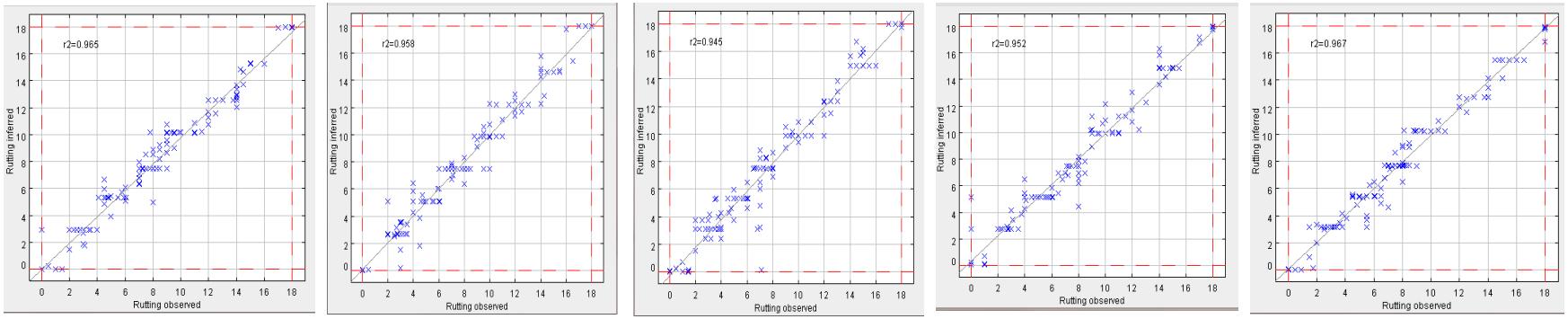

1 2 3 4 5

Rutting Model performance (testing data 20% of all data)

Figure 6.14 Cross validation of rutting models' performance

The coefficient of determination (R^2), estimated root mean square errors (RMSE) and mean absolute error (MAE) for the models were used to compare their efficiency in prediction. Results for cracking and rutting are given in Table 6.7 and Table 6.8 respectively.

Table 6.7 Validation of model performance for cracking

Model No	Training data 80% of all data			Testing data 20% of all data		
	R^2 (%)	RMSE	MAE	R^2 (%)	RMSE	MAE
1	97.2	43.991	25.812	96.7	48.204	26.582
2	97.1	43.297	25.232	96.7	47.095	29.191
3	96.5	49.082	27.675	97.6	42.178	24526
4	96.2	51.048	30.429	97.8	39.318	25.64
5	96	251.977	30.019	98	36.454	26.33

Table 6.8 Validation of model performance for rutting

Model No	Training data 80% of all data			Testing data 20% of all data		
	R^2 (%)	RMSE	MAE	R^2 (%)	RMSE	MAE
1	93.5	1.168	0.77	96.5	0.846	0.646
2	93.3	1.16	0.773	95.8	0.934	0.683
3	93.8	1.125	0.734	94.5	1.115	0.754
4	94	1.091	0.741	95.2	1.003	0.66
5	93.6	1.157	0.77	96.7	0.808	0.626

It can be seen that the model developed for cracking has better accuracy (R^2= 97.2 to 96) than the rutting model (R^2= 94 to 93.3). The RMSE and MAE are also low in rutting model for both training and testing data sets (Table 6.5). These values are higher in cracking data sets (Table 6.4). As explained in section 6.3.1, the wide spread of cracking in various surfaces play a role for variability. However, despite this difference, both models have been good agreement with the measured data.

6.3.3 Sensitivity Analysis

The purpose of the sensitivity analysis was to explore the influence of each input variables on the efficiency of the deterioration prediction models. For instance, the sensitivity investigation was conducted by generating the FIS model by considering the effect of individual input while other inputs remained inactive.

The correlation between the fuzzified and each input variable are shown in Table 6.9.

Table 6.9 Sensitivity level for each input variable

Input Variable	Deterioration model	
	Rutting	Cracking
	R^2 (%)	R^2 (%)
Asphalt Type	46.4	40.3
Aggregate Size	0.9	0.5
Weather Conditions	1.9	1.9
Frequency	27.4	27.1
Void Contents	22.2	43.4
Number of Cycles	40.6	21.4

It can be seen that the determination coefficients for asphalt type, aggregate size, weather conditions, frequency, void contents and the number of cycles were 46.4%, 0.9%, 1.9%, 27.4%, 22.2% and 40.6% for rutting and 40.3%, 0.5%, 1.9%, 27.4%, 43.4% and 21.4 %for cracking respectively. It was noticed, for this data set, that the influence of initial void contents of the mixture was higher than that of other parameters on cracking prediction; and in rutting; the number of cycles has a high impact in model prediction. The impacts of mixture type and load frequencies were also dominant in the model sensitivity in both types of distresses. It is appeared that aggregate size and weather condition has little influence on the model sensitivity although experimental study showed both parameters have significant impact on pavement performance. Overall, single input parameter does not give good sensitivity on the model performance.

To overcome this issue, three variables were kept active in each sensitivity analysis. The combination of these variables is given below.

- Case 1: Surface type, and two other variables are active,
- Case 2: Weather condition and load cycle and one other variable is active
- Case 3: Weather condition and surface type and one other variable is active

The coefficient of determination for each combination is presented in the following Tables 6.8 to 6.10.

Table 6.10 Case 1: Sensitivity level of combined input in asphalt deterioration models when Surface type and two other variables are active

Active input						Correlation (R^2 %)		Sensitivity Level	
Surface type	Agg. size	Weather conditions	Freq.	Void contents	Cycles	Cracking	Rutting		
✓				✓		43.7	48	L	L
✓		✓				42.3	47.9	L	L
✓			✓			48.8	43.7	L	L
✓					✓	86.1	89.9	H	H
✓				✓	✓	88.1	89.9	H	H
✓			✓	✓		49.4	47.2	L	L
✓			✓		✓	92.2	89.1	H	H
✓	✓	✓				51.7	50.7	M	M
✓	✓		✓			51.8	50.2	M	M
✓	✓			✓		53.7	49.4	M	L
✓	✓				✓	92	91.6	H	L

Table 6:8 shows, when combined three variable, model correlation increased significantly. The sensitivity level of the inputs was based on regression analysis if R^2 is <50% Low (L), 50 %< R^2 < 70% Medium (M) and R^2>70% High (H).

In Table 6.10, the highest sensitivity level of combined aggregate size and traffic showed 92% and 91.6% for cracking and rutting respectively. This showed good agreement with the experimental results in Chapter 5, when measured the influence of aggregate size between 14mm Open SMA and 14mm PA. In addition, the combination of load frequencies and number of cycles has high influence in both models with correlation in cracking 92.2% and rutting 89.1% respectively. Furthermore, void contents and the number of cycles has also showed high influence in both models with 88.1% and 89.9% correlation. Finally, weather conditions combined with aggregate

size has medium sensitivity level 51.7% for cracking and 50.7% for rutting, the sensitivity level of asphalt and aggregate sizes and void content was medium.

Table 6.11 presents the results for Case 2.

Table 6.11 Case 2: Sensitivity levels for cracking and rutting when weather condition and load cycle and one other variable are active.

Active Inputs						Correlation		Sensitivity Level	
Weather conditions	Cycles	Asphalt type	Freq.	Void contents	Agg.	Cracking	Rutting	Cracking	Rutting
✓	✓	✓				88.8	84.7	H	H
✓	✓			✓		74.9	76.7	H	H
✓	✓				✓	64.9	58.6	M	M
✓	✓		✓			68	74.6	M	H

Considering the cracking, as shown in Table 6.9, that the asphalt type and initial void contents have highest influence in the cracking, and the aggregate size and frequency has medium influence with the R^2 88.8%, 74.9%, 64.9% and 68% respectively. In rutting, the influence of asphalt type, void contents and frequency showed high influence while the aggregate size showed medium influence with R^2 76.7 %, 74.6% and 58.6% respectively.

Results for Case 3 are presented in Table 6.12.

Table 6.12 Case 3: sensitivity levels for cracking and rutting when weather condition and surface type and one other variable are active.

Active Inputs		Cycles	Freq.	Void contents	Agg.	R^2 (%) Cracking	R^2 (%) Rutting	Sensitivity Level	
Weather conditions	Asphalt								
✓	✓				✓	59.8	54.3	M	M
✓	✓		✓			68	59.8	M	M
✓	✓			✓		53.6	50.8	M	M
✓	✓	✓				88.2	84.7	H	H

It can be seen that in Case 3, No of cycles has high influence in both cracking and rutting with R^2 for cracking and rutting models are 88.2% and 84.7% respectively. The influence of other combinations such as frequency, void contents and aggregate size showed medium influence for both cracking and rutting.

Analysis of above cases showed that influence on model accuracy is greater when multiple variables are considered rather than one single input variable. The results also showed that the combination of asphalt surface type, weather condition and load frequency have most impact on model performance, while combinations of aggregate size and void contents have medium sensitivity.

6.6.4 Development of the Equation of Deterioration Prediction

A multi-input deterioration prediction model is generally used to find a relationship between the dependent variable, which is distress progression or a condition index, and one or more explanatory variables, such as cracking area, age and ESAL (Mahmood, 2015). Subjective indices such as ride quality, condition index, and serviceability, and objective indices such as rutting, roughness, and cracking, are utilised as dependent variables. These performance indices are related to one or more independent variables such as structural strength, traffic loading and environment effects (Prozzi and Madanat, 2004). To develop an equation of deterioration prediction for cracking and rutting, the six independent variables, asphalt types, aggregate sizes, weather conditions, frequency, void content and load pulses are used, by using multiple regression analysis.

The single equation of the prediction model is described consequently:

$$y = a_1 + a_2x_1 + a_3x_2 + a_4x_3 + a_5x_4 + a_6x_5 + a_7x_6$$

Where y = Cracking/or Rutting; X1 = Asphalt Types; X2 = Aggregate Sizes; X3 = Weather Conditions; X4 = Frequency; X5 = Void Content; X6 = No Cycles; $a1$, $a2$, $a3$, $a4$, $a5$, $a6$ and a7 = Coefficients

Table 6.13 X values of independent variables

Independent variables	X	Value
Asphalt Types	X_1	1=HRA, 2=OpenSMA, 3=PA
Aggregate Sizes	X_2	6,10,14
Weather Conditions	X_3	0=Dry, 1=Wet
Frequency	X_4	5=5Hz, 10=Hz
Void Content	X_5	For each type and aggregate size was specific void contents
No Cycles	X_6	1000,2000, ……..,40,000

Table 6.14 Equation of prediction models of cracking and rutting

Distress	Prediction Model	R^2
Cracking	$y = -465.231 + 146.814x_1 - 14.657x_2 + 112.0837x_3 + 41.190x_4 + 14.318x_5 + 0.01x_6$	0.61
Rutting	$y = 6.642 - 5.225x_1 + 0.0050x_2 + 1.810x_3 - 0.105\,x_4 - 0.50x_5 + 0.00029x_6$	0.77

The models and their corresponding coefficients of correlation (R^2) are shown in Table 6.11. It can be seen that rutting model has high correlation, with R^2 value 77%, while the cracking model has medium correlation with R^2 value 61%.

The observed deterioration data which is independent variables of each asphalt mixture was plotted against predicted deterioration data which is dependent variables as shown below.

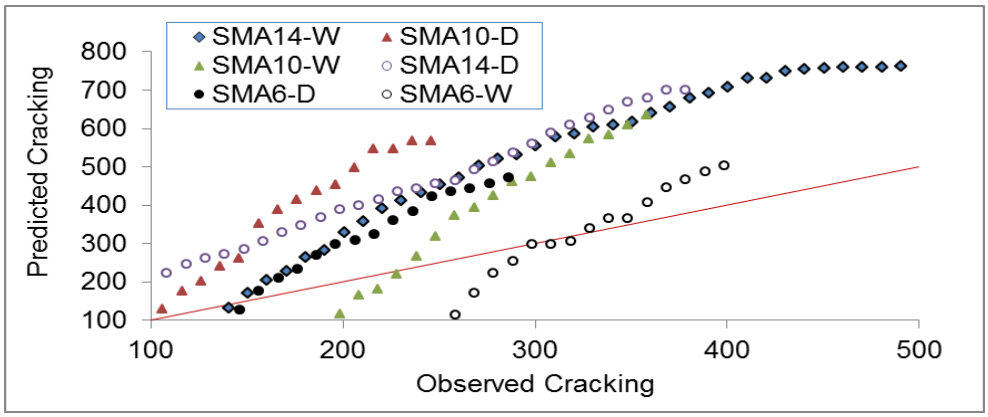

Figure 6.15 Accuracy of the single equation of cracking model for Open SMA

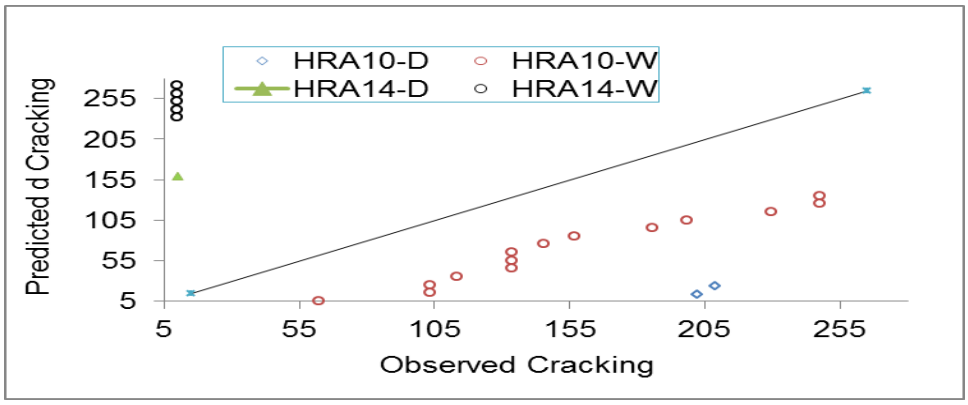

Figure 6.16 Accuracy of the single equation of cracking model for HRA

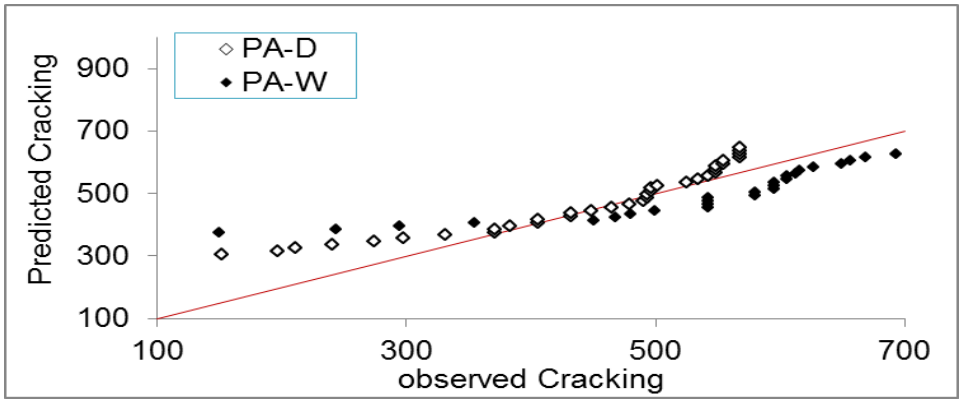

Figure 6.17 Accuracy of the single equation of cracking model for PA

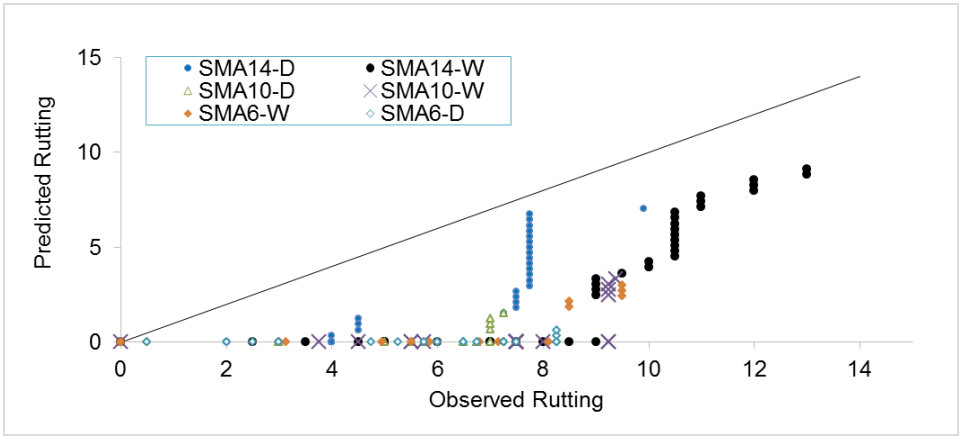

Figure 6.18 Accuracy of the single equation of rutting model for Open SMA

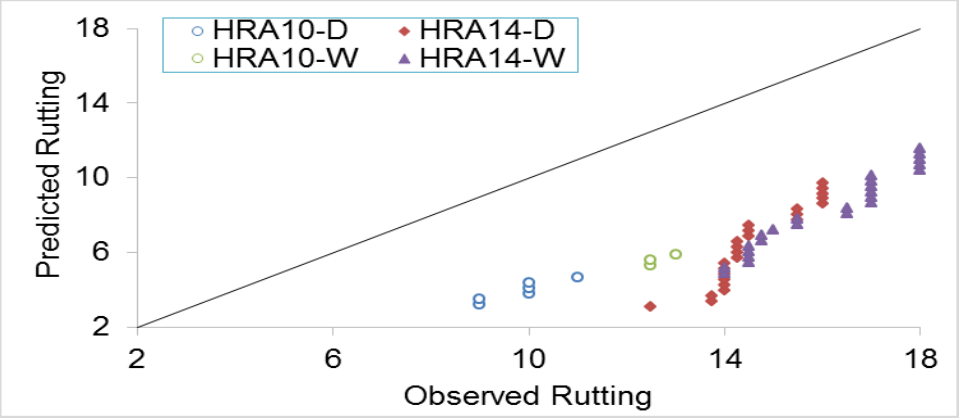

Figure 6.19 Accuracy of the single equation of rutting model for HRA

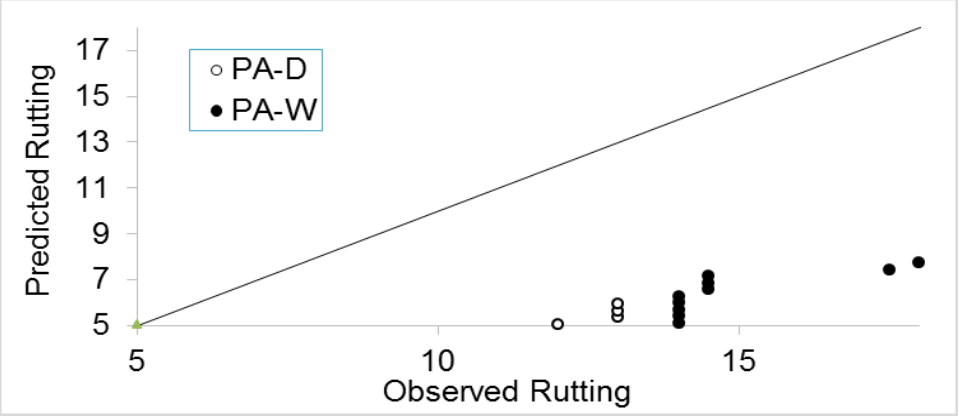

Figure 6.20 Accuracy of the single equation of rutting model for PA

Figures 6.15 to 6.20 show the errors and linear relation in individual asphalt mixture for rutting and cracking. A 45 degree references line was drawn to show the degree of closeness between the predicted and measured values. Table 6:15 shows whether is predicted value are overestimated or underestimated compared to experimental data. It was found that depending in asphalt mixture the regression equations for rutting underestimated the distress while the regression equations for cracking are mixed. It is therefore can only be used as an indicative tool rather than decision making.

Table 6.15 Prediction distress compare to actual value distress

Mixture Type	Cracking	Rutting
Open SMA6-D	*Overestimate	Underestimate
Open SMA6-W	** Overestimate	Underestimate
Open SMA10-D	Overestimate	Underestimate
Open SMA10-W	*Overestimate	Underestimate
Open SMA14-D	Overestimate	Underestimate
Open SMA14-W	*Overestimate	Underestimate
HRA10-D	Underestimate	Underestimate
HRA10-W	Underestimate	Underestimate
HRA14-D	Overestimate	Underestimate
HRA14-W	Overestimate	Underestimate
PA-D	Underestimate	Underestimate
PA-W	*Overestimate	Underestimate

*Distress predicted value started underestimated then became overestimated
**Distress predicted value started underestimated, same value then became overestimated

6.4 Summary

A multi input fuzzy-based deterioration prediction models have been developed to evaluate the combined interaction of traffic loading (frequency and load magnitude) and water on asphalt surfaces. The prediction accuracy of the model was 96.6% and 94.1% with the experimentally measured distresses such as cracking and rutting. Across validation method used to evaluate of the models carried out and both models showed high accuracy across the data set.

The sensitivity analysis to evaluate the influence of each and multiple input variable on the model performance showed that irrespective of mixture type, mixture parameters (aggregate size, void contents), traffic parameters (loading frequency) and environmental factors (wet condition) have an impact on either for cracking or rutting or both. Also, a single equation prediction models based on multiple variable regression analysis were developed, and the rutting showed 77% of correlation while the cracking showed 61%.

Chapter 7 Summary, Conclusions and Recommendations.

7.1 Introduction

The main purpose of this study was to develop a better understanding on the aspect of pore water pressure in pavement and then subsequent damage due to combined action of water and loading (frequencies and magnitude). Concerning this purpose, this research presented a novel laboratory test to investigate the influence of dynamic loading and tyre characteristics on pore water pressure in asphalt surfaces, and subsequently applied this method under a repeated loading condition to evaluate the performance of different asphalt surfaces. Finally, the results obtained from the laboratory investigations were used to develop prediction models. The development of test method, measurement of pore water pressure, performance of different surfaces and prediction models are presented in Chapters 3, 4, 5 & 6 respectively. The results are analysed in detail and discussed in the relevant chapters. This chapter will summarise, and present conclusions drawn from each aspect of the research and recommendations for future research. The main conclusions are presented in Section 7.3 to 7.6 and then recommendations for future research are given in Section 7.7

7.2 Contribution to knowledge

This research project has contributed to the science of pore water pressure in asphalt surface by improving the understanding of factors influence pore water pressure magnitude in asphalt surface. The following four key points highlight the conclusive statements gathered during this research.

1) Develop a laboratory test represented tyre-water-pavement surface interaction (refers to Chapter 3).

2) Measuring water pressure in asphalt surface under dynamic loading when the surface was flooded with water (refers to Chapter 4).

3) The impact of combined water and dynamic loading on asphalt surface damage was successfully represented in the laboratory environment. The result of the test approach has shown a promising future for further development (refers to Chapters 5).

4) Develop a multi input models to predict deterioration of asphalt surfaces when subject to combined action of repeated traffic loads with specific tyre characteristics applied asphalt surfaces submerged with shallow water (refers to Chapters 5 and 6).

7.3 Summary and Conclusion Related Test Development (Chapter 3)

7.3.1 Summary

The primary aim of this chapter was to develop a test method to simulate tyre-water-pavement surface interaction. A conceptual illustration, derived from the literature review, presented in chapter 2, was utilized to develop the test. Initial trials were done in a concrete slab with series of narrow holes. The pores were connected to a manometer by flexible tubes. The slab was then subjected to flooding and 1Hz dynamic compression loading. Based on the preliminary test results, the final test method was designed to select pore water pressure sensor, to develop a test protocol for automatically controlling the applied load at different frequencies and measure water pressure consistently under the slab when the slab is subjected to shallow flooding.

7.3.2 Conclusions

The key conclusions drawn from this investigation are as follows:

- The preliminary study showed that highest water pressure occurs at the middle of the loading plate with the maximum pore water pressure at low frequency loading (1Hz) was around 913Pa. Based on the preliminary results, a 913Pa pore water pressure sensor was used in the adopted test and was optimized to use a single sensor directly under the loading plate.
- The operation of the test was unsafe and inconstant when surface water reached more than 4mm and load frequency exceeded 15 Hz. These observations were used to select appropriate test parameters for subsequent investigations.

7.4 Summary and Conclusion Related to Pore Water Pressure in Pavement (Chapter 4)

7.4.1 Summary

The primary aim of this chapter was to measure water pressure in pavement under dynamic loading when the surface was flooded with water. The adopted test method (Chapter 3) was used to measure water pressure underneath a flooded concrete slab that contains a 2mm continuous pore (cracks) across the full depth. The test was repeated on a slab overlaid with 20mm semi permeable asphalt surface. The slab was subjected to flooding with 2mm and 4mm water and dynamic compression load of a 5kN and 10kN with three tyre tread patterns (square groove, square channel and no tread) with four tread depths (8mm, 3mm, 1.5mm and 0mm). The load was applied at four different frequencies, 1Hz, 5Hz, 10Hz and 15 Hz. The experimental set-up together with detail description of the testing procedure and results analysis are given in chapter 4.

7.4.2 Conclusions

The key conclusions drawn from these investigations are:

- Increasing load frequency increases pore water pressure in the pavement. However, water pressure increases significantly when high frequency loading combined with square types of tread with deep tread depth when water trapped inside the groove. Square tread with channel allows water to drain, which reduces pore water pressure.

- Irrespective of tread pattern, 8mm tread thickness showed the highest amount of water pressure, but the pressure reduces significantly in 1.5mm tread thickness. It is likely that increasing tread depth will increase the water pressure in the pavement.

- Load magnitude has the marginal impact on the pore water pressure. The water pressure diffidence between 5kN and 10kN load was found only range from

3% to 25% in all tread patterns, thicknesses and loading frequencies. Similarly, the depth of surface water appears to have minimum impact on the water pressure. It is likely that pore water pressure will build up if pores are filled with water, and there is a minimum amount of water on the surface.

- The asphalt surface can mitigate water pressure underneath the pavement range from 5% to 38% depending on the vehicle speed, tread patterns and thickness. This large variation also indicates that, for given surface type, the tyre characteristics and vehicles speed will influence the pore water pressure.

- Whilst the magnitude of water pressure is only around 8% of the contact pressure, smaller but continuous voids can significantly increase this pressure, which eventually can lead to degradation of foundation material and progressive deterioration to asphalt surface resulting fretting, ravelling or stripping.

7.5 Summary and Conclusion Related to Asphalt Surface Damage Due to Combined Action of Water and Dynamic Loading (Chapter 5)

7.5.1 Summary

The main aim of this study was to investigate the performance of different asphalt surfaces subjected to concurrent flooding and sinusoidal loading. For this propose, the laboratory test set-up (presented in Chapter 3) was slightly modified to accurately measure distress generated due to continuous action of water and traffic loading.

In this study, granite aggregate and a softer grade bitumen 150/100 pen were used for manufacturing test specimens. Three rang of voids asphalt surface mixtures; a gap graded mixture such as hot rolled asphalt (HRA) and two open-graded mixtures, stone mastic asphalt (Open SMA) and porous asphalt (PA) were used. Each of these mixtures was produced with different sizes of aggregates to evaluate their impact on mixture performance.

All mixtures were tested in dry and in wet conditions by applying vertical dynamic load at 5Hz and 10Hz while the asphalt surface was submerged with up to 2mm water. All specimens went through overnight saturation prior to testing. The test results concerning surface cracking, rutting and other visual distress such as material missing, were measured using digital microscope, camera and straight plate.

7.5.2 Conclusions

The key conclusions are given below:

- The influence of combined water and dynamic loading on surface damage was successfully simulated in the laboratory environment. The outcome of the test method has demonstrated a promising future for further development.

- Depending on the type of asphalt surfaces, the presence of water accelerates surface damage concerning cracking, rutting and other distresses like ravelling.
- The cracking tendency was severe in highly open graded porous asphalt PA, then semi impermeable Open SMA and gap graded hot rolled HRA asphalt mixtures. Compared to dry condition testing, the appearance of surface crack was about seven times faster in porous asphalt tested in wet conditions. It is possible that the water pressure builds up inside the pore exacerbates during cycling loading which then lead to additional stress and strains, resulting accelerated damage. It is interesting to note that whilst porous asphalt is designed to drain water through open voids, the constant presence of water on the surface due to heavy rain combined with loading can significantly diminish their load bearing capacity.

- All tested Open SMA mixtures demonstrated good wet condition rutting resistance compared to porous and hot rolled mixtures, although their cracking resistance was significantly reduced in the presence of water.

- Whilst both 10mm and 14mm HRA showed the best performance regarding resistance to cracking; the rutting was significantly higher compared to the

other two mixtures. However, at the end of 40,000 pulses, the porous asphalt showed significant rutting. The best performance was observed in 10mm SMA.

- In the presence of water, the mixture gradation appeared to have more influence on load bearing capacity than the size of aggregates.

- The impermeable boundary and build up water also have severe negative impact on the mixture performance. The impact was significantly high in open graded mixtures with high air void contents (18–20%). In reality, all mixtures, more importantly to porous asphalt, has to be designed with good interface connect with adequate drainage provisions and need regular maintenance to remove dust and leaves to avoid clogging of the voids.

7.6 Summary related to Surface Deterioration Prediction Model (Chapter 6)

7.6.1 Summary

The primary aim of this study was to develop a multi input models to predict deterioration of asphalt surfaces when subject to combined action of repeated traffic loads with specific tyre characteristics applied asphalt surfaces submerged with shallow water. The results from experimental studies in chapter 4 and chapter 5 were utilized as input variables for the deterioration prediction models. The input parameters were three asphalt surface type (HRA, Open SMA and PA), three aggregate size (6mm, 10mm and 14mm), initial void contents of the mixtures (4-8%, 8-12% and >12%), two load frequencies (5Hz and 10Hz), and two test conditions (wet and dry). The output parameters were cracking and rutting.

Two prediction models were developed. The first model was based on Fussy Inference System (FIS), a widely use soft computing techniques and the second method was a deterministic method using multiple regression analysis. The FIS method gave set of "*if-then*" rules while regression model was used to develop distress equation as an

indicative predictive tool. After developing the model, a cross validation exercise was carried out to evaluate the model accuracy across dataset. In addition, the sensitivity analysis to assess influence each parameter in asphalt performance was conducted.

7.6.2 Conclusions

The key conclusions related to prediction models are given below;

- In the FIS model, the accuracy both models showed more than 90% accuracy with the experimental data. The cross validation method of the model also accurately predicted both distresses from randomly selected dataset.

- The sensitivity analysis to assess the impact of every variable on the model performance pointed that irrespective of mixture type, mixture parameters (aggregate size, void contents), traffic parameters (loading frequency) and environmental factors (wet condition) have an influence either on cracking or rutting or on both. It can be concluded that the FIS based "*If-then*" rules are suitable to predict surface distresses. This method has the potential to extend in other data sets with similar circumstances.

- In the multiple regression analysis, it was found that multiple input based equations to predict rutting and cracking have good agreement with the experimental data with 77% and 61% model correlation respectively. It was also found that depending on the mixture type the models had good model predicted. The model prediction regression equations of rutting for all mixture types were underestimated the deterioration. While in model prediction regression equation for cracking overestimate or underestimate based on mixture type. Therefore, this type of equation could be used as an indicative tool rather than decision making.

7.7 Recommendations and Further Study

In this section, recommendations for a further work are listed based on the knowledge established by the completion of this research. The gaps are identified and outlined which will further add value to the research area.

Recommendations on experimental set-up

1) Manual feeding of water was used to maintain water level during the test. It would be useful to design an automated feeding and drainage system so that operators' involvement could be minimise.

2) The test was applied in the room temperature. It would be useful to develop a temperature control cabinet in order to perform the test in various temperatures including freeze-thaw conditions.

Recommendations on pore water pressure measurements

3) Although, the impact of tyre and traffic parameters on water pressure in pavement was experimentally investigated under limited loading and environmental condition, further works should be carried out on different wider loading and environmental conditions. For example, water pressure under freezing and thawing condition.

4) Moreover, in chapter 4, the results of laboratory work showed differences regarding the performance of asphalts surface under the influence of loading and water and tread pad. It would be appropriate for a further investigation to focus on measure pore water pressure under different asphalt surfaces.

5) Only one pore water pressure sensor was used in this study. The future study can evaluate pore water pressure under series of pressure sensors.

6) It was found in this study that macro texture may have influence on pore water pressure. As macro texture is related to coarse aggregate, it would be interesting to research the effects of aggregate size in asphalt mixture on pore water pressure magnitude.

7) Although influence of idealised tread depth and pattern was investigated in this study and showed a positive correlation between pore water pressure and tread depth. The maximum tread depths used in this study was 8mm. The influence of higher tread depth can be investigated. Additionally, the research could be extended to study the impact of actual tyre tread on the water pressure.

8) The water pressure was measured only in one depth primarily at the interface. It will be worth to extend the investigation to measure pore water pressure at different depths simultaneously by using sensors at multiple depth to investigate the impact of layer thickness on water pressure magnitude.

9) This study has been conducted on idealised pavement, further investigation could be carried out on field cored pavement with different ageing conditions.

Recommendations on asphalt surface performance due to combined interaction of tyre and water

10) More experiments are needed to investigate interaction with the aged asphalt surface. In addition, increase time of wet condition prior to test can be used for further work.

11) Although not conclusive, replacing the filler in mixtures showed improvement in resistant to cracking and rutting. Further studies are needed to validate this.

12) It is also recommended that further study to extend the investigation in high frequencies and also in freeze thaw condition.

13) Furthermore, 3D simulation using CFD and microstructure-based discrete element model could be developed to investigate fluid flow and internal failure mechanisms.

Recommendation related to prediction models

14) In order to improve the accuracy of the prediction model, more data are needed. By implementing recommendations 3-12, it will be possible to improve model accuracy significantly.

15) Both FIS based and regression equations could be used in field data similar testing conditions. In addition, further work should be extended to determine pavement condition index from the distress data. This will help practicing engineers to make effective decision.

X. References

Abaza, K.A. (2016) 'Back-calculation of transition probabilities for Markovian-based pavement performance prediction models', *International Journal of Pavement Engineering*, 17(3), pp. 253-264.

Ahmad, N. (2011) *Asphalt mixture moisture sensitivity evaluation using surface energy parameters.* PhD Thesis, University of Nottingham.

Agatonovic-Kustrin, S. and Beresford, R. (2000) 'Basic concepts of artificial neural network (ANN) modeling and its application in pharmaceutical research', *Journal of pharmaceutical and biomedical analysis*, 22(5), pp. 717-727.

Alliance, A.I. (2018) *Annual Local Authority Road Maintenance Survey*. London: Asphalt Industry Alliance.

Al-Mansour, A.I., Sinha, K.C. and Kuczek, T. (1994) 'Effects of routine maintenance on flexible pavement condition', *Journal of Transportation Engineering*, 120(1), pp. 65-73.

Airey, G.D. and Choi, Y. (2002) 'State of the art report on moisture sensitivity test methods for bituminous pavement materials', *Road Materials and Pavement Design*, 3(4), pp. 355-372.

Airey, G.D., Apeagyei, A.K., and Grenfell, J.R. (2015) 'Influence of aggregate absorption and diffusion properties on moisture damage in asphalt mixtures', *Road Materials and Pavement Design*, 16(sup1), pp. 404-422.

Airey, G., Grenfell, J., Apeagyei, A., Subhy, A. and Presti, D.L. (2016) 'Time dependent viscoelastic rheological response of pure, modified and synthetic bituminous binders', *Mechanics of Time-Dependent Materials*, 20(3), pp. 455-480.

Apul, D.S., Gardner, K., Eighmy, T., Benoit, J. and Brannaka, L. (2002) 'A review of water movement in the highway environment: Implications for recycled materials use', Recycled Materials Resource Center, University of New Hampshire, Durham.

Baladi, G.Y., Schorsch, M. and Svasdisant, T. (2003) *Determining the causes of top-down cracks in bituminous pavement*. available at: https://www.michigan.gov/documents/mdot_rc-1440_82241_7.pdf (Accessed :7 January 2018).

Baldwin, G., Addis, R., Clark, J. and Rosevear, A. (1997) *Use of industrial by-products in road construction-water quality effects*. London: CIRIA.

Berenji, H.R., Chen, Y., Lee, C., Murugesan, S. and Jang, J. (1989) 'An experiment-based comparative study of fuzzy logic control', 1989 American Control Conference. IEEE, 2751-2753.

Borkar, A.D. and Atulkar, M. (2013) 'Fuzzy inference system for image processing', *International Journal of Advanced Research in Computer Engineering & Technology*, 2(3), pp. 1007-1010.

British Standards Institute (1998). *BS EN 1177:1998 Impact absorbing playground surfacing. Safety requirements and test methods.* London: British Standards Institution.

British Standards Institute (2017) BS *EN 1766:2017: Products and systems for the protection and repair of concrete structures. Test methods. Reference concretes for testing.* London: British Standards Institution.

British Standards Institute (2004) *BS EN 12697-35:2004 Bituminous mixtures. Test methods for hot mix asphalt. Laboratory mixing.* London: British Standards Institution.

British Standards Institute (2003) *BS EN 12697-6:2003 Bituminous mixtures. Test methods for hot mix asphalt. Determination of bulk density of bituminous specimens.* London: British Standards Institution.

British Standards Institute (2003) *BS EN 12697-8:2003 Bituminous mixtures. Test methods for hot mix asphalt. Determination of void characteristics of bituminous specimens* . London: British Standards Institution.

British Standards Institute (2016) *BS EN 13108-4:2006 Bituminous mixtures. Material specifications. Hot Rolled Asphalt* . London: British Standards Institution.

British Standards Institute (2016) *BS EN 13108-5:2016 Bituminous mixtures. Material specifications. Stone Mastic Asphalt.* London: British Standards Institution.

British Standards Institute (2016) *BS EN 13108-7:2006 Bituminous mixtures. Material specifications. Porous Asphalt*. London: British Standards Institution.

Browne, D. (2005) *Generator Status Monitoring System.* UG dissertation, University of Cape Town. (Accessed: 28 April 2018)

Brown, S. (1974) 'Determination of Young's modulus for bituminous materials in pavement design', *Highway Research Record,* (431).

Camahan, J., Davis, W., Shahin, M., Keane, P. and Wu, M. (1987) 'Optimal maintenance decisions for pavement management', *Journal of Transportation Engineering,* 113(5), pp. 554-572.

Caro, S., Masad, E., Bhasin, A. and Little, D.N. (2008) 'Moisture susceptibility of asphalt mixtures, Part 1: mechanisms', *International Journal of Pavement Engineering,* 9(2), pp. 81-98.

Castelblanco Torres, A. (2004) *Probabilistic analysis of air void structure and its relationship to permeability and moisture damage of hot mix asphalt.* MSc Thesis, University of Texas A&M. (Accessed: 5 May 2018)

Cerezo, V., Do, M.T., Prevost, D. and Bouteldja, M. (2014) 'Friction/water depth relationship—In situ observations and its integration in tire/road friction models', *Proceedings of the Institution of Mechanical Engineers, Part J: Journal of Engineering Tribology,* 228(11), pp. 1285-1297.

Chen, S. and Chen, Y. (2002) 'Automatically constructing membership functions and generating fuzzy rules using genetic algorithms', *Cybernetics &Systems,* 33(8), pp. 841-862.

Chen, J., Lin, K. and Young, S. (2004) 'Effects of crack width and permeability on moisture-induced damage of pavements', *Journal of Materials in Civil Engineering,* 16(3), pp. 276-282.

Christiansen, B. (2007) 'Atmospheric circulation regimes: Can cluster analysis provide the number?', *Journal of Climate,* 20(10), pp. 2229-2250.

Chu, P.C. and Beasley, J.E. (1997) 'A genetic algorithm for the generalised assignment problem', *Computers & Operations Research,* 24(1), pp. 17-23.

Connell, M. E., Learning to Control a Dynamic Physical System, AAAI, pp. 45646, 1986.

Cook, M. and Dykins, S. (1991) 'Treated permeable base offers drainage, stability', *Roads & Bridges,* 29(5).

Copeland, A., Youtcheff, J. and Shenoy, A. (2007) 'Moisture sensitivity of modified asphalt binders: Factors influencing bond strength', *Transportation Research Record: Journal of the Transportation Research Board,* (1998), pp. 18-28.

Cui, X. (2010) 'Dynamic numerical analysis of antimoisture-damage mechanism of permeable pavement base', *International Journal of Geomechanics,* 10(6), pp. 230-235.

Cui, X., Cao, W., Liu, S. and Dong, L. (2009) 'On dynamic pore pressure in moisture damage of asphalt pavement', *Performance modeling and evaluation of pavement systems and materials: Selected papers from the 2009 GeoHunan international conference.* , 122-128.

Dawson, A. (2008) Water in road structures: movement, drainage & effects. Springer Science & Business Media.

Dehnad, M., Khodaii, A. and Nejad, F.M. (2013) 'Moisture sensitivity of asphalt mixtures under different load frequencies and temperatures', *Construction and Building Materials,* 48, pp. 700-707.

Dehzangi, O., Zolghadri, M.J., Taheri, S. and Fakhrahmad, S.M. (2007) 'Efficient Fuzzy Rule Generation: A New Approach Using Data Mining Principles and Rule Weighting', *International Conference on Fuzzy Systems and Knowledge Discovery.* IEEE, 134-139.

Dixon, J. (1996) *Tyres, Suspension and Handling* (2nd edn), Warrendale, PA: Society of Automotive Engineers.

Dong, Z., Cheng, X., Cao, L. and Tan, Y. (2007) 'Influence of surface drainage conditions on dynamic response of saturated asphalt pavement', *Journal of Highway and Transportation Research and Development (English Edition),* 3(2), pp. 1-6.

Engelbrecht, A. (2007) *Introduction to computational Intelligence*. England: John Wiley & Sons, Ltd.

Eustacchio, E. and Fritz, H. (2014) *Mechanical Tests for Bituminous Mixes-Characterization, Design and Quality Control: Proceedings of the Fourth International RILEM Symposium.* Van Reinhold: New York.

Federal Highway Administration (2009) Pavement Distress Identification Manual for the NPS Road Inventory Program. Avalible at : http://www.wistrans.org/mrutc/files/Distress-ID-Manual.pdf (Accessed: 5 May 2016)

Flynn, L. (1991) 'Open-Graded Base May Lengthen Pavement Life', *Roads and Bridges*, pp. 35-42.

Fromm, H.J. (1974) 'The mechanisms of asphalt stripping from aggregate surfaces', *Journal of the association of asphalt paving technologists*, 43, 191–219.

Fwa, T.F. (2006) *The Handbook of Highway Engineering*. Boca Raton: Taylor & Francis

Gao, J., Guo, C. and Liu, Y. (2015) 'Measurement of pore water pressure in asphalt pavement and its effects on permeability', *Measurement*, 62, pp. 81-87.

Gent, A.N. and Walter, J.D. (2006) 'Pneumatic Tire'. US department of transportation.

George, K., Rajagopal, A. and Lim, L. (1989) 'Models for predicting pavement deterioration ', *Transportation Research Board.* Washington, D.C, 13-17 January. TRB, 25-32.

Georgiou, P. and Loizos, A. (2014) 'A laboratory compaction approach to characterize asphalt pavement surface friction performance', *Wear*, 311(2), pp. 114-122.

Gillespie, T.D., 1992. *Fundamentals of Vehicle Dynamics*. Warrendale, PA: Society of Automotive Engineers.

Glaoui, B., Merbouh, M., Van de Ven, M., Chailleux, E. and Youcefi, A. (2012) 'Thermal fatigue of polymer modified bitumen', *Journal of Thermoplastic Composite Materials*, 25(4), pp. 469-478.

Goodyear (2015) *All-about-tyres/understand-your-tyre/how-tyresare-made.* Available at: http://www.goodyear.eu/home_en/all-about-tyres/understand- your -tyre/how-tyresare-made/#blend (Accessed: 08 September 2015).

Gopalakrishnan, K., Kim, S., Ceylan, H. and and Khaitan, S.K. (2010) 'Natural selection of asphalt mix stiffness predictive models with genetic programming', The Artificial Neural Networks in Engineering. St. Louis, Missouri, November 1-3.

Guillaume, S., Charnomordic, B. and Lablée, J. (2002) *Fispro: An open source portable software for fuzzy inference systems.* Available at: http://www.inra.fr/Internet/Departements/MIA/M/fispro (Accessed: 6 June 2017).

Guo, X., Sun, M. and Dai, W. (2017) 'Analysis of effective pore pressure in asphalt pavement based on computational fluid dynamics calculation', *Advances in Mechanical Engineering*, 9(2). pp.1-14.

Hassan, N.A., Abdullah, N.A.M., Shukry, N.A.M., Mahmud, M.Z.H., Yunus, N.M., Putrajaya, R., Hainin, M.R. and Yaacob, H. (2015) 'Laboratory evaluation on the effect of clogging on permeability of porous asphalt mixtures', *J Teknol*, 76(14), pp. 77-84.

Hainin, M.R., Yusoff, N.I.M., Satar, Mohd Khairul Idham Mohd and Brown, E.R. (2013) 'The effect of lift thickness on permeability and the time available for compaction of hot mix asphalt pavement under tropical climate condition', *Construction and Building Materials*, 48, pp. 315-324.

Hanson, D.I., James, R.S. and NeSmith, C. (2004) *Tire/Pavement Noise Study.* Alabama: National Center for Asphalt Technology.

H. Heisler (1989) *Advanced Vehicle Technology*. London: Hodder and Stoughton.

Henning, T. and Roux, D.C. (2008) *Pavement deterioration models for asphalt-surfaced pavements in New Zealand.* Wellington: NZ Transport Agency.

Highways Agency. (2006) *Design Manual for Roads and Bridges (DMRB), Volume 7: Pavement Design and Maintenance. Section 2, Part 3, HD 26/06: Pavement Design*. London: Department for transport.

Highways England (2012) *Interim Advice Note 154/12*. London: Stationery Office.

Highway Research Board (1962) *The AASHTO road test report 7. Special report 61-G*. Washington DC: HRA.

Hunter, A. and Airey, G. (2005) 'Numerical modeling of asphalt mixture site permeability', *Proceedings of the 84th Transportation Research Board Annual Meeting.* Washington, DC.TRB

Instron (2015) Instron WaveMatrix for Dynamic Testing. Available at: http://www.instron.co.uk/en-gb/products/materials-testing-software/wavematrix (Accessed: 5 May 2015).

Jain, A.K. (2010) 'Data clustering: 50 years beyond K-means', *Pattern Recognition Letters,* 31(8), pp. 651-666.

Jang, J. (1993) 'ANFIS: adaptive-network-based fuzzy inference system', *IEEE transactions on systems, man, and cybernetics,* 23(3), pp. 665-685.

Jansen, S., Schmeitz, A., Maas, S., Rodarius, C. and Akkermans, L. (2014) *Study on some safety-related aspects of tyre use.* Available at: https://ec.europa.eu/transport/road_safety/sites/roadsafety/files/pdf/vehicles/study_tyres_2014.pdf (Accessed: 9 February 2017).

JATMA (2011) *Tyre Industry of Japan*. NC Japan: The Japan Automobile Tyre Manufacturers Association.

Jiang, W., Zhang, X. and Li, Z. (2013) 'Simulation test of the dynamic water pressure of asphalt concrete', *Journal of Highway and Transportation Research and Development,* 7(1), pp. 23-27.

Johnson, D.R. and Freeman, R.B. (2002) *Rehabilitation techniques for stripped asphalt pavements.* Bozeman: Western Transportation Institute.

Gao, J., Chen, H., Ji, T. and Liu, H. (2009) 'Measurement of dynamic hydraulic pressure in asphalt pavement using fiber bragg grating', *Transducer Microsyst.Technol.,* 28(9), pp. 59-61.

Kakar, M.R., Hamzah, M.O. and Valentin, J. (2015) 'A review on moisture damages of hot and warm mix asphalt and related investigations', *Journal of Cleaner Production,* 99, pp. 39-58.

Kandhal, P.S. (1994) 'Field and laboratory investigation of stripping in asphalt pavements: State of the art report', *Transportation Research Record,* (1454).

Karlson, T.K. (2005) *Evaluation of cyclic pore pressure induced moisture damage in asphalt pavement,* PhD thesis, University of Florida. (Accessed: 7 May 2015).

Kennedy, T.W., Roberts, F.L. and Rauhut, J.B. (1979) 'Distresses and related material properties for premium pavements', *Transportation Research Record,* (715).

Kim, Y., Lutif, J.S., Bhasin, A. and Little, D.N. (2008) 'Evaluation of moisture damage mechanisms and effects of hydrated lime in asphalt mixtures through measurements of mixture component properties and performance testing', *Journal of Materials in Civil Engineering,* 20(10), pp. 659-667.

Kok, B.V. and Yilmaz, M. (2009) 'The effects of using lime and styrene–butadiene–styrene on moisture sensitivity resistance of hot mix asphalt', *Construction and Building Materials,* 23(5), pp. 1999-2006.

Kringos, N., 2007. Modeling of combined physical-mechanical moisture induced damage in asphaltic mixes. Delft University of Technology.

Kutay, M.E. and Aydilek, A.H. (2007) 'Dynamic effects on moisture transport in asphalt concrete', *Journal of Transportation Engineering,* 133(7), pp. 406-414.

Kutay, M.E. and Aydilek, A.H. (2009) 'Pore pressure and viscous shear stress distribution due to water flow within asphalt pore structure', *Computer-Aided Civil and Infrastructure Engineering,* 24(3), pp. 212-224.

kwikfit (2018) Tyre Construction - How Tyres Are Made . Available at: https://www.kwik-fit.com/tyres/information/how-tyres-are-made (Accessed: 26 July 2018).

Landau, S. (2004) *A handbook of statistical analyses using SPSS.* CRC.

Li, H.B. and Sheng, Y.P. (2012) 'Study on Vehicle Speed in Pore Water Pressure of Rigid Pavement Base Using Poro-Elasticity', *Applied Mechanics and Materials.* Trans Tech Publ, 2615-2618.

Li, S., Zhang, H. and Sun, L. (2007) 'Development and simulation measurement of dynamic hydraulic pressure', *Journal-Tongji University,* 35(7), pp. 915-918.

Xiaoyong, L.Z.D. (2008) 'Axial symmetric elastic solution of pore water pressure in asphalt pavement under mobile load ', *Journal of Southeast University (Natural Science Edition),* 5, pp. 014.

Lindly, J.K. and Elsayed, A.S. (1995) 'Estimating permeability of asphalt-treated bases', *Transportation Research Record,* (1504), pp. 103-111.

Little, D.N. and Jones, D. (2003) 'Chemical and mechanical processes of moisture damage in hot-mix asphalt pavements', *National seminar on moisture sensitivity of asphalt pavements. ,* 37-70.

Lottman, R.P. (1982) 'Field Evaluation and Correlation of Laboratory Test Method for Predicting Moisture-Induced Damage to Asphalt Concrete'. *Transportation Research Board,* Washington D.C., 1982.

Lytton, R.L. (1987) 'Concepts of Pavement Performance Prediction and Modeling', *Proc., Second North American Conference on Managing Pavements,* November, pp. 3-20.

Mallick, R.B., Cooley, L.A., Teto, M.R., Bradbury, R.L. and Peabody, D. (2003) (2003) *An evaluation of factors affecting permeability of Superpave designed pavements.* Alabam: National Centre for Asphalt Technology.

Masad, E., Birgisson, B., Al-Omari, A. and Cooley, A. (2004) 'Analytical derivation of permeability and numerical simulation of fluid flow in hot-mix asphalt', *Journal of Materials in Civil Engineering,* 16(5), pp. 487-496.

Masad, E., Muhunthan, B., Shashidhar, N. and Harman, T. (1999) 'Internal structure characterization of asphalt concrete using image analysis', *Journal of Computing in Civil Engineering,* 13(2), pp. 88-95.

Masad, E., Birgisson, B., Omari, A. and Cooley, A. (2005) 'Analysis of permeability and fluid flow in asphalt mixes', *Journal of Materials in Civil Engineering,* 16(5).

Rahman, M., Stonecliffe-Jones, M. and Evans, R. (2011) 'Structural assessment of in-service doweled concrete pavement joints', *International Conference Bituminous Mixtures and Pavements, 5th, 2011, Thessaloniki, Greece.*

Miller, J. and Bellinger, W. (2003) Distress identification manual for the long-term pavement performance program .Federal Highway Administration Report: FHWA-RD-03-031.

Mahmood, M.S. (2015) *Network-level maintenance decisions for flexible pavement using a soft computing-based framework,* University of Nottingham Trent, Nottingham.

Mahmood, M., Rahman, M. and Mathavan, S. (2018) 'A multi-input deterioration-prediction model for asphalt road networks', *Proceedings of the Institution of Civil Engineers-Transport.* Thomas Telford Ltd, 1-12.

Mahmood, M., Rahman, M., Nolle, L. and Mathavan, S. (2013) 'A fuzzy logic approach for pavement section classification', *International Journal of Pavement Research and Technology,* 6(5), pp. 620-626.

Moulton, L.K. (1980) *Highway subdrainage design*. Washington, D.C: Federal Highway Administration.

Munakata, T. and Jani, Y. (1994) 'Fuzzy systems: An overview', Communications of the ACM, 37(3), pp. 69-77.

Naik, V.C. (2004). *Fuzzy C-means clustering approach to design a warehouse layout*. MSc Dissertations, University of South Florida.

Navdeep, G. (2017) Artificial Neural Networks, Neural Networks Applications and Algorithms. Available at: https://www.xenonstack.com/blog/data-science/artificial-neural-networks-applications-algorithms/ (Accessed: 8 May 2018).

Negnevitsky, M. (2005) *Artificial intelligence: a guide to intelligent systems.* Addison Wesley.

Nelles, O., Fischer, M. and Muller, B. (1996) 'Fuzzy rule extraction by a genetic algorithm and constrained nonlinear optimization of membership functions', *Fuzzy Systems, 1996., Proceedings of the Fifth IEEE International Conference on.* IEEE, 213-219.

Nicholls, J., Carswell, I., Thomas, C. and Sexton, B. (2010) *Durability of Thin Surfacing Systems. Part 4: Final Report after Nine Years Monitoring.* Wokingham: TRL Ltd.

Nikolaides, A. (2014) *Highway engineering: pavements, materials and control of quality.* New York: CRC Press.

Nielsen, C. (2006) Durability of porous asphalt-International experience. Copenhagen: Danish Road Institute.

Nguyen, T., Byrd, E., Alsheh, D. and and Bentz, D. (1995) 'Relation between adhesion loss and water at the polymer/substrate interface.', Proceedings adhesion society meeting, Hilton Head Island, SC, USA.

Nguyen, D.T. (2016) *Pavement Management System Implementation in Vietnam*. PhD thesis. Kyoto University.

Omega (2015) C Series Universal Analog Input Module. Available at: http://www.ni.com/en-gb/support/model.ni-9219.html (Accessed: 1 May 2015).

Ongel, A.J. (2007) State of the practice 2006 for open-graded asphalt mix design. Available at: http://149.136.36.11/research/researchreports/reports/2007/ucprc-tm-2008-07.pd (Accessed: 7 May 2017).

Osman, S.A. (2005) *The role of bitumen and bitumen/filler mortar in bituminous mixture fatigue.* PhD Thesis. University of Nottingham.

Ozer, H., Al-Qadi, I.L., Singhvi, P., Bausano, J., Carvalho, R., Li, X. and Gibson, N. (2018) 'Prediction of pavement fatigue cracking at an accelerated testing section using asphalt mixture performance tests', *International Journal of Pavement Engineering*, 19(3), pp. 264-278.

Pep Boys (2016) Four tire tread types. Available at: https://www.pepboys.com/tires/treadsmart/tread_type/ (Accessed: 14 August 2016).

Rahimzadeh, B. (2002) *Linear and non-linear viscoelastic behaviour of binders and asphalts.* PhD Thesis. University of Nottingham. (Accessed: 12 March 2018).

Rahman, M. and Thom, N. (2012) *Performance of asphalt patch repairs.* Institution of Civil Engineers: ice.

Rauhut, J.B., Roberts, F.L. and Kennedy, T.W. (1979) 'Response and distress models for pavement studies', *Transportation Research Record*, (715).

Read, J.M. (1996) *Fatigue cracking of bituminous paving mixtures.* PhD Thesis. University of Nottingham.

Read, J. and Whiteoak, D. (2003) *The shell bitumen handbook.* Thomas Telford.

Reid, J. M., G. I. Crabb, J. Temporal and M. Clark (2006) *A Study of Water Movement in Road Pavements*. Available at https://trl.co.uk/reports/PPR082 (Accessed January 12, 2017).

Ridgeway, H.H. (1976) 'Infiltration of Water through the Pavement Surface (Abridgement)', *Transportation Research Record*, (616), pp98-101

Ridgeway, H.H. (1982) 'Pavement subsurface drainage systems', *NCHRP synthesis of highway practice*, (96).

Riza, L.S., Bergmeir, C.N., Herrera, F. and Benítez Sánchez, J.M. (2015) 'frbs: Fuzzy rule-based systems for classification and regression in R', *Journal of Statistical Software*. 65(6).

Roque, R., Birgisson, B., Darku, D. and Drakos, C.A. (2004) *Evaluation of Laboratory Testing Systems for Asphalt Mixture Design and Evaluation*. Available at: http://www.fdot.gov/research/Completed_Proj/Summary_RD/FDOT_BB888_v1_rpt.pdf (Accessed: 3 May 2016).

Saeed, F., Qamariatul, S., Rahman, M. and Woodside, A. (2015) 'The state of pothole management in UK local authority', *Bituminous Mixtures and Pavements.*10-12 June**.** Thessaloniki, pp. 153-159.

Saleh, S.E., Awda, G.J. and Ahmed, N.G., 2008. Development of pavement condition index model for flexible pavement in Baghdad city. *Journal of Engineering*, *14*(1), pp.2120-2135.

Santucci, L. (2002) Moisture Sensitivity of Asphalt Pavements. Available at: https://trid.trb.org/view/986729. (Accessed: 3 may 2017).

Shahin, M.Y. and Walther, J. (1990) *Pavement maintenance management for roads and streets using the PAVER system.* Construction Engineering Research Lab.

Sheta, A. (2006) 'Software effort estimation and stock market prediction using takagi-sugeno fuzzy models', *Fuzzy Systems, 2006 IEEE International Conference on.* IEEE, 171-178.

Shiwakoti, H. (2007) *Development of a rapid test to determine moisture senstivity of HMA (SUPERPAVE) mixtures.* PhD Thesis. University of Kansas.

Sonebi, M., Bassuoni, M. and Yahia, A. (2016) 'Pervious concrete: mix design, properties and applications', RILEM Technical Letters, 1, pp. 109-115.

Sussillo, D. and Abbott, L.F. (2009) 'Generating coherent patterns of activity from chaotic neural networks', Neuron, 63(4), pp. 544-557.

Solaimanian, M., Harvey, J., Tahmoressi, M. and Tandon, V. (2003) 'Test methods to predict moisture sensitivity of hot-mix asphalt pavements', *Transportation Research Board National Seminar. San Diego, California.* , 77-110.

Svasdisant, T., Schorsch, M., Baladi, G. and Pinyosunun, S. (2002) 'Mechanistic analysis of top-down cracks in asphalt pavements', *Transportation Research Record: Journal of the Transportation Research Board,* (1809), pp. 126-136.

TIRERACK (2016) Rotate Direction of Rotation. Available at: https://tires.tirerack.com/tires/Rotate%20Direction%20Of%20Rotation (Accessed: 15 August 2016).

Thom, N. (2008) *Principles of pavement engineering.* Thomas Telford London.

Uysal, O. and Bulkan, S. (2008) 'Comparison of genetic algorithm and particle swarm optimization for bicriteria permutation flowshop scheduling problem', *International Journal of Computational Intelligence Research,* 4(2), pp. 159-176.

Vadood, M., Semnani, D. and Morshed, M. (2011) 'Optimization of acrylic dry spinning production line by using artificial neural network and genetic algorithm', *Journal of Applied Polymer Science,* 120(2), pp. 735-744.

Vaiana, R., Capiluppi, G., Gallelli, V., Iuele, T. and Minani, V. (2012) 'Pavement surface performances evolution: an experimental application', Procedia-Social and Behavioral Sciences, 53, pp. 1149-1160.

Vaidehi, V., Monica, S., Mohamed Sheik Safeer, S., Deepika, M. and and Sangeetha, S. (2008) 'A Prediction System Based Fuzzy Logic', *Proceedings of the World Congress on Engineering and Computer Science.* San Francisco, USA.

Wang, L. and Mendel, J.M. (1992) 'Generating fuzzy rules by learning from examples', *IEEE transactions on systems, man, and cybernetics*, 22(6), pp. 1414-1427.

Wells, R. (2003) 'Synaptic Weight Modulation and Adaptation Part I: Introduction and Presynaptic Mechanisms'.

Willway T, Baldachin L, Reeves S et al. (2008) *The Effects of Climate Change on Highway Pavements and How to minimise them: Technical Report*. Available at: https://trl.co.uk/sites/default/files/PPR184_secure.pdf. (Accessed: 3 June 2018)

Xiaoyong, L.Z.D. (2008) 'Axial symmetric elastic solution of pore water pressure in asphalt pavement under mobile load ', *Journal of Southeast University (Natural Science Edition)*, 38 (5), pp. 014.

Yilmaz, A. and SARGIN, Ş. (2012) 'Water effect on deteriorations of asphalt pavements', *The Online Journal of Science and Technology*, 2(1), pp. 1-6.

Zadeh, L.A. (1965) '*Fuzzy logic and its applications*', Academic Press:New York.

Zadeh, L.A., Fuzzy Logic, IEEE Computer, pp. 83-93, 1988.

Zhou, C., Wang, Z., Chen, J. and Qiao, Y. (2007) 'Numerical computation and analysis on dynamic pore water pressure in asphalt pavement', *International Conference on Transportation Engineering*, 2981-2986.

XI. Appendences

Appendix A

WaveMatrix Software setup to measure pore water pressure.

The software used was the WaveMatrix software for dynamic and fatigue testing as it delivers flexibility for the user to run both a ramp waveform and a cyclic waveform. The test sequence was divided in three steps, each one performing a specific action. This is shown in Figure 1 and explained below, and details of each step are shown in Figures 2 and 3.

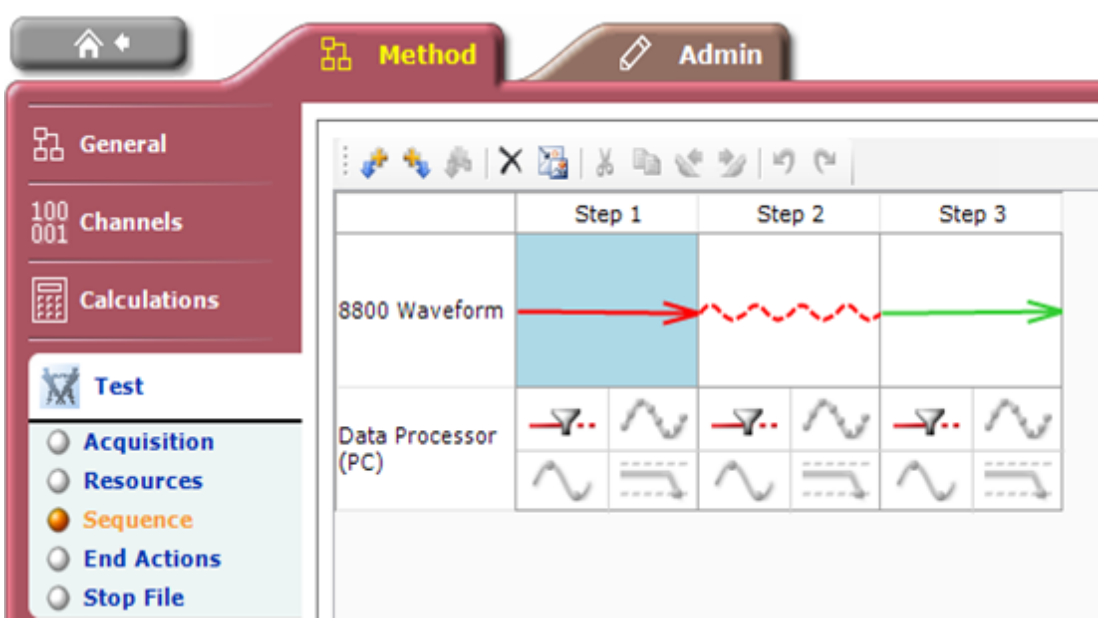

Measure pore water pressure setup

Step 1: Relative Ramp Waveform

- Control Mode: Load
- Ramp Duration: 15

- End Point: load (relative to start point which in this case was always 0 kN)
- Waveform End Action: Immediately Transfer All to Next Step

This step sets the load as the controlled variable. Also, setting ramp duration of 15 s means the impact device will slowly go down to the slab surface until it reaches a required load. Furthermore, the negative sign of the load is related to the direction of the force. This step is performed to secure an accurate value for the load that is applied. Then, the software moves to the next step.

Step 2: Cyclic waveform

- Control Mode: Load
- Amplitude: load required
- Frequency: Set as the test is carried out
- Shape: Sine
- Number of Cycles: 30
- Waveform Starting Phase: 0 Degrees
- End Action: Finish All, then Transfer All to Next Step

This step maintains the load as the controlled variable. Also, the magnitude is load required kN. Frequency set as the test is carried out. The number of cycles is chosen ten after many trails. Ten cycles it has been believed is the proper number of cycles beyond this number no change in pressure magnitude observed, also to save time.

Step 3: Absolute Ramp Waveform

- Control Mode: Position
- Ramp Rate: Duration
- Ramp Duration: 5 s
- End Point (absolute value)
- Wave Form End Action: Finish All, then Transfer All to Next Step

This step changes the control mode to the position as set up as required at the beginning of each test. The duration of the step is 5 second. Then; the software moved to the finish the test and saved the data in excel sheet.

Appendix B

Measured Pore Water Pressure under Concrete Slab

Test No	ID	Frequency	Water Depth 4mm		Water Depth 2mm	
			5KN	10KN	5KN	10KN
Test 1	1.5 SQ	1HZ	2.645	3.559	2.180	3.659
Test 2	1.5 SQ	1HZ	2.712	3.710	2.702	3.600
Test 3	1.5 SQ	1HZ	2.673	3.692	2.234	3.633
Test 1	1.5 SQ	5HZ	3.747	4.321	2.730	3.718
Test 2	1.5 SQ	5HZ	3.839	4.449	2.744	3.752
Test 3	1.5 SQ	5HZ	3.858	4.577	2.793	3.822
Test 1	1.5 SQ	10HZ	3.732	4.775	3.165	4.756
Test 2	1.5 SQ	10HZ	3.600	4.857	3.242	4.851
Test 3	1.5 SQ	10HZ	3.600	4.907	3.149	4.818
Test 1	1.5 SQ	15HZ	4.894	5.213	4.393	4.985
Test 2	1.5 SQ	15HZ	4.870	5.042	4.301	5.011
Test 3	1.5 SQ	15HZ	4.893	5.192	4.893	5.133
Test 1	3 SQ	1HZ	3.029	4.549	2.991	3.150
Test 2	3 SQ	1HZ	3.069	4.662	2.946	3.015
Test 3	3SQ	1HZ	3.080	4.528	2.951	3.015
Test 1	3SQ	5HZ	4.172	5.215	3.897	5.161
Test 2	3 SQ	5HZ	4.236	5.294	3.900	5.240
Test 3	3SQ	5HZ	4.266	5.390	3.796	5.213
Test 1	3 SQ	10HZ	4.693	5.395	3.866	5.309
Test 2	3SQ	10HZ	4.713	5.399	3.877	5.313
Test 3	3SQ	10HZ	4.637	5.431	3.943	5.390
Test 1	3SQ	15HZ	5.330	5.702	4.613	4.861
Test 2	3 SQ	15HZ	5.365	5.873	4.576	4.765
Test 3	3 SQ	15HZ	5.371	5.921	4.578	4.877
Test 1	8SQ	1HZ	4.638	5.692	2.851	3.895
Test 2	8SQ	1HZ	4.163	5.685	2.796	3.826
Test 3	8SQ	1HZ	4.225	5.843	2.800	3.783
Test 1	8SQ	5HZ	4.725	5.454	4.558	5.433
Test 2	8SQ	5HZ	4.701	5.556	4.633	5.240
Test 3	8SQ	5HZ	4.652	5.471	4.601	5.345
Test 1	8SQ	10HZ	5.793	6.002	5.431	5.865
Test 2	8SQ	10HZ	5.861	5.968	5.422	5.932
Test 3	8SQ	10HZ	5.853	6.214	5.329	5.959

Measured Pore Water Pressure under Concrete Slab

Test No	ID	Frequency	Water Depth 4mm		Water Depth 2mm	
			5KN	10KN	5KN	10KN
Test 1	8SQ	15HZ	6.383	6.885	6.166	6.653
Test 2	8SQ	15HZ	6.199	6.889	6.125	6.585
Test 3	8SQ	15HZ	6.237	6.893	6.234	6.596
Test 1	1.5SL	1HZ	2.790	3.690	2.728	3.519
Test 2	1.5SL	1HZ	2.762	3.665	2.656	3.603
Test 3	1.5SL	1HZ	2.729	3.559	2.642	3.548
Test 1	1.5SL	5HZ	2.763	3.844	2.225	3.676
Test 2	1.5SL	5HZ	2.755	3.773	2.222	3.714
Test 3	1.5SL	5HZ	2.779	3.733	2.185	3.704
Test 1	1.5SL	10HZ	2.599	4.867	3.252	4.741
Test 2	1.5SL	10HZ	2.715	4.882	3.154	4.861
Test 3	1.5SL	10HZ	2.612	4.763	3.151	4.755
Test 1	1.5SL	15HZ	3.149	5.192	4.402	4.985
Test 2	1.5SL	15HZ	3.048	5.209	4.321	5.091
Test 3	1.5SL	15HZ	3.112	5.073	4.403	5.042
Test 1	3SL	1HZ	2.043	4.577	1.771	2.128
Test 2	3SL	1HZ	2.054	4.528	1.753	2.105
Test 3	3SL	1HZ	2.104	4.649	1.863	2.066
Test 1	3SL	5HZ	2.362	3.390	1.932	3.325
Test 2	3SL	5HZ	2.343	3.402	1.903	3.290
Test 3	3SL	5HZ	2.294	3.373	1.912	3.319
Test 1	3SL	10HZ	2.504	5.249	1.940	4.798
Test 2	3SL	10HZ	2.422	5.146	1.963	4.679
Test 3	3SL	10HZ	2.462	4.954	1.993	4.798
Test 1	3SL	15HZ	3.501	5.404	2.276	5.269
Test 2	3SL	15HZ	3.462	5.425	2.263	5.413
Test 3	3SL	15HZ	3.329	5.303	2.228	5.282
Test 1	8SL	1HZ	2.820	3.604	2.200	3.493
Test 2	8SL	1HZ	2.758	3.593	2.231	3.520
Test 3	8SL	1HZ	2.803	3.591	2.245	3.524
Test 1	8SL	5HZ	2.939	4.341	2.515	4.271
Test 2	8SL	5HZ	2.956	4.363	2.472	4.281
Test 3	8SL	5HZ	3.023	4.338	2.441	4.232
Test 1	8SL	10HZ	3.392	5.005	3.311	4.809
Test 2	8SL	10HZ	3.399	5.106	3.365	5.044
Test 3	8SL	10HZ	3.390	4.834	3.332	4.802

Measured Pore Water Pressure under Concrete Slab

Test No	ID	Frequency	Water Depth 4mm		Water Depth 2mm	
			5KN	10KN	5KN	10KN
Test 1	8SL	15HZ	4.226	5.467	3.646	5.131
Test 2	8SL	15HZ	4.214	5.329	3.614	5.213
Test 3	8SL	15HZ	4.232	5.319	3.711	5.225
Test 1	NT	1HZ	1.272	1.333	0.692	1.275
Test 2	NT	1HZ	1.315	1.323	0.672	1.302
Test 3	NT	1HZ	1.304	1.303	0.692	1.285
Test 1	NT	5HZ	1.308	1.374	0.867	1.333
Test 2	NT	5HZ	1.346	1.361	0.866	1.335
Test 3	NT	5HZ	1.319	1.377	0.894	1.323
Test 1	NT	10HZ	1.496	1.616	0.974	1.473
Test 2	NT	10HZ	1.544	1.629	0.974	1.507
Test 3	NT	10HZ	1.510	1.582	1.008	1.497
Test 1	NT	15HZ	1.581	1.690	1.024	1.588
Test 2	NT	15HZ	1.618	1.682	1.041	1.534
Test 3	NT	15HZ	1.592	1.651	1.102	1.562

Maximum value of Pore Water Pressure under Concrete Slab

Test No	ID	Frequency	MAX			
			Water Depth 4mm		Water Depth 4mm	
			5KN	10KN	5KN	10KN
Test 1	1.5 SQ	1HZ	2.712	3.710	2.702	3.633
Test 2	1.5 SQ	1HZ				
Test 3	1.5 SQ	1HZ				
Test 1	1.5 SQ	5HZ	3.858	4.577	2.793	3.822
Test 2	1.5 SQ	5HZ				
Test 3	1.5 SQ	5HZ				
Test 1	1.5 SQ	10HZ	3.732	4.907	3.242	4.851
Test 2	1.5 SQ	10HZ				
Test 3	1.5 SQ	10HZ				
Test 1	1.5 SQ	15HZ	4.894	5.213	4.893	5.133
Test 2	1.5 SQ	15HZ				
Test 3	1.5 SQ	15HZ				
Test 1	3 SQ	1HZ	3.080	4.662	2.991	3.150
Test 2	3 SQ	1HZ				
Test 3	3SQ	1HZ				
Test 1	3SQ	5HZ	4.266	5.390	3.900	5.240
Test 2	3 SQ	5HZ				
Test 3	3SQ	5HZ				
Test 1	3 SQ	10HZ	4.713	5.431	3.943	5.390
Test 2	3SQ	10HZ				
Test 3	3SQ	10HZ				
Test 1	3SQ	15HZ	5.371	5.921	4.613	4.877
Test 2	3 SQ	15HZ				
Test 3	3 SQ	15HZ				
Test 1	8SQ	1HZ	4.638	5.843	2.851	3.895
Test 2	8SQ	1HZ				
Test 3	8SQ	1HZ				
Test 1	8SQ	5HZ	4.725	5.556	4.633	5.433
Test 2	8SQ	5HZ				
Test 3	8SQ	5HZ				
Test 1	8SQ	10HZ	5.861	6.214	5.431	5.959
Test 2	8SQ	10HZ				
Test 3	8SQ	10HZ				
Test 1	8SQ	15HZ	6.383	6.893	6.234	6.653
Test 2	8SQ	15HZ				
Test 3	8SQ	15HZ				
Test 1	1.5SL	1HZ	2.790	3.690	2.728	3.603
Test 2	1.5SL	1HZ				
Test 3	1.5SL	1HZ				

Maximum value of Pore Water Pressure under Concrete Slab

Test No	ID	Frequency	MAX			
			Water Depth 4mm		Water Depth 2mm	
			5KN	10KN	5KN	10KN
Test 1	1.5SL	5HZ	2.779	3.844	2.225	3.714
Test 2	1.5SL	5HZ				
Test 3	1.5SL	5HZ				
Test 1	1.5SL	10HZ	2.715	4.882	3.252	4.861
Test 2	1.5SL	10HZ				
Test 3	1.5SL	10HZ				
Test 1	1.5SL	15HZ	3.149	5.209	4.403	5.091
Test 2	1.5SL	15HZ				
Test 3	1.5SL	15HZ				
Test 1	3SL	1HZ	2.104	4.649	1.863	2.128
Test 2	3SL	1HZ				
Test 3	3SL	1HZ				
Test 1	3SL	5HZ	2.362	3.402	1.932	3.325
Test 2	3SL	5HZ				
Test 3	3SL	5HZ				
Test 1	3SL	10HZ	2.504	5.249	1.993	4.798
Test 2	3SL	10HZ				
Test 3	3SL	10HZ				
Test 1	3SL	15HZ	3.501	5.425	2.276	5.413
Test 2	3SL	15HZ				
Test 3	3SL	15HZ				
Test 1	8SL	1HZ	2.820	3.604	2.245	3.524
Test 2	8SL	1HZ				
Test 3	8SL	1HZ				
Test 1	8SL	5HZ	3.023	4.363	2.515	4.281
Test 2	8SL	5HZ				
Test 3	8SL	5HZ				
Test 1	8SL	10HZ	3.399	5.106	3.365	5.044
Test 2	8SL	10HZ				
Test 3	8SL	10HZ				
Test 1	8SL	15HZ	4.232	5.467	3.711	5.225
Test 2	8SL	15HZ				
Test 3	8SL	15HZ				
Test 1	NT	1HZ	1.315	1.333	0.692	1.302
Test 2	NT	1HZ				
Test 3	NT	1HZ				

Maximum value of Pore Water Pressure under Concrete Slab

Test No	ID	Frequency	MAX			
			Water depth 4mm		Water depth 2mm	
			5kN	10kN	5kN	10kN
Test 1	NT	5HZ	1.346	1.377	0.894	1.335
Test 2	NT	5HZ				
Test 3	NT	5HZ				
Test 1	NT	10HZ	1.544	1.629	1.008	1.507
Test 2	NT	10HZ				
Test 3	NT	10HZ				
Test 1	NT	15HZ	1.618	1.690	1.102	1.588
Test 2	NT	15HZ				
Test 3	NT	15HZ				

Minimum value of Pore Water Pressure under Concrete Slab

Test No	ID	frequency	MIN			
			Water Depth 4mm		Water Depth 2mm	
			5KN	10KN	5KN	10KN
Test 1	1.5 SQ	1HZ	2.645	3.559	2.180	3.459
Test 2	1.5 SQ	1HZ				
Test 3	1.5 SQ	1HZ				
Test 1	1.5 SQ	5HZ	3.747	4.321	2.730	3.718
Test 2	1.5 SQ	5HZ				
Test 3	1.5 SQ	5HZ				
Test 1	1.5 SQ	10HZ	3.600	4.775	3.149	4.756
Test 2	1.5 SQ	10HZ				
Test 3	1.5 SQ	10HZ				
Test 1	1.5 SQ	15HZ	4.870	5.042	4.301	4.985
Test 2	1.5 SQ	15HZ				
Test 3	1.5 SQ	15HZ				
Test 1	3 SQ	1HZ	3.029	4.528	2.946	3.015
Test 2	3 SQ	1HZ				
Test 3	3SQ	1HZ				
Test 1	3SQ	5HZ	4.172	5.215	3.796	5.161
Test 2	3 SQ	5HZ				
Test 3	3SQ	5HZ				
Test 1	3 SQ	10HZ	4.637	5.395	3.866	5.309
Test 2	3SQ	10HZ				
Test 3	3SQ	10HZ				
Test 1	3SQ	15HZ	5.330	5.702	4.576	4.765
Test 2	3 SQ	15HZ				
Test 3	3 SQ	15HZ				
Test 1	8SQ	1HZ	4.163	5.685	2.796	3.783
Test 2	8SQ	1HZ				
Test 3	8SQ	1HZ				
Test 1	8SQ	5HZ	4.652	5.454	4.558	5.240
Test 2	8SQ	5HZ				
Test 3	8SQ	5HZ				
Test 1	8SQ	10HZ	5.793	5.968	5.329	5.865
Test 2	8SQ	10HZ				
Test 3	8SQ	10HZ				
Test 1	8SQ	15HZ	6.199	6.885	6.125	6.585
Test 2	8SQ	15HZ				
Test 3	8SQ	15HZ				
Test 1	1.5SL	1HZ	2.729	3.559	2.642	3.519
Test 2	1.5SL	1HZ				
Test 3	1.5SL	1HZ				

Minimum value of Pore Water Pressure under Concrete Slab

Test No	ID	Frequency	MIN			
			Water Depth 4mm		Water Depth 2mm	
			5KN	10KN	5KN	10KN
Test 1	1.5SL	5HZ	2.755	3.733	2.185	3.676
Test 2	1.5SL	5HZ				
Test 3	1.5SL	5HZ				
Test 1	1.5SL	10HZ	2.599	4.763	3.151	4.741
Test 2	1.5SL	10HZ				
Test 3	1.5SL	10HZ				
Test 1	1.5SL	15HZ	3.048	5.073	4.321	4.985
Test 2	1.5SL	15HZ				
Test 3	1.5SL	15HZ				
Test 1	3SL	1HZ	2.043	4.528	1.753	2.066
Test 2	3SL	1HZ				
Test 3	3SL	1HZ				
Test 1	3SL	5HZ	2.294	3.373	1.903	3.290
Test 2	3SL	5HZ				
Test 3	3SL	5HZ				
Test 1	3SL	10HZ	2.422	4.954	1.940	4.679
Test 2	3SL	10HZ				
Test 3	3SL	10HZ				
Test 1	3SL	15HZ	3.329	5.303	2.228	5.269
Test 2	3SL	15HZ				
Test 3	3SL	15HZ				
Test 1	8SL	1HZ	2.758	3.591	2.200	3.493
Test 2	8SL	1HZ				
Test 3	8SL	1HZ				
Test 1	8SL	5HZ	2.939	4.338	2.441	4.232
Test 2	8SL	5HZ				
Test 3	8SL	5HZ				
Test 1	8SL	10HZ	3.390	4.834	3.311	4.802
Test 2	8SL	10HZ				
Test 3	8SL	10HZ				
Test 1	8SL	15HZ	4.214	5.319	3.614	5.131
Test 2	8SL	15HZ				
Test 3	8SL	15HZ				

Minimum value of Pore Water Pressure under Concrete Slab

Test No	ID	Frequency	MIN			
			Water Depth 4mm		Water Depth 2mm	
			5KN	10KN	5KN	10KN
Test 1	NT	1HZ	1.272	1.303	0.672	1.275
Test 2	NT	1HZ				
Test 3	NT	1HZ				
Test 1	NT	5HZ	1.308	1.361	0.866	1.323
Test 2	NT	5HZ				
Test 3	NT	5HZ				
Test 1	NT	10HZ	1.496	1.582	0.974	1.473
Test 2	NT	10HZ				
Test 3	NT	10HZ				
Test 1	NT	15HZ	1.581	1.651	1.024	1.534
Test 2	NT	15HZ				
Test 3	NT	15HZ				

Calculated STDEVA of Pore Water Pressure under Concrete Slab

Test No	ID	Frequency	STDEVA			
			Water depth 4mm		Water depth 2mm	
			5KN	10KN	5KN	10KN
Test 1	1.5 SQ	1HZ	0.034	0.082	0.287	0.092
Test 2	1.5 SQ	1HZ				
Test 3	1.5 SQ	1HZ				
Test 1	1.5 SQ	5HZ	0.059	0.128	0.033	0.053
Test 2	1.5 SQ	5HZ				
Test 3	1.5 SQ	5HZ				
Test 1	1.5 SQ	10HZ	0.076	0.066	0.050	0.048
Test 2	1.5 SQ	10HZ				
Test 3	1.5 SQ	10HZ				
Test 1	1.5 SQ	15HZ	0.014	0.093	0.319	0.079
Test 2	1.5 SQ	15HZ				
Test 3	1.5 SQ	15HZ				
Test 1	3 SQ	1HZ	0.027	0.072	0.025	0.078
Test 2	3 SQ	1HZ				
Test 3	3SQ	1HZ				
Test 1	3SQ	5HZ	0.048	0.088	0.059	0.040
Test 2	3 SQ	5HZ				
Test 3	3SQ	5HZ				
Test 1	3 SQ	10HZ	0.040	0.020	0.042	0.046
Test 2	3SQ	10HZ				
Test 3	3SQ	10HZ				
Test 1	3SQ	15HZ	0.022	0.115	0.021	0.060
Test 2	3 SQ	15HZ				
Test 3	3 SQ	15HZ				
Test 1	8SQ	1HZ	0.258	0.089	0.031	0.056
Test 2	8SQ	1HZ				
Test 3	8SQ	1HZ				
Test 1	8SQ	5HZ	0.037	0.055	0.038	0.096
Test 2	8SQ	5HZ				
Test 3	8SQ	5HZ				
Test 1	8SQ	10HZ	0.037	0.133	0.056	0.048
Test 2	8SQ	10HZ				
Test 3	8SQ	10HZ				
Test 1	8SQ	15HZ	0.097	0.004	0.055	0.036
Test 2	8SQ	15HZ				
Test 3	8SQ	15HZ				
Test 1	1.5SL	1HZ	0.031	0.069	0.046	0.043
Test 2	1.5SL	1HZ				
Test 3	1.5SL	1HZ				

Calculated STDEVA of Pore Water Pressure under Concrete Slab

Test No	ID	Frequency	STDEVA			
			Water depth 4mm		Water depth 2mm	
			5KN	10KN	5KN	10KN
Test 1	1.5SL	5HZ	0.012	0.056	0.022	0.020
Test 2	1.5SL	5HZ				
Test 3	1.5SL	5HZ				
Test 1	1.5SL	10HZ	0.063	0.065	0.058	0.065
Test 2	1.5SL	10HZ				
Test 3	1.5SL	10HZ				
Test 1	1.5SL	15HZ	0.051	0.074	0.047	0.053
Test 2	1.5SL	15HZ				
Test 3	1.5SL	15HZ				
Test 1	3SL	1HZ	0.032	0.061	0.059	0.031
Test 2	3SL	1HZ				
Test 3	3SL	1HZ				
Test 1	3SL	5HZ	0.035	0.014	0.015	0.019
Test 2	3SL	5HZ				
Test 3	3SL	5HZ				
Test 1	3SL	10HZ	0.041	0.150	0.027	0.069
Test 2	3SL	10HZ				
Test 3	3SL	10HZ				
Test 1	3SL	15HZ	0.090	0.065	0.025	0.079
Test 2	3SL	15HZ				
Test 3	3SL	15HZ				
Test 1	8SL	1HZ	0.032	0.007	0.023	0.017
Test 2	8SL	1HZ				
Test 3	8SL	1HZ				
Test 1	8SL	5HZ	0.045	0.014	0.037	0.026
Test 2	8SL	5HZ				
Test 3	8SL	5HZ				
Test 1	8SL	10HZ	0.005	0.137	0.027	0.138
Test 2	8SL	10HZ				
Test 3	8SL	10HZ				
Test 1	8SL	15HZ	0.009	0.082	0.049	0.051
Test 2	8SL	15HZ				
Test 3	8SL	15HZ				
Test 1	NT	1HZ	0.022	0.015	0.012	0.014
Test 2	NT	1HZ				
Test 3	NT	1HZ				

Calculated STDEVA of Pore Water Pressure under Concrete Slab

Test No	ID	Frequency	STDEVA			
			Water depth 4mm		Water depth 2mm	
			5kN	10kN	5kN	10kN
Test 1	NT	5HZ	0.020	0.008	0.016	0.006
Test 2	NT	5HZ				
Test 3	NT	5HZ				
Test 1	NT	10HZ	0.025	0.024	0.020	0.017
Test 2	NT	10HZ				
Test 3	NT	10HZ				
Test 1	NT	15HZ	0.019	0.021	0.041	0.027
Test 2	NT	15HZ				
Test 3	NT	15HZ				

Observed pore water pressure under concrete slab using asphalt overlay

Test No	ID	Frequency	Water Depth 4mm		Water Depth 2mm	
			5KN	10KN	5KN	10KN
Test 1	1.5 SQ	1HZ	2.378	2.631	2.244	2.081
Test 2	1.5 SQ	1HZ	2.254	2.581	2.311	2.098
Test 3	1.5 SQ	1HZ	2.332	2.617	2.262	2.102
Test 1	1.5 SQ	5HZ	2.512	3.244	2.353	3.082
Test 2	1.5 SQ	5HZ	2.462	3.221	2.372	3.095
Test 3	1.5 SQ	5HZ	2.505	3.218	2.362	3.107
Test 1	1.5 SQ	10HZ	3.105	3.311	3.075	3.095
Test 2	1.5 SQ	10HZ	3.014	3.292	3.011	3.091
Test 3	1.5 SQ	10HZ	3.090	3.242	3.050	3.094
Test 1	1.5 SQ	15HZ	3.253	4.111	3.194	3.689
Test 2	1.5 SQ	15HZ	3.249	4.131	3.171	3.660
Test 3	1.5 SQ	15HZ	3.293	4.103	3.163	3.666
Test 1	3 SQ	1HZ	2.462	2.768	2.443	2.551
Test 2	3 SQ	1HZ	2.512	2.773	2.419	2.626
Test 3	3SQ	1HZ	2.505	2.753	2.441	2.575
Test 1	3SQ	5HZ	3.313	3.528	3.028	3.243
Test 2	3 SQ	5HZ	3.360	3.540	3.040	3.339
Test 3	3SQ	5HZ	3.343	3.584	3.044	3.262
Test 1	3 SQ	10HZ	3.530	3.990	3.164	3.342
Test 2	3SQ	10HZ	3.634	3.982	3.172	3.362
Test 3	3SQ	10HZ	3.559	3.995	3.155	3.388
Test 1	3SQ	15HZ	3.690	4.954	3.530	3.698
Test 2	3 SQ	15HZ	3.559	4.949	3.531	3.685
Test 3	3 SQ	15HZ	3.665	4.984	3.534	3.682
Test 1	8SQ	1HZ	3.863	3.263	3.363	2.521
Test 2	8SQ	1HZ	3.787	3.383	3.383	2.551
Test 3	8SQ	1HZ	3.851	3.359	3.369	2.586
Test 1	8SQ	5HZ	3.984	3.540	3.411	4.529
Test 2	8SQ	5HZ	4.103	3.521	3.462	4.564
Test 3	8SQ	5HZ	4.030	3.510	3.420	4.563
Test 1	8SQ	10HZ	4.202	5.567	4.272	4.934
Test 2	8SQ	10HZ	4.277	5.596	4.292	4.984
Test 3	8SQ	10HZ	4.290	5.559	4.259	4.971
Test 1	8SQ	15HZ	5.192	5.765	5.090	5.241
Test 2	8SQ	15HZ	5.042	5.764	5.125	5.262
Test 3	8SQ	15HZ	5.128	5.763	5.250	5.231

Observed pore water pressure under concrete slab using asphalt overlay

Test No	ID	Frequency	Water Depth 4mm		Water Depth 2mm	
			5KN	10KN	5KN	10KN
Test 1	1.5SL	1HZ	1.915	2.145	2.264	2.066
Test 2	1.5SL	1HZ	1.934	2.153	2.253	2.108
Test 3	1.5SL	1HZ	1.948	2.138	2.298	2.102
Test 1	1.5SL	5HZ	1.799	2.358	2.358	3.065
Test 2	1.5SL	5HZ	1.853	2.341	2.361	3.087
Test 3	1.5SL	5HZ	1.836	2.315	2.365	3.094
Test 1	1.5SL	10HZ	2.255	3.372	3.010	3.095
Test 2	1.5SL	10HZ	2.304	3.392	3.012	3.096
Test 3	1.5SL	10HZ	2.175	3.385	3.034	3.088
Test 1	1.5SL	15HZ	2.443	3.411	3.191	3.662
Test 2	1.5SL	15HZ	2.449	3.461	3.191	3.666
Test 3	1.5SL	15HZ	2.460	3.452	3.172	3.692
Test 1	3SL	1HZ	2.158	2.333	2.093	2.096
Test 2	3SL	1HZ	2.160	2.372	2.072	2.078
Test 3	3SL	1HZ	2.165	2.362	2.112	2.066
Test 1	3SL	5HZ	2.363	3.263	2.328	2.284
Test 2	3SL	5HZ	2.410	3.252	2.312	2.307
Test 3	3SL	5HZ	2.403	3.289	2.306	2.288
Test 1	3SL	10HZ	2.818	3.362	2.646	2.343
Test 2	3SL	10HZ	2.851	3.344	2.654	2.382
Test 3	3SL	10HZ	2.881	3.388	2.600	2.391
Test 1	3SL	15HZ	2.962	3.445	2.877	3.082
Test 2	3SL	15HZ	2.877	3.452	2.892	3.013
Test 3	3SL	15HZ	2.918	3.421	2.902	3.006
Test 1	8SL	1HZ	2.452	2.444	2.443	2.635
Test 2	8SL	1HZ	2.486	2.440	2.453	2.647
Test 3	8SL	1HZ	2.511	2.439	2.432	2.665
Test 1	8SL	5HZ	3.223	3.632	3.113	2.561
Test 2	8SL	5HZ	3.274	3.631	3.114	2.637
Test 3	8SL	5HZ	3.292	3.634	3.112	2.586
Test 1	8SL	10HZ	4.061	4.247	3.998	3.054
Test 2	8SL	10HZ	4.069	4.241	3.986	3.015
Test 3	8SL	10HZ	3.994	4.245	3.989	3.042
Test 1	8SL	15HZ	4.162	4.521	4.148	3.699
Test 2	8SL	15HZ	4.236	4.554	4.189	3.684
Test 3	8SL	15HZ	4.242	4.552	4.072	3.662

Observed pore water pressure under concrete slab using asphalt overlay

Test No	ID	Frequency	Water Depth 4mm		Water Depth 2mm	
			5KN	10KN	5KN	10KN
Test 1	NT	1HZ	0.995	1.101	0.840	0.945
Test 2	NT	1HZ	0.969	1.111	0.861	0.923
Test 3	NT	1HZ	0.982	1.120	0.861	0.933
Test 1	NT	5HZ	1.190	1.097	1.111	1.050
Test 2	NT	5HZ	1.167	1.130	1.128	1.025
Test 3	NT	5HZ	1.198	1.114	1.088	1.037
Test 1	NT	10HZ	1.212	1.291	0.662	1.097
Test 2	NT	10HZ	1.210	1.300	0.682	1.130
Test 3	NT	10HZ	1.211	1.292	0.677	1.108
Test 1	NT	15HZ	1.720	1.928	1.925	1.760
Test 2	NT	15HZ	1.761	1.985	1.934	1.799
Test 3	NT	15HZ	1.744	1.949	1.948	1.782

Maxiumum pore water pressure under concrete slab using asphalt overlay

Test No	ID	Frequency	Max			
			Water Depth 4mm		Water Depth 2mm	
			5KN	10KN	5KN	10KN
Test 1	1.5 SQ	1HZ	2.378	2.631	2.311	2.102
Test 2	1.5 SQ	1HZ				
Test 3	1.5 SQ	1HZ				
Test 1	1.5 SQ	5HZ	2.512	3.244	2.372	3.107
Test 2	1.5 SQ	5HZ				
Test 3	1.5 SQ	5HZ				
Test 1	1.5 SQ	10HZ	3.105	3.311	3.075	3.095
Test 2	1.5 SQ	10HZ				
Test 3	1.5 SQ	10HZ				
Test 1	1.5 SQ	15HZ	3.293	4.131	3.194	3.689
Test 2	1.5 SQ	15HZ				
Test 3	1.5 SQ	15HZ				
Test 1	3 SQ	1HZ	2.512	2.773	2.443	2.626
Test 2	3 SQ	1HZ				
Test 3	3SQ	1HZ				
Test 1	3SQ	5HZ	3.360	3.584	3.044	3.339
Test 2	3 SQ	5HZ				
Test 3	3SQ	5HZ				
Test 1	3 SQ	10HZ	3.634	3.995	3.172	3.388
Test 2	3SQ	10HZ				
Test 3	3SQ	10HZ				
Test 1	3SQ	15HZ	3.690	4.984	3.534	3.698
Test 2	3 SQ	15HZ				
Test 3	3 SQ	15HZ				
Test 1	8SQ	1HZ	3.863	3.383	3.383	2.586
Test 2	8SQ	1HZ				
Test 3	8SQ	1HZ				
Test 1	8SQ	5HZ	4.103	3.540	3.462	4.564
Test 2	8SQ	5HZ				
Test 3	8SQ	5HZ				
Test 1	8SQ	10HZ	4.290	5.596	4.292	4.984
Test 2	8SQ	10HZ				
Test 3	8SQ	10HZ				
Test 1	8SQ	15HZ	5.192	5.765	5.250	5.262
Test 2	8SQ	15HZ				
Test 3	8SQ	15HZ				

Maxiumum pore water pressure under concrete slab using asphalt overla

Test No	ID	Frequency	Max			
			Water Depth 4mm		Water Depth 2mm	
			5KN	10KN	5KN	10KN
Test 1	1.5SL	1HZ	1.948	2.153	2.298	2.108
Test 2	1.5SL	1HZ				
Test 3	1.5SL	1HZ				
Test 1	1.5SL	5HZ	1.853	2.358	2.365	3.094
Test 2	1.5SL	5HZ				
Test 3	1.5SL	5HZ				
Test 1	1.5SL	10HZ	2.304	3.392	3.034	3.096
Test 2	1.5SL	10HZ				
Test 3	1.5SL	10HZ				
Test 1	1.5SL	15HZ	2.460	3.461	3.191	3.692
Test 2	1.5SL	15HZ				
Test 3	1.5SL	15HZ				
Test 1	3SL	1HZ	2.165	2.372	2.112	2.096
Test 2	3SL	1HZ				
Test 3	3SL	1HZ				
Test 1	3SL	5HZ	2.410	3.289	2.328	2.307
Test 2	3SL	5HZ				
Test 3	3SL	5HZ				
Test 1	3SL	10HZ	2.881	3.388	2.654	2.391
Test 2	3SL	10HZ				
Test 3	3SL	10HZ				
Test 1	3SL	15HZ	2.962	3.452	2.902	3.082
Test 2	3SL	15HZ				
Test 3	3SL	15HZ				
Test 1	8SL	1HZ	2.511	2.444	2.453	2.665
Test 2	8SL	1HZ				
Test 3	8SL	1HZ				
Test 1	8SL	5HZ	3.292	3.634	3.114	2.637
Test 2	8SL	5HZ				
Test 3	8SL	5HZ				
Test 1	8SL	10HZ	4.069	4.247	3.998	3.054
Test 2	8SL	10HZ				
Test 3	8SL	10HZ				
Test 1	8SL	15HZ	4.242	4.554	4.189	3.699
Test 2	8SL	15HZ				
Test 3	8SL	15HZ				

Maxiumum pore water pressure under concrete slab using asphalt overlay

Test No	ID	Frequency	Max			
			Water Depth 4mm		Water Depth 2mm	
			5KN	10KN	5KN	10KN
Test 1	NT	1HZ	0.995	1.120	0.861	0.945
Test 2	NT	1HZ				
Test 3	NT	1HZ				
Test 1	NT	5HZ	1.198	1.130	1.128	1.050
Test 2	NT	5HZ				
Test 3	NT	5HZ				
Test 1	NT	10HZ	1.212	1.300	0.682	1.130
Test 2	NT	10HZ				
Test 3	NT	10HZ				
Test 1	NT	15HZ	1.761	1.985	1.948	1.799
Test 2	NT	15HZ				
Test 3	NT	15HZ				

Miniumum pore water pressure under concrete slab using asphalt overlay

Test No	ID	Frequency	MIN			
			Water Depth 4mm		Water Depth 2mm	
			5KN	10KN	5KN	10KN
Test 1	1.5 SQ	1HZ	2.254	2.581	2.244	2.081
Test 2	1.5 SQ	1HZ				
Test 3	1.5 SQ	1HZ				
Test 1	1.5 SQ	5HZ	2.462	3.218	2.353	3.082
Test 2	1.5 SQ	5HZ				
Test 3	1.5 SQ	5HZ				
Test 1	1.5 SQ	10HZ	3.014	3.242	3.011	3.091
Test 2	1.5 SQ	10HZ				
Test 3	1.5 SQ	10HZ				
Test 1	1.5 SQ	15HZ	3.249	4.103	3.163	3.660
Test 2	1.5 SQ	15HZ				
Test 3	1.5 SQ	15HZ				
Test 1	3 SQ	1HZ	2.462	2.753	2.419	2.551
Test 2	3 SQ	1HZ				
Test 3	3SQ	1HZ				
Test 1	3SQ	5HZ	3.313	3.528	3.028	3.243
Test 2	3 SQ	5HZ				
Test 3	3SQ	5HZ				
Test 1	3 SQ	10HZ	3.530	3.982	3.155	3.342
Test 2	3SQ	10HZ				
Test 3	3SQ	10HZ				
Test 1	3SQ	15HZ	3.559	4.949	3.530	3.682
Test 2	3 SQ	15HZ				
Test 3	3 SQ	15HZ				
Test 1	8SQ	1HZ	3.787	3.263	3.363	2.521
Test 2	8SQ	1HZ				
Test 3	8SQ	1HZ				
Test 1	8SQ	5HZ	3.984	3.510	3.411	4.529
Test 2	8SQ	5HZ				
Test 3	8SQ	5HZ				
Test 1	8SQ	10HZ	4.202	5.559	4.259	4.934
Test 2	8SQ	10HZ				
Test 3	8SQ	10HZ				
Test 1	8SQ	15HZ	5.042	5.763	5.090	5.231
Test 2	8SQ	15HZ				
Test 3	8SQ	15HZ				

Miniumum pore water pressure under concrete slab using asphalt overlay

Test No	ID	Frequency	MIN			
			Water Depth 4mm		Water Depth 2mm	
			5KN	10KN	5KN	10KN
Test 1	1.5SL	1HZ	1.915	2.138	2.253	2.066
Test 2	1.5SL	1HZ				
Test 3	1.5SL	1HZ				
Test 1	1.5SL	5HZ	1.799	2.315	2.358	3.065
Test 2	1.5SL	5HZ				
Test 3	1.5SL	5HZ				
Test 1	1.5SL	10HZ	2.175	3.372	3.010	3.088
Test 2	1.5SL	10HZ				
Test 3	1.5SL	10HZ				
Test 1	1.5SL	15HZ	2.443	3.411	3.172	3.662
Test 2	1.5SL	15HZ				
Test 3	1.5SL	15HZ				
Test 1	3SL	1HZ	2.158	2.333	2.072	2.066
Test 2	3SL	1HZ				
Test 3	3SL	1HZ				
Test 1	3SL	5HZ	2.363	3.252	2.306	2.284
Test 2	3SL	5HZ				
Test 3	3SL	5HZ				
Test 1	3SL	10HZ	2.818	3.344	2.600	2.343
Test 2	3SL	10HZ				
Test 3	3SL	10HZ				
Test 1	3SL	15HZ	2.877	3.421	2.877	3.006
Test 2	3SL	15HZ				
Test 3	3SL	15HZ				
Test 1	8SL	1HZ	2.452	2.439	2.432	2.635
Test 2	8SL	1HZ				
Test 3	8SL	1HZ				
Test 1	8SL	5HZ	3.223	3.631	3.112	2.561
Test 2	8SL	5HZ				
Test 3	8SL	5HZ				
Test 1	8SL	10HZ	3.994	4.241	3.986	3.015
Test 2	8SL	10HZ				
Test 3	8SL	10HZ				
Test 1	8SL	15HZ	4.162	4.521	4.072	3.662
Test 2	8SL	15HZ				
Test 3	8SL	15HZ				

Miniumum pore water pressure under concrete slab using asphalt overlay

Test No	ID	Frequency	MIN			
			Water Depth 4mm		Water Depth 2mm	
			5KN	10KN	5KN	10KN
Test 1	NT	1HZ	0.969	1.101	0.840	0.923
Test 2	NT	1HZ				
Test 3	NT	1HZ				
Test 1	NT	5HZ	1.167	1.097	1.088	1.025
Test 2	NT	5HZ				
Test 3	NT	5HZ				
Test 1	NT	10HZ	1.210	1.291	0.662	1.097
Test 2	NT	10HZ				
Test 3	NT	10HZ				
Test 1	NT	15HZ	1.720	1.928	1.925	1.760
Test 2	NT	15HZ				
Test 3	NT	15HZ				

Calculated STDVA pore water pressure under concrete slab using asphalt overlay

Test No	ID	Frequency	STDEVA			
			Water Depth 4mm		Water Depth 2mm	
			5KN	10KN	5KN	10KN
Test 1	1.5 SQ	1HZ	0.063	0.026	0.035	0.011
Test 2	1.5 SQ	1HZ				
Test 3	1.5 SQ	1HZ				
Test 1	1.5 SQ	5HZ	0.027	0.014	0.009	0.012
Test 2	1.5 SQ	5HZ				
Test 3	1.5 SQ	5HZ				
Test 1	1.5 SQ	10HZ	0.049	0.036	0.032	0.002
Test 2	1.5 SQ	10HZ				
Test 3	1.5 SQ	10HZ				
Test 1	1.5 SQ	15HZ	0.024	0.014	0.016	0.015
Test 2	1.5 SQ	15HZ				
Test 3	1.5 SQ	15HZ				
Test 1	3 SQ	1HZ	0.027	0.011	0.014	0.039
Test 2	3 SQ	1HZ				
Test 3	3SQ	1HZ				
Test 1	3SQ	5HZ	0.024	0.030	0.009	0.051
Test 2	3 SQ	5HZ				
Test 3	3SQ	5HZ				
Test 1	3 SQ	10HZ	0.054	0.007	0.009	0.023
Test 2	3SQ	10HZ				
Test 3	3SQ	10HZ				
Test 1	3SQ	15HZ	0.069	0.019	0.002	0.009
Test 2	3 SQ	15HZ				
Test 3	3 SQ	15HZ				
Test 1	8SQ	1HZ	0.041	0.064	0.010	0.032
Test 2	8SQ	1HZ				
Test 3	8SQ	1HZ				
Test 1	8SQ	5HZ	0.060	0.015	0.027	0.020
Test 2	8SQ	5HZ				
Test 3	8SQ	5HZ				
Test 1	8SQ	10HZ	0.047	0.019	0.017	0.026
Test 2	8SQ	10HZ				
Test 3	8SQ	10HZ				
Test 1	8SQ	15HZ	0.075	0.001	0.084	0.016
Test 2	8SQ	15HZ				
Test 3	8SQ	15HZ				

Calculated STDVA pore water pressure under concrete slab using asphalt overlay

Test No	ID	Frequency	STDEVA			
			Water Depth 4mm		Water Depth 2mm	
			5KN	10KN	5KN	10KN
Test 1	1.5SL	1HZ	0.016	0.007	0.023	0.022
Test 2	1.5SL	1HZ				
Test 3	1.5SL	1HZ				
Test 1	1.5SL	5HZ	0.027	0.021	0.004	0.015
Test 2	1.5SL	5HZ				
Test 3	1.5SL	5HZ				
Test 1	1.5SL	10HZ	0.065	0.010	0.013	0.004
Test 2	1.5SL	10HZ				
Test 3	1.5SL	10HZ				
Test 1	1.5SL	15HZ	0.009	0.027	0.011	0.016
Test 2	1.5SL	15HZ				
Test 3	1.5SL	15HZ				
Test 1	3SL	1HZ	0.004	0.020	0.020	0.015
Test 2	3SL	1HZ				
Test 3	3SL	1HZ				
Test 1	3SL	5HZ	0.025	0.019	0.011	0.012
Test 2	3SL	5HZ				
Test 3	3SL	5HZ				
Test 1	3SL	10HZ	0.032	0.022	0.029	0.026
Test 2	3SL	10HZ				
Test 3	3SL	10HZ				
Test 1	3SL	15HZ	0.043	0.016	0.013	0.042
Test 2	3SL	15HZ				
Test 3	3SL	15HZ				
Test 1	8SL	1HZ	0.030	0.002	0.011	0.015
Test 2	8SL	1HZ				
Test 3	8SL	1HZ				
Test 1	8SL	5HZ	0.036	0.002	0.001	0.039
Test 2	8SL	5HZ				
Test 3	8SL	5HZ				
Test 1	8SL	10HZ	0.041	0.003	0.006	0.020
Test 2	8SL	10HZ				
Test 3	8SL	10HZ				
Test 1	8SL	15HZ	0.044	0.018	0.059	0.018
Test 2	8SL	15HZ				
Test 3	8SL	15HZ				

Calculated STDVA pore water pressure under concrete slab using asphalt overlay

Test No	ID	Frequency	STDEVA			
			Water Depth 4mm		Water Depth 2mm	
			5KN	10KN	5KN	10KN
Test 1	NT	1HZ	0.013	0.009	0.012	0.011
Test 2	NT	1HZ				
Test 3	NT	1HZ				
Test 1	NT	5HZ				
Test 2	NT	5HZ				
Test 3	NT	5HZ	0.016	0.016	0.020	0.013
Test 1	NT	10HZ				
Test 2	NT	10HZ				
Test 3	NT	10HZ	0.001	0.005	0.010	0.017
Test 1	NT	15HZ				
Test 2	NT	15HZ				
Test 3	NT	15HZ	0.021	0.029	0.011	0.020

Appendix C

Software setup for surface damage

- Set up Instron 8501 and WaveMatrix Software for asphalt surface damage

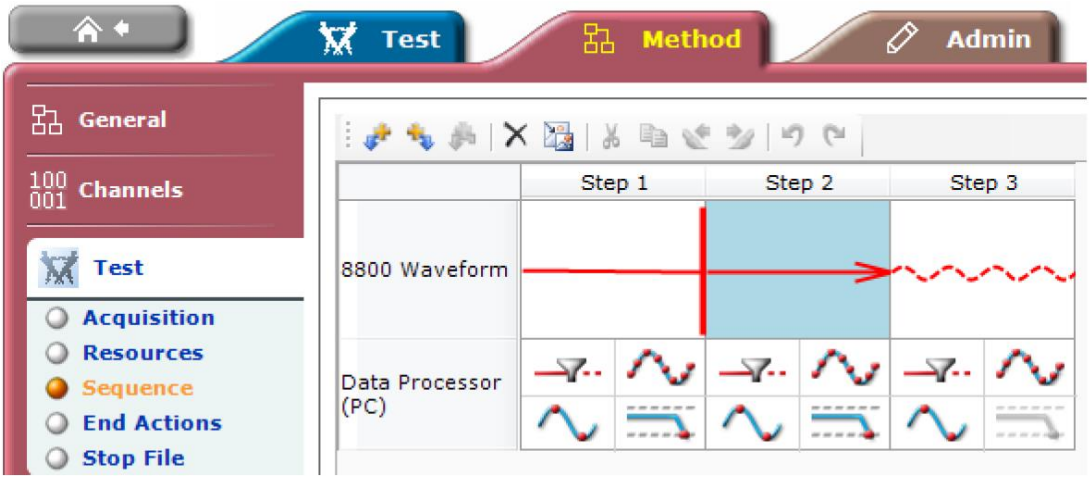

Surface damage test sequence

Step 1: Relative Ramp Waveform

- ✓ Control Mode: Load
- ✓ Ramp Rate: 0.2 kN/s
- ✓ End Point: -4.5 kN (relative to start point which in this case was always 0 kN)
- ✓ Waveform End Action: Immediately Transfer All to Next Step

This step sets the load as the controlled variable. Besides, setting a ramp rate of 0.2 kN/s means the impact device will slowly go down to the slab surface until it reaches a load of -4.5 kN The duration of the step is 22.5 seconds. Furthermore, the negative sign of the load is related to the direction of the force. As soon as this step is finished the software moves to the next step.

Step 2: Absolute Ramp Waveform

- ✓ Control Mode: Load

- ✓ Ramp Rate: 0.1 kN/s
- ✓ End Point: -4.5 kN (relative to start point which in this case was -4.5 kN)
- ✓ End Action: Finish All, then Transfer All to Next Step

This step maintains the load as the controlled variable. Also, the ramp rate is changed to 0.1 kN/s until it reaches a load of -4.5 kN, which is also known as preload. The duration of the step is 1 second. Similarly, the negative sign is again related to the direction of the force. As soon as this step is finished the software moves to the last step. These two steps are performed to secure an accurate value for the load that is applied.

Step 3: Cyclic Waveform

- ✓ Control Mode: Load
- ✓ Amplitude: 0.5 kN
- ✓ Frequency: 5Hz
- ✓ Shape: Sine
- ✓ Number of Cycles: 1000
- ✓ Waveform Starting Shape: 0 Degrees
- ✓ End Action: Finish All, then Wait for All

This step gives the sinusoidal shape to the load application. Similarly, the load is the controlled variable. Besides, the amplitude of the wave is 0.5 kN which indicates that the load will oscillate reaching a maximum value of 5 kN at a frequency of 5Hz. The duration of the step is determined by the number of cycles. Finally, as soon as this step is finished the measurements for cracking and rutting of the asphalt surface are observed.

Appendix D

Mixtures weight volume

HRA-14mm			Unites
% of bitumen (by mass)	Mb	8.2	%
% of aggregate (by mass)	Magg	91.8	%
Sg of bitumen		1.01	
Sg of aggregate		2.70	
Combined sg		2.37	
Combined volume	Vt	1	m^3
Volume of bitumen	VB	0.19	m^3
Volume of aggregate	VAGG	0.81	m^3
Combined volume	VT	100	%
% volume of air	Va	4.5	%
% volume of aggregate	Vagg	77.09	%

HRA-10mm			Unites
% of bitumen (by mass)	Mb	8	%
% of aggregate (by mass)	Magg	92	%
Sg of bitumen		1.01	
Sg of aggregate		2.70	
Combined sg		2.38	
Combined volume	Vt	1	m^3
Volume of bitumen	VB	0.12	m^3
Volume of aggregate	VAGG	0.81	m^3
Combined volume	VT	100	%
% volume of air	Va	4.5	%
% volume of aggregate	Vagg	68.19	%

SMA-14mm			Unites
% of bitumen (by mass)	Mb	5.8	%
% of aggregate (by mass)	Magg	94.2	%
Sg of bitumen		1.01	
Sg of aggregate		2.7	
Combined sg		2.46	
Combined volume	Vt	1	m³
Volume of bitumen	VB	0.14	m³
Volume of aggregate	VAGG	0.86	m³
Combined volume	VT	100	%
% volume of air	Va	8	%
% volume of aggregate	Vagg	78.99	%

SMA-10mm			Unites
% of bitumen (by mass)	Mb	6.2	%
% of aggregate (by mass)	Magg	93.8	%
Sg of bitumen		1.01	
Sg of aggregate		2.7	
Combined sg		2.45	
Combined volume	Vt	1	m³
Volume of bitumen	VB	0.15	m³
Volume of aggregate	VAGG	0.85	m³
Combined volume	VT	100	%
% volume of air	Va	8	%
% volume of aggregate	Vagg	78.18	%

SMA-6mm			Unites
% of bitumen (by mass)	Mb	6.6	%
% of aggregate (by mass)	Magg	93.4	%
Sg of bitumen		1.01	
Sg of aggregate		2.70	
Combined sg		2.43	
Combined volume	Vt	1	m^3
Volume of bitumen	VB	0.16	m^3
Volume of aggregate	VAGG	0.84	m^3
Combined volume	VT	100	%
% volume of air	Va	8	%
% volume of aggregate	Vagg	77.38	%

PA-14mm			Unites
% of bitumen (by mass)	Mb	4.5	%
% of aggregate (by mass)	Magg	95.5	%
Sg of bitumen		1.01	
Sg of aggregate		2.7	
Combined sg		2.51	
Combined volume	Vt	1	m^3
Volume of bitumen	VB	0.11	m^3
Volume of aggregate	VAGG	0.88	m^3
Combined volume	VT	100	%
% volume of air	Va	18	%
% volume of aggregate	Vagg	72.82	%

Mixture volumetric

Hot Rolled Asphalt

HRA-14mm			Unites
Mould dimension	Width	200	mm
	Length	200	mm
	Height	50	mm
Total volume	1 Mould	2000	cm^3
Assume			
	Sg of the mix	2.370	%
Target			
	% of air voids(target)	4.5	%
	% of bitumen (by mass)	8.2	%
	Density(maximum)	2.263	g/cm^3
Total mass		4526.70	g
	Bitumen	371.19	g
	Aggregate	4155.51	g

HRA-10mm			Unites
Mould dimension	Width	200	mm
	Length	200	mm
	Height	50	mm
Total volume	1 Mould	2000	cm^3
Assume			
	Sg of the mix	2.38	%
Target			
	% of air voids(target)	4.50	%
	% of bitumen (by mass)	8.00	%
	Density(maximum)	2.273	g/cm^3
Total mass		4545.80	g
	Bitumen	363.66	g
	Aggregate	4182.14	g

Stone Mastic Asphalt

SMA-14mm			Unites
Mould dimension	Width	200	mm
	Length	200	mm
	Height	50	mm
Total volume	1 Mould	2000	cm^3
Assume			
	Sg of the mix	2.46	%
Target			
	% of air voids(target)	8.00	%
	% of bitumen (by mass)	5.80	%
	Density(maximum)	2.263	g/cm^3
Total mass		4526.40	g
	Bitumen	262.53	g
	Aggregate	4263.87	g

SMA-10mm			Unites
Mould dimension	Width	200	mm
	Length	200	mm
	Height	50	mm
Total volume	1 Mould	2000	cm^3
Assume			
	Sg of the mix	2.45	%
Target			
	% of air voids(target)	8.00	%
	% of bitumen (by mass)	6.2	%
	Density(maximum)	2.254	g/cm^3
Total mass		4508.00	g
	Bitumen	279.50	g
	Aggregate	4228.50	g

SMA-6mm			Unites
Mould dimension	Width	200	mm
	Length	200	mm
	Height	50	mm
Total volume	1 Mould	2000	cm^3
Assume			
	Sg of the mix	2.43	%
Target			
	% of air voids(target)	8.00	%
	% of bitumen (by mass)	6.6	%
	Density(maximum)	2.236	g/cm^3
Total mass		4471.20	g
	Bitumen	295.10	g
	Aggregate	4176.10	g

Porous Asphalt

PA-14mm			Unites
Mould dimension	Width	200	mm
	Length	200	mm
	Height	50	mm
Total volume	1 Mould	2000	cm^3
Assume			
	Sg of the mix	2.51	%
Target			
	% of air voids(target)	18.00	%
	% of bitumen (by mass)	4.5	%
	Density(maximum)	2.10	g/cm^3
Total mass		4116.40	g
	Bitumen	185.24	g
	Aggregate	3931.16	g

Grading Curve Envelopes

Hot rolled asphalt

HRA-14mm		
BS EN 13108-4:2006		
Sieve size (mm)	% retained in Individual sieve	Mass(g)
20	0.00	0.00
14	3.50	145.44
10	21.50	893.43
2	9	374.00
0.5	31	1288.21
0.25	7.50	311.66
0.063	18.50	768.77
pan	9	374.00

HRA-10mm		
BS EN 13108-4:2006		
Sieve size (mm)	% retained in Individual sieve	Mass(g)
14	0.00	0.00
10	0.00	0.00
6.3	1	41.82
2	46.50	1944.69
0.5	12.50	522.77
0.25	15	627.32
0.063	5	209.11
pan	14	585.50

Stone Mastic Asphalt

SMA-14mm		
BS EN 13108-5:2016		
Sieve size (mm)	% retained in Individual sieve	Mass(g)
20	0.00	0.00
14	3.50	149.24
10	49	2089.30
6.3	18.50	788.82
2	6	255.83
0.63	14	596.94
pan	9	383.75

SMA-10mm		
BS EN 13108-5:2016		
Sieve size (mm)	% retained in Individual sieve	Mass(g)
14	0.00	0.00
10	3.50	148.00
6.3	56.50	2389.10
4	17	718.85
2	12.50	528.56
0.065	10.50	443.99
pan	100	4228.50

SMA-6mm		
BS EN 13108-5:2016		
Sieve size (mm)	% retained in Individual sieve	Mass(g)
14	0.00	0.00
10	0.00	0.00
6.3	3.50	146.16
4	63	2630.94
2	6.50	271.45
0.065	16	668.18
pan	11	459.37

Porous Asphalt

PA-14mm		
BS EN 13108-7:2006		
Sieve size (mm)	% retained in Individual sieve	Mass(g)
22.4	0	0
16	6	235.87
11.2	19	746.92
5.6	55	2162.14
2	5	196.56
500	7	275.18
0.63	3.5	137.59
Pan	4.5	176.90

Mass Relation

Stone Mastic Asphalt

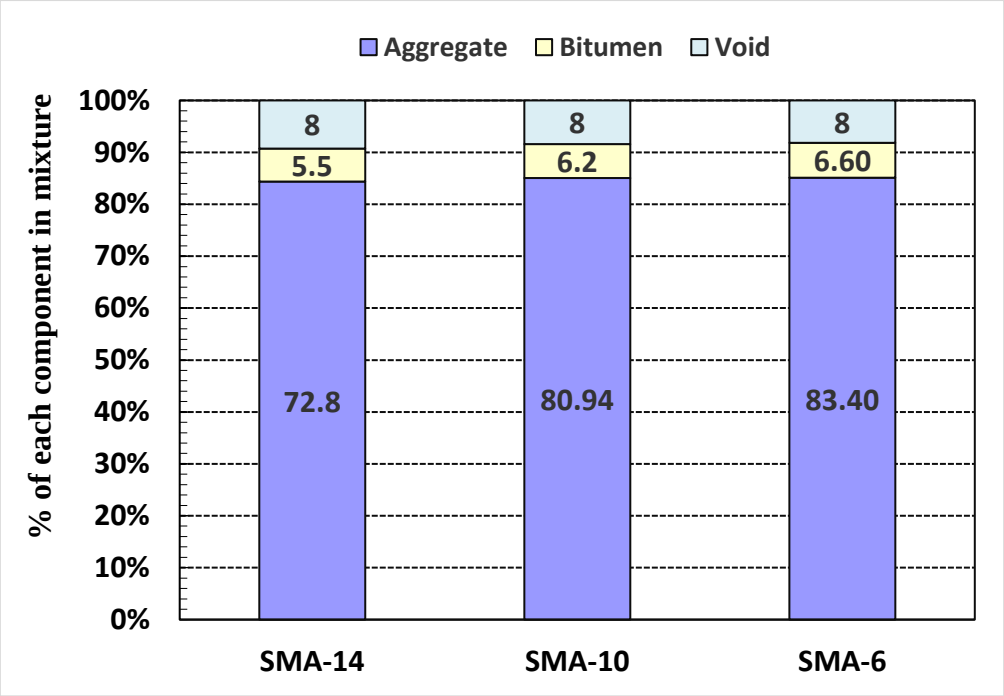

Hot Rolled Asphalt

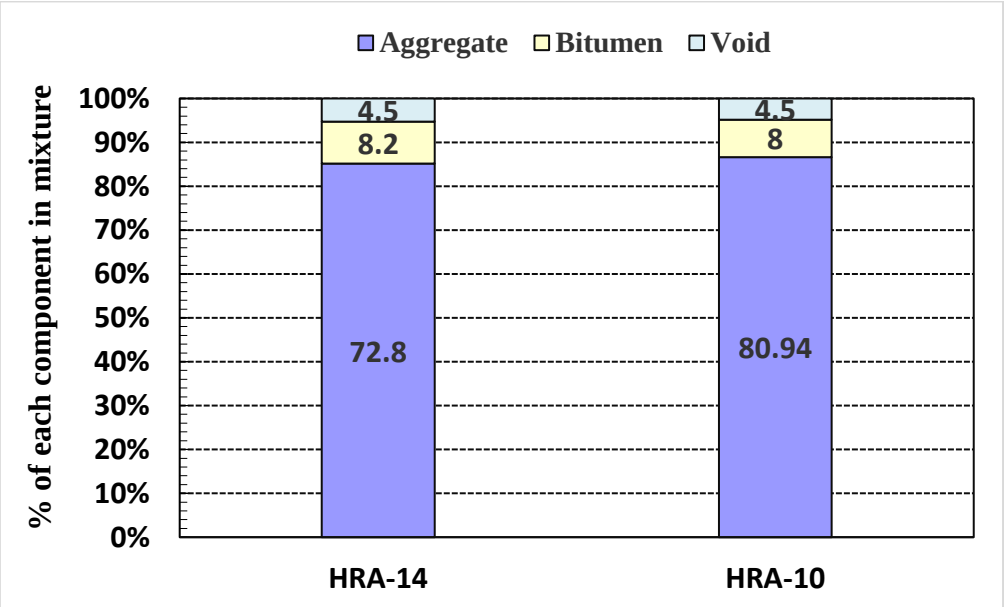

Porous Asphalt

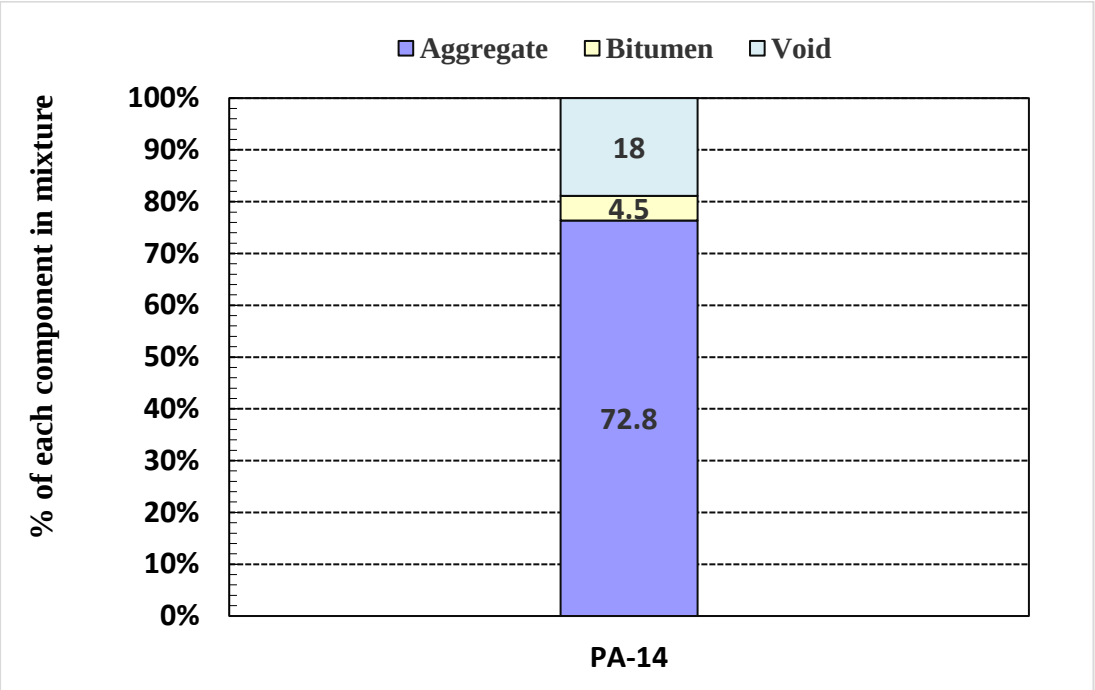

Equations Used in Mixture Design

1. Air void content in Compacted Mixture

The air void content of asphalt mixture was calculated based on the maximum and bulk densities, as it is shown in Eq. (1).

$$V_m = \frac{\rho_m - \rho_b}{\rho_m} \times 100\ \%$$

Where V_m is the air void content in the mixture (%), ρ_m is the maximum density of the mixture (kg/m^3) and ρ_b is the bulk density of the test sample in (kg/m^3)

Bulk Specific Gravity.

2. Bulk Specific Gravity

$$G_{sb} = \frac{P_1 + P_2 + \cdots P_n}{\frac{P_1}{G_1} + \frac{P_2}{G_2} + \ldots \frac{P_n}{G_n}}$$

$G_{sb=}$ Bulk dry gravity of the total aggregate

$P_{1,}$ $P_{2,}$ $P_{n\ =}$ percentage by weight of aggregates, filler and bitumen

G_1, G_2, G_3= bulk specific gravities of aggregates filler and bitumen